SECONDARY ELECTRON EMISSION PROPERTIES AND CHARACTERISTIC ENERGY LOSSES FROM SOME METALS

being

a thesis presented for the Degree of

Doctor of Philosophy at University of Keele

by

Simon Thomas, M.Sc.

Department of Physics,
University of Keele,
Keele, Staffordshire,
England.

October, 1967.

ACKNOWLEDGMENTS

The author wishes to express his gratitude to,

Professor D.J.E. Ingram for the use of his laboratory and research facilities,

Dr. E. B. Pattinson for his constructive criticism and helpful guidance all through this work,

Professor D. E. Davies and Dr. R.G.C. Leckey (now at La Trobe University, Australia) for their help in the early stages of this work,

Professor T. B. Thomas, Dr. B. P. Betts and Dr. (Mrs.) A. T. Betts for their constant encouragement,

Mr. R. M. Allen and colleagues in the Physics Department for useful discussions,

Mr. F. Rowerth and his technical staff for their assistance in constructional work,

Mrs. J. A. Morrough for the typing of the thesis,

The University of Keele for the provision of a research grant and

The Ministry of Defence for a research contract to the University, of which this work forms a part.

SYNOPSIS

Secondary electron emission yield and characteristic energy losses from a number of metals have been measured in the present investigation. Owing to the known adverse effects of poor vacuum conditions and any consequent contamination of the surface on the secondary emission properties, all experiments have been conducted in a clean ultra-high vacuum environment - typical pressure under operating conditions being $< 10^{-9}$ torr and the residual gases analysed by a quadrupole residual gas analyser. Total yield has been measured from Ni, Ag, Pt, Bi and TaC. A quantitative assessment of the variation of the total yield δ with angle of incidence of the primary beam, in the energy range 200 - 1300eV and of the mean depths of origin of secondary electrons in these materials, has been made. The total yield from TaC, which is currently favoured as a low yield material, and the effect of surface conditions on its yield have also been investigated.

Characteristic energy losses have been measured from Ag, Bi, Be, Ta and TaC by using a spherical retarding field energy analyser coupled with electronic differentiation. This technique involves energy modulating the electron beam and extracting the signal using phase sensitive detection methods. The accurate values of energy losses obtained in this manner, established the validity of such a technique and the potential of the analyser in characteristic energy loss studies. In particular, two losses at 15 and 30eV have been observed in TaC which has not been investigated hitherto. New energy losses at 13.5eV in Ag and 7.9 and 12.5eV in Ta

have been found. The various energy losses in the different materials have been attributed to the excitation of volume and surface plasmons and to interband transitions. Intensity variations with changes in environment have also been noted. Both changes in the intensity and shape of the loss peaks with contamination have emphasised the necessity for maintaining the target surface clean under ultra-high vacuum conditions.

CONTENTS

CHAPTER 1

The Basic Processes in Secondary Electron Emission

1.1 Introduction

When electrons with sufficient kinetic energy bombard a solid surface, the surface will emit electrons. The bombarding electrons are considered "primary" electrons and the emitted electrons "secondary"; the entire process being termed "secondary electron emission" (SEE). It was Austin and Starke (1) who, for the first time, in 1902, noticed the phenomenon of secondary electron emission while studying the reflection of cathode rays from metal surfaces. They observed that the number of electrons emitted by the metal was larger than the number hitting it. This could not be explained merely as reflection but rather as the additional liberation of electrons from the metal under the influence of the bombarding electrons.

Ever since the discovery of Austin and Starke, numerous experimental and theoretical investigations have been made concerning the phenomenon of secondary electron emission. The theories range from relatively simple empirical treatments to highly complex quantum mechanical investigations. Considerable experimental evidence has been gathered from metals, insulators and semiconductors under different conditions. Despite the long history of the phenomenon and the vast amount of study on it, many questions have yet to be answered ragarding the actual

production and escape mechanism of secondary electrons.

Secondary emission is predominantly a surface effect since the probability of electron escape decays exponentially with depth. The effects of surface contamination thus become very important. It is frequently very difficult to ascertain whether the experimental results are actually characteristic of the prepared target or of some contaminating element or of some compound formed by the contaminant and the target material. Much experimental effort has been extended in obtaining clean target surfaces, with varying degrees of success. Flashing metallic surfaces at high temperatures probably has been the most successful, but this technique has been limited to a few metals such as tungsten, tantalum and molybdenum. Heat treatment is open to criticism in the case of some metals such as aluminium where the oxide is much less volatile than the metal itself. Thus if the surface is once oxidised, it may not be possible to clean it off purely by heat treatment. Some authors prefer to prepare the targets by evaporation in a good vacuum. In all secondary electron emission studies it is essential to have the best possible vacuum conditions, since the characteristics can vary so much with adsorbed layers of foreign materials.

Early investigations on secondary electron emission had a very straightforward approach. Primary electrons bombard the surface of a material, where, by certain mechanisms, electrons are caused toleave the material. One need only measure the number of so called "secondary electrons" per second as a function of their energy (E) and their direction (θ) i.e. measure $J(E,\theta)$ and construct a theory to satisfy

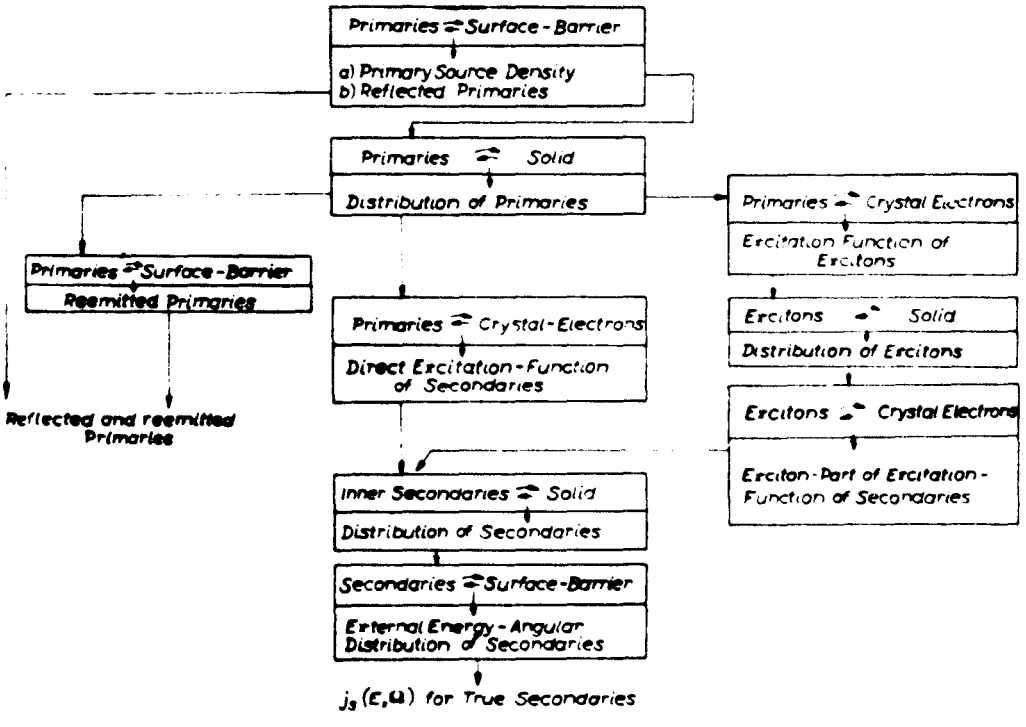

FIG. 1. Scheme of the secondary-emission process.

these results. Even though this approach gives a rough idea of secondary electrons, to completely understand the mechanism of secondary emission within the material, more advanced and complicated approaches must be made.

$J(E, \theta)$ can depend only on the states of the interacting systems, that is to say, on the properties of the primary electron beam and on the physical and chemical properties of the target, such as chemical composition, crystal structure, surface conditions, temperature , etc.

1.2 Qualitative scheme of secondary emission

The phenomenon of secondary emission is a complicated problem in nature. Although the full understanding of the mechanism involved is lacking, several schemes seem to explain logically the different elementary processes involved. These schemes are based on a multiplicity of events transpiring between the penetration of the primary electrons into the solid and the emission of the secondaries.

The interaction of primary electrons with the target and the subsequent emission of secondary electrons have been diagramatically represented by Hachenberg and Brauer (2) as shown in fig. 1.

The process can be explained as follows. 1) The Primary electron beam impinges upon the surface of the target where it interacts with the surface potential barrier and is split into two parts (a) those which are reflected and (b) those which penetrate the surface. 2) Those electrons penetrating the surface interact with the nuclei and electrons of the material and are thus distributed by elastic

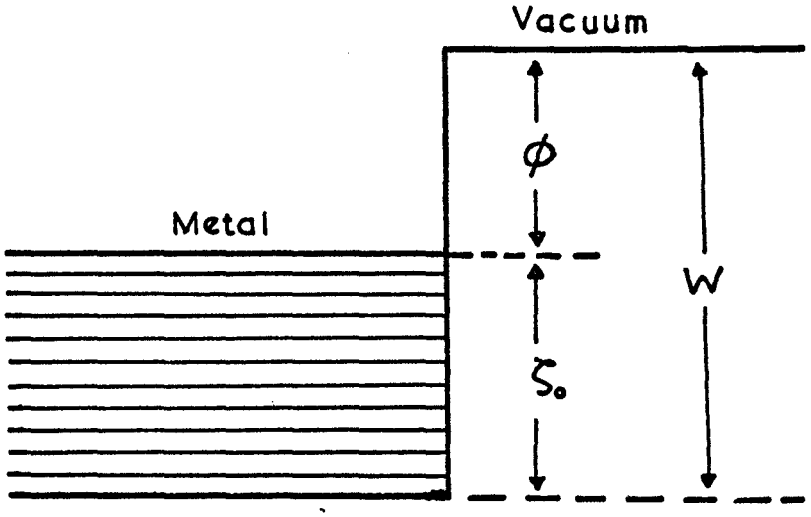

Fig. 2

Electron energy levels inside and outside a metal in vacuum.

collisions with the nuclei and energy is lost through interaction with the electrons. The elastic collisions cause the beam to be split again into various directions, some of which are backscattered towards the surface. These reflected primaries also will produce secondaries part of which will escape into free space (3,4,5). A primary electron going into the solid, owing to the Coulomb forces, excite atomic electrons, at the same time losing a fraction of its initial energy at each excitation or collision. High energy primaries may excite any electrons, but lower energy primaries (~100 ev) will usually excite only conduction band electrons. These "internal secondary electrons" thus generated interact with different components of the solid, such as electrons and phonons and spread towards the surface.

Whether such an electron ever escapes from the surface of the target depends on several factors. The kinetic energy associated with its velocity component perpendicular to the surface must be greater than, W, the difference between the bottom of the conduction band and the vacuum level, when it reaches the surface (fig. 2) (6.7).

An individual electron in the solid will fail to emerge, therefore if 1) its initial energy from the collision with primary electron is less than W 2) it loses sufficient energy from subsequent collisions so that by the time it reaches the surface, its kinetic energy is less than W. 3) It arrives at the surface at an angle such that the velocity component perpendicular to the surface is too small.

With regards to the last, consider an electron with

energy

$$E = \tfrac{1}{2}m\,(V_x^2 + V_y^2 + V_z^2) \geq W$$

Assume that its motion at the surface makes an angle θ with the normal to the surface. For escape

$$\tfrac{1}{2}m\,V_x^2 \geq W$$

or

$$\tfrac{1}{2}m\,V^2\,\mathrm{Cos}^2\theta \geq W$$

i.e.

$$\mathrm{Cos}^2\theta \geq \frac{W}{E}$$

The greatest angle from the normal at which an electron with arrival energy E, can escape from the surface is then

$$\theta_o = \mathrm{Cos}^{-1}\left(\frac{W}{E}\right)^{\frac{1}{2}} \qquad (1)$$

For all $\theta \leq \theta_o$ electrons of kinetic energy E, will escape. The solid angle involved is $\Omega = \int d\Omega = \int_0^{2\pi}\int_0^{\theta_o} \sin\theta\, d\theta\, d\phi$

$$= 2\pi\,(1 - \mathrm{Cos}\ \theta_o)$$

The probability of escape P(E) of an electron of energy E, can be computed. If an isotropic angular distribution of the electrons reaching the surface can be assumed and taking into account the one half space which is of interest

$$P(E) = \frac{\Omega}{2\pi} = (1 - \mathrm{Cos}\ \theta_o) = 1 - \left(\frac{W}{E}\right)^{\frac{1}{2}} \qquad (2)$$

The secondary electrons coming out of the target and their dependence on the various parameters, have been studied in great detail and a brief account of the experimental results will be

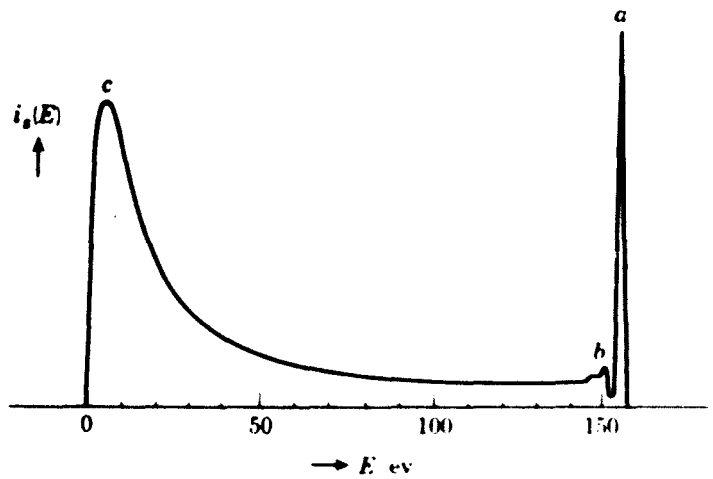

The energy distribution of secondary electrons emitted by silver.

FIG. 3

given so as to enable one to understand the basic processes involved.

1.3 Energy Spectrum

When investigating the secondary electrons, one of the more obvious features which may be studied, is the energy distribution. It is of prime importance both in applications of secondary emission and in the theoretical interpretation of the process.

If the number of secondary electrons emitted by the target, in the energy interval E and E + dE is plotted against E, a typical energy spectrum results. The general form of the distribution curve, resulting from medium values of primary energy E_p ($50 < E_p < 1000$eV) has been demonstrated by Rudberg (8) and one such curve is reproduced in fig. 3, for a silver target bombareded by 155 eV electrons. A number of features immediately become apparent. Three groups of electrons may be distinguished in the distribution curve

1) A group of electrons having the same energy, E_p, as the primary electrons. These can easily be distinguished as the primary electrons which have suffered elastic collisions with the lattice and have merely been reflected. These are called "reflected primaries". These elastically reflected primaries have an energy distribution similar to that of the primaries. The primary electrons are not monoenergetic but rather they have a Maxwellian distribution, it being a function of the cathode temperature. The group of reflected primaries is indicated by peak a in fig. 3.

2) A second group (marked b in fig. 3) falls between E_p and approximately

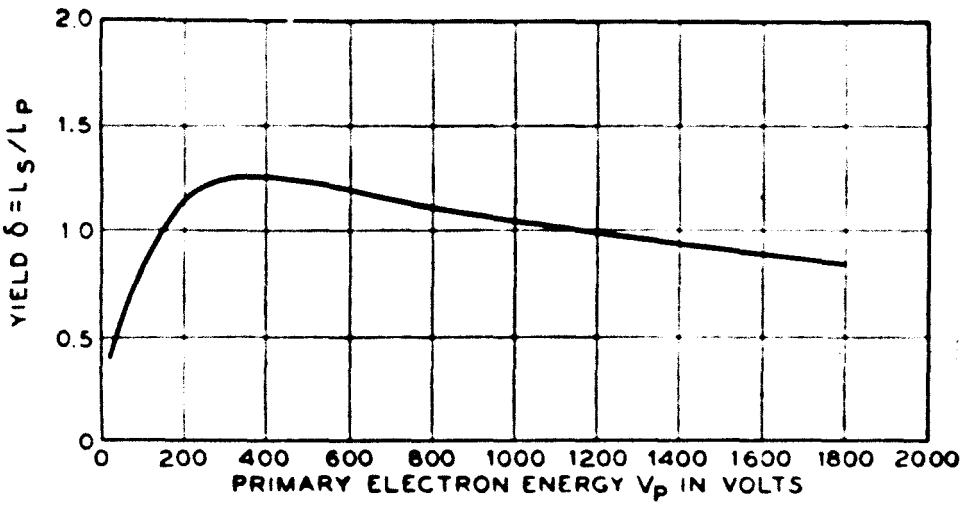

Yield curve for molybdenum.

FIG. 4

account. The discussion has been carried out only to give a useful classification of the secondaries into different groups depending on the amount of energy they possess. Many other indirect processes such as production of tertiary electrons by the true secondaries, the excitation of plasma oscillations and the consequent energy losses of the primary electrons and the release of secondaries by the action of the inelastically reflected primaries, have not yet been considered.

1.4 Yield

The "yield" δ is defined as "the number of secondary electrons emitted on the average by the action of one primary electron" (11). Or, alternatively, it is the ratio of the total secondary electron current (i_s) to the primary electron current (i_p)

i.e. $$\delta = \frac{i_s}{i_p} \qquad (3)$$

One of the most investigated phenomena of secondary emission is the variation of yield, δ, with the primary electron energy, E_p. The plot of δ against E_p, known as the "yield curve" has in general the same shape for all materials. A typical yield curve is reproduced in fig. 4, for a molybdenum target (12). For low E_p, δ is much less than unity, increases to a maximum value, δ_{max} (for metals not greater than $\delta = 2$) for E_p equal to a few hundred eV ($E_{p\ max}$). δ then decreases slowly as E_p is increased further.

The yield symbol is sometimes written as δ_{tot}, to indicate that the secondary current includes all the three groups of secondaries.

If however, the "true yield" is to be considered, it is usually written as δ true, and is defined as the ratio of the true secondary electrons to the primary electrons producing them.

A simple relationship between δ_{true} and δ may be easily worked out (2).

$$\delta_{true} = \frac{i_{s\ total} - i_p(\eta + r)}{i_p - r i_p} \qquad (4)$$

where i_s total is the total secondary current η and r are the fractions of inelastically reflected and elastically reflected primary electrons. Upon using the equation (3) one gets

$$\delta_{true} = \frac{\delta - (\eta + r)}{(1 - r)} \qquad (5)$$

The first important fact one observes in yield curves, is the similarity in shape, for almost all targets. Various authors (13, 14, 15) explain the characteristic curves in different ways, but all have to consider how internal secondaries are produced and how they escape.

When the primary electron has very small energy, its depth of penetration is small and the probability of the internal secondary emerging is governed only by the angular probability (assuming no collision loss of energy on the way to the surface for the small penetration depth) and should be constant. Thus the yield, per primary should increase as the primary energy since the energy determines the number of internal secondaries created. Therefore, in the range of very small

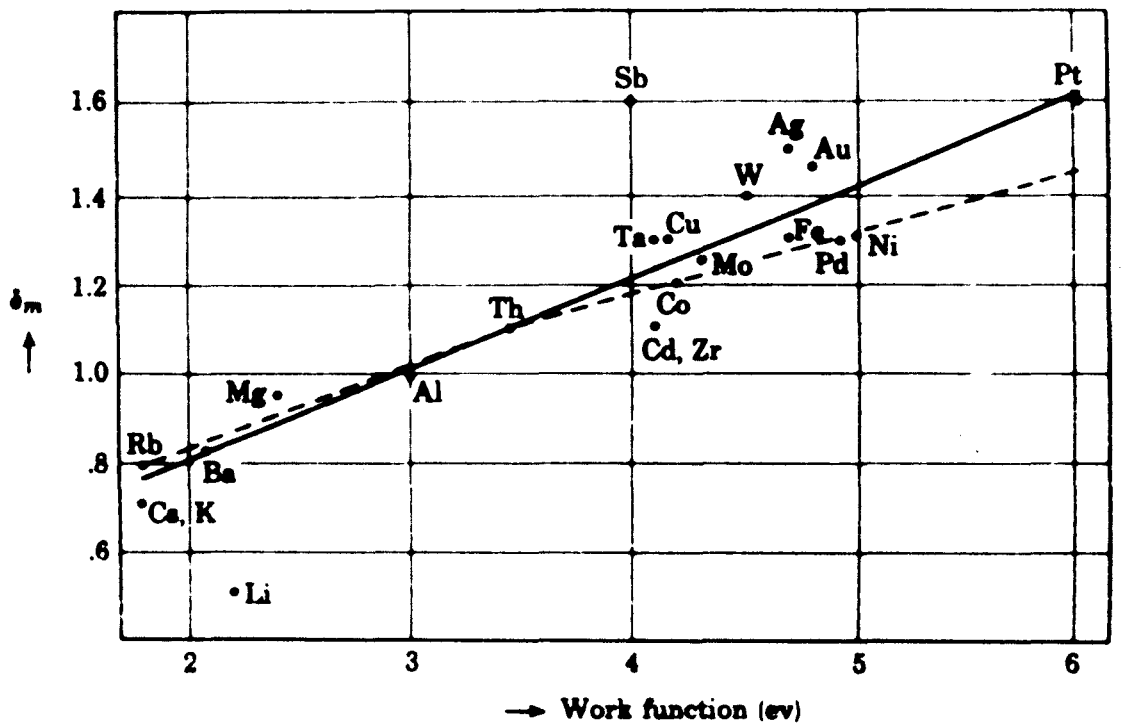

FIG. 5 Correlation between maximum yield and work function. The solid line shows the trend of experimental points. The dashed curve is a plot of $\delta_{max} = (0.35\,\Phi)^{\frac{1}{2}}$ according to Baroody (22).

primary energies, δ is approximately proportional to E_p. As the primary energy is increased, the number of internal secondaries still increases proportionately. However, many of these are now produced at a considerable depth, and some lose so much energy through repeated collisions on the way to the surface, or are backscattered, that the number of actual escaping secondaries does not increase proportionately.

As the penetration depth increases further, the collision loss phenomenon becomes more important until a δ_{max} is reached at some $E_{p\ max}$. At still greater E_p the yield decreases because a greater number of internal secondaries are created at considerable depth than near the surface. Near the surface, the high energy primary electron has too large a velocity to excite atomic electrons to the emission level, passing in and out of close proximity too quickly.

Though this explanation is extremely qualitative and aimed at explaining the shape of the yield curve, some of the experimental results in SEE can be explained on the above background.

1.5 Correlation of δ_{max} and Workfunction ϕ

McKay (3) tried to correlate the maximum yield and work function. He plotted δ_{max} for a few polycrystalline surfaces against the work function values, compiled from Becker (16) (fig. 5). This approach shows some interesting relationships. There appears to be a tendency for materials with high work functions to have high yields. Baroody finds from his theory a relationship $\delta_{max} \propto \phi^{\frac{1}{2}}$, shown as dotted line in fig. 5, (22). However, the inference should not be made, as McKay

points out, that by increasing the work function of a metal the SE yield will be increased. Often the inverse statement seems to be more reliable. It is believed that the work function itself plays a relatively minor role in determining the yield, but that it is linked with other properties of the metal which play a dominant role in determining the yield. In fact, McKay states that a relationship nearly as reliable may be obtained by plotting δ_{max} against the density of the target.

A number of authors have tried to investigate the effect of the work function on the yield, without varying any other parameter which might affect the yield. One method was to deposit a thin layer of a different element on the target, in which case the change in work function could be measured independently. De Boer and Bruining (17) argue that if the thickness is less than a monomolecular layer, the contribution to the yield due to secondaries in this adsorbed layer is negligible provided E_p is greater than 50 eV. This method has been used by Sixtus (18) using thorium on tungsten, Treloar (19) with barium on tungsten, Coomes (20) with thorium on tungsten and McKay (21) with sodium on tungsten. All the results, except that of Coomes, show an increase in yield when the work function is lowered. Sixtus and Treloar obtained relations of the form

$\log \delta = A - b\phi$, where ϕ is the work function and A & b are constant for a given metal and E_p. This equation holds only for adsorbed layers which are thinner than those for minimum work function.

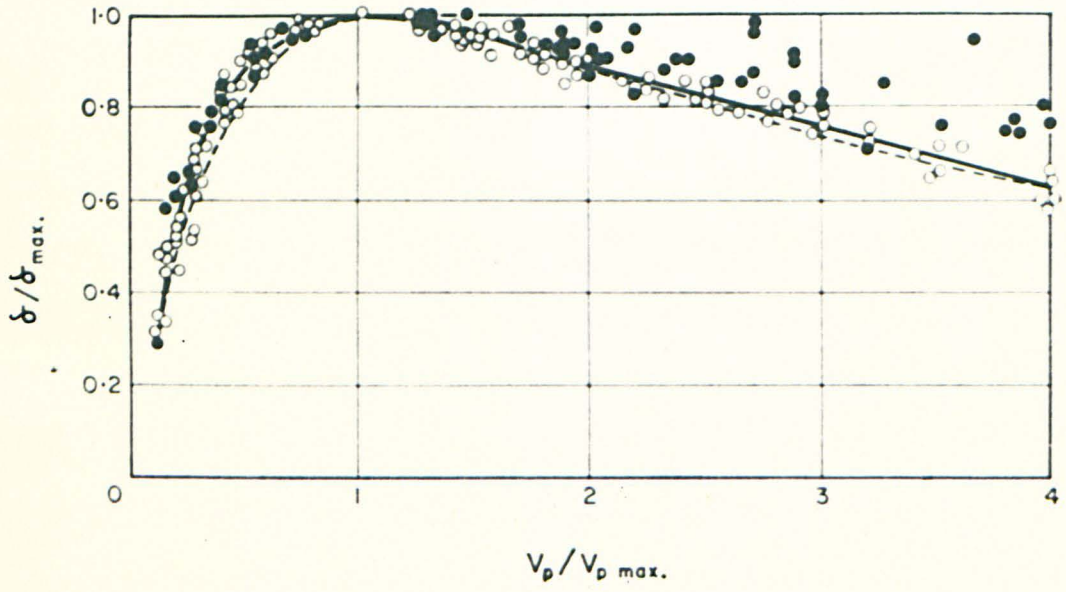

FIG. 6

1.6 Normalised Yield

As indicated previously, the general shape of yield curves for all metals is quite similar. Baroody (22) made this similarity particularly conspicuous by normalising the curves i.e. he plotted δ/δ_{max} against $E_p/E_{p\ max}$. Presented in this form, the curves for different metals lie in a narrow range so that the representation is nearly a "universal yield curve" for all metals (fig. 6). Kollath (23) added further results, the yields being "corrected" for rediffused primary electrons using an equation similar to (5). In fig. 6 the open circles refer to measurements corrected for rediffused primaries. The nature of the Universal yield curve will be discussed in greater detail in Chapter IV.

1.7 Temperature Dependence of Yield

Most investigators do agree that true secondary emission in metals is independent of the temperature of the emitter surface. Certain complications do occur however, since the changes in temperature of the target may alter the density of adsorbed gas if present and may possibly change the crystal structure or the roughness of the surface. Any of these may influence the yield. However, when these complications are not present, many experimenters (20, 21, 24, 25) have found no significant change at all in the yield of metals with temperature. Morozov (26) and Wooldridge (27, 28) have shown that for cobalt, iron, molybdenum and nickel the SE temperature coefficient must be less than the temperature coefficient of linear expansion.

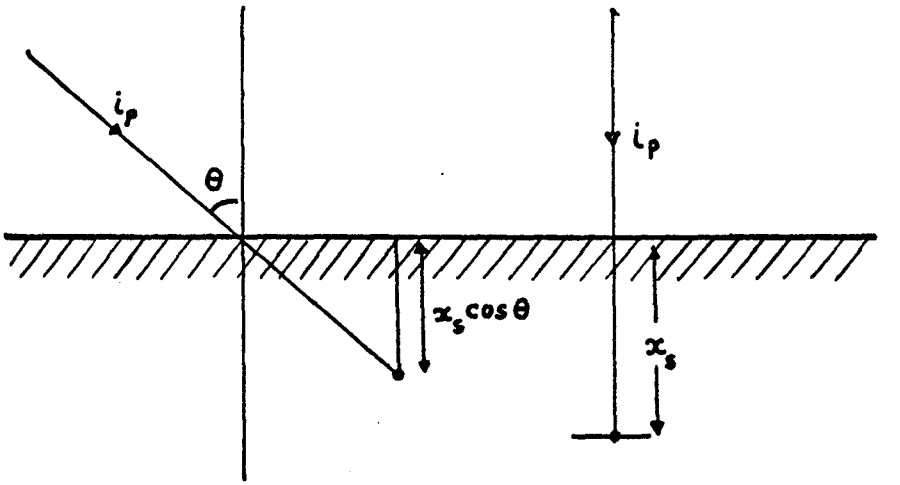

FIG. 7. Dependence of the mean depth of origin of secondaries with angle of incidence of primaries.

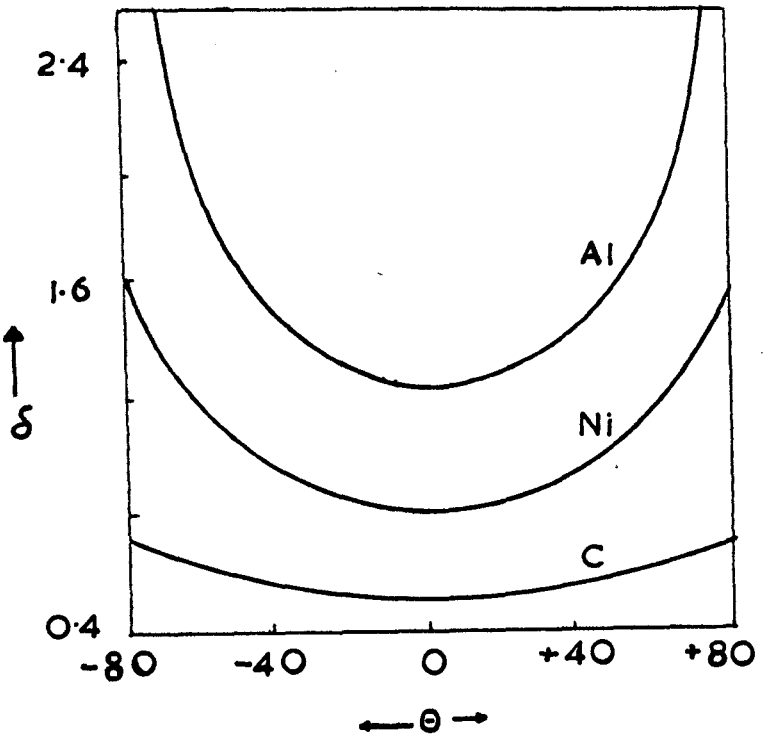

FIG.8. Variation of δ with θ for a primary energy of 2.5 KeV.

Blankenfield (29) found no variations greater than 1% for nickel in the temperature range from 20°C to 400°C. Only Sternglass (30) found a temperature dependence which might be due to adsorption of layers at the surface, especially since he did not have any provision for heat treatment.

It must be added here that many workers do find variation in semiconductors and insulators. For Ge, Johnson and McKay (31) found a continuous decrease by 5% in a temperature range of 20° to 600°C. Since the study of SE from semiconductors and insulators in itself is a special field and since in the present investigation only metals are studied the variation of yield with temperature in semiconductors and insulators will not be considered here.

1.8 Dependence of δ on the angle of incidence of the Primaries

Numerous investigators have determined the secondary emission yield with primary electrons under oblique angle of incidence and have observed a larger yield than under normal incidence (32, 33, 34). The general effect of oblique incidence may be seen from fig. 7 where for normal incidence of the primaries the mean depth of origin of secondaries is x_s. For oblique incidence, the secondaries produced at the end point of x_s, will be only at a distance $x_s \cos \theta$ from the surface, where θ is the angle of incidence, and thus have less chance of being absorbed. However, this dependence is more predominant when $E_p > E_{p\,max}$ where the yield is mainly limited by the absorption of secondaries. Little variation should be expected for low primary energies and this has been

verified experimentally (35).

Muller (36) investigated aluminium, nickel and carbon targets at E_p = 2.5 keV and the results are shown in fig. 8. With greatly oversimplified assumptions, he showed that $\delta \propto \frac{1}{\cos \theta}$.

Bruining (34, 35) assuming that the secondaries are absorbed exponentially with distance, derived a relation

$$\delta_\theta = \delta_o \exp\{\alpha x_s(1 - \cos\theta)\} \qquad (6)$$

where

δ_θ and δ_o are the yields at angles of incidence θ^o and 0^o.

x_s - mean depth of origin of the secondaries

α - coefficient of absorption of secondaries.

Bruining used the equation (6) to calculate the mean depth of origin of secondaries in nickel since

$$x_s = \frac{\ln(\frac{\delta_\theta}{\delta_o})}{\alpha(1 - \cos\theta)} \qquad (7)$$

Assuming the value of α for nickel to be 1.5×10^6 cm.$^{-1}$ (Becker, 37) Bruining computed the value of x_s to be about 30 Å for nickel.

Jonker (38) showed that for many metals $E_{p\ max}$, in addition, increased with angle of incidence according to $\frac{1}{\sqrt{\cos\theta}}$, but this relationship seems to be less valid in the evidence of recent experiments by Young (39).

This consistent increase in yield with angle of incidence is true only if the target surface is extremely smooth. For rough surfaces the variation is less singificant, obviously because the angle of incidence on such a surface is ill-defined.

1.9 Surface Effects

It has been established by many workers (16, 40) that the work function of a surface depends upon the orientation of the exposed crystal face. Nichols' (40) data for example shows that the work function of tungsten varies from 4.35 volts for the (111) crystal direction to at least 4.65 for the (110) direction. As discussed in section 1.5, the change in work function could alter the yield to a certain extent. Hence, it is to be expected that different crystal faces will have different yields. If we assume Treloar's formula $\log \delta = A - b\sqrt{}$ (section 1.5), a rough estimation of the change in the yield, with a change of the crystal direction from (111) to (110) of tungsten shows that there would be a change of some 3% in δ_{max}. Beckow (41) measured δ_{max} for a single copper crystal and found that it had a different value for each crystal face, being a maximum for the (100) face. However, Wooldridge's theory (42) implies that factors other than work function due to crystal orientation may influence the yield. By and large, all researchers do report that any given face of a crystal exhibits a characteristic yield. However, care should be taken when trying to correlate this information to experimental results, as a given polycrystalline substance need not necessarily exhibit all crystalline faces to the surface with equal probability. On the contrary, unless the experiment is precisely designed to locate a given lattice plane, the probability of the surface being inhomogeneous as to orientation of crystal faces is high.

Experimental evidence shows that a rough or porous surface has a lower secondary emission yield than a smooth one. This is

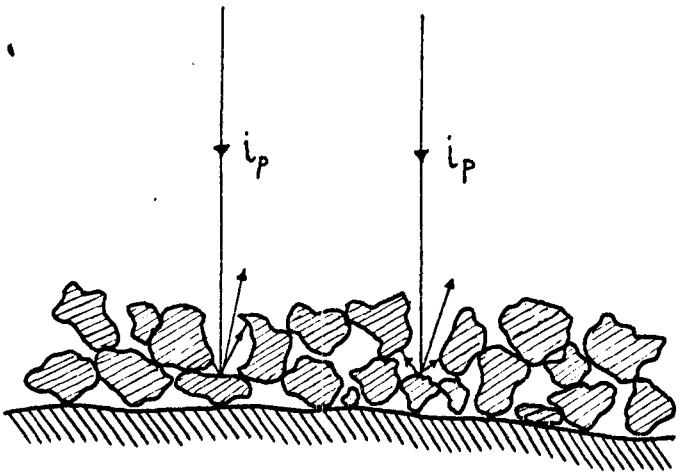

FIG. 9

Diagram showing the nature of a 'rough' surface and its influence on the escape of secondaries

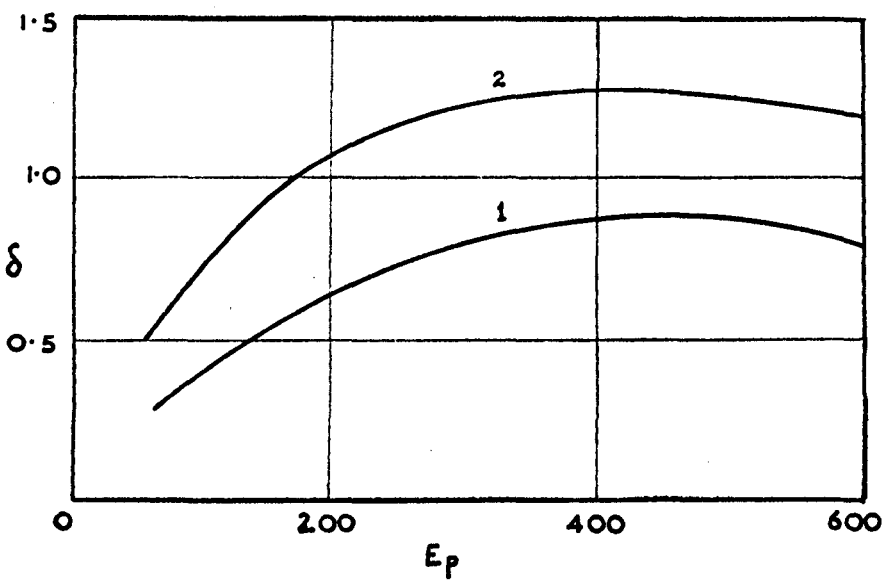

FIG. 10

Variation of δ with surface roughness

1. Soot; 2. Smooth Carbon

qualitatively explained (11) by postulating that a rough surface can be thought of as consisting of a number of "holes" or "wells" which form miniature Faraday cages out of which the secondaries cannot escape (fig. 9). Rashkovskii (43) actually obtained profilograms of a number of blackened and roughened surfaces and showed that the structure is in fact very similar to that shown in fig. 9. Many secondary emitting surfaces used commercially in applications where a low secondary emission is required, are made deliberately rough.

In section 1.5 it was said that the work function of a surface could be altered by an adsorbed metallic layer on the surface. The same will be true for adsorbed gases. If the layer is very thick, the yield may be expected to be altered appreciably. However, a mon-atomic layer probably has a yield of the order of 0.02 at E_p around 200 eV (17), indicating possibly that the variation for layers of this thickness is primarily due to variation of the work function. Recent low energy diffraction experiments have shown the change in crystal structure with adsorbed gases (44). Heat treatment is one common method used by many authors to remove the adsorbed impurity layers. This procedure in some cases is unreliable as the crystal structure itself may be altered by heat treatment. Also, when gas layers are being removed it is extremely difficult to distinguish the thickness and uniformity of remaining layers. Finally, the surfaces may become oxidised which will give unreliable data. Further heating of the surface will not necessarily elminate this problem either, as oxygen may not be removed by heat treating alone, but may require heat treatment in an atmosphere of hydrogen, for example, the subsequent water vapour then being removed by simple heating in vacuum.

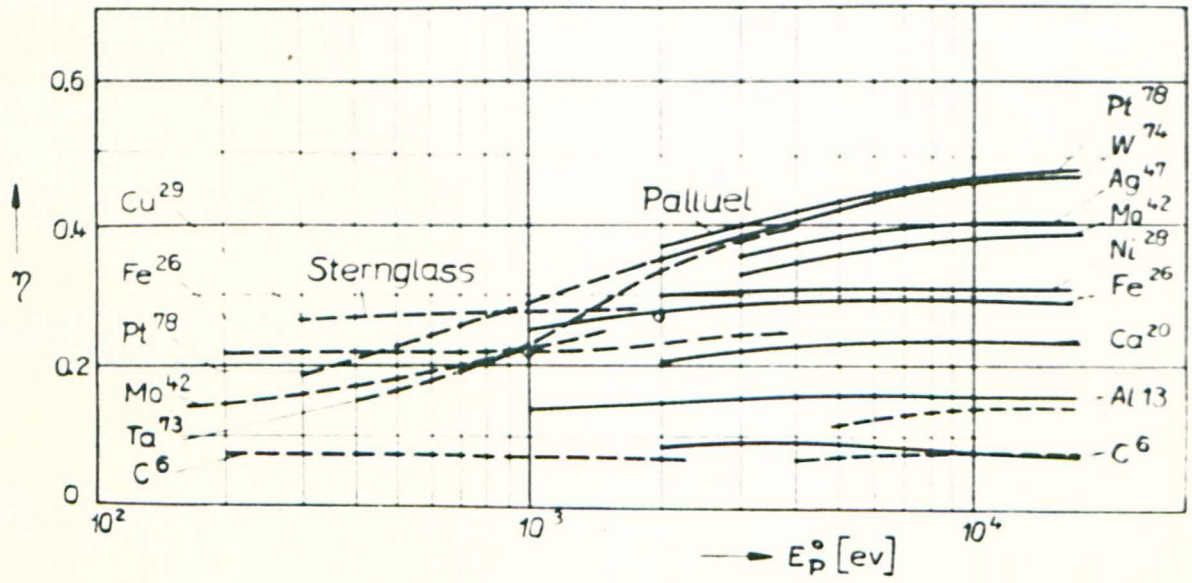

Rediffusion coefficient η of different metals.

FIG. 11

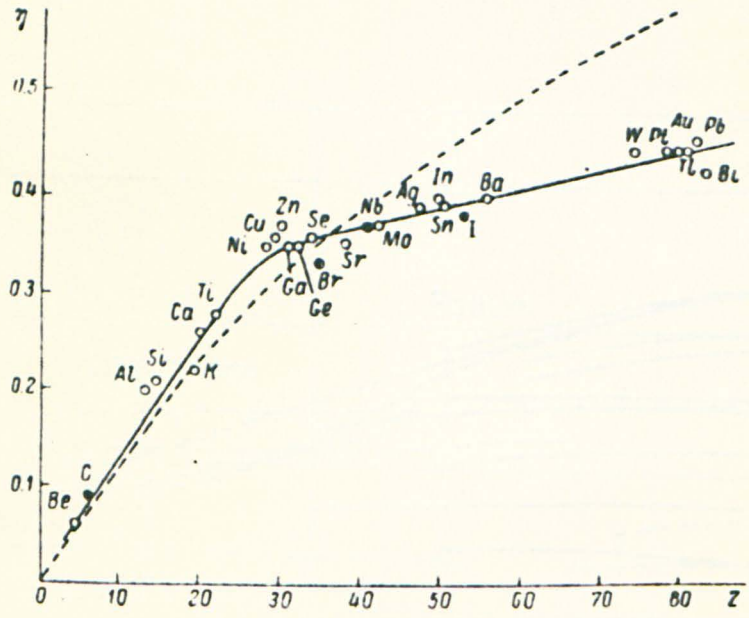

Dependence of the inelastic electron scattering coefficient of elements on the atomic number, $\eta(Z)$.

FIG. 12

1.10 Backscattered Primaries

In section 1.3, the secondaries have been categorised into "true secondaries" (below 50eV), inelastically reflected primaries and elastically reflected primaries. Since elastically reflected primaries in many cases are so few, they with inelastically reflected primaries can be grouped together as rediffused primaries and expressed as a fraction η of the primary electrons. Thus it is easy to separate the rediffused or backscattered fraction η of the primaries by means of a retarding potential of about 50eV. Measurements of the inelastic electron scattering coefficient η have been carried out by many authors (45, 46, 47, 48). Fig. 11 indicates η plotted against primary energy for a number of metals. η seems to approach an upper limit between 0.05 and .5 with increasing primary energy. Furthermore many authors are of opinion that for all metals the curves rise starting from low energies up to about 15 keV. However referring to the papers by Bronshtein and Segal (4, 5) one can see that a plot of η against E_p has in some cases the shape similar to the total yield, i.e. there is a maximum at a low primary energy after which it falls off or keeps a steady value as the energy increases. The metals involved according to these authors include beryllium, silver and bismuth.

Most authors do agree upon the fact that in the range of moderate primary electron energies E_p 2 - 5 keV, where $d\eta/dE_p \simeq 0$, the value depends only on the atomic number Z of the element. Fig. 12 shows a plot of η for the investigated elements. It can be seen that all the points lie close to some curve which increases monotonically with Z (the continuous curve in fig. 12).

The energy distribution of backscattered electrons has been studied by many workers, the classic example being the one by Rudberg (8). The energy distribution curve of these electrons runs nearly horizontal (fig. 3). Just below the primary energy, the continuum is superposed by single sharp peaks, indicating that a primary on penetration into the solid, undergoes single discrete losses of energy. These energy loss peaks are characteristic of the target and are often referred to as the "characteristic energy losses". In these cases, electrons have either raised crystal electrons from deeper levels into the conduction band or have eventually excited "plasma oscillations" comparable to that in a gaseous plasma. This phenomenon of plasma oscillations has recently been studied in great detail both theoretically and experimentally by many authors. It is of great value in enabling one to have a better understanding of the structure of solids. In the present work also, particular emphasis has been laid on the study of characteristic energy losses and plasma oscillations and hence a deeper account of the whole phenomenon will be given in Chapter III.

Even though the phenomenon of plasma oscillations has been studied in great detail, a complete understanding of the inelastic scattering of electrons is lacking. As far back as 1954, Sternglass (52) suggested that the inelastic interactions with the bound electrons in a solid dominate the electron scattering. Recently, however, the elastic mechanism of electron scattering by interaction with the nuclei has gained favour (53, 54, 55). According to Everhart (53), single Rutherford-type interactions with nuclei,

which produce an immediate deflection by an angle greater than 90°, play the dominant role. Neglecting electron deflections through angles less than 90° and assuming that the electrons are retarded in accordance with Whiddington's Law (Chapter IV) Everhart obtained the following formula for η of elements

$$\eta = \frac{a - 1 + 0.5^{a}}{1 + a} \tag{8}$$

where

$$a = \frac{\pi Z^{2} e^{4} N}{m^{2} C A} \tag{9}$$

Z - atomic number

e - electronic charge

N - Avogadro's number

m - mass of the electron

C - Whiddington's Constant

A - atomic weight of the element.

Formula (8), according to Everhart, is valid at not too low values of E_p. He estimated the lower limit to be 0.17 keV for Al and 1.9 keV for Au. From equations (8) and (9) it follows that $\eta = f(Z^2/A)$ or since $\frac{A}{Z} \simeq$ a constant we simply have $\eta = f(Z)$. The experimental results agree quantitatively with the calculated ones (if C is selected empirically) only for $Z < 40$ (dashed curve in fig. 12). Nakhodkin and Archard (54, 55) consider that in the case of the elements with $Z > 40$, multiple elastic deflections through small angles play the main role and Everhart's approximation is not valid.

The inelastic scattering of electrons from compounds has been investigated much less than that from elements. In the region of moderate energies there are only isolated data for some random representatives of various types of compounds. Müller (56), Saldick and Allen (57) investigated the inelastic scattering of β particles and concluded that the inelastic electron scattering coefficient of a compound is equal to the inelastic scattering coefficient of an element - which will be called the "equivalent element" - if the effective atomic number of the compound Z_{eff} is equal to the atomic number Z of the element. According to them, one can use the concept of Z_{eff} of a compound, if the scattering and the retardation of an electron during its motion in this compound are due to its interactions with individual atoms of the compound. These authors calculated Z_{eff} of a compound B_mC_n.

According to Müller

$$Z_{eff} = \frac{mA_BZ_B + nA_CZ_C}{mA_B + nA_C} \qquad (10)$$

But according to Saldick and Allen

$$Z_{eff} = \frac{mZ_B^2 + nZ_C^2}{mZ_B + nZ_C} \qquad (11)$$

where Z_B and Z_C are the atomic numbers of elements forming the compound; A_B and A_C are their atomic weights. The two formulae, however, give similar values of Z_{eff} for the same compound. The experimental data obtained in (56) and (57) for primary energies of the order of 1 MeV show that the equivalent elements can be found from equations (10) and (11).

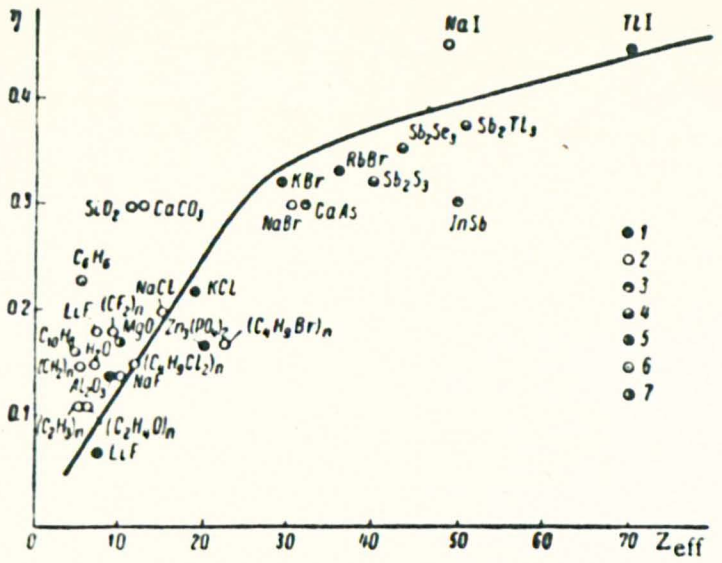

Fig.13. Dependence of the inelastic electron scattering coefficient of compounds on their effective atomic number, $\eta(Z_{eff})$. 1) [11], E_p = 20 keV; 2) [12, 18], E_p = 2-5 keV; 3) [19], E_p = 1.5 keV; 4) [15], E_p = 2-3 keV; 5) [17], E_p = 3-4 kev; 6) [13], E_p = 2.5 keV; 7) [16], E_p = 2 keV. The continuous curve shows the dependence $\eta = f(Z)$ for elements.

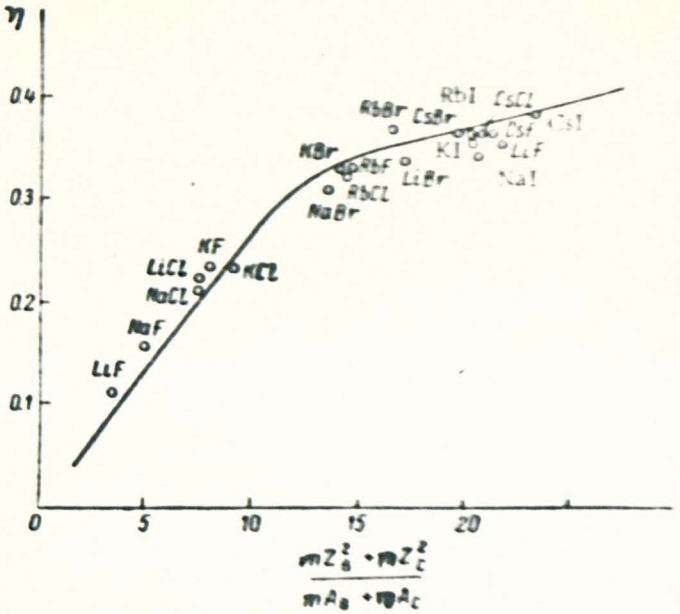

Fig.14. Dependence of the inelastic electron scattering coefficient of alkali-halide compounds on the quantity $(mZ_B^2 + nZ_C^2)/(mA_B + nA_C)$. The continuous curve gives the dependence $\eta(Z^2/A)$ for elements.

However, in the moderate energy region the results of investigations of the inelastic reflectionof electrons from compounds are contradictory. Fig. 13 shows the plot of η against Z_{eff} for a number of compounds in the primary energy region 2 - 20 keV. The continuous curve is the experimentally determined dependence of η on Z for elements. Even though the values of η of some compounds are close to η of equivalent elements, this in general is not true, especially for compounds with small values of Z_{eff}.

Extending Everhart's method, Gomoyunova and Letunov (58) derived a formula for the equivalent element of a compound.

According to them

$$\frac{mZ_B^2 + nZ_C^2}{mA_B + nA_C} = \frac{Z^2}{A} \qquad (12)$$

Considering this equation, the scattering coefficient η is found to be governed not by the effective atomic number Z_{eff} but by the effective value of the quantity Z^2/A. This applies to all alkali--halide compounds and to some other substances. In fig. 14 is given a plot of η against $(mZ_B^2 + nZ_C^2)/(mA_B + nA_C)$. The continuous curve gives the dependence of $\eta(Z^2/A)$ for elements.

It must be said that despite all the good agreement between the experimental and theoretical curves, one cannot help questioning some of the basic assumptions of Everhart and others. For example, all of them do neglect multiple scattering. It is quite possible for the electron to be backscattered after multiple scattering. Also, the validity of Whiddington's Law is questionable. However, for the basic understanding

FIG. 15

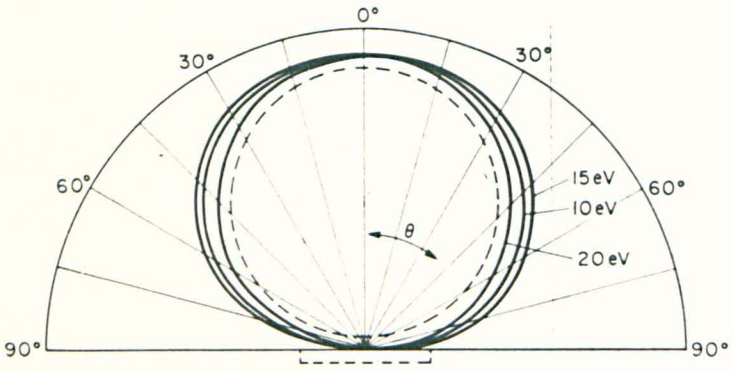

The angular distribution of true secondaries of various energies emitted from a nickel target.

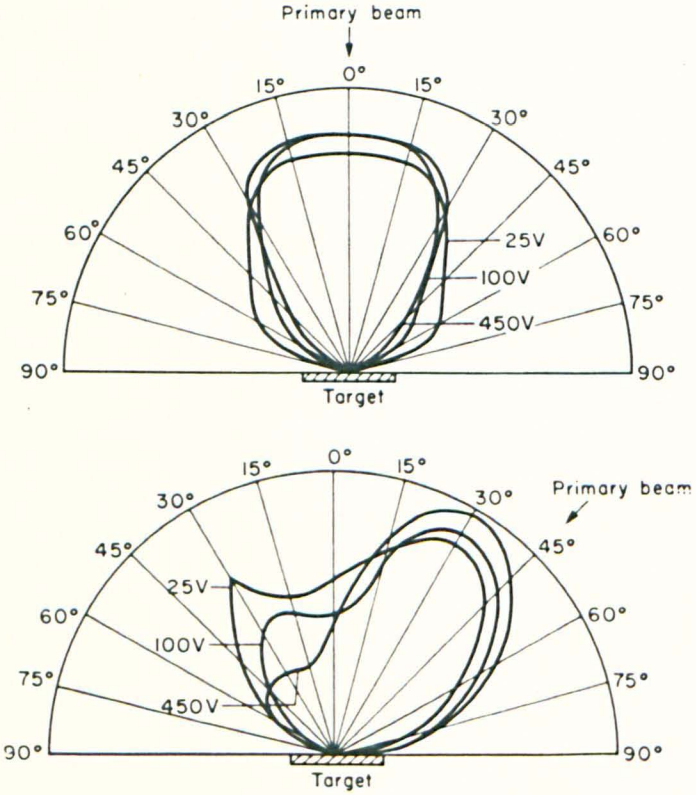

The angular distribution of rediffused primary electrons at various bombarding energies and two angles of incidence.

FIG. 16

of the very complicated phenomenon of secondary electron emission, such assumptions may have to be made until further progress is made.

1.11 Angular Distribution of Secondaries

The energy angular distribution of the secondaries is a function which is of great significance in the formulation of any theory of SEE. In spite of its significance not much work has been done on this. The classical work in this field was done by Jonker (59, 60) studying the angular distribution of secondaries from a nickel target. Alekseev and Borisov (61) studied the same using MgO layers as target. The lack of sufficient data might be due to the technical difficulties in the construction of an apparatus capable of distinguishing electrons according to their energy and angle.

Jonker using moderate primary energies and Ni as the target, separated secondaries of low energies into different groups with energy 1.5eV, 10eV, 20eV, etc. Fig. 15 is reproduced from his paper. It can be seen that the low energy secondaries have an approximate cosine distribution. A true cosine law is drawn dotted in the figure for comparison. This law is followed almost exactly for secondaries of 20eV energy but a slight flattening of the polar diagram appears for secondaries of lower energy. Jonker observes that the distribution curves do not depend on the crystal structure of the target and also he does not find any fine structure in the distribution. Owing to the cosine distribution of true secondaries outside the target, theoreticians infer that the distribution of the directions of internal secondaries inside the

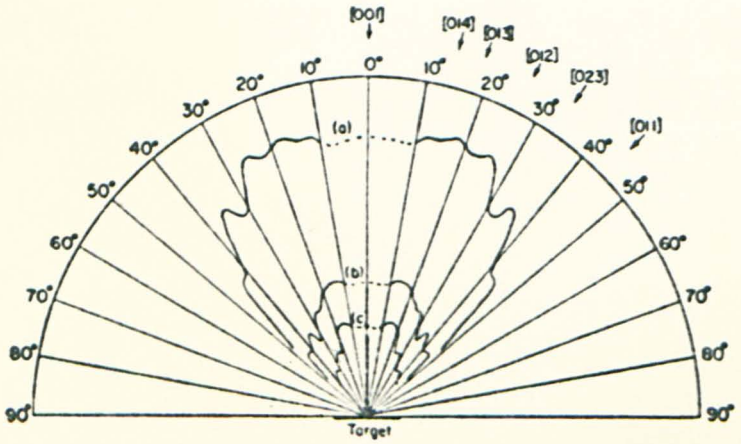

.. Copper crystal, (001) face, 250-volt primary beam at normal incidence. Curve (a) is for 0–10 ev secondaries; index of refraction 1.29. Curve (b) is for 10–20 ev secondaries; index of refraction 1.36. Curve (c) is for 20–40 ev secondaries; index of refraction 1.48.

FIG. 17

solid must be isotropic and this in fact forms one of the corner-stones of the theory of secondary electron emission.

For backscattered primaries also, Jonker found an approximate cosine distribution. With oblique angle of incidence of the primary beam, the curves are slightly dented in the direction of the incident beam. The elastically reflected primaries, on the other hand, have a distinct maximum in the direction of the incident beam. In addition, with oblique incidence of the primaries there will occur distinct peaks in the direction of the "optically" reflected primary beam (fig. 16).

Despite the very conclusive experimental evidence obtained by Jonker, one wonders if the perfect cosine distribution is not a bit over-simplified, especially owing to the few data available from other materials. Experimental workers often tend to assume the cosine distribution and presume that there are no particularly interesting or noteworthy features in the distribution curve.

More recently, however, Burns (62) studied the angular distribution of slow electrons from specified faces of single crystals of both copper and nickel, and has observed some striking departures from the cosine law.

Fig. 17 shows a typical polar distribution curve from the (001) face of a copper crystal for a primary beam of energy 250eV at normal incidence. There is a central peak which, according to Burns' explanation, consists of secondaries scattered inelastically along the (001) direction and superimposed on this central peak appear smaller maxima in (015), (014), (013), (012), (023) and (011) directions.

Burns concludes that the angular distribution of secondaries from single crystals of copper and nickel is not a simple cosine distribution as Jonker found, but instead it possesses a number of weak maxima superimposed upon a background which has approximately a cosine distribution. Needless to say that more investigation should be directed in this direction, for a clear and complete understanding of the angular distribution of secondary electrons both from single crystals and polycrystalline targets.

1.12 Fine Structure in Energy Distribution of Secondary Electrons

The general shape of the energy distribution of secondary electrons from a metal target is a smooth curve, with the true secondary maximum at two or three electron-volts and another peak corresponding to the reflected primaries (fig. 3). However, some workers have observed some fine structure in the energy spectrum of secondaries from a number of different metals. They were first discovered by Haworth for Mo and for Cb (63). Kollath (64) Harrower (65) and Zinke (66) also found similar subsidiary maxima above 50 eV up to 300eV - i.e. in the range of rediffused primaries. These subsidiary maxima or "humps" indicate that electrons are being preferentially emitted at certain fixed energies. These humps are independent of the primary energy and are characteristic of the target. Many authors are still rather sceptical about these humps, especially when considering the conditions under which they are obtained. The targets were subjected to excessive heat treatment, with a view to obtaining clean surfaces. For example, Harrower heated Mo at 2000°K and W at 2600°K, for 15 hours, "to drive out impurities

TABLE I. COMPARISON OF CALCULATED AUGER ENERGIES WITH OBSERVED SUBSIDIARY MAXIMA OF W ACCORDING TO HARROWER[a]

Auger transition	Calculated value	Observed value
	Both electrons originally in same band	
$5d - 6sp$	$51 - 2 \times 19 = 13$	13
$5p - 6sp$	$63 - 2 \times 19 = 25$	25
$4d - 6sp$	$245 - 2 \times 19 = 207$	212
$4p - 5d$	$450 - 2 \times 51 = 348$	340
$4p - 5s$	$450 - 2 \times 93 = 264$	264
	Electrons originally in different bands	
$(4s - 4p) - 5s$	$(590 - 450) - 93 = 47$	46
$(4p - 4d) - 5d$	$(450 - 245) - 51 = 154$	160
$(4p - 4d) - 4f$	$(450 - 245) - 31 = 174$	173
$(4d - 4f) - 5d$	$(245 - 31) - 51 = 163$	164
$(4d - 4f) - 6sp$	$(245 - 31) - 19 = 195$	199
$(5s - 4f) - 6sp$	$(93 - 31) - 19 = 43$	38

[a] G. A. Harrower, *Phys. Rev.* **102**, 340 (1956).

within the target meterial". Lander (67) explained these humps as due to Auger processes (68). Briefly, the Auger effect can be explained as follows. An electron is excited from a deep level D (fig 18) by a primary collision. The vacancy created in band D is filled with an electron of the next higher band C. The energy $(E_D - E_C)$ released by this process does not appear as an electromagnetic radiation quantum outside the solid but instead is used for exciting an electron from the band C or even from the upper band A. The electron then appears outside the solid with an energy $(E_D - E_C) - E_A$, if it comes from the band A. On the other hand if this electron comes from the band C itself, its energy will be $(E_D - 2E_C)$. Harrower could explain all the subsidiary maxima observed for W, as due to Auger transitions. It is interesting to compare the calculated Auger energies and the subsidiary maxima of W obtained by Harrower, Table 1.

Theoretically , the Auger process is definitely one means by which primary electrons can lose energy and also secondaries can be emitted preferentially. But looking at Harrower's observed energy distribution curves, one cannot help being suspicious and sceptical, especially since these so-called humps are so ill-defined. For a heavy metal, there can be a large number of Auger transitions, since Auger transitions are possible even though the corresponding optical transitions areforbidden by selection rules. The existence of subsidiary maxima in the case of insulators has not yet been proved with certainty. According to the interpretion by Auger process it would be quite natural to expect similar maxima for insulators as well.

1.13 Secondary Emission from Insulators

Even though in the present work, only secondary emission from metals was studied, a very brief account of the secondary emission from insulators and metal compounds would not be out of place. In many ways, the properties of insulators are very much more complicated than those for pure metals. Besides, it is much more difficult to make measurements on insulators. However, from the point of view of technical applications, this class of materials is probably more important than metals, since high secondary emission yields are obtainable and secondary emission multiplication is possible.

Most insulators have a $\delta - E_p$ curve similar in shape, although not necessarily in magnitude, to that for metals. The maximum yield from insulators lies in the range 0.96 (WS_2) to 18 (MgO) with somewhat higher values for single crystals (e.g. 24 for a single crystal of NaBr).

Unlike in metals, the yield from insulators may change considerably with temperature, owing to the difference in mechanism by which internal secondaries lose energy. In a metal there are many free and bound electrons with which the secondaries can make collisions involving the transfer of large or small amounts of energy. This process may continue until the secondaries are brought into thermal equilibrium with the lattice. However, in an insulator the minimum energy which can be lost by the process is equal to the energy gap between the bottom of the conduction band and top of the valence band. In MgO for example, this is at least 5.6eV and for most insulators it is of comparable magnitude. Once the electrons have fallen to an energy of about 5eV the only

mechanism by which they may lose energy is by collisions with lattice defects and electron-phonon interactions. In a single crystal, the number of collisions with lattice defects will be small and although the number of electron-phonon interactions may be large the amount of energy lost by each collision will be small. Provided the energy required for the emission of an electron at the vacuum interface is small compared to the electron affinity of the crystal, electrons with only a few eV energy will have a high probability of travelling large distances with sufficient energy to be emitted. This explains the high secondary yield and high $E_{p\ max}$ for many insulators especially alkali halides and alkaline earth oxides.

In insulators free from a large number of lattice defects, one would expect the influence of phonon interactions to predominate and hence δ and $E_{p\ max}$ to decrease with temperature. This, in fact, has been experimentally observed by many authors.

Geyer studied the energy distribution of "true" secondaries for various thicknesses of NaCl and MgF_2 on a nickel substrate and found a similar distribution as in metals. The most probable energy of the secondaries was found to nearly 1eV. Even though only a few insulators have been studied, it is generally accepted that the mean energy and the most probable energy of emission of secondaries from insulators, are considerably less than from metals. Very little is in fact known about reflected primaries, from insulators, the range of primaries, etc. Until these and many other properties of insulators are studied in greater detail - despite the technical difficulties - a full understanding of the mechanism of secondary emission from insulators will be impossible.

1.14 Malter Effect

In 1936 L. Malter (69) presented the results of an investigation of secondary emission from a target, composed of an aluminium plate with an oxidised surface layer, which was covered with Caesium Oxide. Such a layer can be represented by the symbol (Al) - Al_2O_3 - Cs_2O. When bombarded with a primary electron beam of a few hundred eV, he obtained emission currents from the target which were as much as one thousand times the primary current.

Time effects were apparent however; the emission current did not reach its full value until some time after the bombardment began. When the primary beam was switched off the secondary current dropped rapidly at first and then decayed from a small value over a period of several hours. This phenomenon, after the investigator, is called "Malter effect".

Malter showed that the yield varied as a power law of the collector voltage

$$\delta = M V_{coll}^{n}$$

where M and n are constants.

Malter and later Koller and Johnson (70) interpreted these results in terms of the charging up of the target surface. Since δ is greater than one, when the insulating target surface is bombarded with the primary beam, it becomes positively charged while the other face is at ground potential. Although the potential difference across the insulator is not large, the very small thickness of the insulator makes the field intensity very large. The intensity is great enough to cause field emission from the aluminium and aluminium oxide. Hence this effect is also termed "thin film field emission". In addition, the oxide becomes polarised and both the

polarisation and the surface charge persist after the removal of the primary beam until neutralised by leakage and by a portion of the field emission.

This phenomenon has attracted many investigators, partly because of its intrinsic interest and partly because it suggests a method of obtaining high yield surfaces of commercial value, if it could be stabilised. Quite a lot of work has been done in this field and most workers do confirm Malter's results and explanations. However, it must also be emphasisedthat a complete understanding of the whole mechanism of Malter effect is still lacking.

1.15 Conclusion

In this Chapter, the basic processes involved in secondary electron emission have been discussed, together with various mechanisms which can contribute to the generalised SEE. To understand the need for the present work, it is first necessary to consider the previous experimental work in this field, which will be given in Chapter II.

CHAPTER II

Review of Some Experiments on SEE

2.1 Introduction

Having discussed some of the basic processes involved in secondary electron emission in the previous chapter, it may be worthwhile to give a brief account of some of the experimental work done previously, on some of the properties of SEE. This will enable one to have an insight into the different techniques used and also the problems encountered. Such a thorough background is essential if one wishes to improve upon the techniques used and to obtain more reliable and reproducible results. Irreproducibility seems to be a feature all too common in SEE work.

2.2 Preparation of Clean Surfaces

It is imperative that in any study of the SE properties of a surface, for reproducible results genuinely characteristic of the surface studied, the surface must be "clean". To define such a surface, we may adopt the recent definition given by Allen et al. (71) which states that an atomically clean surface is "one free of all but a few per cent of a single monolayer of foreign atoms, either absorbed on or substitutionally replacing surface atoms of the parent lattice". If such a clean surface is exposed to a gas at atmospheric pressure, it is subjected to $\sim 3 \times 10^{23}$ molecular impacts per $cm.^2$ per second. Many of the gas molecules do not rebound elastically, but are adsorbed onto the clean surface. This process

of adsorption continues, until the surface is covered by many layers of molecules.

At a pressure of 10^{-7} torr, assuming a sticking coefficient of unity, a clean surface will adsorb a monolayer in a few seconds. Most sticking coefficients are found to be fairly high, of the order of 0.1 - 0.5 and vary with coverage and temperature (72). Bloomer and Haine (73) investigated the adsorption of oxygen on a clean tungsten surface and found the time required to produce a monolayer to be given by $t_m = \frac{2.4 \times 10^{-6}}{P}$ secns, where P is pressure in torr. Hence in an investigation of clean surfaces, it is essential to have a residual gas pressure that can be maintained below 10^{-9} torr.

Clean surfaces may be prepared on metallic and non-metallic substrates by several techniques, the principal methods being

1) Vacuum evaporation
2) High temperature heating
3) Chemical reaction
4) Ion bombardment cleaning
5) Crystal cleaving
6) Field desorption

Perhaps the simplest and the most versatile method for producing a clean surface is by the evaporation of the meterial on to a suitable substrate. The material to be evaporated is initially heated to a temperature just below the temperature at which it has an appreciable vapour pressure. The impurities which are more volatile than the material are therefore eliminated by evaporation. A further temperature rise

vaporises the purified material -- leaving behind the less volatile contaminants. The structure of evaporated films is found to be highly dependent on the condition of the substrate surface, the initial temperature of the substrate, any subsequent heat treatment, and the evaporation rate.

Atomically clean surfaces of a number of high melting point metals and non-metals can be generated easily by heating the material to a high temperature. This method is applicable only to those materials whose surface impurities possess a higher vapour pressure than the base material or decompose at temperatures below the melting point of the base material. The generation of clean surfaces by heating to a high temperature is not as straightforward as it may appear. Surface impurities may diffuse into the bulk rather than leave as gaseous species. Or in some cases, the impurities dissolved in the bulk material will tend to diffuse towards the surface. This has been demonstrated for molybdenum, tungsten, tantalum and rhenium where carbon diffused to the surface formed carbon monoxide and carbon dioxide, on letting some oxygen into the system (74). Heating can also in some cases alter the nature of the surface. Some crystallographic planes may grow at the expense of others and thermal etch-pits may appear. Clearly, there are many pit-falls which must be kept in mind when using this apparently straightforward technique.

Cleaning a surface by chemical reaction is in some ways a round-about method. In principle the surface is heated in a reactive atmosphere and the reaction products volatilise at these temperatures and leave the

surface. The reactant gas must be of the highest purity to prevent contamination and should not interact to any great extent with the underlying surface material or else there will be chemical etching. Chemical reaction techniques are usually used in conjunction with one of the other cleaning techniques.

In the ion bombardment technique, the crystal to be cleaned is kept in a pure inert atmosphere of argon at a pressure of about 10^{-3} torr. The bombarding positive ions are produced in an externally maintained discharge. Atomically clean surfaces of W, Ti, and Ni have successfully been produced by this technique. It must be said that this method is limited in its applications, since it is unlikely that gas molecules will be completely prevented from entering the structure of the surface in the case of the more reactive metals.

Clean surfaces can be produced by breaking or cleaving single crystals in high vacua. Cleaving is usually accomplished by forcing a wedge into a small oriented slot in the crystal. In most cases, the strain thus produced affects the nature of the surface. The availability of almost perfect large single crystals limits the general application of the technique but the greatest limitation is the small number of materials which are brittle and fracture along a given cleavage plane.

Under favourable conditions clean surfaces can be prepared by using high electrostatic field techniques. Field evaporated surfaces are usually produced in field ion microscopes by increasing the potential of the tip so that the field is about 10^9 volts/cm near the surface of the tip (75). This leads to the removal of loosely held protruding surface atoms and

produces perfectly regular surface structures. The field desorption technique can be applied to a wide variety of materials. But unfortunately, it can only prepare clean surfaces with an area of approximately 10^{-10} cm^2.

Having prepared a clean surface it is highly essential to keep it free from contamination. This can be achieved only by maintaining the surface under ultra-high vacuum conditions.

2.3 Preparation of Low Yield Surfaces

In many instances, the emission of secondaries from an electrode of a valve or other electronic device may have a disturbing influence on its performance. Examples of this are secondary emission from the control grid of a transmitting valve, the secondary emission from the cavity gaps of a klystron and charging up of the insulating supports and glass walls of the envelope.

Frequently, in such cases where secondary emission is undesirable, instead of modifying the surface of the emitting electrode, a more satisfactory method is to arrange an extra electrode to prevent the escape of secondaries, as in the case of a pentode.

In high power transmitting valves, the tetrode is still used on account of its lower anode capacity. It has been stated (76) that a coating of sintered zirconium powder is usually sufficient to reduce the secondary emission of the anode, although in very large valves, operated at high temperatures, powdered tungsten carbide has been used.

A simple laboratory method used by many authors, to reduce the secondary emission is to coat the surface with soot. Bruining et al. (77)

investigated the secondary emission from soot and found a low value for the yield. The actual value of the yield was found to be dependent on the "roughness" of the surface.

In high power transmitting valves if the secondary yield rises above unity, a negative grid transconductance occurs and undesirable oscillations may be excited in the grid circuit. Boumeester (78) describes a tube which uses a zirconium grid or a molybdenum-tungsten grid coated with a layer of zirconium oxide which is reduced to zirconium metal during tube processing. Another method is to paint the grids with a solution of CrO_3 in water and subsequently to reduce to Cr_2O_3 by heating the parts to red heat in a stream of hydrogen. Another very important compound - from the point of view of the present work - which has been used is tantalum carbide. This may be obtained by stoving tantalum in a CO atmosphere.

The influence of resonance secondary electron emission from the cavity gaps of klystrons, known as the "multipactor effect", can cause serious loss of power. Kreuchen and Diserens (79) describe how the effect may be elminated by coating the cavity gaps with a material such as tantalum carbide. After this suggestion, and with the cooperation of the laboratory of the above authors, a thorough investigation of secondary emission properties of TaC was undertaken and forms part of this dissertation.

2.4 Yield Measurements

The secondary electron emission yield has been defined as the

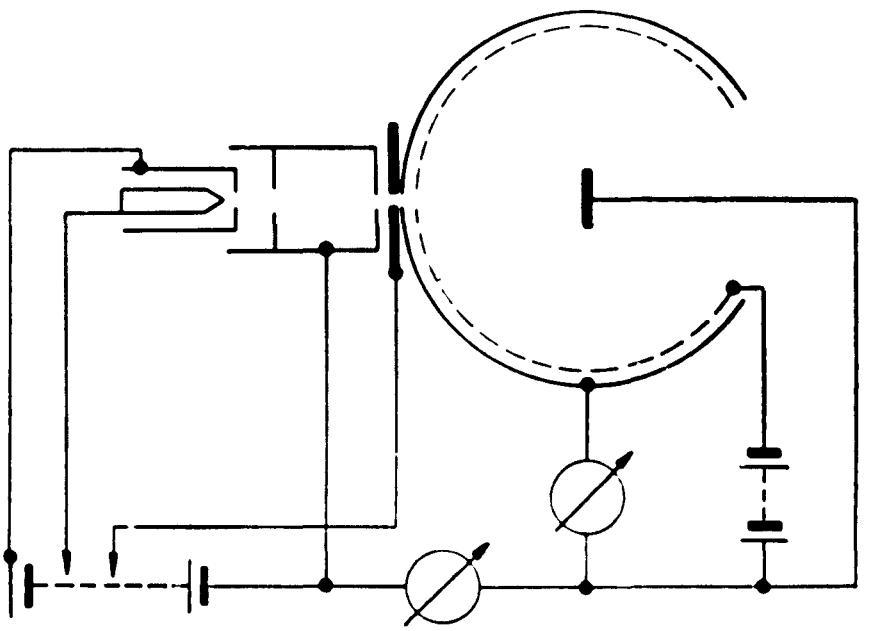

Device to determine the yield and rediffusion coefficient of metals and semiconductors.

FIG. 19

number of external secondaries produced by one primary electron. Or it is simply the ratio of the total secondary current leaving the target to the impinging primary electron current.

In general, the measurement of the yield is simple, particularly for metals. The general arrangement for the measurement of yield is given in fig. 19. The primary electrons come from a directly heated filament or an indirectly heated cathode. They are accelerated to the target by applying a potential difference between the target and the cathode. Usually the target is in the form of a small plate and is surrounded as completely as possible by a spherical collector. The secondary electrons emitted by the target are collected by the spherical collector and a sensitive galvanometer records them as the total secondary current. Normally the collector is held at a positive potential with respect to the target so that all the electrons are dragged to the collector. If a second galvanometer is connected to the target circuit it measures the difference between the primary and secondary current i.e. $(i_p - i_s)$. If on the other hand this measuring device is connected to the target and collector combined, it records directly the actual primary current i_p. When a simple spherical collector is used in this way to record the secondary current, an error is involved owing to the occurrence of tertiary electrons emitted from the collector wall. These electrons are generated by reflected and rediffused primaries, from the inner wall of the collector and can partly return to the target. Some authors coat the inner surface of the wall by soot or some other low yield substance to reduce the effect of tertiaries. However, it is not completely eliminated by coating with such a material.

TABLE 2

Secondary Emission Yield of Pure Metals

Atomic No.	Metal	δ_{max}	E_{pmax}	E_p^1	E_p^2
3	Li	0.52	100		
4	Be	0.5	200		
5	B	1.2	150	50	550
11	Na	0.82	300		
13	Al	0.97	300		
14	Si	1.1	250	120	520
19	K	0.53	175		
25	Mn	1.35	200	50	750
26	Fe	1.3	200	120	1400
28	Ni	1.35	450	140	1100
29	Cu	1.28	600	200	1500
47	Ag	1.56	800	140	> 2000
73	Ta	1.25	600	275	1500
74	W	1.35	650	250	1500
78	Pt	1.5	750	350	3000
79	Au	1.79	1000	150	> 4000
83	Bi	1.15	550	180	1600

A more satisfactory method is to suppress these tertiary electrons by arranging a spherical grid inside the collector and at a negative potential with respect to it, but at the same time having a positive potential with respect to the target. It has been shown (4) that a potential difference of 30 - 40 volts is sufficient to completely suppress the tertiary electrons from the collector. Furthermore, such an arrangement enables, by suitable choice of potentials at the electrodes, to separate the "true" secondaries from the elastically and inelastically reflected primaries.

A list of the yield values obtained from a number of pure metals is given in Table 2. δ_{max} is the maximum yield occurring at a primary energy $E_{p\ max}$. E_p^1 and E_p^2 represent the two primary energies at which the yield is equal to unity. It must be said that differences as big as $\pm$ 10% do exist between data given by different authors. This could very well be due to the difference in surface structure of the samples examined and to adsorbed surface layers.

Measurement of yield from insulators is not as simple as in the case of metals. When such a surface is bombarded by electrons, the surface either charges up or down, depending on whether δ is greater than or less than unity. It is required that either the surface potential be measured with SE measurement or be kept fixed. Depending on the choice, the methods could be classified as static or dynamic.

One of the simplest static methods is to use a low current density electron beam to bombard the surface. The surface potential changes slowly and the yield can be plotted as a function of time. By

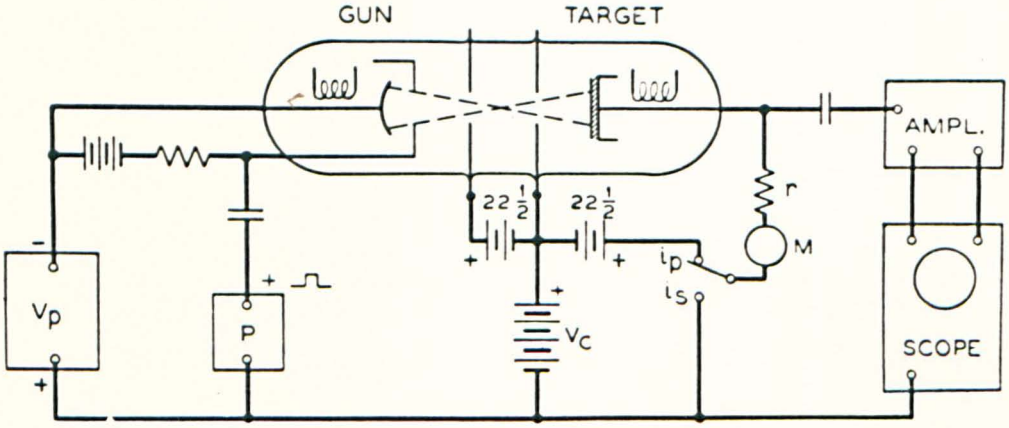

–Schematic for SE yield determination by direct pulsing method.

FIG. 20

extrapolation the actual yield can be deduced from this apparent yield. However, in this method extremely low current density has to be used to obtain the slow change in surface potential.

Most recent work on insulators is done using the dynamic method, where pulse techniques are employed. The direct pulsing technique was first used by Johnson (8) and the circuit is shown in fig. 20. The primary electron source is kept at a negative potential ($-V_p$), but the beam is normally cut off by the negative grid bias. The back of the target is connected through a small resistor to ground and the voltage developed across it is amplified and displayed on an oscilloscope. Due to the small but finite conductivity of the target, the target surface is normally at ground potential. The pulser then delivers a short ($\sim$ 1 μ sec.) flat topped pulse to the grid which turns on the primary beam for this interval. This is synchronised with a fast horizontal sweep on the oscilloscope. The current through the load resistor produces a pulse on the oscilloscope. By varying the recurrence frequency of the pulse a sufficient time can be allowed between pulses so that the target surface again reaches ground potential. This method or its varied forms can be used to measure δ of insulators quite accurately.

2.5 Measurements of the Inelastic Reflection Coefficient

It has been said in section 1.3. that the spectrum of secondary electrons consists of the so-called "true" secondaries with energies between 0 and 50eV and of inelastically and elastically reflected primaries above 50eV. The fraction of elastically and inelastically reflected primaries, η

is not small in either metals of insulators. η is related to the total yield δ by the simple relation $\delta = \delta_{true} + \eta$

In recent years the measurement of η has gained considerable recognition and space in the literature on SEE (45, 46, 47, 48, 52).

The same experimental set up (fig. 19) used in the measurement of yield, can be employed in measuring η as well. In so doing, the spherical grid inside the collector needs to be kept at -50V with respect to the target. Owing to this retarding field, all electrons with energy less than 50eV will be returned to the target and those with energy above 50eV be collected by the collector.

Such measurements of the inelastic reflection coefficient and the energy distribution of the inelastically reflected electrons offer a means of shedding new light on the relative importance of elastic and inelastic processes involved in secondary emission.

The basic theories of secondary emission (Chapter IV) usually do not take into account the role of inelastically reflected primary electrons in the production of slow secondaries and assume that all the slow secondary electrons are knocked out of the target by the primaries as they move into the interior of the target. If the range of primary electrons in the target is R and the depth from which a secondary electron can escape into vacuum is x_s, then for primary energy greater than $E_{p\ max}$, $R > x_s$. For such energies, there are two electronic currents in the "output zone" of secondaries (x_s), namely, the incoming primaries and the reverse outgoing inelastically reflected primaries. These inelastically reflected electrons returning from the interior of the material, emerge through the

output zone with reduced energy and with a cosine distribution in escape angle. The rate of energy loss and the path length (Chapter IV) of the backscattered electrons in the secondary escape region are comparable to that of the incoming primaries even when the inelastic reflection coefficient is relatively small. Since the energy dissipation close to the surface is proportional to the observed secondary yield - confirmed experimentally (81, 82) - the inelastically reflected electrons can contribute very substantially to secondary formation.

Considerable amount of work has recently been done, in an attempt to determine the extent to which inelastically reflected primary electrons are responsible, for the production of slow electrons within the solid, capable of subsequent escape, The contribution to secondary yield, by the inelastically reflected primaries was first noticed by Stehberger (83). More recently it has been studied by Dobretsov and Matskevich (84) Bronshtein and Segal (4, 5), Kanter (85) and others.

According to the above authors δ_{true} itself is produced by the primary electrons and the inelastically reflected primaries. That fraction due to the primaries is represented by δ_p. Dobretsov and Matskevich determined the fraction δ_p using the formula

$$\delta_p = \frac{\delta_{tot} - \eta}{(1 + \beta \eta)} \qquad (13)$$

where δ_{tot} is the observed total yield including slow secondaries and inelastically reflected primaries, η , is the inelastic reflection coefficient, β is a factor accounting for the increased efficiency of the

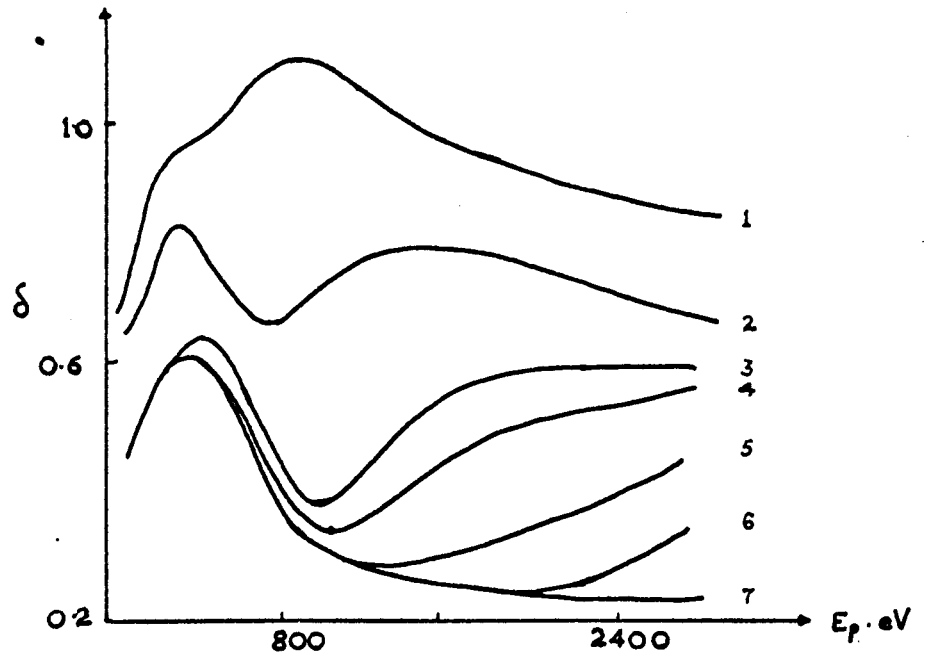

FIG. 21

$\delta(E_p)$ curves for evaporated Be on Pt. (1) d = 15 atomic layers, (2) 33; (3) 63; (4) 100; (5) 190; (6) 370; (7) Solid Be layer.

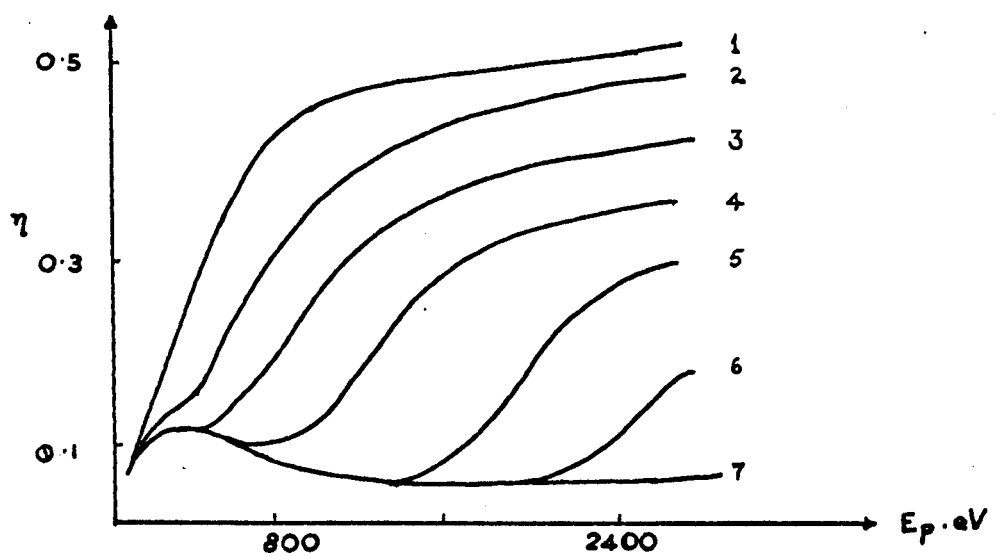

FIG. 22

$\eta\ (E_p)$ curves for Be on Pt

backscattered electrons in forming secondaries. They suggested that β would lie between 1 and π.

Recently Bronshtein and Segal made measurements of η and δ from thin layers of various thicknesses deposited on substrates, to obtain values for β.

The work of Bronshtein and Segal is of interest as it attempts an experimental determination of (1) the role of inelastically scattered electrons in secondary emission; (2) the range of primary electrons; and (3) the range of secondary electrons. The method is based on a study of the yield of thin films of one substance A, evaporated on to a suitably matched substrate B. The combination of the substrate B and the thin film A can be divided into three cases.

(1) The case of the "zero" substrate when the coefficient of inelastic reflection $\eta_B << \eta_A$; $\delta_B < \delta_A$;

(2) a "mirror" substrate when $\eta_B >> \eta_A$; $\delta_B >> \delta_A$;

(3) an "equivalent" substrate when $\eta_B \approx \eta_A$ but $\delta_B \neq \delta_A$.

For Be, a "mirror" substrate, namely Pt, was chosen and for every layer of Be deposited on Pt, $\delta - E_p$ and $\eta - E_p$ graphs were drawn. Fig. 21 and fig. 22 show typical sets of curves for Be of various thicknesses on Pt. From these characteristic curves one can see that there are definite "breaks" from the limiting curve which is characteristic of solid Be. For a given thickness of the Be film, as primary energy is increased there is a transition from the characteristics of Be to Pt. This transition or "break" occurs at a higher E_p for thicker films.

These experimental curves were used by Bronshtein and Segal to determine the range of the primary electrons, the effectiveness of inelastically reflected primaries on secondary emission and the range of secondary electrons.

2.5.a Range of Primary Electrons

As seen from fig. 22 the inelastic reflection coefficient for platinum is practically constant, $\eta \approx 0.45$, at high primary energies - above 800eV. The platinum substrate therefore acts like a "mirror" from which about half of the electrons are reflected with a small loss of energy. Before a primary electron can come out as an inelastically reflected electron, it must pass through the Be layer of thickness 'd', get reflected by the substrate and then pass through the layer in the reverse direction. If the thickness of the layer 'd' is so large that for a primary energy, E_p there are no electrons which are able to pass through to the substrate and back again and then to come out with an energy $\geq$ 50eV, then the total effective ionisation range R of the primaries - neglecting the range of 50eV electrons - can be evaluated.

There are two separate cases to be reckoned with.

Case 1 There are certain materials like platinum, where there are a large number of inelastically reflected primaries, close to the primary E_p (52). In such cases R = 2d as given by Dobretsov and Matskevich (84) and Holliday and Sternglass (46).

Case 2 In the case of certain light metals (e.g. carbon) the number of electrons with energy close to the primary energy is comparatively small.

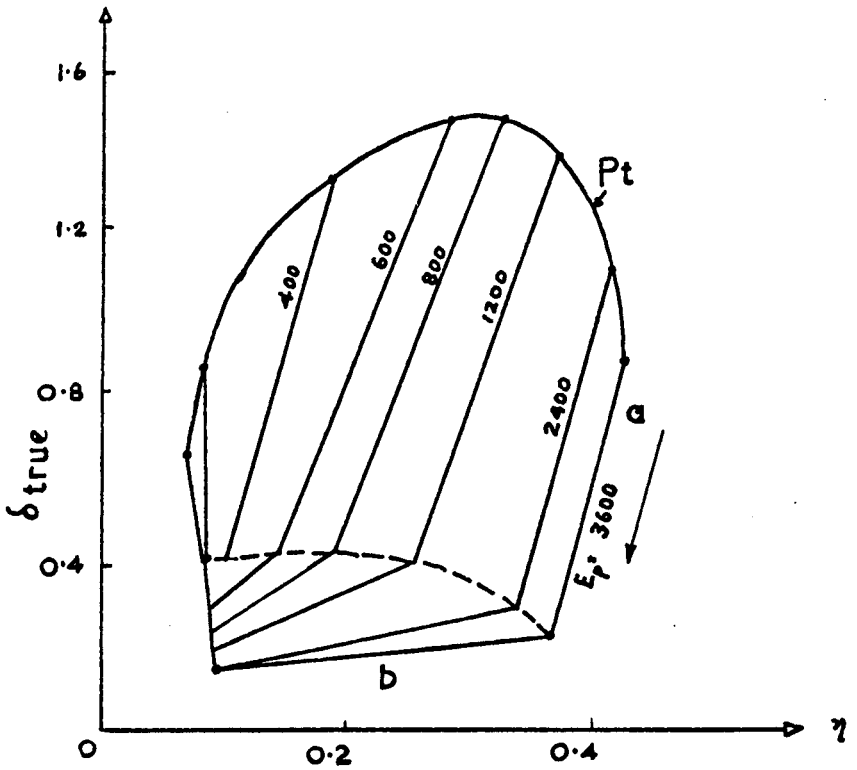

FIG. 23

δ_{true} vs η curves for Be layers on Pt.
The arrows show the direction of increase of thickness of the Be layers. The dotted line connects the break points which correspond to d = x_s = 12 atomic layers.

Consequently after a second passage through the layer they cannot be detected experimentally. The experimentally observed values of 'd_1' in this case, turns out to be low ($d_1 < d < R/2$). In this case Bronshtein and Segal evaluated R by using the approximate relation

$$R = \left(\frac{1 + k^n}{k^n}\right) d_1 \qquad (14)$$

Here k is given by $E_m = kE_p$, E_m being the energy corresponding to the maximum of the distribution function of electrons inelastically reflected by the substrate, when a beam of energy E_p is incident on it. n is given by the assumed relation

$$R = A^n E_p^n \qquad (15)$$

(A is a constant)

The relation between R and E_p for Be was found to be $R \propto E_p^n$ where $n = 1.5$ for $E_p > 800$eV. For bismuth and silver the corresponding relations were found to be $R \propto E_p^{1.4}$ and $R \propto E_p^{1.2}$ respectively.

2.5.b Role of Inelastically Reflected Electrons in SEE

As is already established, the secondary electron emission coefficient of true secondaries (energy < 50eV) is

$$\delta_{true} = \delta - \eta$$

From fig. 21 and fig. 22 one can construct a graph of δ_{true} against η for Be for E_p constant (fig. 23), since both δ_{true} and are parametrically dependent on thickness. For $E_p > 600$eV the curves have two straight portions with different slopes. The slopes of the upper portion (a)

for all E_p values, are approximately equal and for the lower parts (b) the slopes decrease with increasing E_p.

The shape of the curves may be explained as follows:- Platinum has both a high δ and η, i.e. it emits a large number of slow secondaries δ_{true}. When these two groups of electrons enter the Be layer, even though for thin films of Be, the fast (η) electrons are not absorbed, the slow electrons are completely absorbed. So even for a large change of δ_{true}, η has not changed substantially and hence the large slope in the region (a). The absorption process for slow electrons emitted by the platinum does not depend on E_p and it occurs for such thin films of Be, that η does not change significantly for all E_p. Therefore, the slopes in the region (a) are approximately the same for all E_p. In the region (b) there occurs a decrease in the number of electrons inelastically reflected by the platinum substrate, which can come out through the Be layers of increasing thickness and consequently in the number of slow secondaries produced by them in Be. The slope of the region (b) characterises the "effectiveness" of inelastically reflected electrons η, in producing slow secondaries.

Now δ_{true} itself may be written as $\delta_{true} = \delta_p + \delta_1$ where δ_p is the fraction produced by the direct primaries and δ_1 by the inelastically reflected electrons. δ_1 may be written as $\delta_1 = S\,\eta$, where S is the effectiveness of inelastically reflected primaries in the production of slow secondaries, i.e. the number of slow secondaries produced by one inelastically reflected electron in the region x_s

$$\therefore \quad \delta_{true} = \delta_p + S\eta$$

and also

$$\left.\frac{d\delta_{true}}{d\eta}\right|_{d > x_s} = S \qquad (16)$$

i.e. the "effectiveness", S, can be defined as the slope of the line E_p = constant in the region (b).

From the above graphs S, δ_1, δ_p, δ_1/δ_p and S/δ_p may be computed for E_p = constant.

Bronshtein and Segal calculated the value of δ_1/δ_p to be about 0.5 i.e. the role played by the "reverse" (inelastically reflected) current in the formation of slow secondaries is approximately half as much as that played by the "direct" current. The ratio S/δ_p is the factor β in equation (13) due to Dobretsov and Matskovich. The value turns out to be of the order of 4 to 5 which is higher than the theoretical maximum which is π . It is instructive to note that Kanter (85) working independently got a value of 4.9 for β.

The above method of calculating the value of S has been criticised by Gomoyunova (86). The equation used by Bronshtein and Segal is

$$\delta_{true} = \delta_p + S\eta$$

for $d > x_s$, we have $\frac{d\delta_p}{d\eta} = 0$

So $\frac{d\delta_{true}}{d\eta} = S + \frac{dS}{d\eta}\eta$

It is evident from this that $\frac{d\delta_{true}}{d\eta} = S$ only when $\frac{dS}{d\eta} = 0$.

Gomoyunova argues that since the excitation probability is dependent on the energy, $\frac{dS}{d\eta}$ cannot be zero.

So $$S + \frac{dS}{d\eta}\,\eta = C \qquad (17)$$

- C is a constant. Solving the differential equation

$$S = C + \frac{A}{\eta} \qquad (18)$$

where A is a constant. However small the factor $\frac{A}{\eta}$ may be, the fact is that it does exist.

2.5.c Range of Slow Secondaries

It has already been noted in fig. 23, the $\delta_{true} - \eta$ graphs break for all E_p, at one and the same thickness - d = 12 atomic layers for Be. That thickness, at which the slow secondary electrons emitted by the platinum substrate are absorbed, can be considered to be the range in Be of slow secondaries (or their production zone). That for Bi was found to be $\simeq$ 7 atomic layers, and for silver the value ranged from 12 - 20 atomic layers.

2.6 Energy Distribution of Secondary Electrons

To understand the processes responsible for secondary electron production, a knowledge of the distribution in energy of the secondaries is essential. A great deal of work in the past has therefore been directed towards obtaining energy distribution curves for a wide variety of materials and a large range of primary electron energies.

Measuring the energy distribution of true secondaries is basically

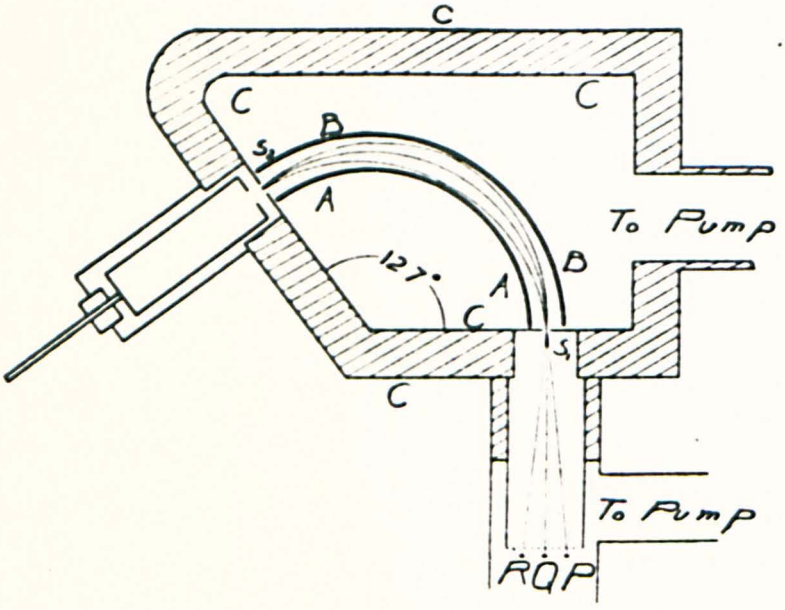

FIG. 24 127° electrostatic analyser of Hughes and McMillen (87)

a problem in electron optics. This is studied mainly by one of the following methods

1) Transverse Electric (TE)

2) Transverse Magnetic (TM)

3) Longitudinal Magnetic (LM)

4) Retarding Field (RF)

An electron spectrometer using the transverse electric field was first described by Hughes and Rojansky (86, 87). It utilises the refocussing property of a two dimensional, inverse first power, electrostatic field. Let an electron be moving from a certain point in this field, perpendicularly to the radius passing through that point, with just the right velocity, so that under the influence of the electric field, it describes a circular path concentric with the axis of the field. If so, all other electrons having the same velocity and starting from the same point, but moving initially in slightly different directions from that of the first electron, will describe orbits which re-focus at the point which is $\frac{\pi}{\sqrt{2}} = 127^{\circ} - 17'$ from the starting point. Hence this analyser is often called the "127° electrostatic analyser".

The first 127° analyser used by Hughes and McMillen is diagrammatically shown in fig. 24. The analyser consists of two concentric arcs subtending an angle of 127° at the centre. When they are kept at a potential difference V_a, the radial field between them permits electrons of a corresponding energy V_o to be refocussed at the exit slit according to the relation

$$V_a = 2V_o \ln\left(\frac{b}{a}\right) \qquad (19)$$

where b and a are the respective radii of the outer and inner arcs. Consequently a measured spectrum of electron energies is linear against voltage applied to the analyser. However implicit in the analyser design is the fact that the sensitivity is proportional to the energy of the electrons being measured. Hence the analyser discriminates against slow electrons, the effect being most severe at energies approaching zero. Besides, the resolution is dependent on the geometrical parameters of the analyser. The analyser displays an electron spike at V volts as a peak with a half width $V_{\frac{1}{2}}$ given by (88).

$$2\left(\frac{V_{\frac{1}{2}}}{V}\right) = \frac{\left(S + \frac{4}{3} r_o \alpha^2\right)}{r_o} \qquad (20)$$

where "S" is the slit width, " r_o" mean radius of the cylindrical arcs and α the acceptance angle in radians.

It was J. J. Thomson, who used the transverse magnetic (TM) method to determine the specific charge of electrons. Under the influence of a uniform magnetic field, an electron of velocity v is bent around into a circle of radius r given by $v = \frac{e}{m} \cdot r \cdot H$ (21)
An electron spectrometer using the transverse magnetic field was first designed by Ramsauer (89) for slow electrons and since then, has been repeatedly used for determining the energy distribution of the secondaries. Rudberg (90) used this method in studying the energy losses of electrons. The electrons coming off the target in some given direction are fed into the magnetic analyser consisting of a semi-circular apertured tube in a uniform transverse magnetic field. The current to a Faraday cage collector at the output end of the analyser is obtained as a function of the magnetic

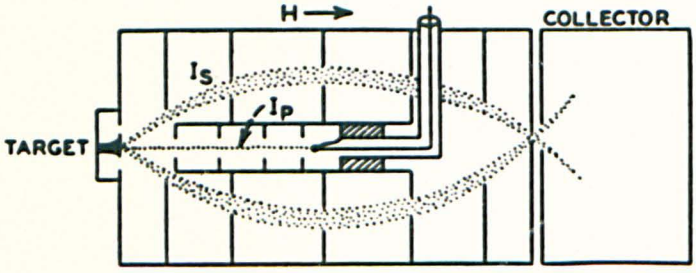

—Measurement of secondary electron velocity distribution with a longitudinal magnetic field.[163]

FIG. 25

field and this gives the energy distribution directly. In order to avoid any deflection of the primary beam in the magnetic field the beam must be arranged parallel to the magnetic field. Consequently the primary beam must be orthogonal to the secondary beam. The resolution is again dependent on the energy of the electrons. Rudberg obtained a resolution of ~ 0.6%.

In the longitudinal magnetic (LM) method the magnetic field is applied parallel to the primary beam. The method was originally used by Klemperer for β-rays and adapted by Kollath (91) for secondary electrons. The scheme of the spectrometer is shown in fig. 25. Apertures are set up so that secondaries emitted within a certain cone enter the linear analyser. The axial focussing properties of the magnetic field are used to select secondaries of a given velocity. The entrance slit of the Faraday cage collector is situated at the focal plane. When the strength of the magnetic field is varied, electrons of different energy are focussed into the cage and the current to the cage gives directly the energy distribution. Since electrons in a cone are selected, there are more electrons available for measurement and hence a small primary current can be made use of.

The retarding field method was probably first used by Lenard to study the energy distribution of photoelectrons. The principle has been borrowed to study the energy distribution of secondary electrons. In the simplest case, the electrons emitted radially from the target move against a spherically symmetrical field. Only those electrons, with sufficient energy to overcome the potential barrier between the target and the collector, are collected by the collector. Hence the collector current is a measure of all the electrons above this energy. A graph drawn between the retarding

voltage and the collector current is the integral of the energy distribution. Hence the first derivative gives the actual energy distribution. Many workers have employed the retarding field method owing to the sheer simplicity of the method though the theoretical resolution might not be as good as the other methods. In the present investigation also the retarding field method has been used and hence it is dealt with in greater detail in section 5.3.a.

A number of investigators have studied the energy distribution of secondary electrons, using one or the other of the above mentioned methods. Basically the shape of the energy distribution curve for various materials, is similar (fig. 3). The most common features of the distribution are the "slow secondary peak" (section 1.3) occurring at a few electron volts and the elastically reflected primary peak occurring at the primary energy. In between, the distribution is "rather smooth". However, a number of workers (63, 64, 65, 66) have observed fine structure in this region which was explained on the basis of Auger electron emission (section 1.12). The most interesting information about the solid state structure and the energy levels, however, comes from the study of inelastically reflected primary electrons. A study of the energy distribution of these electrons enables one to understand the scattering mechanisms and the energy losses.

It was Erik Rudberg, in 1929, working in Stockholm, who for the first time reported, in his doctorate thesis, on the investigation of energy losses of electrons when reflected from the surface of a solid. This was followed by a series of papers (90, 8) giving the quantitative results on energy loss study. His was probably the first quantitative determination

of energy losses of electrons, though Brown and Whiddington (92) noted qualitatively a "gap" in the energy spectrum of secondaries near the primary peak.

Rudberg clearly demonstrated that when electrons impinge on solid surfaces there are characteristic values of energy losses forming a kind of line spectrum of the energy spectrum. He christened these energy losses as "characteristic energy losses" (CEL). Following Rudberg, a number of workers have studied characteristic energy losses of electrons from a number of materials and the results obtained are voluminous. Since the present investigation also is directed towards a study of the CEL of electrons, a detailed account of the previous investigations will not be out of place and is given in the next Chapter.

2.7 Conclusion

An account of the methods employed in measuring the yield and energy distribution of secondary electrons is given in this chapter. Besides mentioning some of the important results obtained in the previous investigations, a brief account has been given on the precautions to be taken for obtaining reproducible results.

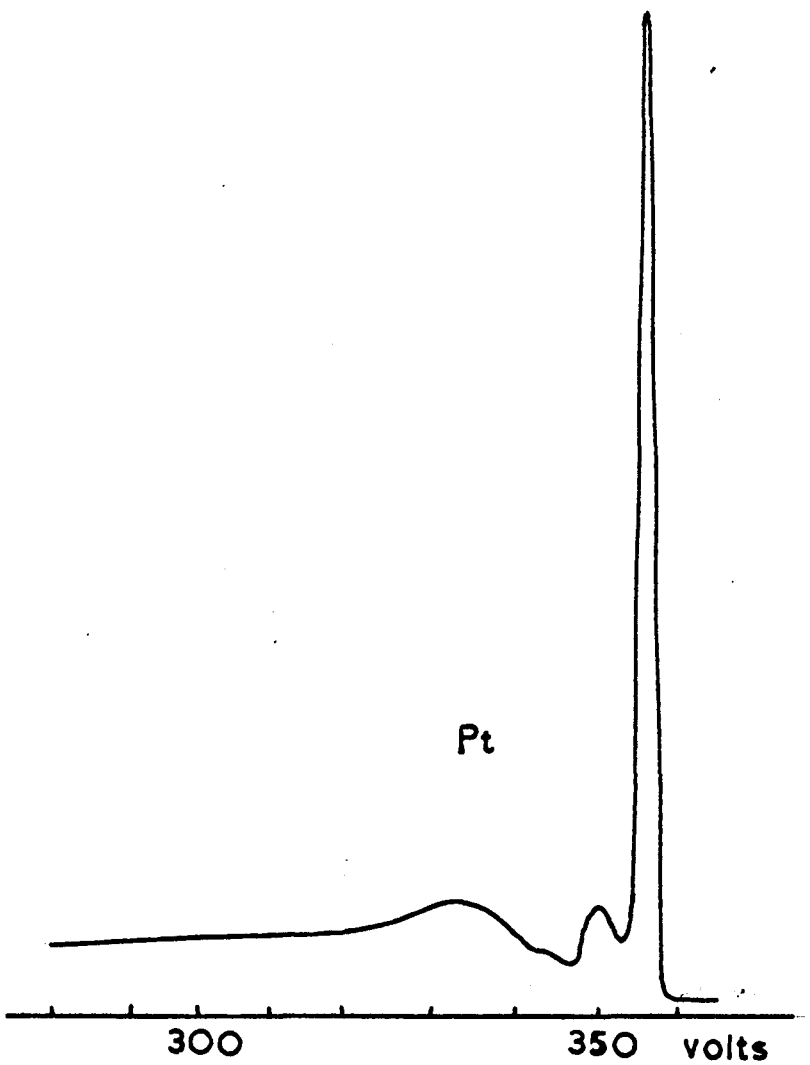

FIG. 26

Energy loss spectrum for Platinum. Rudberg (90)

CHAPTER III

On the Study of Characteristic Energy Losses of Electrons

3.1 Introduction

One of the most important results of the study of the energy distribution of secondary electrons has been a knowledge of the energy losses suffered by the primary electrons scattered by the target material. A knowledge of the energy losses helps to have a better understanding of the energy levels of the solid, the various excitations which take place within the solid, the processes involved in the scattering of electrons and the consequent emission of secondary electrons. It is not surprising then that a large amount of work is currently being done on the inelastic scattering of electrons and energy losses.

3.2 Experimental Observation of Characteristic Energy Losses

As has already been said in section 2.6, it was Rudberg who for the first time, made a quantitative assessment of the characteristic energy losses of electrons, by studying the energy distribution of electrons reflected from a solid target. A typical CEL spectrum, obtained by Rudberg (90) for platinum is shown in fig. 26. The large peak represents the elastically reflected primary electrons. On the lower energy side of this peak, are two maxima, which represent electrons having lost a certain amount of energy. The distances of these peaks from the reflected primary peak are a measure of the CEL of the

electrons. Rudberg was able to show that the energy loss values are characteristic of the scattering material and are not dependent on the primary energy of the electrons. He also found, within the limits of his apparatus, that the energy losses were independent of the angle of incidence of the primary beam, the angle of observation and the thickness of the sample.

Rudberg's work was followed by extensive investigations of Haworth (94, 95) and Farnsworth and his co-workers (96, 97), on both polycrystalline targets and single crystals. They also used similar techniques as Rudberg. However, in the later stages Farnsworth used a 127° electrostatic analyser. Haworth took extreme care to obtain a clean surface. These early workers studied electrons reflected from a solid target.

It was Ruthemann (98, 99) who first studied high energy electrons of several keV transmitted through thin metallic films and observed energy losses. He called these energy losses "discrete" and attempted to identify them with X-ray transitions. The term "characteristic energy losses" coined by Rudberg has been more acceptable to many, than Ruthemann's "discrete energy losses". The reason is that the term "discrete" in spectroscopic language implies a sharp line. However, in the energy spectrum the energy loss peaks are not always sharp. Hence the term "characteristic energy losses" is preferred. Nevertheless, some authors do refer to the losses as discrete energy losses and still some others as "eigen losses".

In energy analysis, each author used one or the other of the

FIG. 27

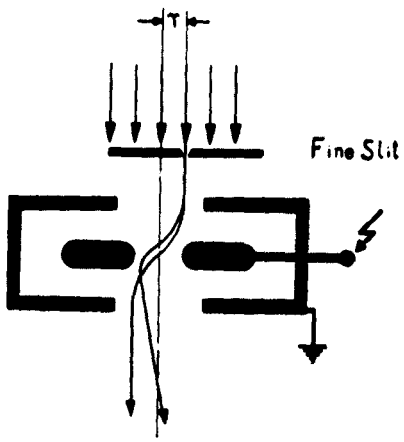

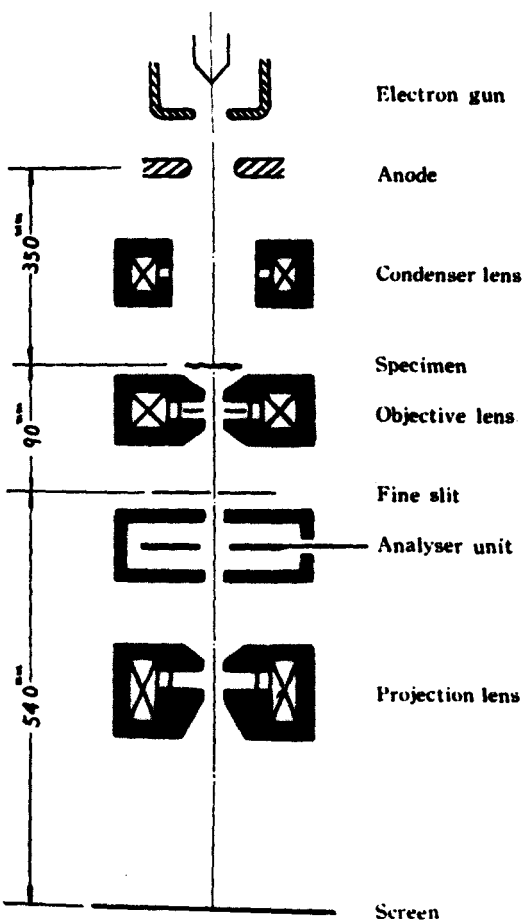

FIG. 28 Möllenstedt type analyser

methods described already in section 2.6. Very high resolution is required in the spectrometry of characteristic energy losses of electrons transmitted through thin films. Ruthe-mann used a transverse magnetic field analyser with a large orbital radius. He obtained a resolution $\frac{\Delta V}{V} = \frac{1}{2000}$.

Following Ruthemann's work, more workers adopted the "transmission method" of studying characteristic energy losses, whereby fast electrons of several keV energy were transmitted through thin metal films and the energy spectrum of the outcoming electrons studied. Consequently more refined methods of analysis of the energy spectrum were sought for.

It was a breakthrough when Möllenstedt (100) introduced a new electrostatic energy analyser, which could be incorporated in standard electron microscopes. This analyser has been used by a great many workers (101, 102, 103) and is shown in fig. 27. This is simply an electrostatic saddle field lens in which the chromatic aberration is very strong. A parallel beam of electrons with different energies, enters the lens, through a very narrow slit at some distance from the axis. As shown in fig. 27 the different electrons with different energies are deflected in different directions. In the electron microscope, these deflections are magnified by the projection lens and the pencils are focussed onto a fluorescent screen or photographic plate. The schematic of such an analyser used with a conventional electrostatic microscope is given in fig. 28. To obtain the highest resolution, a very fine slit is needed but this will reduce the intensity. Möllenstedt countered this by placing a

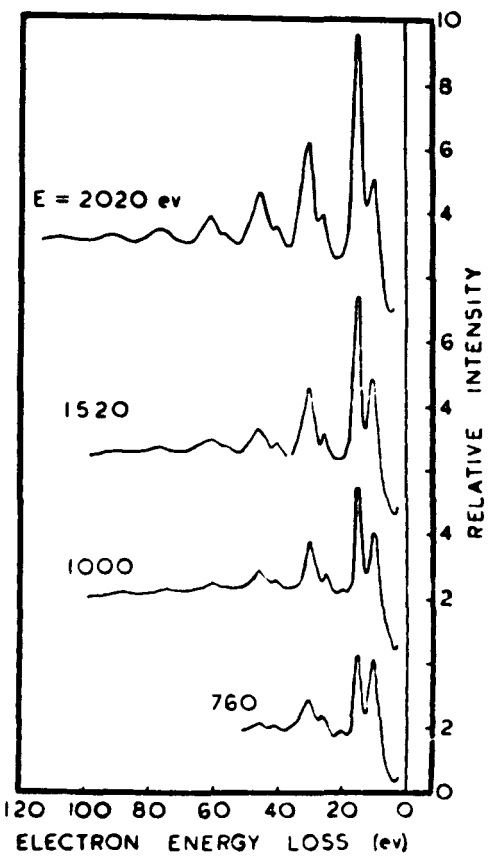

Characteristic energy loss spectra of Al for four different primary energies

FIG. 29

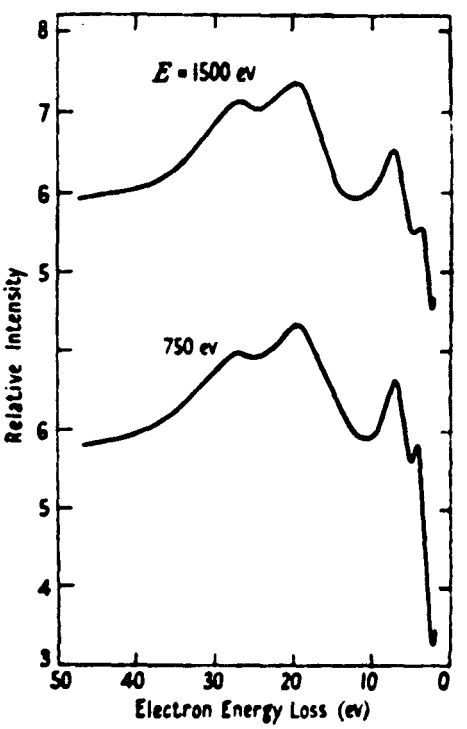

Characteristic loss spectra of copper for primary electron energies of 750 and 1500 ev. The spectra have been normalized for equal intensities of the 19·9 ev peak.

FIG. 30

collimating lens in front of the analyser lens. The resolution usually found in this type of analyser is about one part in 40,000. Möllenstedt achieved one part in 70,000 with his refined instrument.

The scattering targets used in these investigations can be classified into two categories: specimens used in transmission and those used in reflection. The transmission specimens are thin foils ranging from 30 Å to several hundred Å in thickness which are prepared by different methods, the most common one being by evaporation in vacuum, onto a substrate which can be removed. In reflection work also many authors have prepared "thick films" by evaporation, in order to obtain clean surfaces.

Characteristic energy loss values have been determined for most of the elements in the periodic table and a number of compounds and alloys. A typical characteristic energy loss spectrum obtained by reflection from an Al target for different primary energies is shown in fig. 29, as given by Powell and Swan (104). Al is one of the few elements which give very narrow loss peaks. More often the loss peaks are much wider as in the case of copper, fig. 30 (105). Since Al shows particularly sharp maxima and narrow lines, most authors have studied this element. Though all these authors claim to have determined these losses with an accuracy of 0.1eV, it is very surprising - rather unfortunate - that their results for the same loss in Al range over more than 4eV. The discrepancy in the energy loss values can be as high as 20% or more, from author to author. It is interesting to compare the energy loss values from Al obtained by some authors and these are tabulated in table 3. The table shows that the different energy losses are multiples of a basic loss and the basic loss

Table 3. Values for characteristic energy losses in aluminium as given by various authors

Ruthemann (1948)	(7)	14·7	—	29·6	—	44·3	—	59·3	73·8	—
Lang (1948)	—	14·5	—	29·4	—	44·2	—	58·6	75·2	90·4
Möllenstedt (1949)	7	15	22	—	—	—	—	—	—	—
	9	18	—	36	—	54	—	—	—	—
Boersch (1954)	8·7	14·9	—	29·8	—	—	—	—	—	—
Klein (1954)	6·8	14·9	21·9	30	—	44·6	—	—	—	—
Gauthé (1954)	—	16·5	—	—	—	—	—	—	—	—
Marton and Leder (1954)	6·2	13·9	19·2	27·8	3·5	—	—	—	—	—
Watanabe (1954 a)	6·5	14·8	23	29·5	—	45	—	—	—	—
Blackstock *et al.* (1955)	—	14·8	—	30·0	—	44·2	—	59·8	—	—
Haberstroh and Raether (1955)	—	15·0	—	29·4	—	—	—	—	—	—
Möllenstedt and Dietrich (1955)	6·8	15·8	22·5	—	—	—	—	—	—	—
Haberstroh (1956)	(7)	15·2	—	30·6	—	—	—	—	—	—
Jull (1956)	7·0	14·6	20·5	29·2	—	43·8	—	58·4	73·0	—
Leder (1956)	7	14·6	22	29·2	38	44·5	—	—	—	—
Simpson *et al.* (1956)	—	15	—	—	—	—	—	—	—	—
Meyer (1957)	—	15·0	—	—	—	—	—	—	—	—
Fert and Pradal (1958)	7·8	15·8	23·5	31·6	39	47·4	54·6	63·2	79	—
Leder and Simpson (1958)	7·5	15·0	22	30	—	—	—	—	—	—
Leder and Marton (1958)	—	15·0	—	—	—	—	—	—	—	—
	—	15·3	—	—	—	—	—	—	—	—
Marton *et al.* (1958)	6·3	15·3	—	—	—	—	—	—	—	—
Powell and Swan (1959)	10·3	15·3	25·6	30·5	41·1	46·1	56·0	61·4	77·0	91·8
Kunz (1962)	6	15·0	—	—	—	—	—	—	—	—
Boersch, Miessner and Raith (1962)	—	14·7	—	—	—	—	—	—	—	—
Klemperer and Shepherd (1963 a)	(7)	15·4	(23)	30·9	(39)	46·1	—	—	—	—

itself varies from 13.9 to 18eV. Some observe a lower loss at $\simeq$ 7eV, whereas some others don't. Powell and Swan (104) observed a lower loss at 10.3eV.

Characteristic energy losses have also been observed in compounds and alloys. Leder and Marton (107) observed that the energy spectra of elements and their compounds were very much alike with only a small increase in the energy loss values. A typical spectrum for Sb and Sb_2S_3 is reproduced in fig. 31. Watanabe (101) and Best (108) also found the same trend. However, it must be said that there are exceptions to this general rule of similarity of the spectra, as in the case of Al and Al_2O_3, where the losses are $\simeq$ 15eV and $\sim$ 23eV respectively.

The CLL of some intermetallic compounds have been studied by Gauthe (109), Powell (110), Klemperer and Shepherd (111) and others. The loss spectra are significantly different from a simple superposition of the loss spectra of the parent metals. Loss values are found to vary between the loss values of the component metals, depending on the composition of the alloy. Klemperer and Shepherd quantitatively studied the correlation between the energy loss values and the composition of the alloy obtained by chemical analysis.

The large discrepancy in all the energy loss values has been ascribed to both the bulk and the surface contaminations. Surface impurities may be of two kinds. One may be present at the beginning of the investigation and may or may not slowly change under the action of the electron beam. The second is a beam-borne impurity accumulating at the rate of bombardment of the surface and is practically unavoidable in dynamic

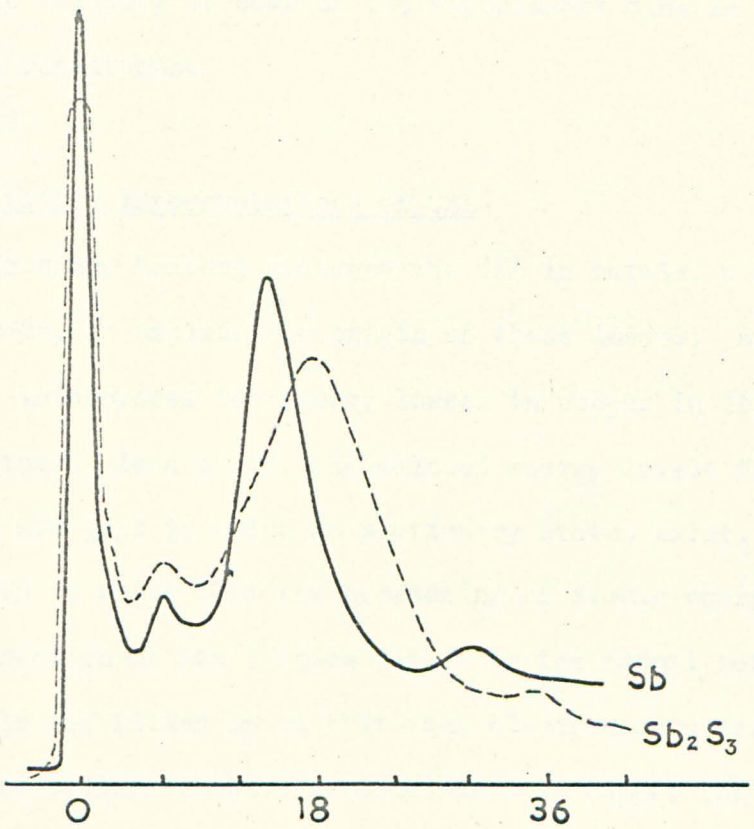

FIG. 31

Energy loss spectrum for Sb and Sb_2S_3

demountable vacuum systems (106). There is indication in the literature that the rate of accumulation may be slowed down or reversed by raising the temperature of the target surface. Considering the enormous effect of contamination on the energy loss values, one can see the necessity for maintaining the target clean in an ultra-high vacuum. One may even question the validity of some of the experiments done in such extremely poor vacuum conditions.

3.3 Qualitative Interpretations of CEL

Ever since Rudberg measured the CEL in metals, a number of attempts have been made, to explain the origin of these losses. Rudberg and Slater (93) interpreted the energy losses in copper in terms of the band scheme of atoms. In a solid, the allowed energy levels fall in bands between which there are gaps in which no stationary states exist. These bands may be considered to arise from the broadening of atomic energy levels due to the mutual interaction of the lattice ions. In the normal metal, the allowed energy levels are filled up so that each electron occupies the lowest level accessible according to Pauli's principle. In copper the least firmly bound electrons occupy levels in a band arising from the perturbation of the 3d and 4s levels of atomic copper. Incident primary electrons are considered to cause transitions from the occupied 3d levels of the band to 4s levels and others above, thus losing energy. Slater and Rudberg, using the density of states curve and approximate wave function corresponding to each level calculated the relative probability of the different energy losses. They found good agreement between theory and experiment for the

first two loss peaks in the spectrum.

There can be little doubt of the validity of the interpretation, for it not only rests on some quite basic features of the band theory, but is also supported by the close correlation between the loss value obtained by Rudberg and the optical absorption peaks obtained by Minor (112). Since the optical absorption also is due to the same mechanism this agreement is necessary.

There have been a few attempts to correlate the energy losses with X-ray data. A few lines in the loss spectrum have been tentatively identified with optical transitions, in particular in the soft X-ray region (113, 103). This method has been successful only in the case of a very few elements. Most of the attempts remain qualitative probably owing to the skimpy optical information.

A different type of identification of the transitions involved, may be offered by the remarkable degree of coincidence of the numerical values of the energy loss lines, with the differences between fine structure absorption maxima in the K or L edge in the X-ray spectra. Since the X-ray K-edge corresponds to a transition of a K-electron to the first unoccupied level above the Fermi level and the maxima of absorption of the fine structure, to transitions to higher allowed levels, it is quite plausible to account for the CEL as due to excitations of the valence electrons to the same higher energy levels. Cauchois (114) thus compared the CEL of Al with the fine structure of the X-ray K-absorption edge. However, she made the comparison with the maxima in the transmission curve.

Watanabe correctly pointed out that the comparison should be made with the maxima of absorption. Since then, Leder and his colleagues (115) have compared the energy losses with the X-ray fine structure, for a very large number of metals and found considerable agreement.

Sternglass (116) has suggested that characteristic energy losses can be interpreted in terms of individual atomic ionisation and excitation and found good agreement in the case of Al. This has not been favoured by other workers who studied other elements and also compounds.

All the above interpretations involve single electron interactions. A completely new and additional mode by which electrons can lose energy in a solid, has been suggested by Bohm and Pines (49 - 51) in what is now known as the Plasma Oscillation theory. They treated the density effect on the long range Coulomb interaction in metals in terms of the collective plasma model. When an electron interacts with such a solid state plasma, it excites collective plasma waves and in the process loses a certain quantum of energy. The plasma oscillation theory has been extremely successful in explaining many of the characteristic energy losses in solids, which have remained anomalous on single electron interaction theory. Thus it is not surprising that this theory has drawn much attention and a quite substantial amount of theoretical work has been done on it. A more detailed account of the theory will be given in the next section.

3.4 Plasma Oscillations in Metals

A system composed of a large number of positive ions and free electrons with zero total charge was first called a "plasma" by Langmuir

in 1928. Physical examples of a plasma can be seen in gas discharges and in the ionosphere. Such plasmas as occur in a gas discharge tube have been studied both theoretically and experimentally for many years and interest in them has recently been intensified owing to their application in thermonuclear devices.

Owing to the relatively large mass of the positive ions, the motion of the ions is not very significant compared to the motion of the electrons. For most practical purposes, it may be assumed that the electron gas moves in a positively charged fluid of uniform density, which is called the "background of positive charge". It is assumed that the time average of the charge density of ions and electrons together is zero everywhere.

Owing to the thermal fluctuations, the electronic charge density is constantly changing from place to place. Let us suppose that, as a result of the thermal motion, the electronic charge density in some region is reduced below the average. The background of positive charge will not be completely neutralised in that region and the resulting positive charge will attract neighbouring electrons. The tendency is to restore charge neutrality. By the time neutrality has been established, the electrons have acquired sufficient momentum and so overshoot the mark. This produces an excess negative charge which causes the electrons to be repelled outwards again. In time, the motion is reversed and a systematic oscillation of the charged region is set up. It was Tonks and Langmuir in 1929 (117) who first observed these oscillations and because of the close similarity of these oscillations to the oscillations of a thin jelly plasma, they christened these oscillations "Plasma Oscillations".

These are longitudinal oscillations analogous to sound waves. Langmuir and Tonks studied these oscillations in greater detail and calculated the frequency of oscillation. The angular frequency

$$\omega_p = \left(\frac{4\pi n_o e^2}{m}\right)^{\frac{1}{2}} \qquad (22)$$

where n_o is the electron density

e - the electronic charge

and m - mass of the electron.

ω_p is often called the "plasma frequency". For a typical gaseous plasma density of 10^{12} electrons/cc, the plasma frequency is about 10^{10} Hz.

A metal also, may be considered to be an example of a plasma, because it consists of positive ions arranged on a crystal lattice, together with valence or conduction electrons, which are more or less free. Though much oversimplified, it may be assumed that the ion-core electrons are tightly bound to the nuclei and the valence electrons are completely free. This theory, proposed by Sommerfeld and known as the free electron theory, assumes that the average field acting on an electron is zero (7) and hence the potential of the field, a constant. This is not quite true, since it is well known that the potential within the metal is periodic with the period of the lattice. Besides, in a metal there are something like 10^{23} electrons/cc and hence these electrons are very close together. The Coulomb force, consequently, can be very large. It is not, however, fair to say that in the Sommerfeld theory of free electron gas, the Coulomb interaction is completely ignored. In fact, the average potential energy due to this interaction, may be considered to be implicit in the depth of the potential box, in which the electrons move.

Sommerfeld's theory was improved upon by Hartree (7, 118, 119). He, however, ignored the Coulombic interaction and considered the electron to be moving in the field of the ions and the field due to the average charge density of the remaining electrons. The Hartree method is equivalent to the use of a total wave function, which is the product of one electron functions. This theory has the same success as the Sommerfeld theory in calculations depending on the density of states. However, it completely fails, for example, in the calculation of cohesive energies.

A further improvement was made by Hartree and Fock (7, 119) who used a total wave function consisting of a determinant of one electron functions. Again the Coulomb interaction is neglected. However, it includes another sort of correlation among the positions of electrons with parallel spins only. Thus the probability of two electrons with identical spatial quantum numbers and parallel spin approaching each other is lowered. The correlation is "accidental" due to the Pauli's principle rather than to the Coulomb repulsion.

A major improvement in the description of the interacting electron gas occurred when Bohm and Pines (49 - 51) advanced the "plasma theory", following up the concept of the classical plasma and plasma oscillations, as observed by Langmuir and Tonks. Bohm and Pines took into account the long range Coulomb interaction whose effect is described by the plasma oscillations. It may be fair enough to consider the metal as a solid state plasma. But there is a distinct difference between the classical gaseous plasma and the solid state plasma. In the former, the density of electrons is small enough ($\sim 10^{12}$/cc) for their motion to

be treated by classical mechanics or Maxwell-Boltzmann statistics. The motion of the high density ($\sim 10^{23}$/cc) electron gas in a metal, however, must be treated by quantum mechanics or Fermi-Dirac statistics.

The frequency of plasma oscillations may be simply derived by using classical electrodynamics (120) even though the same result may be obtained by using rigorous quantum mechanics (121, 122).

Let the average spatial density of electrons be n_o, so that the average electronic charge density is $-n_o e$, where $-e$ is the charge of the electron. The uniform charge density of the positive background is thus $n_o e$. Also let n^1 be the actual density of electrons, which is a function of position and time. This, in fact, is the instantaneous average over a region small compared with the whole volume of the metal, but still containing a large number of electrons. The excessive positive charge density is $e(n_o - n^1)$.

The restoring field E is found by using Poisson's equation

$$\nabla \cdot E = 4\pi e(n_o - n^1) \tag{23}$$

If ξ is the displacement of the electron gas from equilibrium (over and above the thermal motion) the particle current density $n^1\dot{\xi}$ satisfies the equation of continuity.

$$-\frac{\partial n^1}{\partial t} = \nabla \cdot (n^1 \dot{\xi}) \tag{24}$$

An approximation is now made, namely that the amplitude of the oscillation is small. This being so, ξ is small, so that n_o is not very different from n^1. Then

$$\nabla \cdot (n^1 \xi) = n^1 (\nabla . \xi) + (\nabla n_o).\xi \approx n^1 \nabla . \xi$$

From equation (24)

$$-\frac{\partial n^1}{\partial t} = n^1(\nabla.\dot{\xi}) \tag{25}$$

Integrating with respect to time

$$-\int\frac{\partial n^1}{\partial t}\,dt = \int n^1(\nabla.\dot{\xi})\,dt$$

i.e.
$$n_o - n^1 = n_o(\nabla.\xi) \tag{26}$$

Combining equations (23) and (26)

$$\nabla.E = 4\pi n_o e(\nabla.\xi)$$

$$\therefore \quad E = 4\pi n_o e\,\xi \tag{27}$$

No additive constant is required since E is zero at $\xi = o$, i.e. at equilibrium there is no restoring field.

For an electron in an electric field, the equation of motion is

$$m\ddot{\xi} = -eE \tag{28}$$

where m is the mass of the electron.

Hence from (27) and (28)

$$m\ddot{\xi} + 4\pi n_o e^2\xi = o \tag{29}$$

which is the equation of motion of a simple harmonic oscillator, oscillating at an angular frequency

$$\omega_p = \left(\frac{4\pi n_o e^2}{m}\right)^{\frac{1}{2}} \tag{30}$$

which is the plasma frequency.

The polarisation current density is given by

$$j = \alpha\frac{\partial E}{\partial t} \tag{31}$$

where α is the polarisability. The quantity j, also satisfies the continuity equation

$$-e \frac{\partial}{\partial t} (n_o - n^1) = \nabla . j \tag{32}$$

Combining (31) and (32)

$$-e \frac{\partial}{\partial t} (n_o - n^1) = \alpha \nabla . \frac{\partial E}{\partial t}$$

$$-e \frac{\partial}{\partial t} (n_o - n^1) = \alpha \frac{\partial}{\partial t} \nabla . E \tag{33}$$

Using equation (23)

$$-e \frac{\partial}{\partial t} (n_o - n^1) = 4\pi \alpha e \frac{\partial}{\partial t} (n_o - n^1)$$

$$\alpha = -\frac{1}{4\pi} \tag{34}$$

The dielectric constant of a metal is (7)

$$\varepsilon = 1 + 4\pi \alpha \tag{35}$$

which vanishes at the plasma frequency ω_p because of equation (34).

In the above calculation of ω_p, the thermal motion of the electrons has been neglected. A more refined classical treatment (50) shows that the angular frequency is ω_p, only for long waves, but increases as the wavelength λ decreases. The dispersion relation is found to be approximately

$$\omega^2 = \omega_p^2 + k^2 \overline{v^2} \tag{36}$$

where $k = \frac{2\pi}{\lambda}$ is the wave number of the plasma wave and $\overline{v^2}$ is the mean square velocity of the electrons.

From quantum mechanical calculations Pines and Bohm (50) obtained the dispersion relation to be

$$\omega \simeq \omega_p \left(1 + \frac{3 \zeta_o k^2}{5m \omega_p^2} + \frac{\hbar^2 k^4}{8m^2 \omega_p^2}\right) \tag{37}$$

where ζ_o is the energy of an electron at the top of the Fermi band.

In fact, the dispersion is not very great, ω never differing from ω_p by more than a few per cent, because there is an upper limit to k which is known as the cut-off wave vector and represented by k_c. Plasma oscillations do not occur above this wave vector k_c or below the corresponding wavelength

$$\lambda_c = \frac{2\pi}{k_c} \tag{38}$$

λ_c is about twice the interelectronic distance r_e, since it is meaningless to talk about organised oscillations of an electron gas with wavelength less than the interelectronic distance.

If the effect of dispersion is neglected, we may assume that the plasma oscillations in a metal, can be represented approximately, by a finite set of harmonic oscillators, with angular frequency ω_p. The energy of such an oscillator must have values $(N + \frac{1}{2})\hbar\omega_p$, where N is a positive integer or zero. The zero point energy of the oscillator is thus $\frac{1}{2}\hbar\omega_p$. The energy required to raise the oscillator from one state to the next higher - the excitation energy - is $\hbar\omega_p$. Pines (121) gave the name "plasmon" for the quantum of plasma oscillation. Thus the excitation energy of a plasmon is $\hbar\omega_p$.

It is interesting to compare $\hbar\omega_p$ with ζ_o, the maximum kinetic energy of any electron at 0^oK, according to the Sommerfeld-Hartree theory of a free electron gas.

It is found to be (119, 120)

$$\hbar\omega_p = 0.94\, r_e^{\frac{1}{2}}\, \zeta_o \tag{39}$$

where r_e is measured in Bohr units. Now $0.94\, r_e^{\frac{1}{2}} > 1$ for all metals

so that $\hbar\omega_p > \zeta_o$. At normal temperatures T, a few electrons near the Fermi surface are excited and their thermal energies are of the order of KT which is very much smaller than ζ_o. Thus $\hbar\omega_p$ is very much greater than the thermal energy of an electron and this means, temperature excitation of plasmon is highly improbable. Some other means, such as the passage of a fast charged particle, is required to excite a plasmon in a metal.

Thus when a high energy beam of electrons is shot through a thin film, it excites plasmons and in the process loses energy equivalent to that of the excited plasmons. Consequently, the emergent electron loses $\hbar\omega_p$, $2\hbar\omega_p$, $3\hbar\omega_p$ and so on, according to the number of plasma quanta.

Bohm and Pines have shown that the energy loss ΔE should vary with the scattering angle θ of the electron, in the manner

$$\Delta E = \hbar\omega_p + \frac{3\zeta_o P^2}{5m\hbar\omega_p}\theta^2 \qquad (40)$$

where P is the momentum of the incident primary electron and ζ_o the Fermi energy.

The plasma theory predicts a maximum energy loss and hence a maximum angle of scattering θ_c, which is given by

$$\theta_c = \frac{\hbar k_c}{P} \qquad (41)$$

where k_c is the cut-off wave vector. Pines calculated the value of k_c (123) as

$$k_c = 0.353\, k_o r_e^{\frac{1}{2}} \qquad (42)$$

where k_o is the wave number of an electron at the top of the Fermi band and r_e the average interelectronic distance in Bohr units.

3.5 Surface Plasmons

The longitudinal oscillations described above are due to the electron volume density fluctuations in the bulk of the material. Ritchie in 1957 (124) showed that one can also regard the charge density fluctuations at the surface of the material which is separated from the vacuum. He noted that for such a semi-infinite plasma, there existed not only the bulk plasma oscillations of frequency ω_p in the interior of the plasma, but also surface plasma oscillations of frequency $\frac{\omega_p}{\sqrt{2}}$, at the interface between the plasma and vacuum. One can thus make a distinction between "volume plasmons" of frequency $\omega_p/\sqrt{2}$. The energy of the surface plasmons then will be $\frac{\hbar\omega_p}{\sqrt{2}}$

A more generalised formula for the surface plasma frequency was derived by Stern and Ferrell in 1960 (125) for the case of a dielectric medium instead of vacuum. They used the dielectric model of a plasma (section 3.6) and the frequency dependent dielectric constant as given by (126, 127).

$$\varepsilon_p(\omega) = 1 - \frac{\omega_p^2}{\omega^2} \qquad (43)$$

where ω_p is the classical plasma frequency and $\varepsilon_p(\omega)$, the dielectric constant of the metal plasma.

The semi-infinite electron gas is considered to be bounded by a semi-infinite non-absorptive dielectric, of dielectric constant ε_B.

The electric potential distribution set up by a classical charge wave bound to the surface must satisfy Laplace's equation within the metal and dielectric medium. The boundary conditions, for the existence of an oscillating wave across the interface yield the relation (125)

$$\varepsilon_p(\omega) = - \varepsilon_B \tag{44}$$

One may assume that the dielectric layer has approximately a frequency independent dielectric constant ε_B, which is legitimate for dielectric layers on metal surfaces. On substitution for $\varepsilon_p(\omega)$ from equation (43) the resonant frequency for the surface wave is obtained as

$$\omega_s = \frac{\omega_p}{\sqrt{1 + \varepsilon_B}} \tag{45}$$

For a metal bounded by vacuum $\varepsilon_B = 1$ and hence

$$\omega_s = \frac{\omega_p}{\sqrt{2}} ,$$

as obtained by Ritchie.

If we have two metals in contact, with plasma frequencies ω_{p_1}, and ω_{p_2} then the resonant frequency is given by (125)

$$\omega_s = \left[\tfrac{1}{2} \left(\omega_{p_1}^2 + \omega_{p_2}^2 \right) \right]^{\frac{1}{2}} \tag{46}$$

Experiments have recently been carried out to verify the existence of surface plasmons and the agreement with the theoretical values and experimental values has been remarkably good. The experimental evidence will be discussed in section 3.7.

3.6 Dielectric Theory of Energy Losses

So far, in treating the collective oscillations of the conduction electron-ion core plasma, we assumed the core electrons to be tightly bound. Even in metals where the core electrons are tightly bound, the periodic field of the ionic lattice must have some effect on the frequency of the plasma oscillations. To account for the effect of the lattice field, Wolff in 1953 (128) suggested the electron mass 'm' be replaced by an effective mass m^*. But Hubbard (129) and Kanazawa (130) pointed out that the effective mass theory is basically a one-zone theory and is valid only if the effect of virtual inter-zone transitions can be neglected. But Adams (131) is of the opinion that the inter-zone transitions can be considerable and hence the effective mass treatment of plasma oscillation is not valid.

The close relationship between the characteristic losses in a solid and its optical properties has been pointed out by Marton, Leder and Mendlowitz (107), Fröhlich and Pelzer (132), Hubbard (133) and Nozieres and Pines (126). These authors have found that characteristic energy losses can be interpreted in terms of the frequency dependence of the complex dielectric constant $\epsilon(\omega)$. According to this dielectric theory the complex dielectric constant is

$$\epsilon(\omega) = \epsilon_1(\omega) + i\,\epsilon_2(\omega) \qquad (47)$$

This constant may be considered to be a characteristic of the longitudinal displacement of charges, when an electron enters the solid and acts on the electrons of the atom.

The condition for the existence of undamped longitudinal waves is (132)

$$\varepsilon(\omega) = 0 \tag{48}$$

as has already been noted in section 3.4 (equations 34 and 35). For a free electron gas, on the basis of the Drude free eledtron theory (134) the two parts of the dielectric constant can be expressed as

$$\varepsilon_1(\omega) = 1 - \frac{\omega_p^2}{\omega^2} \cdot \frac{1}{1 + \frac{1}{\omega^2\tau^2}} \tag{49}$$

$$\varepsilon_2(\omega) = \frac{1}{\omega\tau} \frac{\omega_p^2}{\omega^2} \cdot \frac{1}{1 + \frac{1}{\omega^2\tau^2}} \tag{50}$$

where τ is the relaxation time and ω_p the plasma frequency.
In the case of a free electron gas, collective oscillations will be set up when $\varepsilon_1 = 0$ if $\omega\tau >> 1$ (121).
Under these conditions, from equation (49) it can be seen that

$$\omega = \omega_p \text{ - the plasma frequency.}$$

The energy lost by an electron traversing the medium, according to this theory is proportional to the imaginary part of $\varepsilon(\omega)$ (107, 132, 133).

$$\Delta E = \mathrm{Im}\left|\frac{1}{\varepsilon(\omega)}\right| = \frac{\varepsilon_2}{\varepsilon_1^2 + \varepsilon_2^2} \tag{51}$$

The complex dielectric constant $\varepsilon(\omega)$ is related to the optical constants n and k, the index of refraction and extinction coefficient respectively (135).

$$\varepsilon(\omega) = (n + ik)^2 \tag{52}$$

$$\varepsilon_1(\omega) = n^2 - k^2 \tag{53}$$

$$\varepsilon_2(\omega) = +2nk \tag{54}$$

Measurements of n and k as a function of the photon energy $\hbar\omega$, yield the values of $\varepsilon_1(\omega)$ and $\varepsilon_2(\omega)$, from which the energy spectrum can be derived. This, in fact, does offer a means of studying the characteristic energy loss spectrum.

After having briefly outlined the basic concepts of the plasma oscillation theory, a brief account of the experimental studies on plasmons will be given in the next section. Many of the critical features of the plasmons have been experimentally verified. These studies might bring out some of the short-comings as well.

3.7 Plasmon Studies

With the development of the plasma oscillation theory, many authors tried to identify the characteristic energy losses in terms of plasmon excitation. Thus when a beam of electrons bombards a metal surface or traverses a thin metal film, there is a good chance that some electrons will lose an energy $\hbar\omega_p$, others 2 $\hbar\omega_p$, 3 $\hbar\omega_p$ and so on. The energy to excite a single volume plasmon thus is

$$\hbar\omega_p = \frac{h}{2\pi} \left(\frac{4\pi n_o e^2}{m}\right)^{\frac{1}{2}}$$

where h - Planck's Constant

n_o - the free electron density

e - the electronic charge

m - the mass of the electron

The electron density is calculated assuming all the valence electrons to be free. Substituting the values of n_o, e, m and h

$$\hbar\omega_p = 28.8 \left(\frac{Zd}{A}\right)^{\frac{1}{2}} \text{ eV} \qquad (55)$$

where Z is the number of valence electrons

d - the density of the metal

and A - the atomic weight.

For example using three electrons per atom to be free for Al, in equation (55)

$$\hbar\omega_p = 15.8\text{eV}$$

Considering the difficulty associated with the measurement of energy losses, the experimental values agree very closely with this value.

However, a distinction must be made between two groups of metals. For the metals, which have sharp loss lines, like Al, Mg, Be, Ti etc., the agreement is remarkably good. But for some metals like Cu, Zn, Au, etc., which have broad loss bands, the agreement is not satisfactory. The disagreement is not surprising since 'n_o' refers to the entirely free electrons. The disagreement may arise from several other phenomena, namely interband transitions and interaction of the electron gas with core electrons.

Where the free electron theory agrees with experimental results, further conclusions from the plasma theory have been tested. The mean free path Λ for the excitation of a plasmon has been calculated theoretically by Bohm and Pines (50) by Blackstock, Ritchie and Birkhoff (138) and by Quinn (139) in 1962. Blackstock and others (138), using a transmission method, measured the mean free paths in thin Al films as a function of primary energy. If the foil thickness D, is larger than the mean free path, Λ , then

$$\Lambda = D \frac{J_o}{J_1} \qquad (56)$$

where J_o and J_1 are the areas under the transmitted peak and first loss peak. For Al, the agreement between the experimental and calculated value is extremely close. In all fairness to the experiments, it must be said that the determination of the thickness of the thin films can be very difficult and different methods often lead to variations as much as 50%!

Another experiment which furnished further support for the plasma theory was the measurement of the energy losses as a function of the scattering angle. Equation (40) gives the variation of the energy loss with scattering angle θ, as

$$\Delta E = \hbar\omega_p + \frac{3}{5}\frac{\zeta_o p^2}{m\hbar\omega_p}\theta^2 \qquad (40)$$

Watanabe (101) measured the energy losses as a function of the angle through which the electron is scattered. The linear relationship between ΔE and θ^2 has been verified for Al, Be, Mg, Na and Li.

From the above measurements Watanabe calculated the cut-off wave vector beyond which the collective oscillations do not occur. He measured the maximum scattering angle θ_c which is given by equation (41).

$$\theta_c = \frac{\hbar k_c}{p}$$

When θ approaches θ_c, the electron loss intensity drops quickly to zero. For Al, the theoretical value of θ_c is about 11 milliradians for the beam of 25keV used by Watanabe. This is only roughly compatible with the experimental value of Watanabe which is between 12 and 16 milliradians. In 1964 Schmüser (140) carried out some very precise measurements which yielded values of θ_c very much closer to the theoretical values than Watanabe's values.

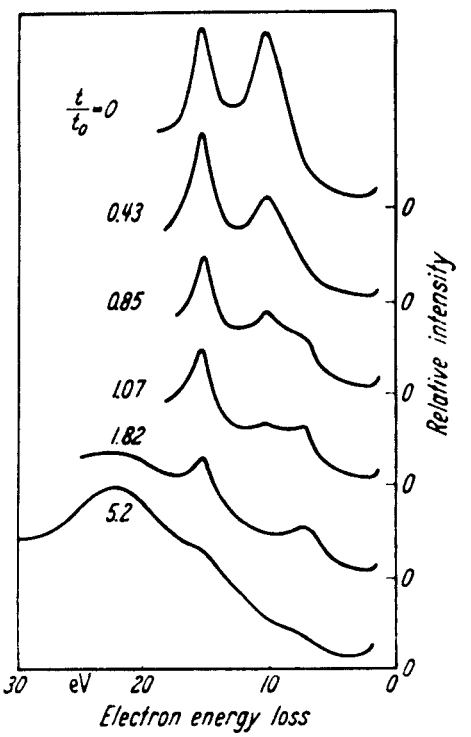

. Portions of the characteristic loss spectrum of Al in progressive stages of oxidation. t is the time elapsed after evaporation of the Al and t_0 is the time in which the measured intensity of the plasma loss is decreased to half its initial value. In the latest stage ($t = 5{,}2\,t_0$) the volume loss (15 eV), the surface loss (10,5 eV), and the surface loss on the oxidised surface (6,5 eV) have nearly disappeared and the broad loss at ~ 23 eV of aluminum oxide remains

FIG. 32

Many of the CEL observed in compounds (107, 108) can be explained as due to plasmon excitation. Neglecting the core polarisability again, the plasmon energy $\hbar\omega_p$ can be calculated and compared with the observed energy losses. The total number of valence electrons should be taken in the case of compounds (123). For example, Al_2O_3 has 24 free electrons per molecule, six from Al and 18 from O. There has been surprisingly good agreement between the plasmon energy calculated in this way and the observed energy losses for some compounds (123).

It has been said in section 3.5 that besides volume plasmons of frequency ω_p there are surface plasmons of frequency $\frac{\omega_p}{\sqrt{2}}$ at the metal to vacuum interface. The prediction of the existence of surface plasmons by Ritchie (124) has been borne out in a series of experiments by Powell, Swan and co-workers (104, 105, 108, 110, 137, 145). They studied electrons reflected from freshly evaporated layers. The energy spectrum was plotted immediately after evaporation, prior to and during the formation of an oxide layer. They obtained the spectrum at regular intervals. One of the typical spectra, is given in fig. 32 for Al. Their measurements showed that there was initially a volume plasma loss at $\hbar\omega_p = 15.9$eV and in addition a surface plasma loss at $\frac{\hbar\omega_p}{\sqrt{2}} = 10.3$eV present. As the oxide layer was formed the surface plasma loss at 10.3eV decreased in intensity and a new modified surface plasma loss at an energy 7.1eV appeared. The energy of the modified surface plasmon is in good accord with what would be expected for the metal - -metallic oxide interface. Using equation (45) the dielectric constant

of the oxide layer Al_2O_3 is found to be 1.9 which may be compared with a value of 1.76 obtained from the optical data. Similar results have been obtained for other metals.

The electron energy loss, at the interface of two metallic layers, each with a frequency dependent dielectric constant, as calculated from equation (46) has also been observed by Axlerod in 1964 (141) in layered films of Bi and Mg. The existence of these surface plasma losses in particular seems to establish firmly the collective nature of electron dynamics in a metal.

In interpreting an energy loss spectrum, one should be able to distinguish between volume and surface plasma losses. Raether and co-workers (134, 140, 142-144) employed the fact that in transmission, the intensity of surface plasmon decays with θ^{-3} where θ is the scattering angle, while volume loss decays as θ^{-2}. A simpler experimental method has been given by Klemperer and Thirlwell in 1966 (146). They found, studying reflected electrons from a solid target, that the ratio of the number of electrons suffering volume plasma loss to that of surface plasma loss decreased with increasing angle of incidence of the primary beam.

Ferrell in 1958 (147) predicted another interesting phenomenon of the plasmons. According to him, a plasmon could decay by emitting an electromagnetic radiation of frequency ω_p - wavelength $\lambda_p = \frac{2\pi c}{\omega_p}$ which could be detected experimentally. The predicted radiation has in fact been detected by Steinmann (148) as well as Brown and others (149) from thin silver film.

They observed the wavelength of the radiation to be 3300 Å, in good agreement with the theoretical value of 3290 Å. Similar radiation has been detected from Al and Mg (150) and in Cd, In and Zn (151).

Ferrell and Stern (152) recently discussed the possibility of exciting plasma oscillations at the frequency ω_p, in thin metals by using polarised light. The light must be polarised in the plane of incidence and incident at a large angle of incidence for such an excitation. The experimental evidence of such a photon excitation of plasma oscillations, has been obtained recently for silver films by a few authors (153, 154). Furthermore, Ritchie in 1965 (155) calculated the probability that a photon incident normally on a thick foil would excite a surface plasmon through the intermediary of an intraband electronic transition. Williams, Arakawa and Emerson (156) in 1967 supported Ritchie's argument from the evidence of experimental data on Al.

From reflectance data, the optical constants n and k can be determined. Equations (53) and (54) yield the values of ϵ_1 and ϵ_2. The energy loss function is given by equation (51)

$$-\mathrm{Im}\left\{\frac{1}{\epsilon(\omega)}\right\} = \frac{\epsilon_2}{\epsilon_1^2 + \epsilon_2^2} = \frac{2nk}{n^2 + k^2}$$

For surface plasmons, the loss function is $-\mathrm{Im}\left(\frac{1}{\epsilon(\omega) + 1}\right)$. When these functions are plotted against ω, the peaks in the distribution correspond to the volume or surface plasmons. The experiments conducted in these lines, yielded extremely accurate values of the plasma frequency and energy losses (157, 158, 159).

3.8 Conclusion

All the above mentioned experiments are sufficient evidence for the validity of the concept of plasma oscillations in solids and the fact that electrons can lose energy by exciting plasmons. In particular, the experimental evidence of surface plasmon has consolidated the plasma oscillation theory. However, it must be remembered that the success of plasma oscillation theory in no way excludes the possibility of band to band transitions as a cause for energy loss.

CHAPTER IV

On the Theories of Secondary Electron Emission

4.1 Introduction

In the previous chapter, an account was given of the processes by which primary electrons lose discrete amounts of energy and emerge as inelastically reflected primaries. But these inelastically reflected primaries form only a small fraction of the total number of secondaries emitted. Any study of secondary electron emission would be incomplete without a basic knowledge of the various theories accounting for the larger fraction of lower energy electrons, and hence a very brief survey of these different theories will now be given.

At present there are a large number of theories in the field, mutually inclusive and most overlapping, in describing some particular aspect of the experimental results under different conditions. There are particular theories, dealing with, the variation of yield with primary energy, the energy distribution of secondary electrons, and the angular distribution of secondaries. Some are qualitative and others quantitative. Despite all the different theories available, it is only fair to say, that the theoretical understanding of SEE, is still quite incomplete.

Many authors consider the phenomenon of SEE as occurring in two distinct steps. Firstly, the primary electrons traverse the medium and by collisions with the lattice electrons, lose energy and produce "internal secondaries". Secondly, the subsequent cascade process, in which these

secondaries diffuse through the solid, multiplying and losing energy "en route", until they either return into the sea of conduction electrons, or reach the surface with sufficient energy to emerge as true secondary electrons. The validity of this simple, general picture may be questionable. Nevertheless, some very useful theories have been built upon it and it will need a lot of disproving before we can disregard it.

4.2 Semi-Empirical Theories

The earlier theories formulated by Salow (160), Bruining (11), Jonker (38) and Baroody (22) were all semi-empirical in nature. The above-mentioned division of the process of SEE, into two distinct steps of the energy loss of primaries and the consequent production of internal secondaries and the escape of these internal secondaries, made the calculations simpler.

Without paying much attention to the actual velocity distribution of internal secondaries, Bruining assumed that δ may be written as

$$\delta = \int n(x,E_p) f(x) dx \qquad (57)$$

where $n(x,E_p)$ is the average number of internal secondaries produced per incident primary of energy E_p, in a thickness dx, at a depth x below the surface, and f(x) the probability for such a secondary to escape from the surface. Whether the primary produces internal secondary electrons throughout its path in the material or merely near the end of a free path, is immaterial at this juncture.

In this analysis a few assumptions are made which make the

calculations easier, though not more accurate.

1) The primaries, for the present, are considered to be incident normally on the surface.

2) The primaries as they enter the solid move along straight lines, along the direction of incidence; this assumption thus neglects elastically and inelastically reflected primaries.

3) The production mechanism of internal secondaries and the emission processes are completely independent.

4) The velocity distribution of the internal secondaries may be completely ignored and only the number is to be considered.

5) The number of internal secondaries produced is proportional to the energy loss per unit path length of the primary electron

$$\text{i.e.} \qquad n(x,E_p) = -\frac{1}{\varepsilon_e}\frac{dE}{dx} \tag{58}$$

where $\frac{1}{\varepsilon_e}$ is the proportionality constant. ε_e may be considered to be the average excitation energy required to produce a secondary.

6) The probability, that an internal secondary produced at a depth x, may escape from the surface is determined, by an exponential absorption, without considering the physical processes involved.

$$\text{i.e.} \qquad f(x) = B\, e^{-\alpha x} \tag{59}$$

where α is the absorption coefficient and B, a constant.

Equation (57) may now be written as

$$\delta = -\frac{B}{\varepsilon_e}\int \frac{dE}{dx}\, e^{-\alpha x} dx \tag{60}$$

All the semi-empirical theories involve some form of this relation.

4.2.a Power Law (161)

This law assumes that the primaries lose energy in accordance with the equation

$$\frac{dE}{dx} = -\frac{A}{E^{n-1}} \tag{61}$$

where A is a constant, characteristic of the material and (n-1) an arbitrary power, i.e. the energy loss is inversely proportional to some power of the energy and hence the name "power law".

When integrated the equation (61) becomes

$$E^n(x) = E_p^{\,n} - Anx \tag{62}$$

If n = 2 we get

$$E^2(x) = E_p^{\,2} - 2Ax \tag{63}$$

This is the celebrated Whiddington's Law (162) used by Bruining, Baroody and Jonker in their calculations.

When the energy of the primaries becomes zero, i.e. when $E^n(x) = 0$, they have attained their maximum range x = R. Then

$$R = \frac{E_p^{\,n}}{An} \tag{64}$$

Substituting this in equation (62) we get in general

$$E^n(x) = An(R-x) \tag{65}$$

$$\frac{dE}{dx} = \frac{d}{dx}\left[(An)^{\frac{1}{n}}(R-x)^{\frac{1}{n}}\right] = \frac{(An)^{\frac{1}{n}}}{n}\left[-\frac{(R-x)^{\frac{1}{n}}}{(R-x)}\right]$$

Substituting in equation (60), we get

$$\delta = \frac{B}{\varepsilon_e} \int_0^R \left(\frac{An}{n}\right)^{\frac{1}{n}} \frac{(R-x)^{\frac{1}{n}}}{(R-x)} \cdot e^{-\alpha x}\, dx \qquad (66)$$

For purposes of integration, substitute

$$y^n = \alpha(R-x) \qquad (67)$$

Then

$$\delta = \frac{B}{\varepsilon_e} \left(\frac{An}{\alpha}\right)^{\frac{1}{n}} e^{-\alpha R} \int_0^{y_m} e^{y^n}\, dy \qquad (68)$$

where $y_m^n = \alpha R$ i.e. where $x = 0$.

Since we are interested in the dependence of δ on E_p, introduce

$$r^n = \alpha R = \alpha \frac{E_p^n}{An} \qquad (69)$$

Then

$$\delta = \left(\frac{B}{\varepsilon_e}\right) \left[\frac{An}{\alpha}\right]^{\frac{1}{n}} e^{-r^n} \int_0^r e^{y^n}\, dy \qquad (70)$$

$$\delta = \left(\frac{B}{\varepsilon_e}\right) \left(\frac{An}{\alpha}\right)^{\frac{1}{n}} G_n(r) \qquad (71)$$

which defines a new function $G_n(r)$. Ultimately, one wishes to express δ/δ_{max} in terms of $\frac{E_p}{E_{p_{max}}}$. So one has to maximise the equation (70).

Let r_m be the value of r, when δ becomes a maximum, δ_{max}.

Maximising the equation (70), it can be readily shown that

$$\delta_{max} = \frac{B}{\varepsilon_e} \left(\frac{An}{\alpha}\right)^{\frac{1}{n}} \left(\frac{1}{n\, r_m^{n-1}}\right)$$

$$= \frac{B}{\varepsilon_e} \left(\frac{An}{\alpha}\right)^{\frac{1}{n}} G_n(r_m) \qquad (72)$$

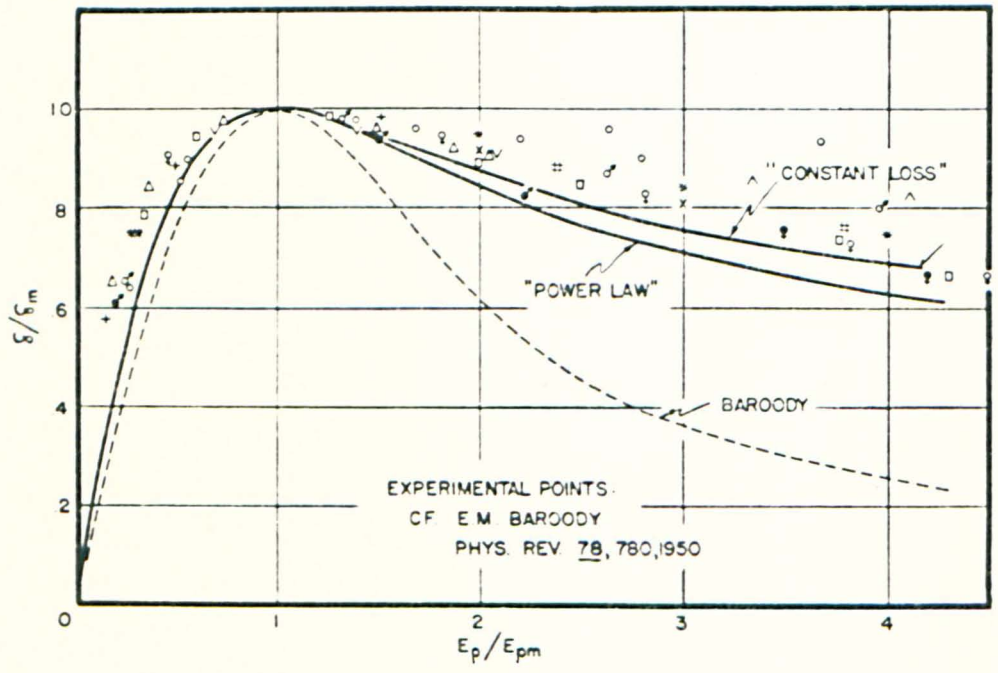
10
8
6
4
2
0
1
2
3
4
δ/δ_m
E_p/E_{pm}
"CONSTANT LOSS"
"POWER LAW"
BARODY
EXPERIMENTAL POINTS
CF E M BARODY
PHYS. REV. 78, 780, 1950

FIG. 33

By dividing (71) by (72) and substituting $r = \left(\frac{E_p}{E_{p_{max}}}\right) r_m$

$$\frac{\delta}{\delta_{max}} = \frac{G_n\left(\frac{E_p}{E_{p_{max}}} \cdot r_m\right)}{G_n(r_m)} \tag{73}$$

Thus the result of introducing reduced variables is to eliminate all those constants A, B, ε_e, which are characteristic of the material. If all materials had the same value of n, the reduced yield curves should all follow a single "universal curve". This fact was pointed out first by Baroody (22). Like Bruining, Baroody assumed n = 2; i.e. he assumed Whiddington's Law. Bruining found the value of $r_m = 0.92$. So for n = 2, equation (73) becomes

$$\frac{\delta}{\delta_{max}} = 1.85\, G_2(0.92\, E_p/E_{p_{max}}) \tag{74}$$

Baroody's universal yield curve, from equation (74), is shown in fig. 33. It can be seen that there is serious deviation from the experimental universal yield curve, particularly for values of $E_p/E_{p_{max}} > 1$. This indicates that perhaps the value n = 2 is too high.

From equation (69) it can be seen that

$$E_{p_{max}} = \left(\frac{2A}{a}\right)^{\frac{1}{2}} r_m \tag{75}$$

if Whiddington's law is assumed. The value of r_m, according to Bruining, is 0.92. Becker (37), from his study of transmission of electrons through thin nickel films found a value for $a = 1.5 \times 10^6 \text{cm.}^{-1}$. Terrill (163) from his experiments got a value for $2A = 3.5 \times 10^{12} (\text{eV})^2/\text{cm}$ Substituting these values in equation (75), $E_{p_{max}} = 1420\text{eV}$ for nickel whereas the experimental value is only 500eV.

4.2.b Jonker's Modification (38)

Considering the large disagreement between the experimental results and the theoretical predictions Jonker attempted to modify the above theory. However, he too assumes Whiddington's law, for the rate of energy loss of primary electrons. He assumes that the internal secondaries move in straight lines from their point of origin towards the surface. The distance the electron has to travel before reaching the surface must be measured from the point of origin to the surface, along the direction of flight. Thus, an electron originating at a depth x, below the surface, but moving at an angle ϕ , to the normal to the surface, has to travel a distance $\frac{x}{\cos\phi}$. In considering the probability of escape of secondaries, in equation (59), x has to be replaced by $x/\cos\phi$. Further, he assumes that the internal secondaries produced, at any point in the medium, are isotropically distributed. Taking into account these factors, he derives a universal yield curve, which is an improvement on Baroody's curve. However, the deviation from the experimental curve is quite considerable.

Jonker extends the theory to the case, where the primary beam is incident on the surface, at an angle θ to the normal. In such a case, internal secondaries dislodged at a distance x, on the path of the primary electrons, are located only at a distance $x \cos\theta$, and accordingly the absorption factor in equation (59) becomes $\exp(-\alpha x \cos\theta / \cos\phi)$. Consequently he derives the relation

$$E_{p_{max}} = r_m \left(\frac{2A}{\alpha \cos\theta}\right)^{\frac{1}{2}} \qquad (76)$$

He finds good agreement between this relationship and his measurements on nickel, nickel carbide and lithium. Also he finds a relationship between δ_{max} and θ. Above all, pursuing the same lines as the theory given above, Jonker gets a theoretical universal yield curve, valid for all materials and for all angles of incidence.

Considering the large deviation of the theoretical curve, obtained by using the power law for energy loss, from the experimental curve, one begins to wonder if a power law for $\frac{dE}{dx}$ is valid at all. If so, one expects that n should be less than 2.

4.2.c The "Constant Loss" Theory

In earlier studies, the quadratic dependence of E_p, on the range R, - Whiddington's law - has been investigated by studying very fast electrons transmitted through thin films. For low energy electrons ($100eV < E_p < 10keV$) the result obtained from the study of high energy electrons is simply extrapolated.

However, Young, in 1956 (39) performed transmission experiments through thin uniform layers of Al_2O_3, using electrons of energy in the range 0.3 to 7.25keV. He found from his experiments, that the practical range R, of electrons in Al_2O_3, follows the relationship

$$R = 0.0115\ E_p^{1.35} \qquad (77)$$

where R is in mg/cm^2 and E_p in keV.

Young's results are in good agreement with those obtained by Hoffmann (164). It is also interesting to compare the values of the

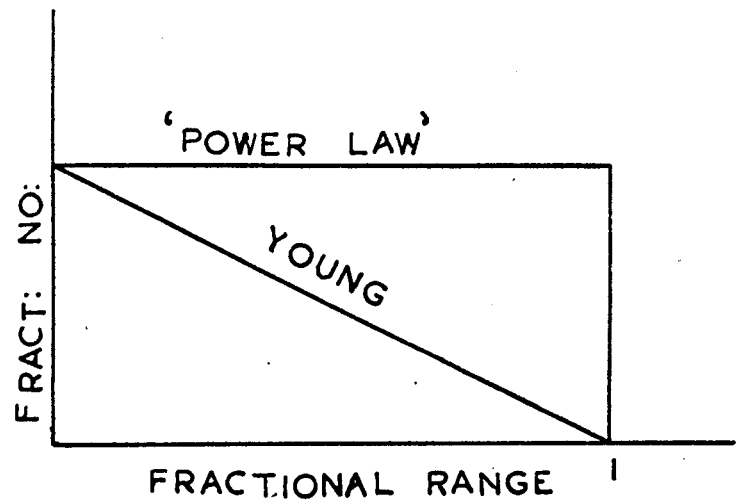

FIG. 34

Idealised representation of Young's transmission results

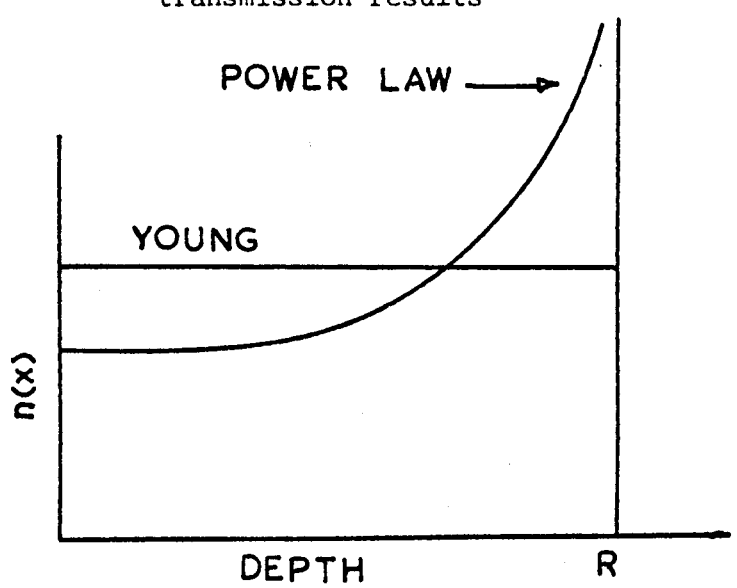

FIG. 35

Energy dissipation according to Young (39)

range, obtained by Bronshtein and Segal (4,5). They found that, for Be, $R \propto E_p^{1.5}$ and for Bi, $R \propto E_p^{1.4}$. Since Young's experiment covers the energy range which is of particular interest to the secondary emission studies, it is more appropriate to use a value $n = 1.35$ in equation (64) for the range of primaries, rather than using Whiddington's law.

In his experiments, Young also makes it clear that some of the tacit assumptions of the previous theory are wrong. In the "power law" theory, it is assumed that the range of all primaries measured along the direction of incidence is the same, as shown in fig. 34. But from his experiments, he finds that the transmitted fraction of electrons decreases approximately linearly with the fractional range (fig. 34). It is, hence, imperative that the scattering of primaries be considered.

In addition, according to the "power law" theory, the energy loss of the primary beam per unit path length, dE/dx, increases with decreasing energy. Since the production function of secondaries, $n(x, E_p)$ is proportional to $\frac{dE}{dx}$, it increases rapidly near the end of the primary range as shown in fig. 35. Thus the "power law" implies that more electrons are produced deeper down in the metal. Young's experimental evidence directly opposes this. He finds that the energy dissipation is approximately constant throughout the range. Thus, one can call a theory based on these facts, a "constant loss" theory.

Assuming the validity of Young's results one can modify the elementary theory of SEE so as to account for the scattering of the primaries. One needs only replace $-\frac{dE}{dx}$ in equation (60) by its

effective value $\frac{E_p}{R}$, and integrate between 0 and R.

Thus the yield equation is

$$\delta = \frac{B}{\varepsilon_e} \frac{E_p}{R} \int_0^R e^{-\alpha x} dx \qquad (78)$$

Assuming the range-energy relation of the primaries to be of the form given in equation (64) and proceeding as in section 4.2.a, one gets

$$\delta = \frac{B}{\varepsilon_e} \left(\frac{An}{\alpha}\right)^{\frac{1}{n}} g_n(z) \qquad (79)$$

where $z^n = \alpha R$ and $g_n(z) = \frac{1 - \exp(-z^n)}{z^{n-1}}$

The reduced yield curve is of the form

$$\delta/\delta_{max} = \frac{g_n\left(z_m \cdot \frac{E_p}{E_{pmax}}\right)}{g_n(z_m)} \qquad (80)$$

A plot of this "constant loss" reduced yield curve is given in fig. 33, for a value n = 1.35. It is seen that the agreement is better than the "power law" curve.

4.2.d Sternglass' Theory

None of the above theories, takes into account the elastically and inelastically scattered primaries. Sternglass (165) has developed a theory of SLE which takes into account the inelastically reflected fraction, η . Despite all the oversimplified assumptions made by him, it is interesting in that the theory brings out the relationship between SEE and atomic shell structure. He, however, employs many of the assumptions made in section 4.2.a. But according to him, the scattering

of the primary electron beam is so strong, that an initially parallel beam quickly fans out and loses its original direction. He argues that beyond a certain depth, the primaries diffuse at random. This characteristic mean depth λ_{sp}, corresponds to a depth for which the total angle of deflection is approximately $\pi/2$ relative to the direction of the incident primaries. Thus λ_{sp} is essentially the momentum-loss mean free path and is a function of the primary energy. He then simplifies the theory by assuming that all secondaries are produced at this mean depth λ_{sp} and in the equation (60), x is replaced by λ_{sp} and in the equation (60), x is replaced by λ_{sp}.

At this point he introduces the inelastic reflection coefficient η, and a factor k, representing the mean fractional energy of these electrons with respect to the primary energy. He thus obtains

$$\delta = \frac{B}{\epsilon_e} (1 - \eta k) E_p e^{-a\lambda_{sp}} \qquad (81)$$

Next, he uses the Bethe expression (166) to arrive at the dependence of λ_{sp} on E_p,

$$-\frac{dE}{dx} = \frac{(2 \pi Ne^4)}{E} \sum_{n,l} Z_{n,l} \ln\left(\frac{2E}{I_{n,l}}\right) \qquad (82)$$

where N, is the number of atoms per unit volume, $Z_{n,l}$ the number of electrons in the shell n,l and $I_{n,l}$ the binding energy of the electrons in the shell n,l. He calculates $a\lambda_{sp} = \beta E_p^{\frac{1}{2}}$ (83)

where β is a constant.

Thus substituting in equation (81) he gets

$$\delta = \frac{B}{\epsilon_e} (1 - \eta k) E_p \exp(-\beta E_p^{\frac{1}{2}}) \qquad (84)$$

where β contains the term $\sum_{n,l} Z_{n,l}/\sqrt{I_{n,l}}$. This indicates the importance of the role of the inner atomic shell in SEE. To prove the validity of equation (84) Sternglass plots a graph of $\ln(\delta/E_p)$ versus $E_p^{\frac{1}{2}}$ which ought to give a straight line. For silver he finds good agreement in the range between 150eV and 1500eV. Finally, Sternglass derives the reduced yield curve of the form

$$\delta/\delta_{max} = \frac{E_p}{E_{p_{max}}} \exp\left[2\left\{1 - \left(\frac{E_p}{E_{p_{max}}}\right)^{\frac{1}{2}}\right\}\right] \qquad (85)$$

According to Sternglass, the agreement between (85) and the experimental curve is very satisfactory.

The fact that Sternglass takes into account the inelastic reflection coefficient η, is certainly an improvement upon the previous theories. Recent experiments (4,5) suggest that a substantial number of true secondaries can be produced by the inelastically reflected primaries. The effectiveness of this fraction of electrons η, has been calculated by Dobretsov and Matskevich (84) and a theory which takes into account this fact has recently been developed by Izmailov (167). Some of the conclusions drawn by Izmailov are surprising. He does not agree to the whole concept of a "universal curve". Since the true yield is partly due to the inelastically reflected primaries η, which in turn varies with energy, the author rejects the idea of a universal curve, even though the shapes of such curves may be similar.

4.3 "Free Electron" Theory

An alternate theory has been put forward by Kadyschevitsch (168) and by Baroody (22) on the basis of the Sommerfeld model of a "free electron" gas. According to this theory secondary electrons are produced by collision processes with conduction electrons of the metal, which are effectively "free". The secondary electrons thus produced undergo multiple eleastic collisions so that a certain fraction of them are eventually able to escape from the surface.

4.3.a Kadyschevitsch's Theory

Kadyschevitsch's line of argument is as follows. He assumes that the number of bound electrons which can be emitted as secondary electrons is negligible and hence one needs only take into account the interaction between the primary electrons and the "free" conduction electrons.

A relatively fast primary electron thus encounters an effectively free electron and communicates momentum to it in a direction normal to the primary direction of motion. If the primary direction is perpendicular to the metal surface, the secondary electron produced in this way will never be moving in a direction to enable it to leave the surface, no matter how energetic it may be. However, the secondary may suffer an elastic collision with a lattice ion, so that, while retaining its energy the direction of motion is changed. Now its energy normal to the surface may be sufficient to take it out of the metal.

Kadyschevitsch calculates the probability that a primary at a depth x within the metal, moving at an angle θ to the normal, will

transfer sufficient energy to a secondary, so that if it continued moving freely, it would leave the surface of the metal. This obviously vanishes when $\theta = 0$. In the actual case, the collisions of primaries and secondaries are to be accounted for. If Λ_1 is the mean free path of the primaries for all types of collisions within the metal, then the probability of a primary reaching a depth x, without suffering a collision will be $\exp(-x/\ \Lambda_1 \mathrm{Cos}\ \theta)$. Taking Λ_2 to be the mean free path of the secondaries, a similar expression will give the probability of a secondary leaving the metal without undergoing a collision which would prevent it from escaping from the surface.

The mean free paths are written as

$$\frac{1}{\Lambda_1} = \frac{1}{\lambda_1} + \frac{1}{l_1} \quad ; \quad \frac{1}{\Lambda_2} = \frac{1}{\lambda_2} + \frac{1}{l_2} \tag{86}$$

where λ_1 and λ_2 are the mean free paths for inelastic collisions with the metal electrons and l_1 and l_2 those for elastic collisions with lattice ions. Whereas, λ_1 and λ_2 reduce the secondary emission, by reducing the energy of primary and secondary, l_1 and l_2 can give rise to a finite probability, that true emission will occur even if $\theta = 0$. Kadyschevitsch calculated the probability that a secondary produced at a depth x, suffers one or more elastic collisions, which deviates it finally without energy loss into a suitable direction which enables it to leave the front surface of the metal. Making further calculations, he finds an expression for the yield at normal incidence

$$\delta = \frac{0.13\ \pi\ \Lambda_1\ \Lambda_2^2}{l_2 E_p(\ \Lambda_1 + 0.56\ \Lambda_2)} \tag{87}$$

As a rough approximation Λ_2 may be taken to be independent of energy for slow secondaries and Λ_1 proportional to E_p^2. This leads to a reduced yield curve of the form

$$\frac{\delta}{\delta_{max}} = \frac{2(E_p/E_{pmax})}{1 + (E_p/E_{pmax})^2} \qquad (88)$$

The theory has been extended to calculate the variation of δ with the angle of incidence of primaries and the energy distribution of secondaries in energy and direction.

In comparing Kadyschevitsch's theory, with experiment, it will probably fail at high energies because of the interaction of the primaries with the core. Also, at lower energies the assumption that Λ_1 is proportional to E_p^2 is no longer true.

4.3.b Baroody's Theory

Baroody uses the Sommerfeld model, to formulate a theory of SEE. Since the temperature dependence of SEE from metals is negligible, Baroody treats the electrons as a completely degenerate Fermi-Dirac gas at absolute zero temperature. So in the momentum space, all states within a sphere of radius P_F about the origin (the momentum corresponding to the Fermi energy $\zeta_o = \frac{P_F^2}{2m}$) are occupied, while states of greater momentum are empty.

Baroody assumes the path of the primary to be straight, and the velocity of the primary, v, to be large compared to the velocity of the conduction electrons. The primaries collide with these electrons and impart momentum to them. To calculate the momentum transferred,

in such a collision, he assumes a simple Coulomb force between a primary and a conduction electron. At this point it may be remarked, that the assumption of a simple Coulomb force in the case of metals is not quite correct. The simple reason is that the highly mobile conduction electrons tend to prevent the field around the extra primary electron from penetrating far into space. Thus an exponentially decreasing screened potential would give a better representation, as has been noted by Bohm and Pines (49-51) and others. Assuming the simple Coulomb interaction, the momentum transferred to the conduction electron, in a direction perpendicular to the primary path is calculated to be

$$\Delta P = \frac{2e^2}{v\rho} \tag{89}$$

where e - the electronic charge

v - velocity of the primary electron

ρ - the distance of closest approach

between the two electrons.

So the effect of a passing primary on all the conduction electrons at a distance ρ, is to shift the centre of momentum sphere by ΔP. From this it is possible to calculate the number of secondaries produced $N(\mu, x)$, per unit primary path at a depth x, for which the momentum is larger than μP_f, where μ is an arbitrary factor. If the electrons are to be emitted from the surface $\mu > 1$.

Baroody finds:

$$N(\mu, x) = \frac{B\zeta_o^2}{E(x)(\mu^2-1)} \tag{90}$$

where E(x) is the primary energy at a depth x

$$B = 2.95 \times 10^{8} (eV)^{\frac{1}{2}} \text{ cm.}^{-1}$$

From equation (90) one sees that the number of internal secondaries produced with energy close to the Fermi energy ($\mu \simeq 1$) becomes very large and for $\mu = 1$ becomes infinite. This is a consequence of the Coulomb law assumption, because the interaction with electrons far away from the primary, corresponding to a large value of ρ , leads to small energy loss. Introduction of the above-mentioned screened Coulomb field would remove this difficulty.

In order to calculate E(x), Baroody uses Whiddington's law

$$E^2(x) = E_p^{\,2} - 2Ax \tag{91}$$

Substituting (91) in equation (90) and differentiating one gets the number of secondaries produced per primary in a slab dx, and with a momentum between μP_F and $(\mu + d\mu)P_F$

$$N(\mu, x)d\mu dx = \frac{2B\,\zeta_\sigma^{\frac{1}{2}}\,\mu d\mu dx}{(E_p^2 - 2Ax)^{\frac{1}{2}}(\mu^2 - 1)} \tag{92}$$

In order to discuss the yield, Baroody introduces two mean free paths λ_s and λ_a. λ_s refers to the scattering of secondaries by lattice vibrations and λ_a refers to inelastic collisions with other electrons i.e. "absorption". λ_a and λ_s correspond to Kadyschevitsch's λ_2 and l_2. Baroody then considers two extreme cases $\lambda_s >> \lambda_a$ and $\lambda_s << \lambda_a$. He finds that both cases in a first approximation, result in the same dependence of the yield on primary energy. He then derives the reduced yield curve to be

$$\frac{\delta}{\delta_{max}} = 1.85\, F\left(0.92\, \frac{E_p}{E_{p_{max}}}\right) \tag{93}$$

This is of the same form as the reduced yield in the semi-empirical theory.

One interesting outcome of Baroody's theory is the dependence of δ_{max} on ϕ - the work function. He finds $\delta_{max} = (0.35\ \phi)^{\frac{1}{2}}$ where ϕ is in eV. It may be mentioned, however, that the work function is brought into the theory through the production mechanism of secondaries rather than the escape mechanism. If $\mu_o P_F$ is the minimum momentum perpendicular to the surface, required by an electron, to escape from the surface,

$$\mu_o^2 P_F^2/_{2m} = \zeta_o + \phi \tag{94}$$

or

$$\zeta_o = \frac{\phi}{(\mu_o^2 - 1)} \tag{95}$$

Comparing equations (92) and (95), the number of secondaries produced is proportional to $\zeta_o^{\frac{1}{2}}$ and hence proportional to $\phi^{\frac{1}{2}}$.

Baroody's theory also permits one to calculate the energy distribution of the secondaries, the results of which are in agreement at least qualitatively. He finds theoretically, a secondary maximum to occur at an energy of 0.7 ϕ in most cases.

4.4 Wave Mechanical Theory

All the semi-empirical theories, though yielding reasonable agreement with the experimental results in some cases, approach the problem without any considerable regard to the physical processes involved. In addition some of the assumptions made, are far too oversimplified. Baroody in his theory, for example, assumes that the incident primary electrons interact only with the "free" conduction electrons.

Fröhlich (169) points out that a completely free electron gas cannot produce secondary emission, since conservation of energy and momentum for the system consisting of the incident electron plus the free electron gas will make it impossible for secondaries to be emitted in a direction opposite to the direction of incidence of the primary.

To improve upon the previous theories a wave mechanical theory has been developed by Fröhlich (169), Woodridge (42), Dekker and van der Ziel (170). There have been a number of modifications to the theory by many investigations (171, 172). A brief account of their method of approach only will be given here.

In this theory the lattice electrons are represented by Bloch functions (7) of the type $U_k(r)e^{i(k.r)}$ where k is the wave vector, r the positional co-ordinates and the function $U_k(r)$ has the period of the lattice. Woodridge (42) considers the primary electron to be free, owing to its large velocity. It may be then represented by a plane wave of the type, exp i(K.R) where K is the wave vector and R the positional co-ordinates, of the primary electron. The effect of the primary beam of electrons is a perturbation on the lattice electrons, this inducing transitions of the latter to higher energy states. Hence the basic problem, in the theory of production of secondaries, consists of calculating the number of transitions per unit time $P(K,k \rightarrow K^1,k^1)d\Omega'$, where K^1 and k^1 represent the wave vectors of the particles after collision and $d\Omega'$ the solid angle into which the primary is scattered.

The immediate problem arising is to find out the perturbation potential due to the interaction of the primary and lattice electrons.

The simple Coulomb law of force, which gives

$$V(R, r) = \frac{e^2}{|R - r|} \tag{96}$$

has been used by many authors (42, 169, 170). However, in the evidence of the plasma theory, this simple law does not hold good, in the case of metals. In a metal, the "extra" primary electron has a tendency to push the conduction electrons away from it. This results in the formation of local space charges, which effectively screen the field of the primary, at long range. Hence a screened potential should be expected in metals, as borne out by the plasma theory. In that theory the interaction between a primary and the lattice electrons is split into two parts.

1) An "organised" part consisting of the long range interaction with the electron gas as a <u>whole</u>, resulting in plasma oscillations and the emission of electrons which have lost discrete amounts of energy. This has already been discussed in Chapter 3.

2) An "unorganised" short range part consisting of interaction with the <u>individual</u> lattice electrons. This part is more relevant in the present case. This is represented by a screened potential of the type (173)

$$V(R, r) = \frac{e^2}{|R-r|} \exp\left[-\lambda(R - r)\right] \tag{97}$$

where λ, the screening parameter, is determined by the properties of the electron gas and is of the order of 10^8 cm.$^{-1}$, for metals.

The significance of such a screened potential is uncertain

according to some authors. Neufield and Ritchie (174) conclude that the above formula is not applicable where the velocity of the incident primary electron is large compared to the root mean square velocity of the plasma electrons. Also according to Fröhlich (175) the use of a screening factor independent of energy is incorrect for the range between 50eV and 1 keV. Recently, Baroody (172) extended the theory of Dekker and van der Ziel (170) with an unscreened Coulomb potential.

However, assuming the simple Coulomb law, Dekker and van der Ziel (170) first calculate the transition probability from the state corresponding to k, K to k^1, K^1. Furthermore, they find an expression for the transitions per unit time as

$$P(K,k \rightarrow K^1, k^1)d\Omega' = \frac{4m^2e^4K^1}{K\hbar^4 q^4} |I|^2 d\Omega' \qquad (98)$$

where $q = K-K^1$ and I is defined by the integral

$$I = \int_e^{i(q.r)} \psi_k(r) \psi_{k1}(r) dr \qquad (99)$$

Non-zero transition probability between the two states exists if $E^1 - E = 0$. i.e. the energy of the system is conserved. The selection rule governing the momenta is given by

$$K + k - K^1 - k^1 + 2\pi H = 0 \qquad (100)$$

where H is the reciprocal lattice vector. This is simply an expression for the conservation of momentum.

When a screened potential of the type given in equation (97) is used instead of a simple Coulomb interaction, van der Ziel shows that the only modification is that q^4 in equation (98) is replaced by $(q^2 + \lambda^2)^2$ where λ is the screening parameter.

Van der Ziel shows that for metals the transitions for which

$H \neq 0$, contribute very little to the production of secondaries. Consequently Woodridge's theory which lays so much emphasis on the bound electrons, loses much of its attradtion. Marshall (171) and Baroody (172) support this conclusion, at the same time justifying Baroody's free electron theory of SEE. For Baroody's free electron model $H = 0$ and $\lambda = 0$.

The energy loss suffered by the primary electron, calculated on the basis of $H = 0$ leads to a Bethe-type law (166)

$$-\frac{dE}{dx} \simeq \frac{\pi N e^4}{E} \log \left(\frac{E}{e_x E_\lambda}\right) \qquad (101)$$

where N is the number of conduction electrons/cc.

e_x is the base of natural logarithm

$E_\lambda = \frac{\hbar^2 \lambda^2}{2m} \simeq 40\text{eV}$ for $\lambda \simeq 10^8$ cm.$^{-1}$

Thus since the logarithm varies slowly with E, Whiddington's law is a good approximation.

The above approach gives an account of the production of internal secondaries in the metal. But to account for the secondary electrons emitted from the metal surface, it is necessary to study the escape mechanism of the internally produced secondaries. This could be done in a simplified manner on the basis of the assumptions made by Baroody.

Wolff (176) is strongly opposed to the idea of "lumping the process into an effective absorption coefficient α , for the internal secondaries". He is of the opinion that the escape mechanism is more important than the production of these internal secondaries.

Wolff gives a theory of electron cascade process in which these secondaries diffuse through the solid, multiplying and losing energy "en route", until they either are emitted as true secondaries or return to the sea of conduction electrons. He observes that the energy losses suffered by the cascade electrons, are due mainly to their interaction with the conduction electrons. Since the temperature has little effect on SEE, electron-phonon interactions are very much less important than electron-electron collisions. He uses a screened Coulomb field to describe the electron-electron interaction. In order to describe the electron cascade process, he uses the same equation as used by Marshak (177), for neutron absorption. He proceeds to solve the transport equation describing the electron cascade process within the metal, using a number of simplifying assumptions and arrives at a theoretical curve for the energy distribution of the emitted secondaries. He then normalises the theoretical curve to the same area as experimental ones. His results are good fits with the alkali metals.

Besides studying the energy distribution of the secondaries, he is able to obtain an expression for the total yield and also a relationship between the total yield and the work function.

The quantitative agreement is not outstanding!

4.5 Conclusion

One can thus see that there exists a large number of theories on SEE, each with somewhat different assumptions and variations upon the working model, and all seem to have some merits. Earlier theories,

though semi-empirical, seem to account satisfactorily for the reduced yield curve. These theories do not bother about the actual physical processes involved. On the other hand wave mechanical theories, while trying to give an insight into such processes, fail to provide reasonable agreement with experimental results.

Most theories fail in giving a correct energy distribution of the secondaries. Wolff's cascade theory in general accounts for the shape. The experimental evidence of Auger processes in SEE, suggests that probably the distribution is made up of pieces of Wolff's cascade process and the Auger process. In addition, there are many other phenomena like "plasma oscillations", which are too complex, perhaps, to be covered by a single theory.

CHAPTER V

The Present Experimental Investigation

5.1 Introduction

Most of the previous studies on secondary electron emission have been done in glass systems under comparatively poor vacuum conditions. Under such conditions, the target surfaces become contaminated quickly and consequently the emission properties are affected. It is thus not surprising that there exists large discrepancies in the results obtained by different authors. Hence, it is essential to perform the experiment in ultra-high vacuum conditions, if one wishes to obtain reproducible results, genuinely characteristic of the material investigated. In the present investigation, which has formed part of a programme of research on SEE with the support of the Ministry of Defence, the total yield δ, of a number of substances under ultra-high vacuum conditions has been measured. In particular, owing to the lack of sufficient quantitative data on the variation of the yield with the angle of incidence of primaries, this aspect has received special attention. Yield measurements have been made on silver, nickel, bismuth, platinum and tantalum carbide. Though the yields of the first four materials have been measured before, angular dependence has been studied only for nickel. Tantalum carbide, which is favoured as a low yield material (section 2.3) has not been studied before.

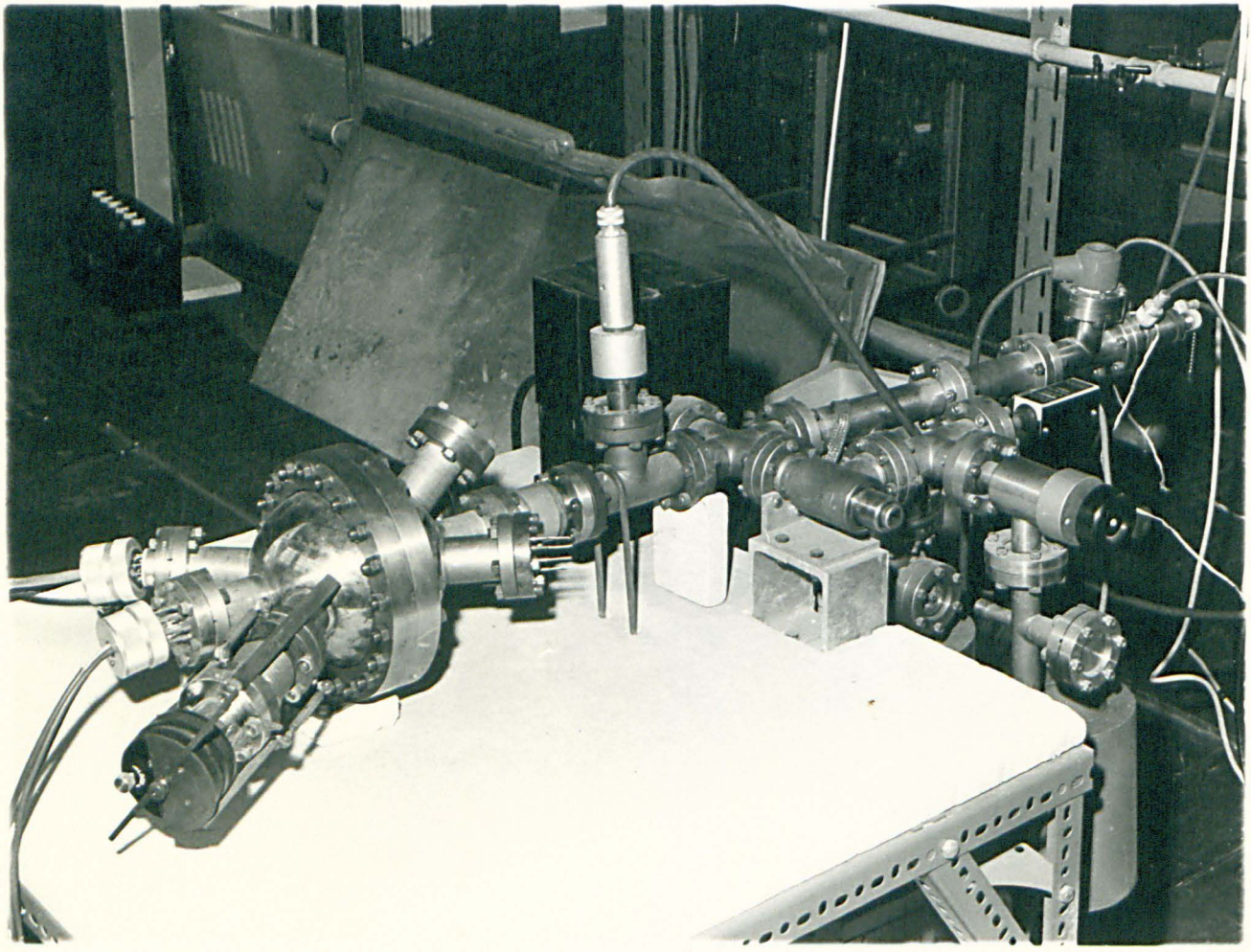

FIG. 36

In the light of the recent advances in the theory of characteristic energy losses, plasmons etc., measurements in this field are particularly important, especially in controlled environmental conditions, where the importance of surface aspects can be studied. A particular feature of the present experimental apparatus is that it can be made to serve the dual role of yield measurement and accurate measurement of characteristic energy losses, using the retarding field method coupled with electronic differentiation. This is perhaps the first time such a technique has been used in the studyof the characteristic energy losses of electrons. The materials investigated include Silver, Bismuth, Beryllium, Tantalum and Tantalum Carbide. Though the first three materials have been investigated before, using different techniques, there are large discrepancies in the results from author to author. In the process of studying TaC, it was felt necessary to study Ta as well, to see if there is any correlation between the energy losses of the element and compound. All the present investigations have been conducted in ultra-high vacuum conditions.

5.2 Experimental Apparatus

The experimental apparatus consists mainly of a spherical manifold made of stainless steel (fig. 36) attached to which there are appendages for an electron gun, molecular gun and feedthroughs for the various electrical connections to the target, and the heating filament used to outgas the target. There is also a viewing port. Inside the spherical manifold is a spherical suppressor grid, made of tungsten mesh.

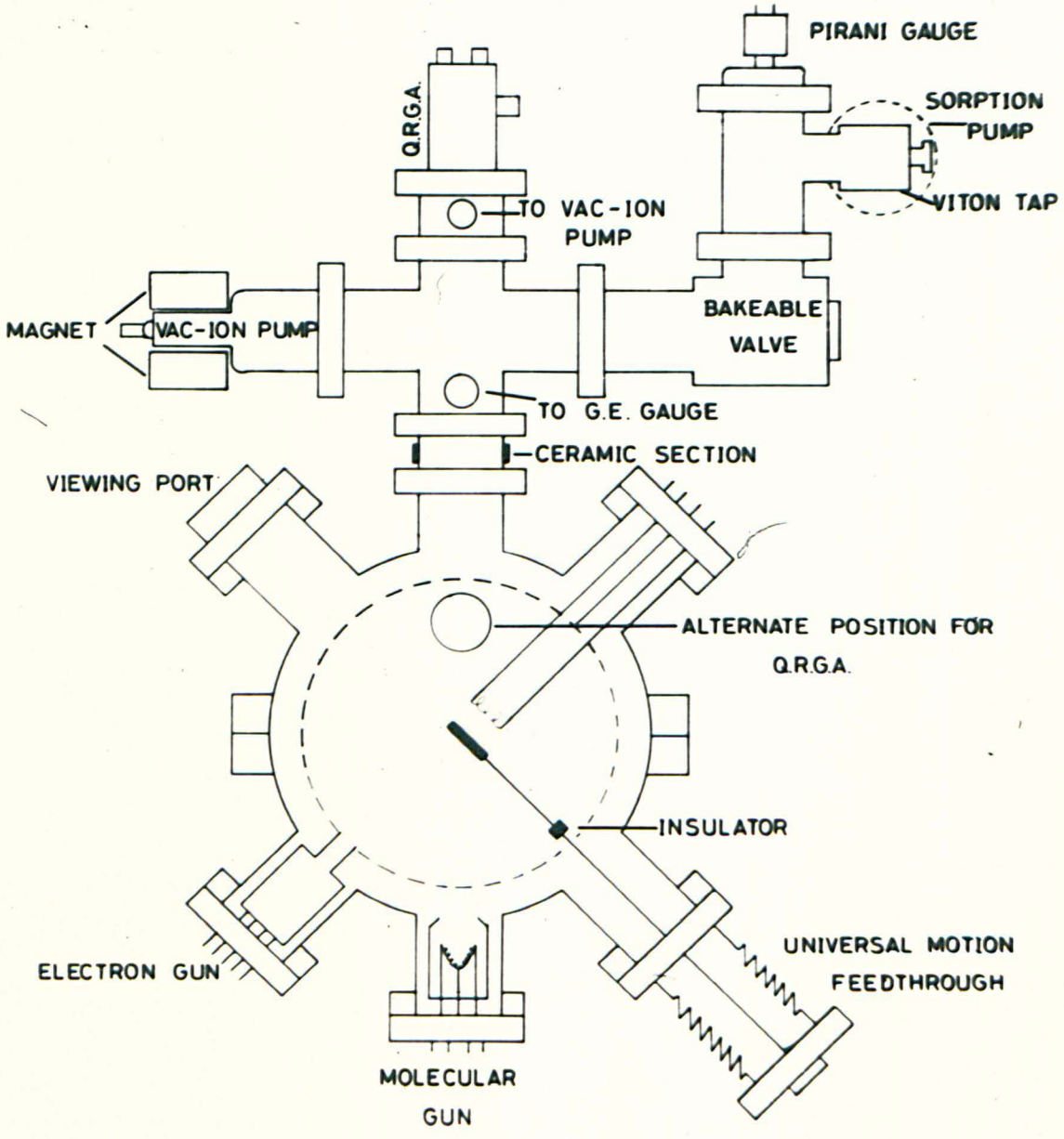

FIG. 37 SCHEMATIC OF THE EXPERIMENTAL SET-UP.

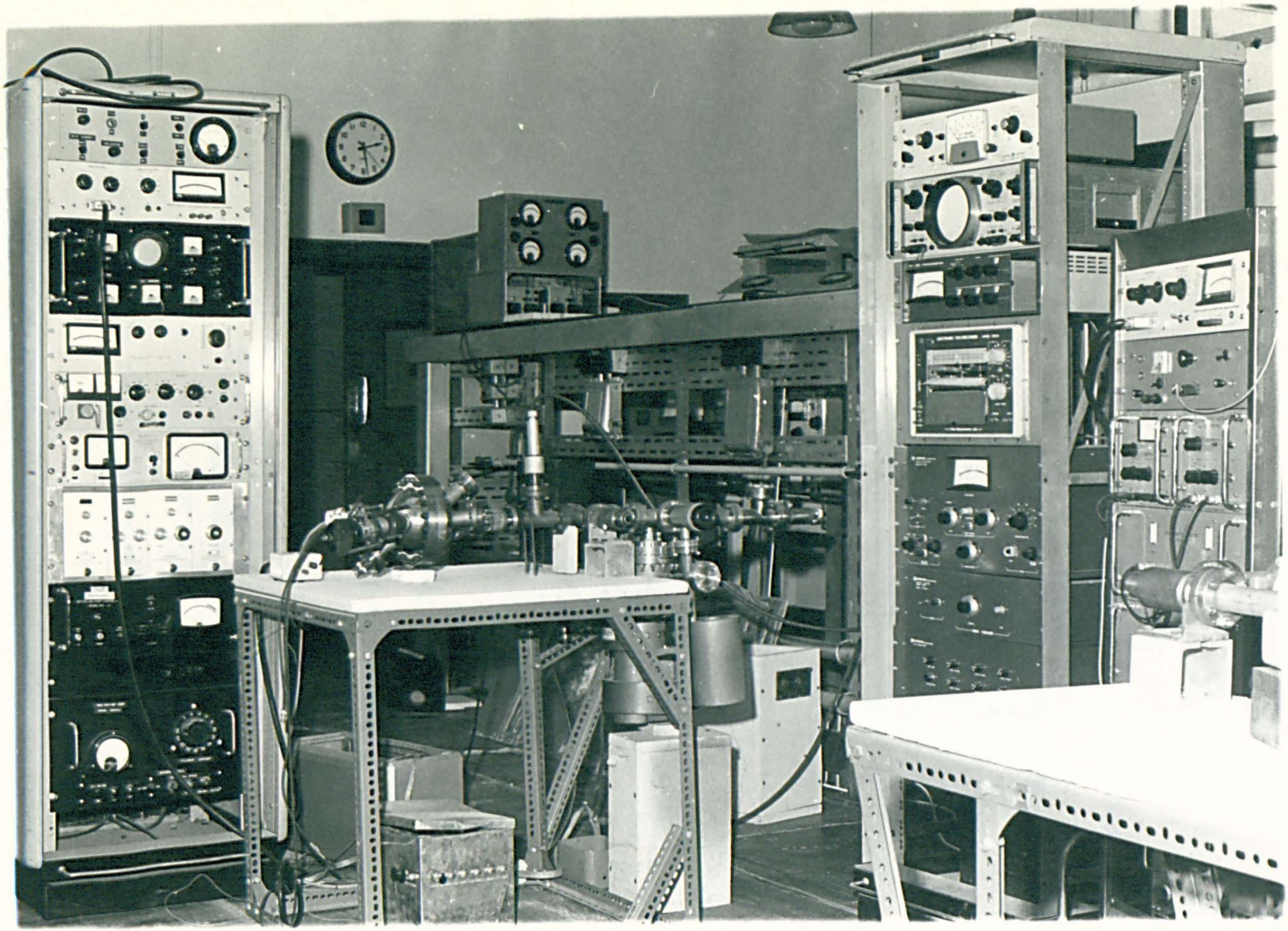

FIG. 38

This is used to suppress the tertiary electrons from the collector, in the measurement of the total yield and in the energy distribution studies it is used as the retarding field electrode. The target is positioned at the centre of the sphere by a "universal motion" feed-through. A schematic diagram is given in fig. 37 which gives the relative positions of the various components.

The system is pumped from atmospheric pressure to $\sim 10^{-3}$ torr by a Sorption pump, the pressure being measured by a Pirani gauge. The system is then isolated and pumped to lower pressures by two Vac-ion pumps. These lower pressures are measured by a General Electric triggered discharge gauge and the quadrupole residual gas analyser, which was incorporated, as the name suggests, in order to have a knowledge of the residual gases present in the system. In addition, there are power supplies for the electron gun, Vac-ion pumps and for thin film deposition. Two electrometers are used to measure the target current and collector current. Each one of the essential components will be described below. A general view of the whole set-up is shown in the photograph (fig. 38).

5.2.a Vacuum System

Owing to the known adverse effects of contamination on secondary emission properties, it is imperative that any reliable study should be made in ultra-high vacuum conditions. In the present investigation special emphasis has been laid on this aspect and all measurements have been made in a clean ultra-high vacuum. The materials used in

constructing such a system satisfied several fundamental criteria. These included low vapour pressure, chemical inertness, impermeability to gases and ease of manipulation. Taking into account these factors, a stainless steel system was preferred to a glass system. Most earlier workers have used glass systems. Recent experiments (178) in surface physics have cast some doubts on the suitability of glass as a material for ultra-high vacuum systems. Glass has been proved to be a source of contamination. It has been shown to decompose when baked at over 350°C, giving off products containing N^+ and K^+ ions. To minimise the effects of residual magnetism on slow electrons, the stainless steel chosen for the construction of the present system was EN 58 ELC. This particular steel also has a low carbon content, thus minimising the possible production of CO_2/CO from carbon which can under certain circumstances migrate to the surface during baking and combine with the residual oxygen atoms.

The spherical manifold, which acts as the collector of secondary electrons, has a diameter of 6 inches and is formed of two hemispherical halves. The appendages for electron gun, molecular gun, and electrical feedthroughs, have an outer diameter of $1\frac{1}{2}$". They were argon-arc welded onto the sphere. The spherical manifold is electrically isolated from the rest of the system by a ceramic insulating section. All connections of the vacuum system used "Varian" type "conflat" flanges. The two hemispheres, constituting the spherical manifold, also are sealed together with two such large diameter conflat flanges welded onto the two halves.

In selecting the pumps used, the conventional rotary pumps and diffusion pumps were rejected owing to their inherent snags of backstreaming of contaminating vapours. Even though this may be reduced to a minimum by several traps or complicated baffles, in addition to the fact that the pumping speed is reduced, the vacuum still is not absolutely devoid of contaminants. Sternglass (52) reports that when an oil diffusion pump is used, a film of amorphous carbon builds up on the target under electron bombardment. The solution in any static system is to do away with rotary pumps and diffusion pumps. The rotary pump is replaced by a "sorption" pump and a Vac-ion pump takes the place of the diffusion pump.

The sorption pump can take the pressure in the system from the atmospheric down to 10^{-3} torr or less. The pumping action of the sorption pump is achieved by the sorption of gas molecules by a chilled molecular sieve - a processed mixture of oxides of aluminium and silicon. Liquid nitrogen is used as the chilling agent. After a pump-down is completed, it is sufficient to warm it up to room temperature for a fresh cycle, thus letting the pumped gas escape. The advantages of the sorption pump are that, besides being devoid of any pump oil, it has no moving parts, operation is free from noise and vibration, and no power supply is required.

The getter-ion pump consists of a titanium anode of honeycomb structure positioned equidistant from two titanium cathodes. The action of the ion-pump depends on the formation of a cold cathode discharge which produces active sputtered titanium. The permanent removal of

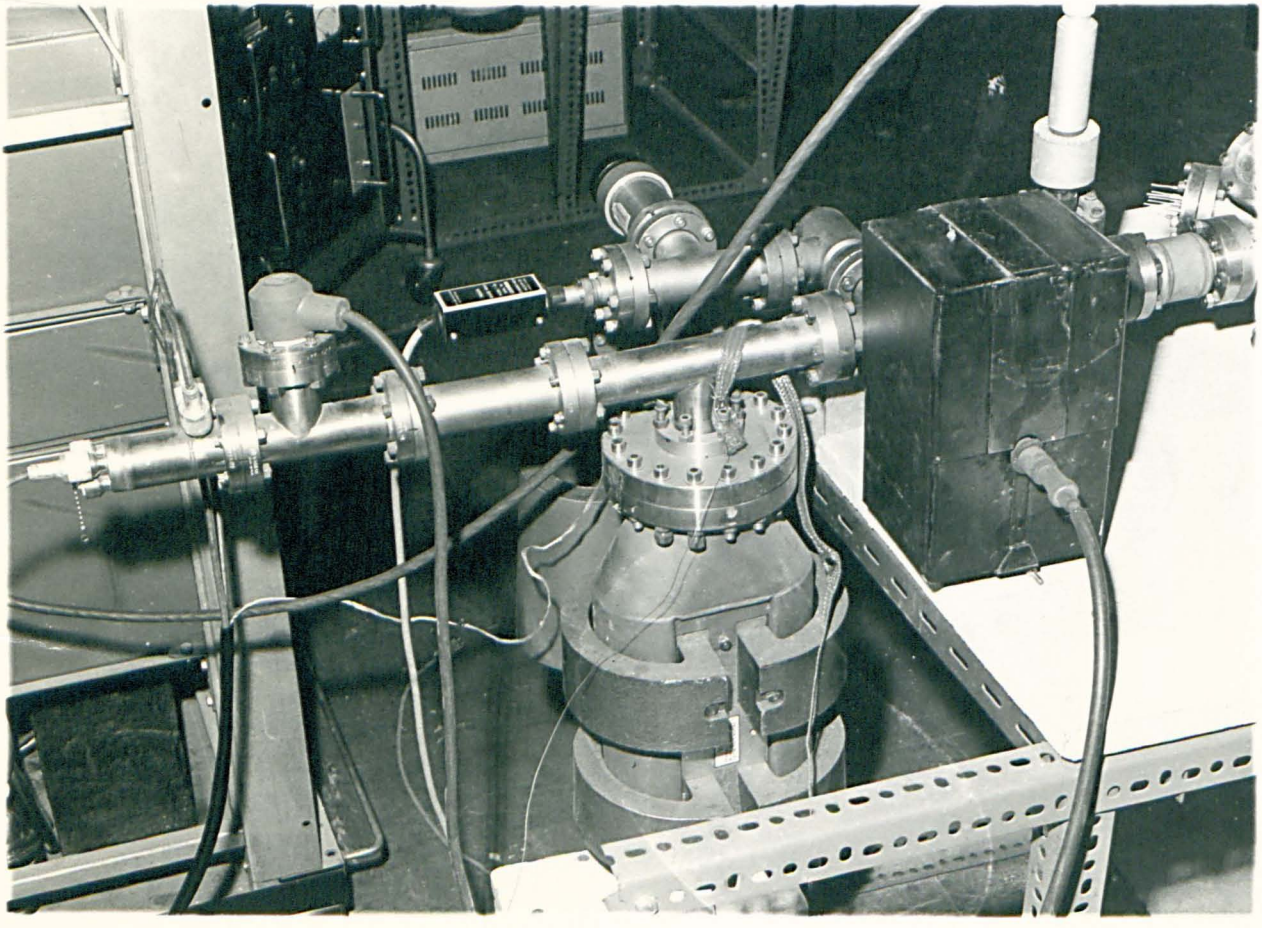

FIG. 39

active gas molecules and atoms from the system is achieved by chemical combination with sputtered titanium to form chemically stable compounds, whereas the inert gases are pumped by ion burial. A strong magnetic field is maintained between the electrodes by means of a permanent magnet, which increases the path length and hence collision frequency of the ions by spiralling them, before they are collected by the electrodes.

The Vac-ion power supply provides a stabilised 3kV to the anode of the pump and measures the current through the pump. Since the pumping speed of the Vac-ion is constant at pressures below 10^{-3} torr, the current through the pump is directly proportional to the pressure. Hence the current meter can be used to measure the pressures directly. However, the lowest pressure that can be read accurately is $\sim 2 \times 10^{-9}$ torr.

The pumping system consists of one sorption pump, two Vac-ion pumps, a Viton tap, and a bakeable valve. The relative positions are shown in the photograph (fig. 39). Just above the sorption pump is a small side arm which is fitted with a safety valve for the release of excess pressure in the sorption chamber, when the unit has returned to room temperature again after being refrigerated to evacuate the system. The Viton tap, above the sorption pump, can seal it from the rest of the system. Following the Viton tap is a Pirani gauge head (Edwards Type M.6A) which measures the pressure in the system from the atmospheric to 10^{-3} torr. A bakeable valve following the gauge head can completely seal off the system from the sorption pump and Pirani gauge.

The whole system, with the exception of the sorption pump and its Viton tap, is bakeable to a temperature of $450^{\circ}C$.

There are facilities, however, for the independent baking of either of the two Vac-ion pumps. The reason for using two Vac-ion pumps, rather than a large single one is as follows. To attain pressures below 10^{-10} torr, the whole of the system (with the previous exception) has to be baked at 450°C. Though it is possible to bake a Vac-ion pump with its magnet in position to a temperature of 300°C, which is too low for the most effective outgassing, the field strength of the magnet is lowered, causing a significant deterioration in the pumping speed. Thus for the best results the pump must be baked without its magnet and the system must also be pumped simultaneously. This necessitates a second Vac-ion pump. In practice, the two pumps are operated and baked alternately in a reciprocal outgassing procedure. Another important reason for two pumps is that there is a small fraction of gas pumped reversibly, this being released in baking as has been noted by Hall (179). Thus by a succession of reciprocal pumping-baking cycle, most of the gas can be removed by irreversible trapping. Initially the present system was provided with two 8 litres/sec. Vac-ion pumps. Later one of them was replaced by a larger 50 litres/sec. pump to facilitate easier starting.

Even though pressures above 2×10^{-9} torr may be measured directly by the Vac-ion pump current, for lower pressures, this cannot be employed. For such pressures a General Electric triggered discharge gauge was used. This instrument utilises a cold cathode discharge in a magnetic field to provide a stable measure of pressure in the range 10^{-4} to 10^{-13} torr. The gauge tube features a momentarily energised hot filament to trigger instant starting under ultra-high vacuum. The tube

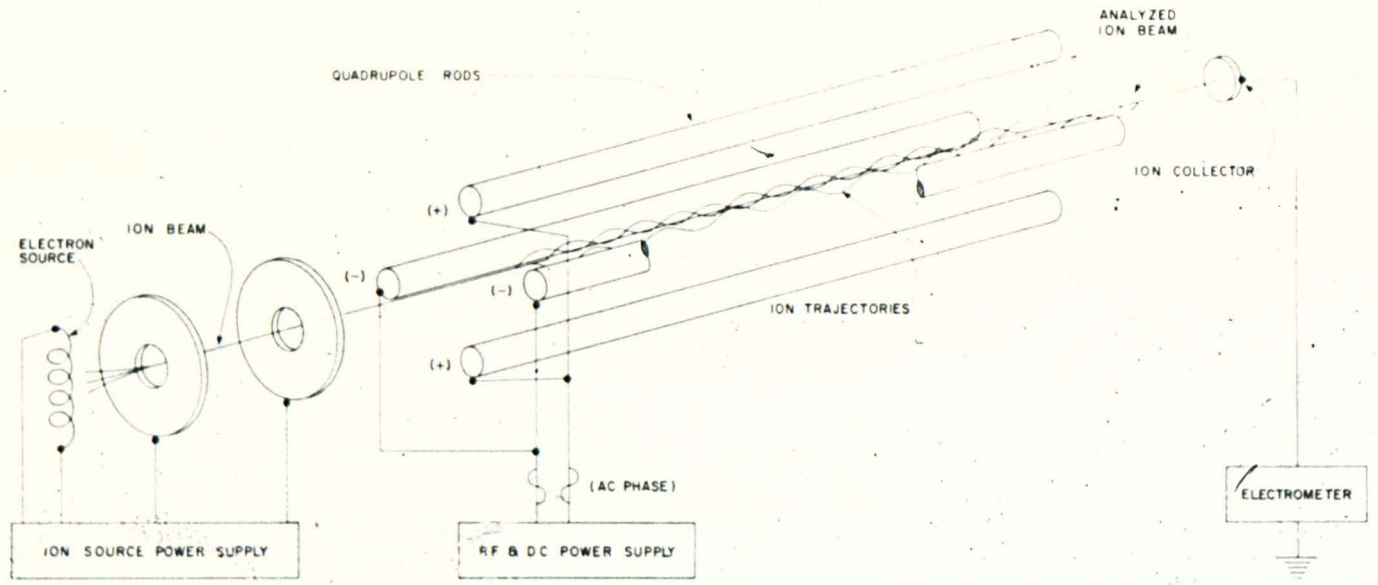

SCHEMATIC OF THE VARIAN QUADRUPOLE GAS ANALYZER

FIG. 40

itself is rigidly constructed in stainless steel with a ceramic metal feedthrough bakeable to 450°C.

5.2.b Quadrupole Residual Gas Analyser

In any ultra-high vacuum a knowledge of the residual gases is particularly important, especially since ion-pumps have different speeds for different gases. In the present investigation, a quadrupole residual gas analyser was used to provide information on the residual gases present in the system. One main advantage of the quandrupole mass filter is that it does not require any magnetic field, the presence of which in other gas analysers can introduce considerable shielding difficulties.

The quadrupole mass analyser consists essentially of an ion source, four long cylindrical rods arranged in a square array - the quadrupole - and an ion collector. A simple schematic representation of such an assembly is given in fig. 40.

The quadrupole consists of, ideally, four long hyperbolic cylinders in a square array. For ease of construction, they are approximated into circular cylinders. The radius of a circle inscribed in the array is equal to the radius of the electrodes. The opposite pairs of rods are connected electrically. To the two opposite pairs, is applied a d.c voltage superimposed on which is an r.f voltage. The d.c voltage U is opposite in sign and the r.f voltage shifted in phase by 180°, on the two pairs.

The trajectory of ions in this quadrupole field is described by equations of motion which can be transposed into Mathieu's differential

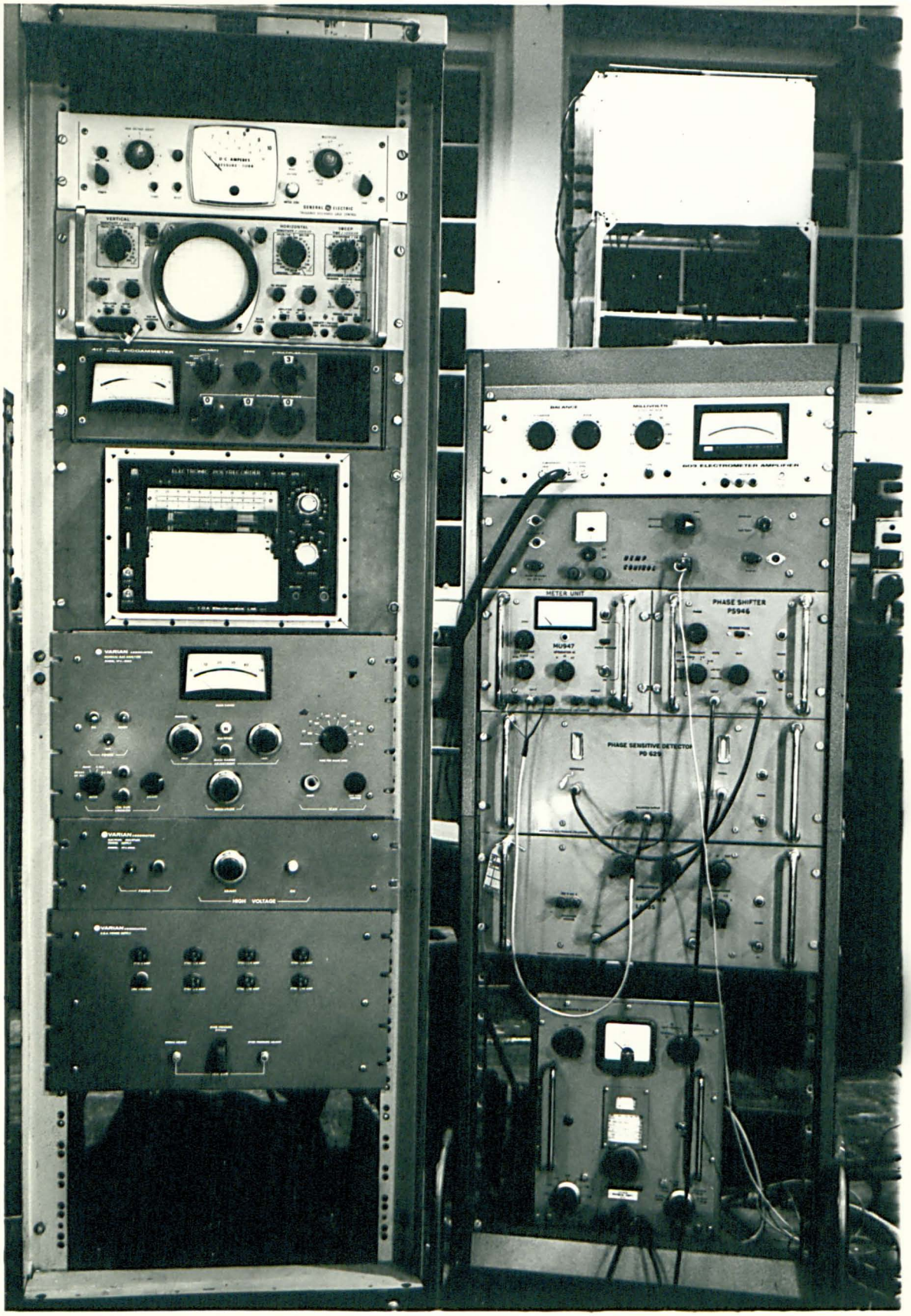
VERTICAL
HORIZONTAL
SWEEP
METER UNIT
HU947
PHASE SHIFTER
PS946
PHASE SENSITIVE DETECTOR
PD 625
HIGH VOLTAGE

FIG. 41

equations. The analysis shows that the injected ions perform oscillations perpendicular to the axis of the quadrupole which remain below a maximum amplitude only for a certain e/M ratio. Ions with the correct e/M ratio pass through the analysing space to the collector. All other ions perform unstable oscillations with rapidly rising amplitudes so that they hit the rod electrodes. Normally a spectrum of ions can be obtained by sweeping the d.c and r.f voltages simultaneously so that their ratio remains constant.

An ion collector collects the analysed ions and the electrometer amplifier records the current, the output of which may be displayed by either an oscilloscope or recorder. With a simple electrometer detection, the minimum detectable partial pressure is $\sim 5 \times 10^{-11}$ torr. By attaching an electron multiplier, partial pressures as low as 5×10^{-13} torr can be easily detected. The positive ions striking the first dynode emit secondary electrons which are then focussed to the next dynode. By successive multiplication, the current is amplified.

In normal use, a spectrum ranges from 0 to 50 a.m.u., thus including all common organic and inorganic gases, though another range 10 to 250 a.m.u. permits detection of heavier hydrocarbons. Typical resolution i.e. $\frac{M}{\Delta M}$ in the lower mass range is 50. (ΔM is taken to be the half width of the peak at a mass number M). The spectrum can be scanned automatically at different rates ranging from 3 seconds/a.m.u. to 1 millisecond/a.m.u., for the 1-50 a.m.u. range. The Q.R.G.A. measures the total pressure, partial pressures and also it can be used as a leak detector. A general view of the Q.R.G.A. control units is shown in the photograph (fig. 41).

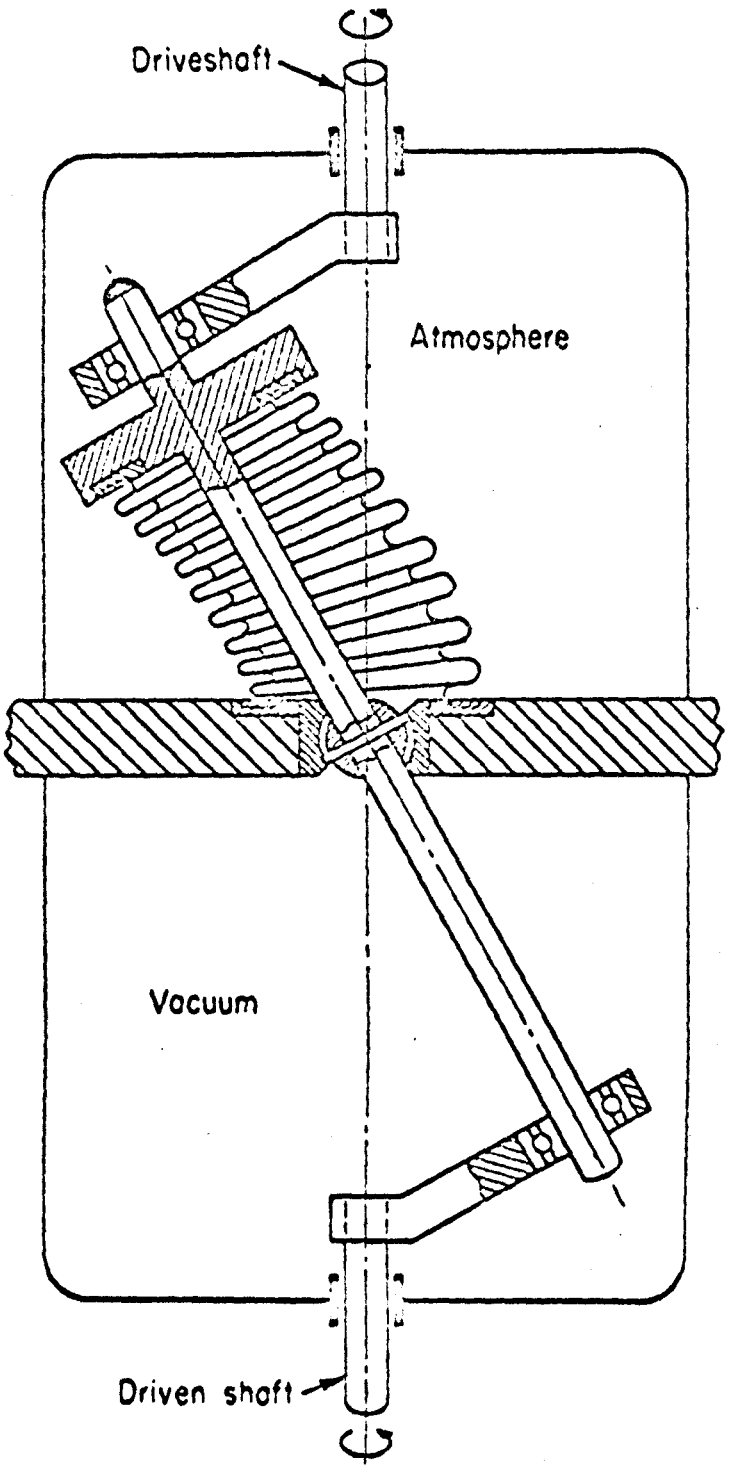

FIG. 42

5.2.c Electrical Feedthroughs

In order to make connections to the components in the ultra-high vacuum chamber special electrical feedthroughs have to be used. These must be able to provide perfect sealing and to withstand high bake-out temperatures. Two varieties of such electrical feedthroughs have been used. One such, manufactured by Varian, has eight kovar wires brazed to a circular ceramic disc, which in turn is attached to a stainless steel flange. Though the performance of this type is good, it has in practice been found to be somewhat fragile and susceptible to mechanical failure. The other variety, manufactured by Ferranti, features individual ceramics sealed into a stainless steel plate. This is found to be much more rugged although the leakage resistance of this type is not so good. In case of failure, the leads can be repaired individually. The ones used here, have 8 or 10 leads.

A more difficult problem is to introduce translational and rotational motion into an ultra-high vacuum system. Translational motion is usually achieved by using metallic bellows which may be compressed or extended. An arrangement using an offset bellows may be used to introduce rotary motion. A combination of the two can provide a "Universal motion" feedthrough. The method of operation of the Ultek feedthrough used in the present case, is shown in fig. 42. The general view of this universal motion feedthrough may be obtained from fig. 36. Calibrated scales attached to the bellows and the rotating head, show the translational and rotational displacements.

Though the target is mounted on the shaft, it has to be insulated

electrically from the feedthrough which makes contact with the spherical manifold. This is done by having a ceramic section between the target and the shaft. The electrical connection to the target is then made through an ordinary feedthrough.

5.2.d Magnetic Shielding

One of the problems associated with using Getter-ion pumps is the stray magnetic fields of the magnets which can affect the slow electrons. Hence to minimise the effect of the field, the system has to be shielded. This was done by means of a complementary pair of shields, one made of "Netic" material and the other of "Co-Netic". These materials were supplied by The Perfection Mica Co., Chicago. "Netic" material has a comparatively low permeability, but saturates at a very high flux density. "Co-Netic" has a higher permeability but lower saturation density. The Vac-ion pumps were shielded by a box made of Netic, which attenuated the field so that the intensity outside was low enough to prevent saturation of the Co-Netic material. The field intensity in the immediate vicinity of the pump was reduced to about 1 oersted. The spherical manifold was surrounded by a Co-Netic shield, which reduced the field to a few milli-oersted as measured on a thin film Hall effect device. Both Netic and Co-Netic materials are highly malleable, and withstand mechanical shock and baking temperatures, without deteriorating in performance. The electron gun also was effectively shielded by a thin Co-Netic foil enclosure. In addition to shielding magnetically, the Co-Netic around the spherical manifold acts as an additional electrostatic shield, when appropriately earthed.

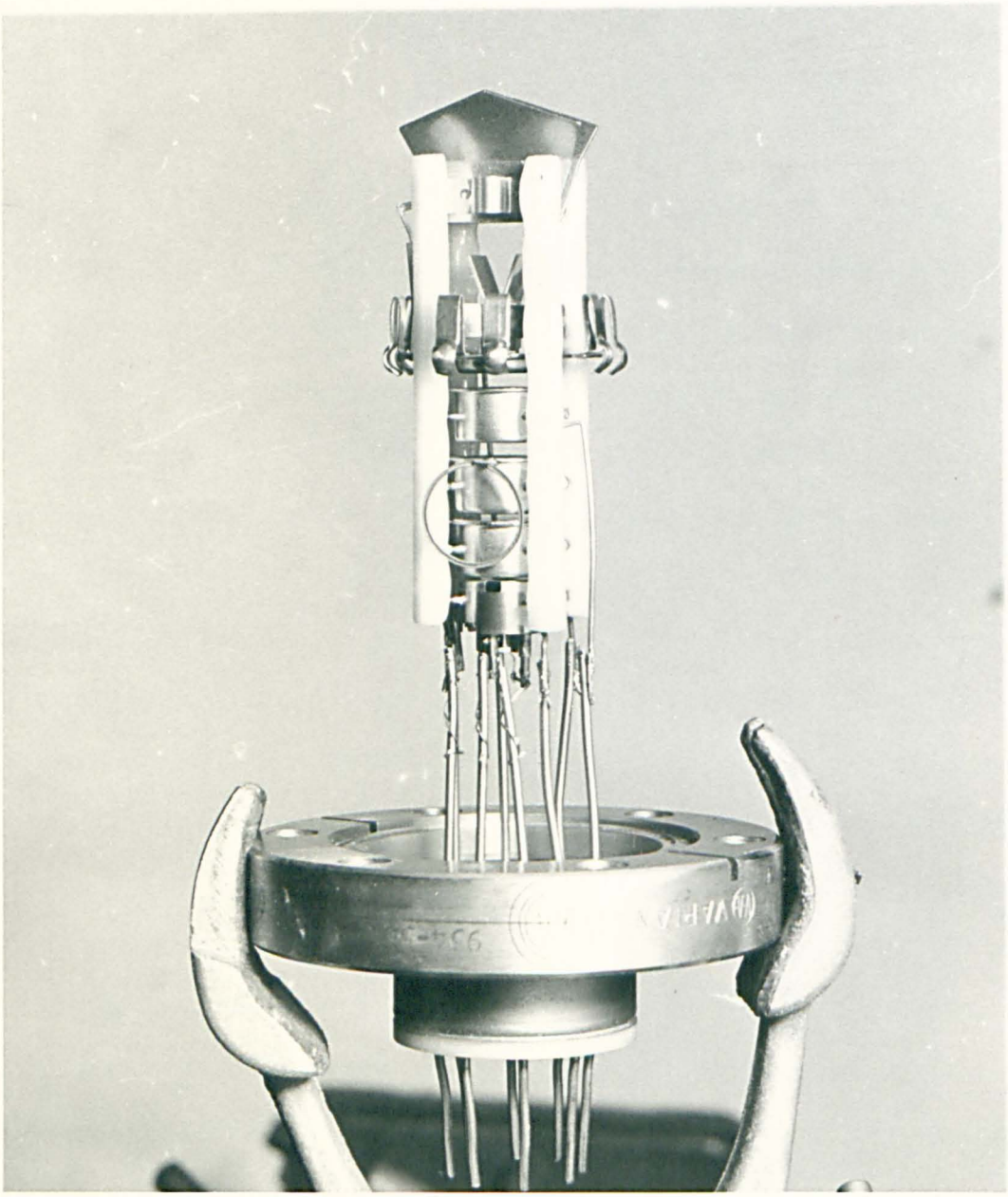

FIG. 43

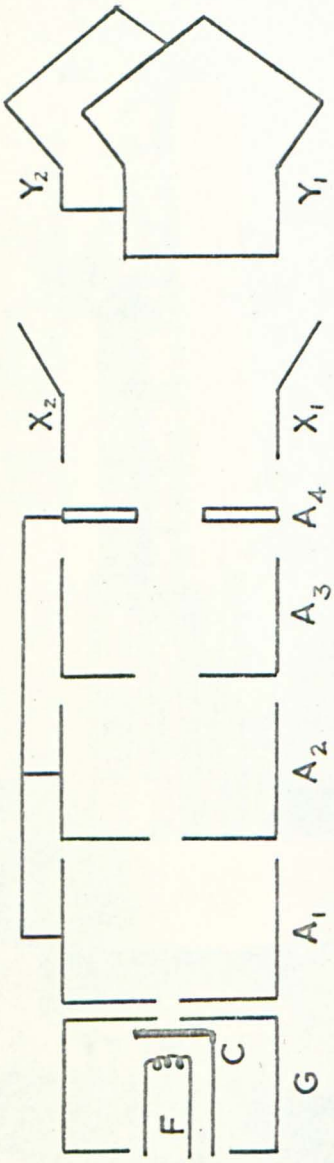

FIG. 44. Schematic of the electron gun electrodes.

5.2.e Electron Beam Supply

The primary electron beam bombarding the target surface, was derived from an electron gun. The gun used in the present study was a standard one, as found in a DG7-37 CRO tube, and using electrostatic focussing and deflection. A general view of the gun may be obtained from the photograph (fig. 43) and a schematic representation of the electrodes is given in fig. 44. The gun is capable of operating in the energy range 0.5keV to 2.5keV. It employs an oxide coated cathode, indirectly heated by a filament. In case of damage or expiry of the life, the cathode and the filament can be replaced. Immediately in front of the cathode is the "grid" which is a cylindrical electrode with an aperture. The negative bias on the grid normally controls the beam intensity. The cylindrical electrodes A_1, A_2 and the final anode, A_4 (fig. 44) are connected together. A_3 is the focussing electrode which is at a positive potential with respect to the cathode. The electrostatic deflection plates X_1, X_2 and Y_1, Y_2 provide deflection of the beam in two perpendicular directions.

The circuitry of the electron beam used is shown in fig. 45. The heater filament operates normally at 0.3 amp and 6.3 volts, the power being supplied from a car battery. Since the target has to be held at ground potential, the negative high voltage is applied to the gun cathode, and the electrodes A_1, A_2 and A_4 are at ground potential. A highly stabilised high voltage supply-variable in the range 0 - 3kV (John Fluke and Co., type 413C) - provided the cathode potential. The negative grid bias voltage and the focussing voltage were obtained from dry batteries

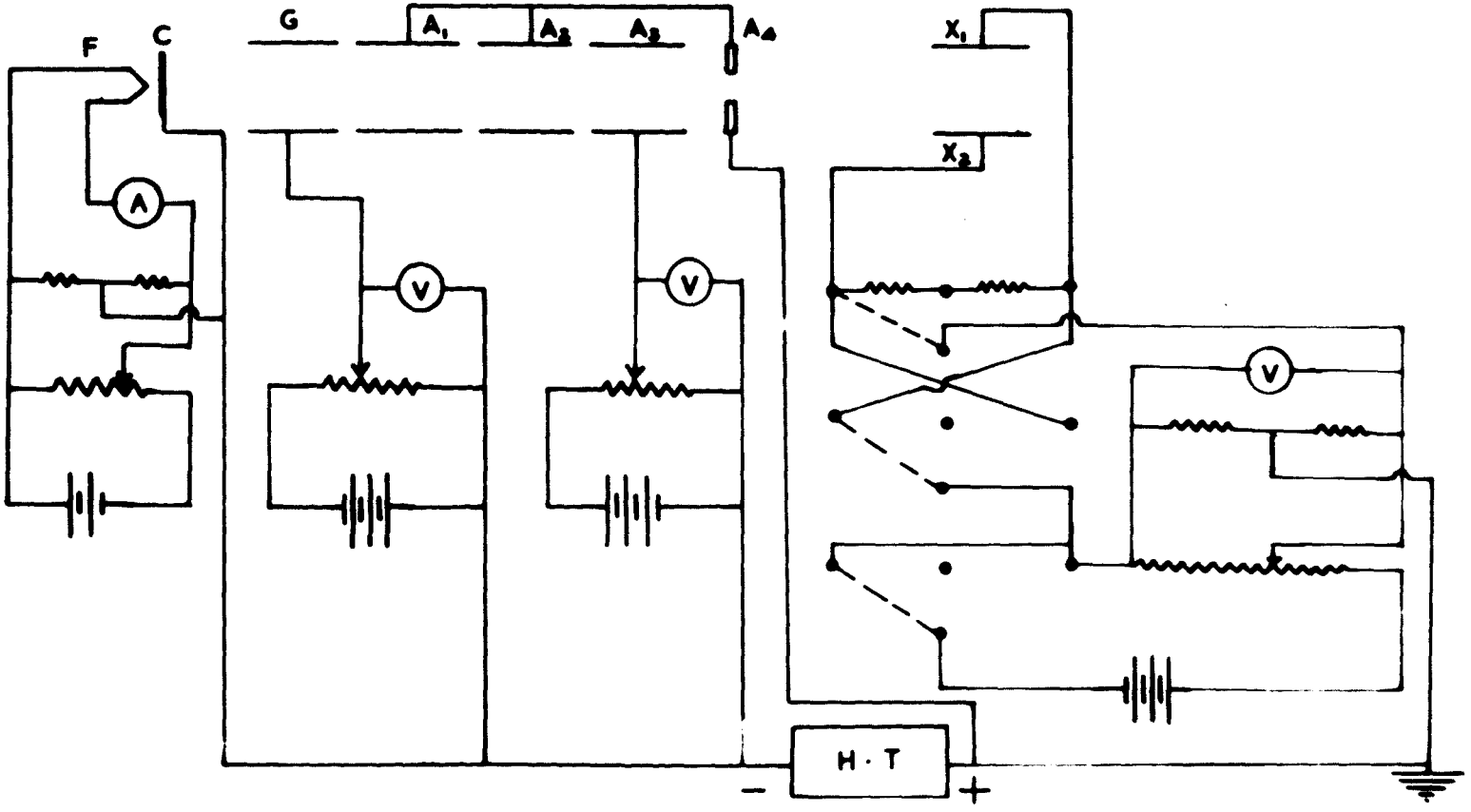

FIG. 45. ELECTRON BEAM CIRCUIT

and were variable. Though in normal operation the X and Y deflection plates were earthed, by applying the suitable voltages, the beam could be deflected to any spot on the target. The gun was surrounded by a Co-Netic foil enclosure, which, apart from being a magnetic shield, stopped stray electrons from the gun directly reaching the collector.

Another C.R.O. tube, containing an identical electron gun, situated outside the vacuum system but fed from the same power supply, was used to monitor the position and focussing condition of the beam on the target.

5.2.f The Spherical Grid

In measurements of the yield, the spherical manifold collected the secondaries emitted from the target. Inside the spherical collector was a spherical anti-dynatron grid which suppressed the tertiary electrons from the collector. In the study of the energy distribution of secondaries, this acted as a retarding field electrode. The spherical grid was made from tungsten mesh of density 64 x 64 meshes/sq. inch and of transparency 87%. The mesh was supplied by the Wire Weaving Company, Holland. The simple but elegant technique used by Todd (180) was employed in making the spherically shaped metal grid without distortion. However, the method was much simplified for the present case.

The wire mesh was allowed to form a tight dome over a 5" diameter glass bulb. A tungsten ribbon was fastened around the perimeter to form a tight belt and the two loose ends of the belt were welded together. Then the wire mesh was folded back over the ribbon belt and

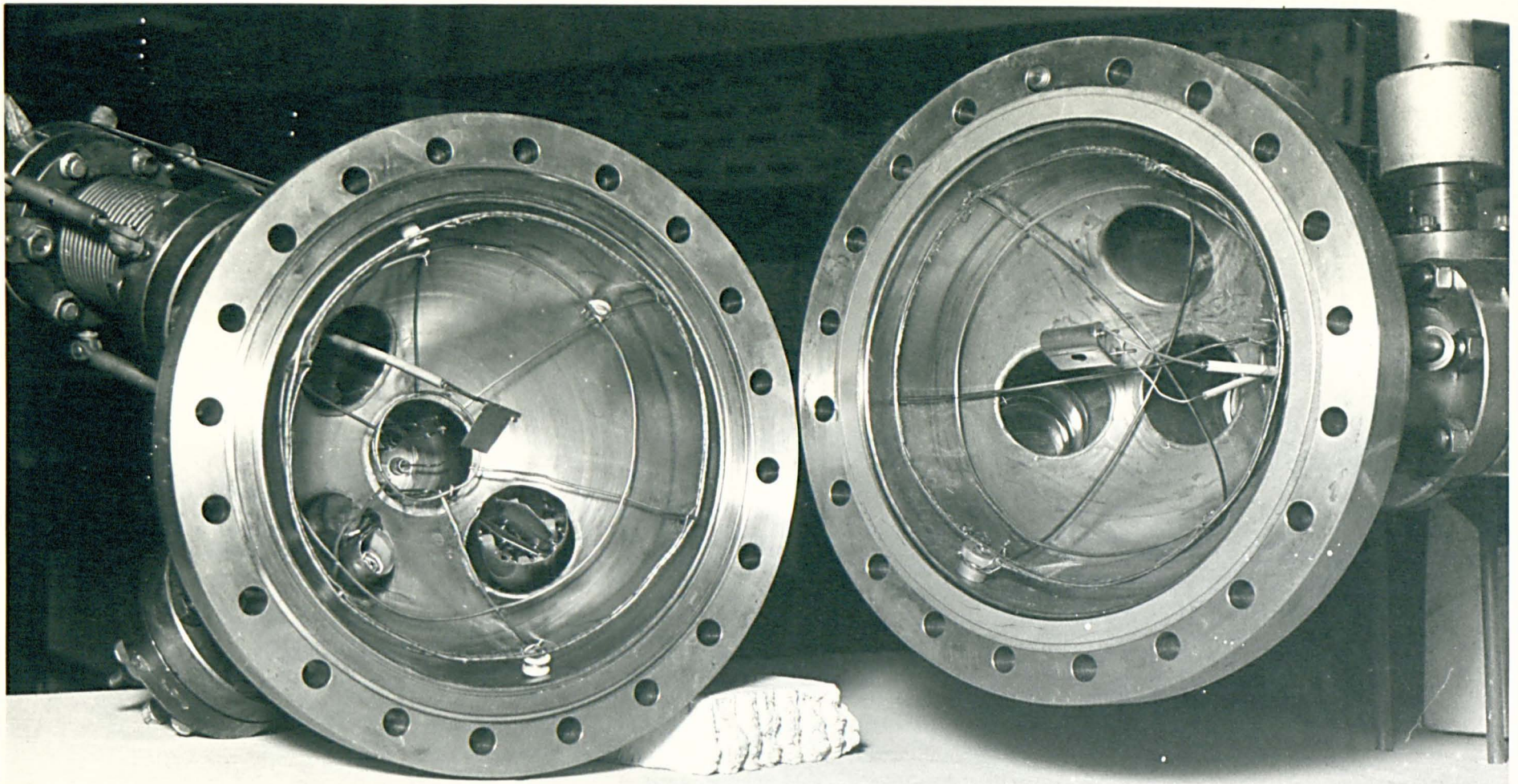

FIG. 46

another belt fastened around so that a sandwich was formed with the mesh in between the two ribbon belts. The dome was then gently removed from the glass bulb and the sandwiched edge welded all around. For better mechanical strength, however, two or three nickel wires were used as skeletons onto which the dome was formed. Two such hemispherical domes formed a perfect spherical grid. The grid was insulated from the spherical collector by attaching a few ceramic (alumina) rollers to the nickel skeletons. Fig. 46 gives a photograph of the inside of the spherical manifold, with the target at the centre, and the spherical suppressor grid surrounding the target.

5.2.g Film Deposition Unit

Some of the targets were prepared by depositing thick films in vacuo. The deposition was done by an Edwards automatic evaporation control system coupled with a film thickness monitor. This could also be used to outgas the evaporant and the molecular gun at a suitable temperature and to deposit a film at a desired rate to a predetermined thickness. The thin film thickness monitor employs a quartz crystal vibrating in the shear mode at a frequency 6MHz. The frequency is lowered with the deposition of films onto the crystal and the change in frequency is a measure of the mass deposited.

5.3 Experimental Techniques and Procedure

Conventional methods were used in measuring the yield. The characteristic energy losses were studied by a retarding field energy

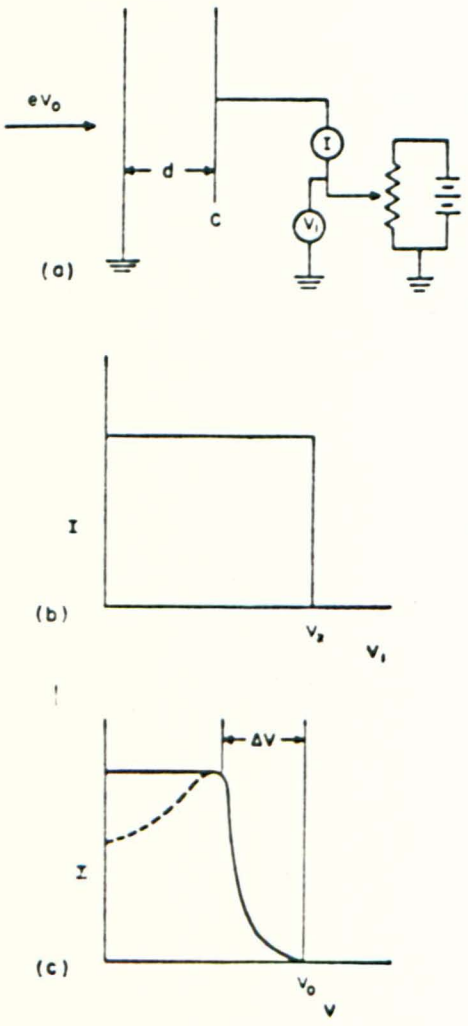

FIG. 47. (a) Basic retarding field analyzer. (b) Ideal retarding field cutoff curve for monoenergetic particles. (c) Usual retarding field cutoff curve. The slope on the rise is due to trajectory effects. The effect of reflection is shown in the dotted curve.

analyser incorporating electronic differentiation. The basic principle of the retarding field energy analyser and the method by which the retarding field plot is differentiated, are briefly discussed.

5.3.a Retarding Field Energy Analysers

A commonly adopted method in the analysis of total kinetic energy of a stream of charged particles is to use a retarding electrostatic field, where the kinetic energy is deduced from the height of the potential barrier that the particles can just surmount. Owing to the simplicity of the principle and the high resolving power, such analysers have drawn much attention recently and a number of sophisticated analysers are available today (181, 182, 183). Unfortunately, it is not always recognised that the potential barrier height is not a measure of the total kinetic energy but of the momentum in a direction perpendicular to the equipotential lines. In many cases the distinction can be overlooked.

In the simplest case of the retarding vield analyser, which has a parallel plate geometry, a beam of infinitesimal extent and perfect collimation, with kinetic energy $E = eV_o$ enters from the left (fig. 47(a)). The beam is retarded by an axially directed electrostatic field between the electrodes and collected at C. If the beam is monoenergetic, a curve plotted with the collector current against the retarding voltage - retarding field curve - has a shape as shown in fig. 47(b). However, in practice the beam will have a finite diameter and angular aperture θ . In parallel plate geometry, the finite diameter causes no difficulty, but the finite angular aperture means that

the kinetic energy of the beam is divided into two parts associated with the axial and transverse components of momentum according to the relation

$$\frac{E_{trans}}{E_{axial}} = \tan^2 \theta \qquad (102)$$

In such a case, since only the axial momentum will be effective in overcoming the retarding potential, the cut-off curve just tails away (fig. 47(c)) and has a base with ΔV (184).

$$\frac{\Delta V}{V_o} = \frac{\Delta E}{E} = \sin^2 \theta \qquad (103)$$

ΔE represents an energy "aberration" and limits the resolution. In principle, it may be reduced by aperturing the beam in angle.

One of the major drawbacks of all retarding field analysers is that the response at an energy E_o is $\int_{E_o}^{\infty} I(E)dE$ rather than the actual $\left| I(E) \right|_{E_o}$ of most other analysers. In most cases the desired quantity is $\left| I(E) \right|_{E_o}$. Although such integral curves may be graphically differentiated, the error in such a procedure may be as great as 20%. In the present study this integral plot is differentiated electronically.

Normally three different types of retarding field analysers may be distinguished according to the location of the retarding field with respect to the collector of electrons and according to the potential of the collector.

In the simplest case, the retarding field is in front of the collector, the collector itself being the retarding electrode.

This is shown in fig. 47(a). By gradually changing the retarding potential, the current collected can be measured. Boersch (185) with his sophisticated analyser using this principle obtained an accuracy of 0.004eV in a beam of 60keV.

In the second version, the collector of the beam current is constantly at anode potential. The retarding potential is on a separate electrode, normally a mesh grid, in front of the collector. This arrangement is conveniently called an electron "filter" - since it graudally filters faster and faster electrons out of the beam, when the bias of the electrode is increased. Historically, Boersch (186) used the filter to remove the inelastically scattered electrons from electron micrographs and diffraction pictures. A number of authors have made use of the electron filter lens as a velocity analyser.

In the third type of the retarding field analyser, the electron beam is transmitted through the Faraday cage collector, which has an entrance aperture and an exit aperture. Behind the exit aperture is arranged the retarding field which gradually reflects faster and faster electrons back into the collector cage, with increasing retarding potential. This has often been called an electron mirror analyser.

In all these types, to obtain high resolution a very narrow, substantially parallel beam, of preferably small intensity, which enters the retarding field at right angles to the equipotentials, is necessary. So much so, a beam generated by a point source with a finite angular aperture - as in the case of secondary emission - cannot be analysed

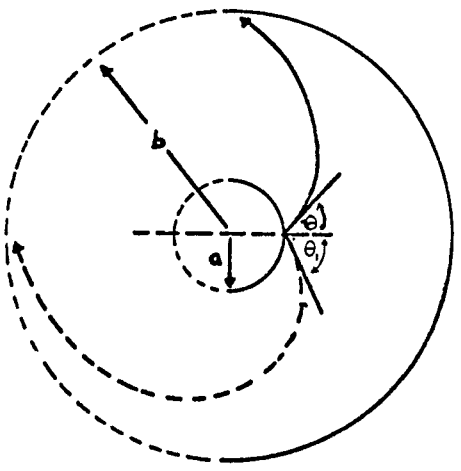

FIG.48. Limiting trajectories for the spherical (dotted line) and hemi-spherical (solid line) retarding analyzer.

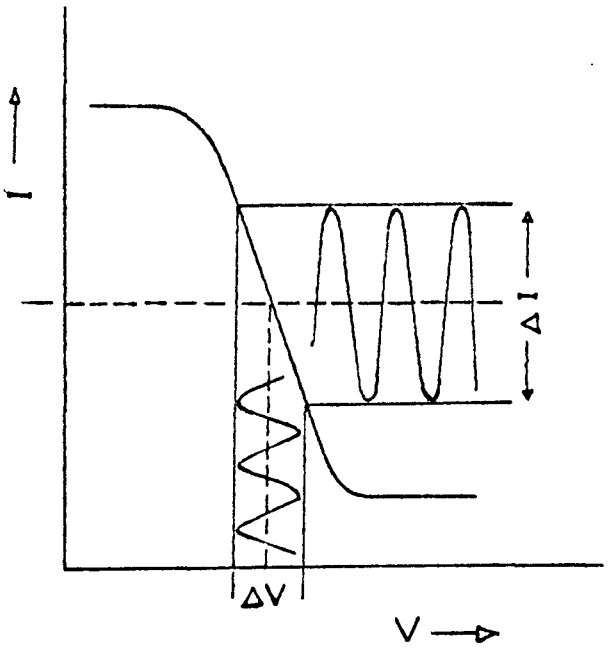

FIG.49. Integral curve of current versus retarding voltage showing the a.c. output current ΔI resulting from the a.c. modulating voltage ΔV.

easily with such an analyser, unless a small pencil is selected from it. This of course reduces the intensity. However, such a beam can be analysed with one of spherical geometry. This type of spherical condenser analyser seems to be the ideal one for obtaining an ideal cut-off curve and hence better resolution (184).

The geometry of the trajectories is not so simple as in the case of parallel field, but since the paths are solutions of a central field problem, they may be determined analytically. A theoretical analysis has been given by Simpson (184). For simplicity, an analyser consisting of two spheres of radii 'a' and 'b' (fig. 48) is considered. Analysis shows that the trajectory of a particle leaving the inner sphere at an angle θ, is an ellipse. It can be shown that $\frac{\Delta E}{E} = (\frac{a}{b})^2 \sin^2 \theta$. When the electrons are emitted from the inner sphere through all angles up to $\pi/2$, the maximum $\Delta E/E$ is given by

$$\frac{\Delta E}{E} = (\frac{a}{b})^2 \qquad (104)$$

This is the ideal case where the emitter also has spherical shape. It has been shown by Soboleva (187) that ΔE is higher if a disc or cube is used instead of the sphere.

In the above analysis, a simplified two electrode system is considered. In such a case even if all the electrons with sufficient kinetic energy reach the collector, they may not be collected altogether, since they can liberate fresh secondaries from the collector. The answer to this problem is to use the three element analyser of the filter type. Here a spherical grid of high transparency is used as a filter electrode, with the retarding potential on it. The spherical collector can be kept at ground potential and this gets rid of many problems of detection.

The negative potential of the grid suppresses the tertiary electrons from the collector. There is really little evidence in the literature as to the range of energy that can be studied with this type of analyser. At higher voltages, there is the possibility of the breakdown of the gap between the grid and collector. Also if the mesh is extremely fine and flexible, the mere electrostatic attraction between the sphere and the mesh is sufficient to cause buckling and hence shorting. Typically, in the present study the grid has a diameter of 13 cms. and the target at the centre an area $\sim$ 1 sq.cm. The energy range studied is 200 to 500eV.

The one common "disadvantage" shared by all retarding field energy analysers is that at a given energy E, the output of the analyser is the sum of all electrons with energy sufficient to overcome the potential barrier (181, 184). The graph of I, as a function of V, the retarding potential, is the integral of the energy distribution of electrons.

$$\therefore \quad I = \int_{V}^{\infty} I(V)dV \qquad (105)$$

This is disadvantageous with respect to the signal to noise ratio and because the energy spectra are more difficult to interpret. This difficulty may be alleviated by differentiating the integral plot by the use of an a.c modulation system as proposed by Leder and Simpson (188). Consider an integral curve shown in fig. 49. Let a small a.c voltage ΔV be superimposed on the retarding voltage V. The resultant collector current I has an a.c component ΔI, whose amplitude is proportional to the slope of the integral curve at the d.c level V. ΔI has the same frequency as ΔV. If ΔV is decreased in amplitude this difference curve

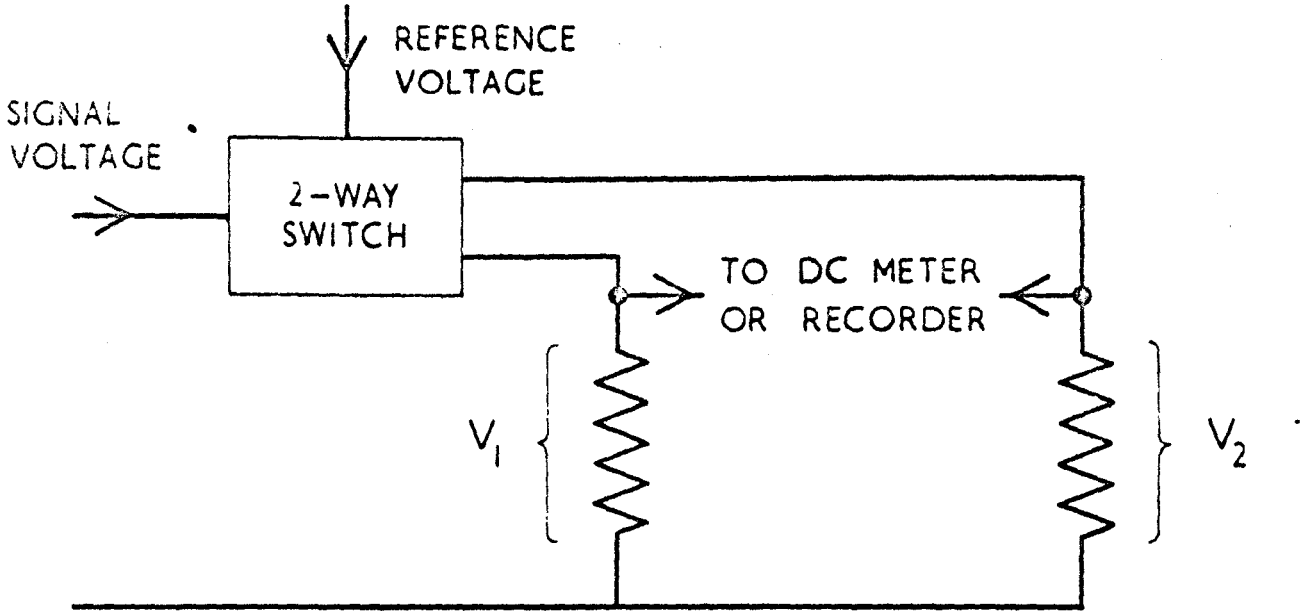

FIGURE 50

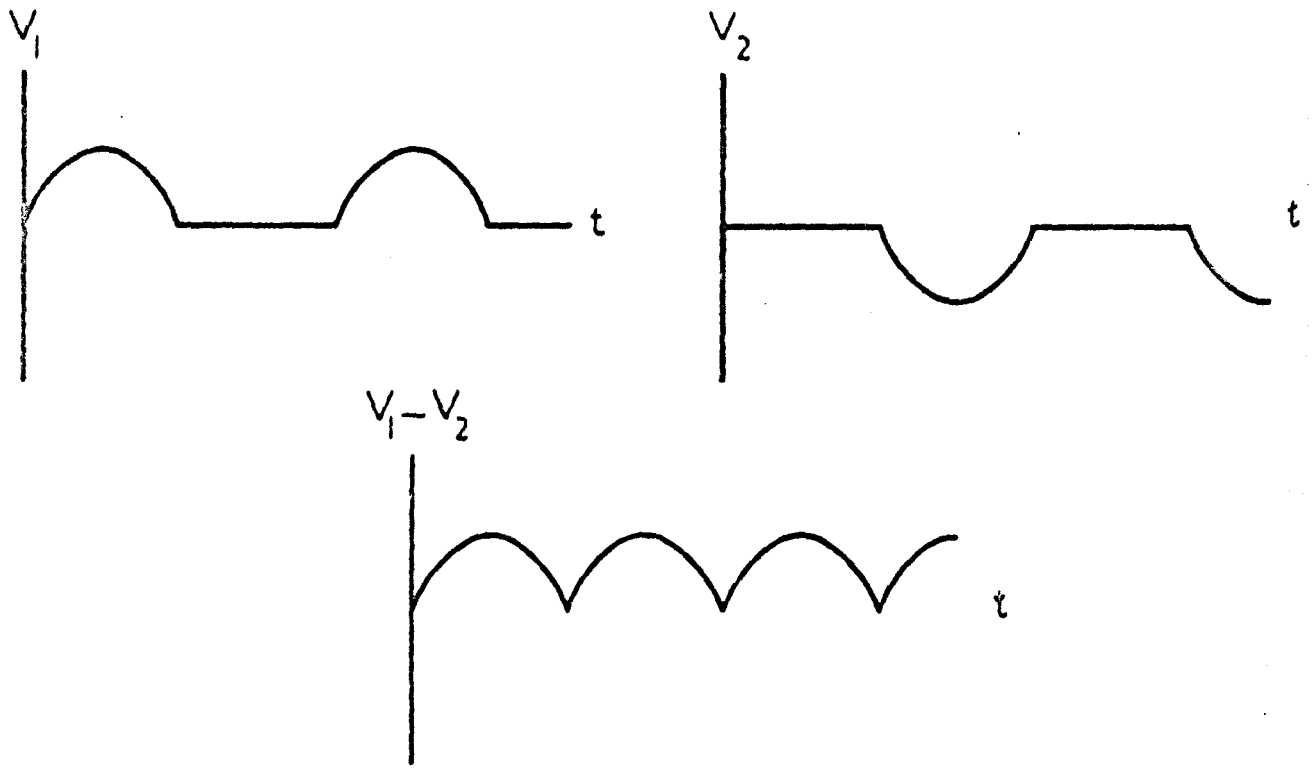

FIGURE 51

will approach a true differential curve. This small a.c component of the current can be detected and amplified to obtain the true energy distribution.

5.3.b Phase Sensitive Detection

When the above-mentioned integral retarding plot is differentiated, using the modulation technique, one is interested in the a.c component ΔI at the modulating frequency. This signal has to be amplified and detected. The amplification may be done by an electrometer. The amplified a.c component has to be extracted from the noise and then converted into a d.c signal, so that it can be recorded by a chart recorder. In the present experiments this was accomplished by a phase sensitive detector (P.S.D.).

A phase sensitive detector is a very elegant device which compares the test signal with a reference signal and gives a d.c output. Basically it consists of a two-way switch - a chopper in reverse - operated by a reference voltage derived from the modulation oscillator (fig. 50). Let the reference voltage be $V_r \sin \omega t$ and if the signal contains an "in phase" component $V_s \sin \omega t$, the switching action gives full wave rectification of this component and a d.c voltage proportional to V_s will appear at the output terminals (189, 190). Components of the signal input at other frequencies (apart from harmonics of ω) will give at the output an a.c voltage at the beat frequency. Thus the response of the system to noise in the signal will depend on the time constant T, of the d.c measuring device and the P.S.D. acts as a selective rectifier of bandwidth $\frac{1}{T}$. A typical d.c meter or recorder has a response time of

the order of 1 second so that the bandwidth is not greater than 1 Hz.

Because of its ability to pick out a signal from a wide spectrum of unwanted frequencies - noise - the P.S.D. has often been called a synchronous detector, coherent detector, lock-in amplifier, homodyne detector, etc. If the signal and the reference voltages have the same frequency and phase, the voltages V_1 and V_2 appearing across the two load resistors are shown in fig. 51. It can be easily seen from the figure that the balanced output gives a full wave rectification.

Mathematically, the operation performed by the P.S.D. corresponds to multiplying the signal by a square wave; that is, by a function $kf_2(t)$ where k is a constant and

$$f_2(t) = \sin \omega t + \frac{1}{3} \sin \omega t + \text{---} \qquad (106)$$

So if the signal input voltage is $V_1 f_1(t)$, the output is

$$V_{out} = kV_1 \int_0^T f_1 f_2 dt \qquad (107)$$

Thus the phase sensitive detector performs a Fourier analysis of $f_1(t)$ and extracts the component corresponding to sin ωt.

5.3.c Pumping-down Procedure

Having sealed the vacuum system, the following procedure was adopted in the pumping-down. With all valves closed, the sorption pump was refrigerated by surrounding it with liquid nitrogen in a Dewar flask. The Viton tap was opened and a Pirani gauge measured the pressure in the region before the bakeable tap. When the indicated pressure was a few microns, the bakeable tap was opened so that the sorption pump now pumped the

whole system, the pressure again being recorded by the Pirani gauge. When the pressure had fallen below 10^{-3} torr (which typically would take 10-15 minutes) both Vac-ion pumps were switched on. Usually the passage of a high current through a pump, while the pressure was high, caused considerable outgassing and the pump became hot. In such an event the pumps were switched off or the two pumps used alternately. When the Vac-ion pump started pumping in the correct mode, the pressure fell rapidly. The Viton tap and the bakeable tap were then closed. A base pressure of 10^{-6} torr was reached within about 30 minutes. When the Vac-ion pump had reached equilibrium with the outgassing rate of the unbaked system (usually at a pressure of $\sim 10^{-7}$ torr) the gaskets and the welded joints were carefully exposed to a narrow stream of hydrogen. Any leaks in the system were indicated as a change in the current through the pump, since the pumping speed for hydrogen is nearly three times that of air. Smaller leaks could be detected using the triggered discharge gauge in the same manner. For extremely small leaks the quadrupole residual gas analyser was perhaps the most sensitive leak detector. The analyser was manually adjusted so that the electrometer reading corresponded to the hydrogen peak. With exposure to a hydrogen stream again, any leaks were quickly shown by the change in the intensity of the peak.

In the event of no leaks being found, the system was baked. The manifold was enclosed in an asbestos oven, 2' x 2' x 1½' in size, with heating elements attached to the inner walls. The temperature of the oven was gradually raised (not faster than 15°C/minute) to about 450°C. The system was baked typically for a couple of days. In the baking process

the two Vac-ion pumps were baked in a reciprocal manner as described in section 5.2.a. In the system used, a pressure of 10^{-8} torr was inevitable and 10^{-10} torr was routine after baking. With a lot of care 10^{-11} torr and below could be reached.

5.3.d Target Preparation

In the present investigation, the materials studied were Silver, Bismuth, Beryllium, Nickel, Platinum, Tantalum and Tantalum Carbide. Special care has been taken to obtain clean surfaces. Ag, Bi and Be were prepared by evaporation from the molecular guns. The molecular guns consisted of a conical basket filament, made of Ta, W and Mo respectively, for Ag, Bi and Be. The evaporants, supplied by Koch-Light Laboratories, Ltd., were of spectroscopic purity. Nickel, Platinum and Tantalum were in the form of rectangular discs 1 cm x 1 cm. Before mounting these targets in the system, they were mechanically polished with a fine rouge and then carefully cleaned in acetone. The tantalum carbide target was in the form of a thick layer on a copper substrate $1\frac{1}{2}$ cm x 0.7 cm. The process of preparation was as follows. Tantalum carbide mixed in ethyl acetate with a nitrocellulose binder was painted on the copper surface. After vacuum stoving at 980°C for 10 minutes the surface was etched in nitric acid. This commercially prepared target was supplied by the E.M.I. Ltd.

Those targets which were not prepared by evaporation could be outgassed by a projection lamp filament of 1kW power, located immediately behind the target. The projection lamp filament was sufficient to bake the

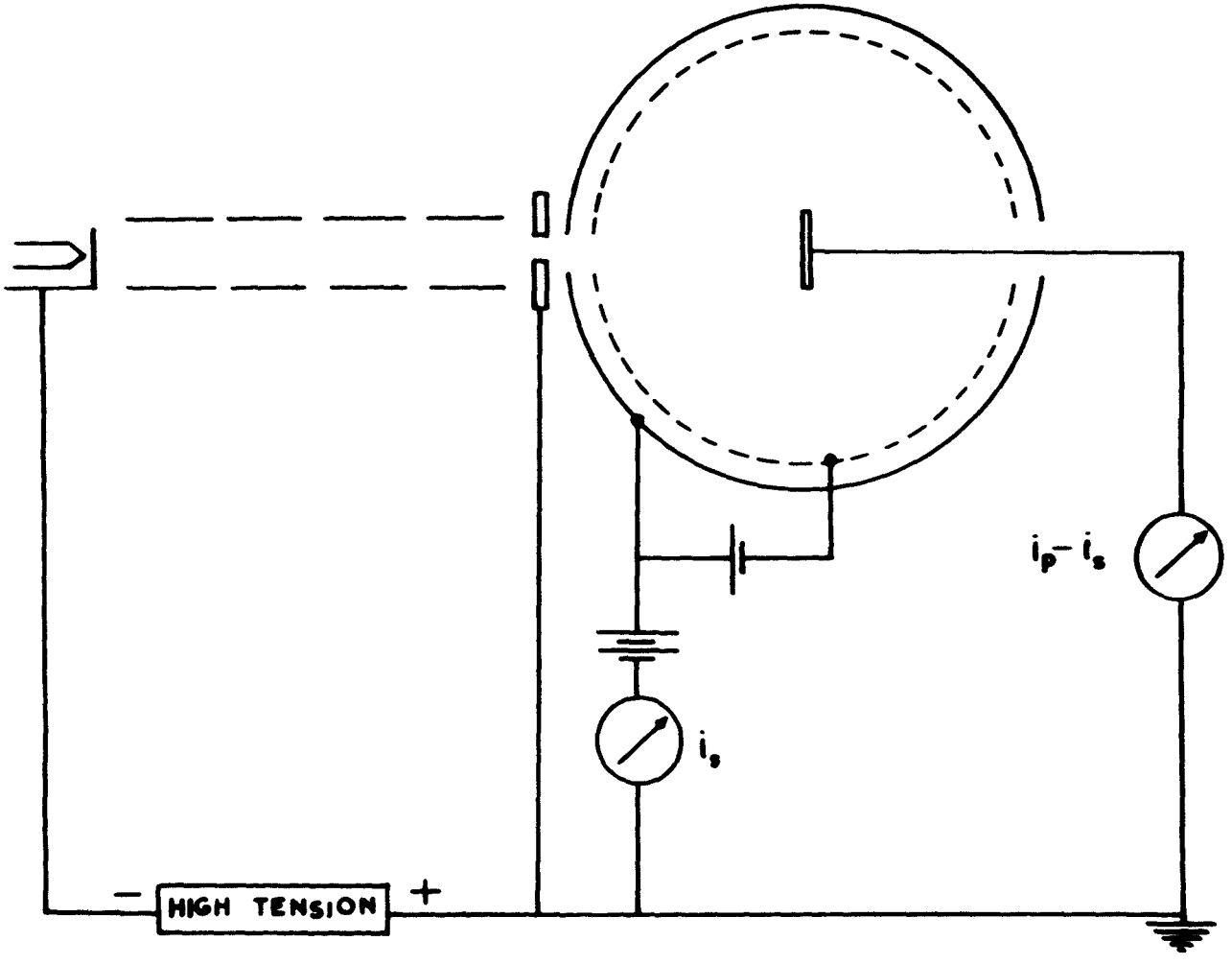

FIG. 52. SCHEME TO MEASURE THE YIELD.

whole spherical manifold up to 250°C. The temperature of the heating filament was measured by an optical pyrometer.

5.3.e Measurement of the Yield

Conventional circuitry, as given in fig. 52, was used in measuring the yield. The measuring devices used were extremely accurate. Since the target had to be kept at ground potential, the negative high voltage was applied to the cathode of the gun to accelerate the primary electrons. The target current and collector current were measured by two Keithley type 409 and 417 picoammeters, respectively. When measuring the total yield, the collector was kept at +60 volts and the spherical grid at +10 volts, with respect to the target which was at ground potential, thus aiding all the secondaries to be collected. When the inelastic reflection coefficient η, was measured the spherical grid was at -50 volts with respect to the target. From the collector current i_s and the target current $(i_p - i_s)$, the yield $\delta = \frac{i_s}{i_p}$ was calculated.

The targets Ni, Pt, and TaC were outgassed and cleaned by heat treatment for 10 - 12 hours, before measurements were made. The yield measurements were made in the primary energy range 150eV to 1300eV. This was done in steps of 20eV from 150eV to 600eV and then onwards in 50eV steps. The primary currents used were of $\sim 10^{-7}$ amp. Measurements were made with decreasing primary energy as well and the mean values taken. This showed that there was no secondary emission "hysterisis". When the primary voltage was changed, the grid bias and the focussing voltage were also adjusted for proper focussing of the beam on to the target,

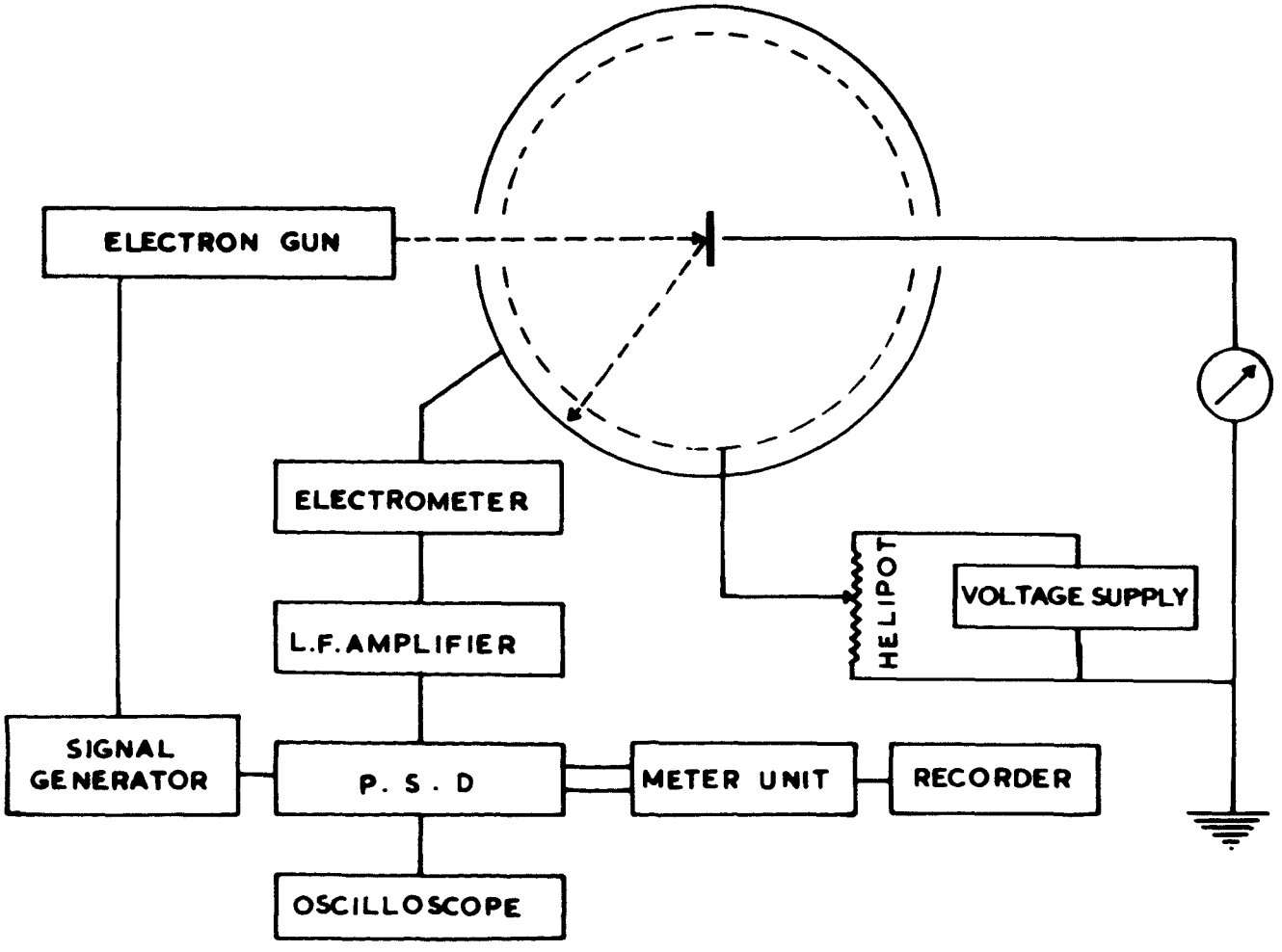

FIG. 53. SCHEMATIC OF THE SET-UP USED IN THE C.E.L STUDY.

as seen from the monitor screen. Normally the electron beam spot had a diameter < 0.5 mm.

When the X and Y deflection plates were at ground potential, the beam was incident normally. The angle of incidence of the primary beam on the target was altered by rotating the universal motion feedthrough, the actual angle being read from the circular scale attached to the feedthrough. Angles of incidence up to 60^{o} only were studied in the present case.

5.3.f Study of the Characteristic Energy Losses

Characteristic energy losses from Ag, Bi, Be, Ta and TaC were studied by the new retarding field analyser. The primary energies were of low range 150eV to 400eV. It must be said that the characteristic energy losses are independent of the primary electron energy. Since the present analyser is more suitable for low primary energies, the above range was adopted.

The system used in this study is diagram-matically represented in fig. 53. In the electrical differentiation of the integral retarding plot (section 5.3.a) the ideal place to apply the modulating voltage is on the grid. But when this was done it was found that the capacitive pick-up on the collector was comparable to the electron signal itself. A solution to this problem has been suggested in this work. However, in order to study the high energy end of the distribution, it was found sufficient to apply the modulating voltage to the cathode, so that the primary beam of electrons becomes energy modulated.

A variable frequency signal generator provided both the a.c modulating voltage and the reference voltage to the P.S.D., through a potential divider. The a.c. modulating voltage was of the order of 250 mV. In order to minimise the possible effect of interclectrode capacitance very high frequencies of modulation were not used. Too low a frequency - comparable to the mains frequency - was also not chosen. As a happy compromise, in the present system, a frequency of 450 Hz was used. Other frequencies were also tried with the same success. It must be emphasised that the frequency does not have any influence on the actual working of the analyser.

The retarding voltage was provided from a Keithley type 241 regulated voltage supply. The voltage was scanned by a 1 Megohm helipot driven by a variable speed motor. Instead of scanning through the whole range of primary voltage, only the high energy end, this being the section of particular interest in the measurement of characteristic energy losses, was scanned by the helipot. For example, for a primary voltage of 300 V, a constant backing voltage of 220 V was maintained on the grid and the rest was scanned by the helipot. This renders the quantitative determination of loss peaks more accurate. Normally the voltage was scanned at a rate of 8 volts/minute.

The collector current was amplified by a Keithley type 603 electrometer. The input resistance usually used was 1 Megohm. The d.c component of the output was blocked by a capacitor and the a.c component fed into a Brookdeal type LA635 low frequency amplifier. The output of the L.F. amplifier formed the signal to the P.S.D. The phase

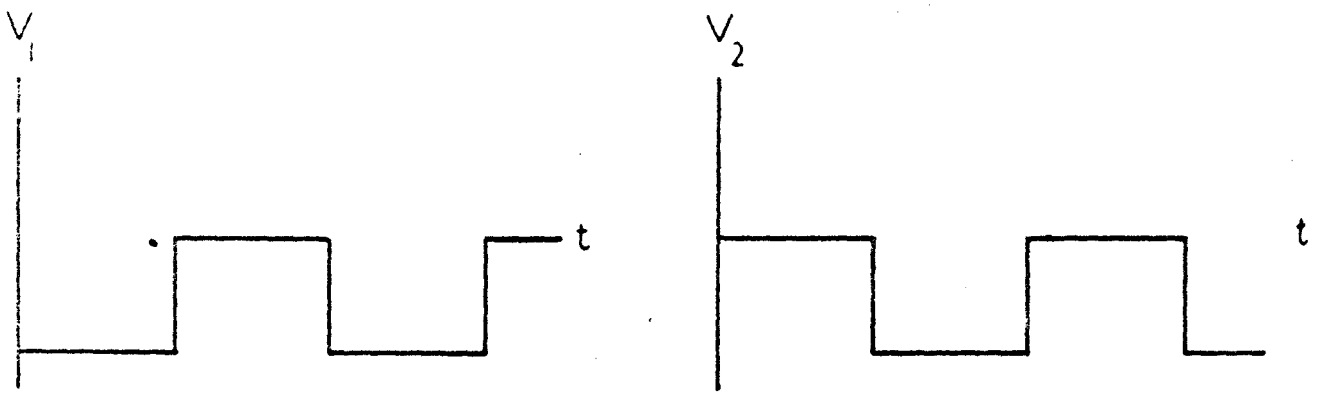

FIGURE 54.a

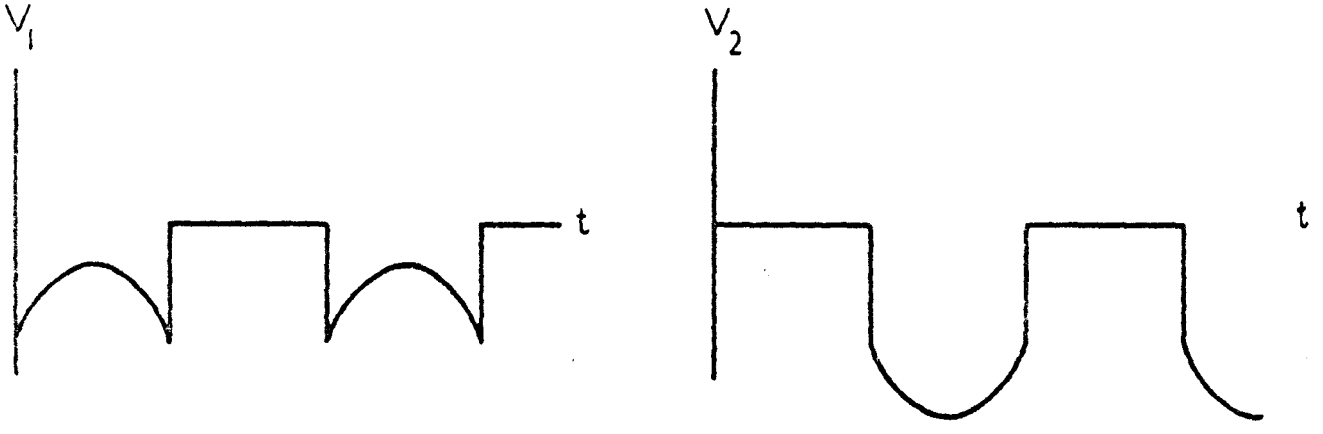

FIGURE 54.b

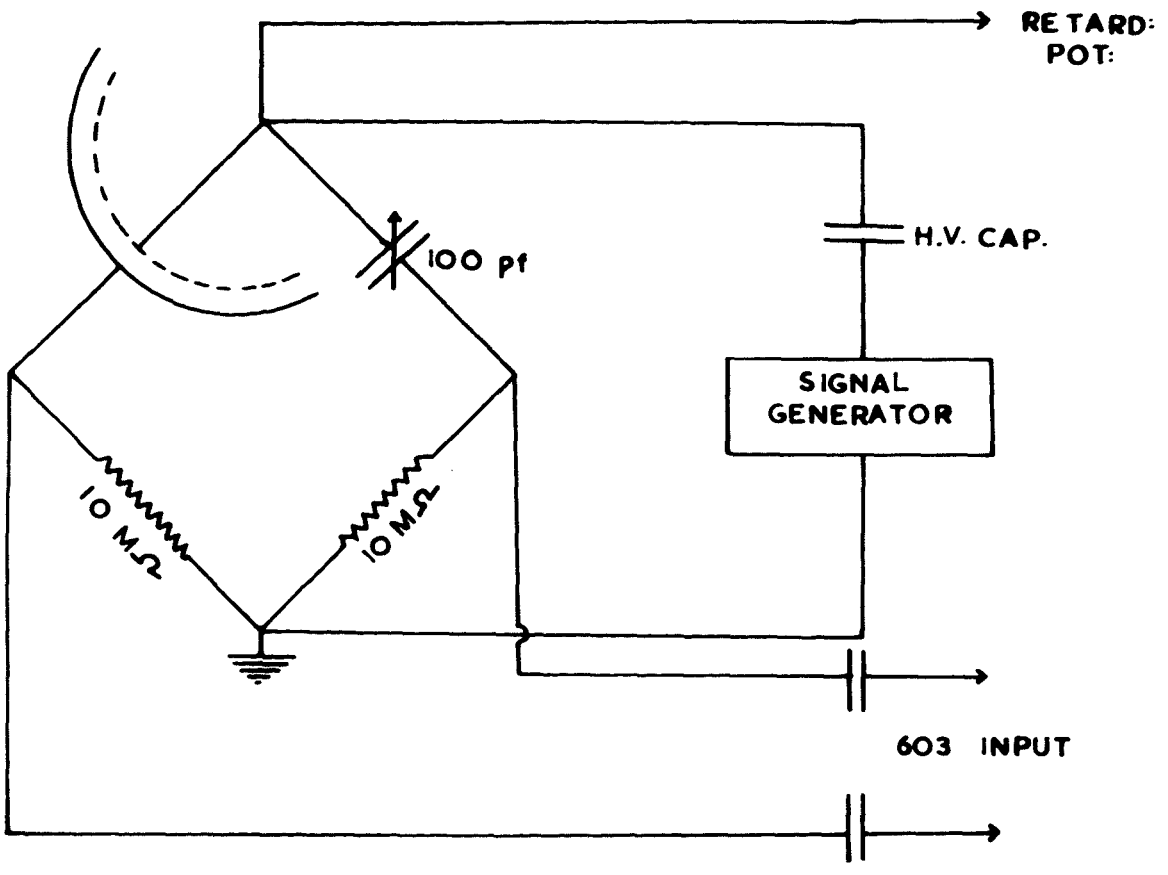
RETARD:
POT:
100 pf
H.V. CAP.
SIGNAL
GENERATOR
10 MΩ
10 MΩ
603 INPUT

FIG. 55

of the reference voltage could be checked by means of a Hewlett-Packard 130 oscilloscope, so that the shape of V_1 or V_2 (fig. 51) was displayed. However, in the PD629 phase sensitive detector, since valves are used and with the current being unidirectional, the switching wave form of fig. 51 cannot be realised. The wave forms obtained in actual practice are shown in fig. 54(a), when there is no signals and fig. 54(b) when the signal is of the same frequency and phase as the reference voltage. If not in phase, the additional phase shifter was adjusted. The balanced output of the P.S.D. was then fed into the metre unit, the output of which was recorded on a Moseley model 680M chart recorder. As already said, when the a.c modulating voltage is on the spherical grid, the capacitive pick-up on the collector can be considerable. This problem may be solved by using an a.c bridge as shown in fig. 55. Here the differential amplifying property of the Keithley model 603 amplifier is employed. The interelectrode capacitance between the grid and the collector forms one arm of an a.c bridge. The capacitive component is annulled by adjusting the variable capacitance to be equal to the interelectrode capacitance.

5.4 Conclusion

In the course of the present chapter, an account of the experimental set-up, the techniques used and the procedure taken, in measuring the yield and the characteristic energy losses, has been given. The working principle of the new retarding field analyser has been discussed. The working potential of this analyser can be estimated from the results obtained, which are given in the next chapter.

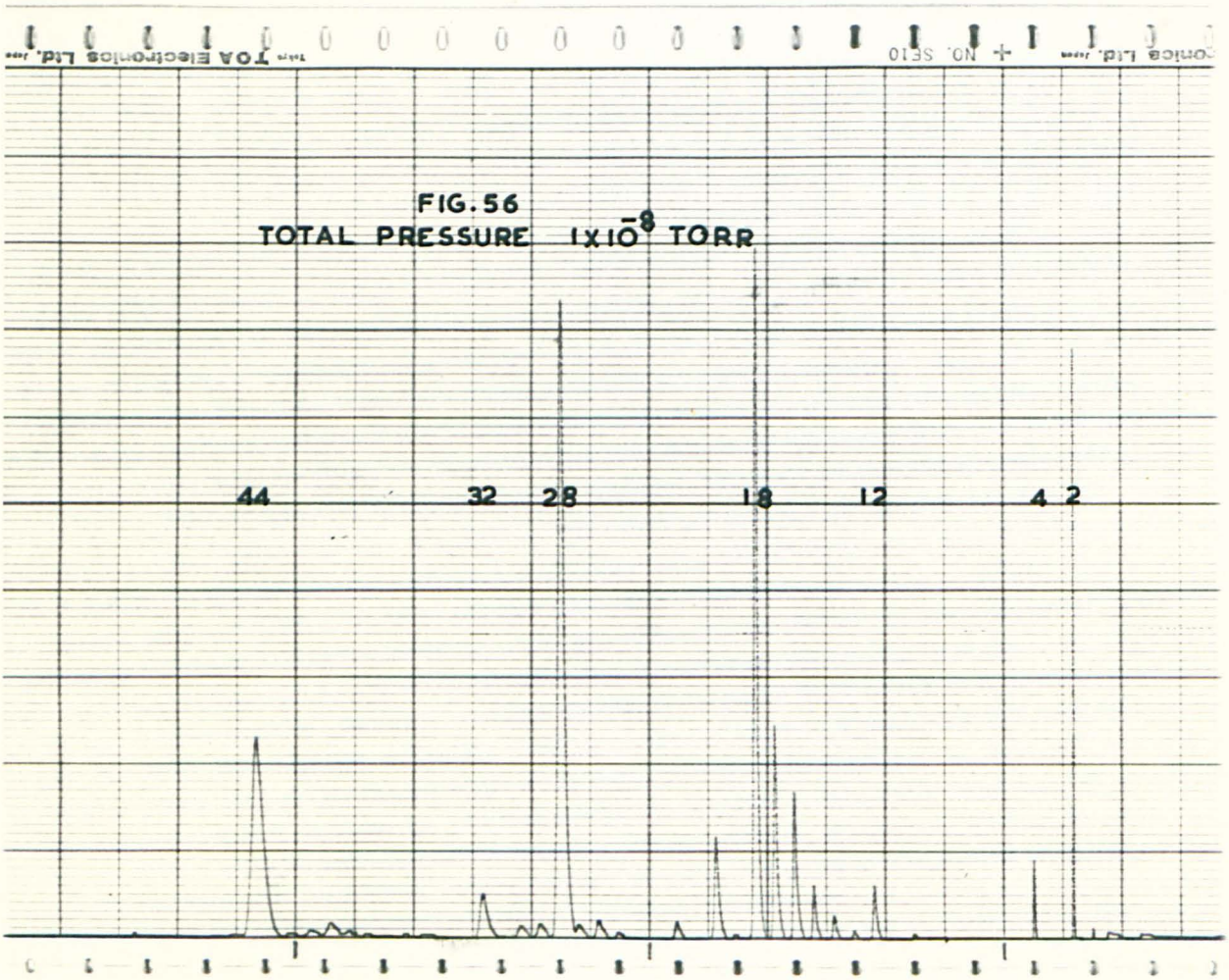
FIG. 56
TOTAL PRESSURE 1X10⁻⁸ TORR
44
32
28
18
12
4
2

CHAPTER VI

Results and Discussion of Results

6.1 Introduction

The results of the experiments conducted, will be given in this chapter. The first section contains an analysis of the residual gases present in the system, using the quadrupole residual gas analyser. The second section deals with the results of yield measurements from the different targets under different conditions. The final section gives an account of the characteristic energy losses of electrons from different materials, obtained using the spherical retarding field energy analyser.

6.2 Residual Gas Analysis

The residual gases present in the system under various conditions were analysed by the quadrupole residual gas analyser. A typical spectrum of the gases present in the unbaked stainless steel system, when the electron gun is not operating, is given in fig. 56. The spectrum ranges from 0 to 50 a.m.u. The total pressure in the system is 1×10^{-8} torr.

The peak heights in this spectrum do not represent the actual partial pressures of gases in the system. To obtain the absolute values of partial pressures one has to "correct" the peak heights, by taking into account the ionisation cross-section for the particular gas. For instance, taking the 28 peak to have a normalised cross section of 1, one should multiply the H_2^+ peak by 3.1 and CO_2^+ peak by 0.71 (191).

In fig. 57 is given a histogram representing the quadrupole

CORRECTED PARTIAL PRESSURES DURING BAKE - OUT.

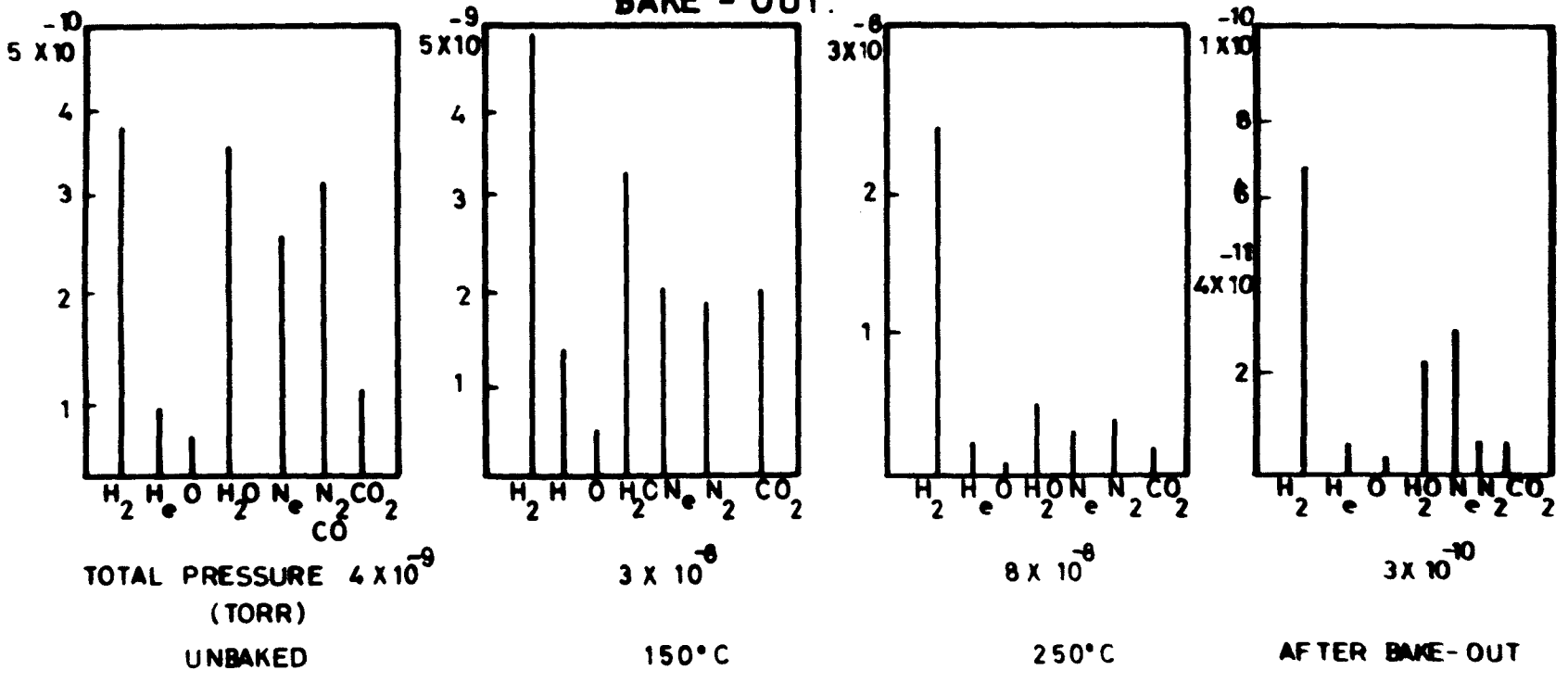

TOTAL PRESSURE 4×10^{-9} (TORR)

UNBAKED

3×10^{-9}

150°C

8×10^{-8}

250°C

3×10^{-10}

AFTER BAKE-OUT

FIG 57

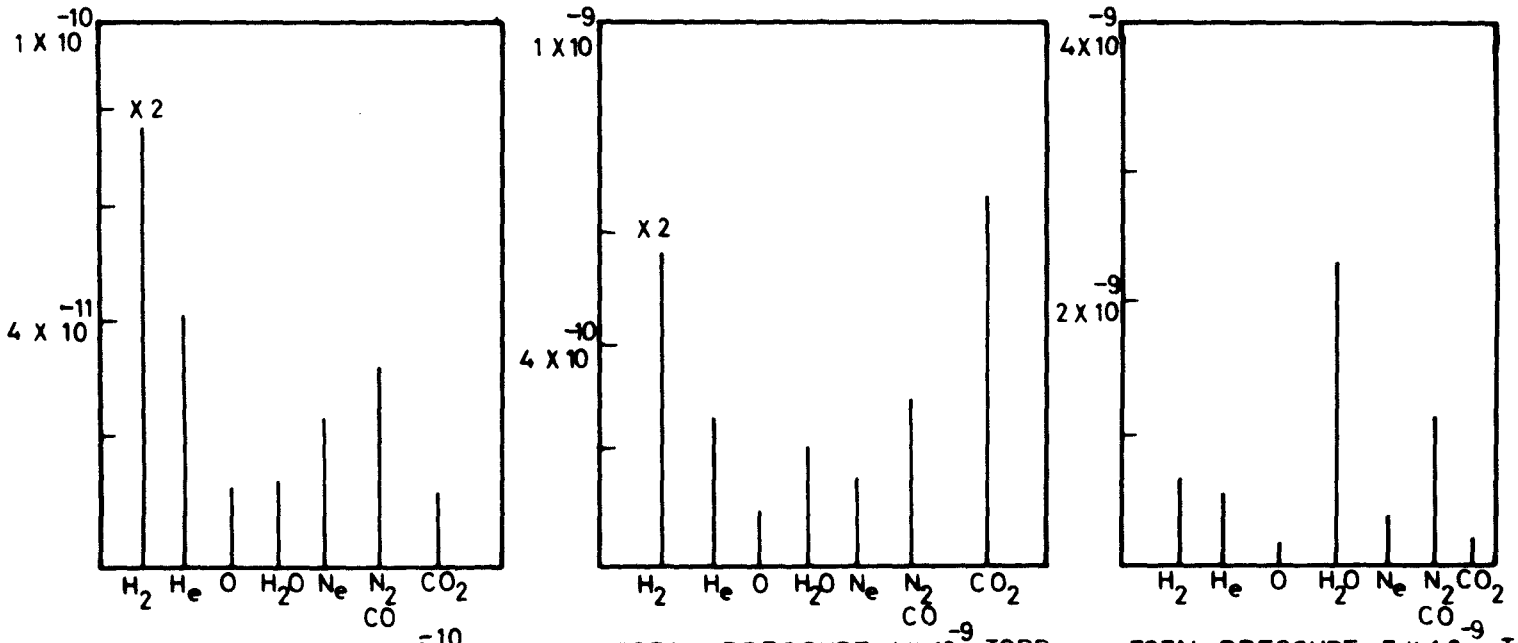

TOTAL PRESSURE 4×10^{-10} TORR

GUN FILAMENT COLD

(a)

TOTAL PRESSURE 4×10^{-9} TORR

GUN FILAMENT 60%

(b)

TOTAL PRESSURE 7×10^{-9} TORR

GUN FILAMENT 100%

ELECTRON BEAM SWITCHED ON

(c)

FIG. 58.

spectra obtained at various stages of the bake-out cycle, of the manifold system. The bake-out cycle lasted 48 hours, rising upto a temperature of 250°. The corrected values of the partial pressures before bake-out, at temperatures 150°C and 250°C and after bake-out are given. The last one was taken after the system had been cooled down to room temperature and the electron gun not operating. It is seen that after bake-out, hydrogen is by far the most abundant gas in the system. The fractions of water vapour and carbon dioxide are small. Surprisingly enough, a considerable amount of neon is present.

It is perhaps more important to analyse the gases present while the electron gun is operating, because it is under these conditions that the target is being bombarded by the electron beam. Fig. 58 gives the corrected values of the partial pressures while the cathode is being heated up by the gun filament. Fig. 58(a) shows the spectrum with cathode cold. When the cathode is raised to 60% of the normal operating temperature, the total pressure goes up by about a factor of 10. The partial pressures of the predominant gases are shown in fig. 58(b). H_2O and CO_2 are evolved relatively more abundantly.

Fig. 58(c) shows the partial pressures, while the electron gun filament is operating at normal temperatures and the primary electron beam of energy 900eV bombarding a silver target. Under these conditions water vapour is the most abundant gas, with a considerable amount of He also present. On the other hand, hydrogen is relatively only a small fraction. It is observed that as soon as the electron gun filament is switched off, the H_2O peak diminishes in height rapidly, being pumped away by the Vac-ion pump.

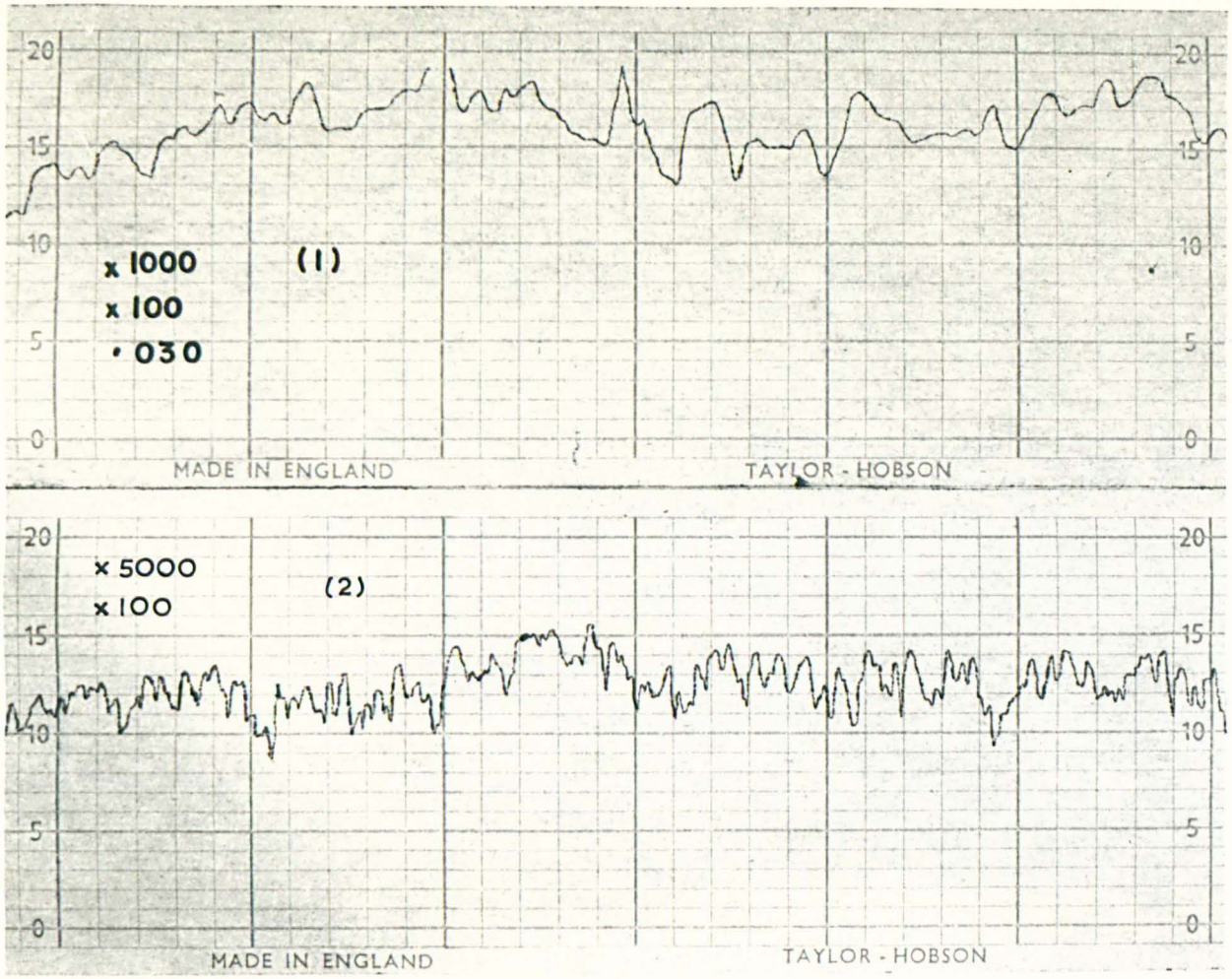

FIG. 59 Profile of the TaC surfaces

(1) Rough surface (x1000 vertically, x100 horizontally)

(2) Smooth surface (x5000 vertically, x100 horizontally)

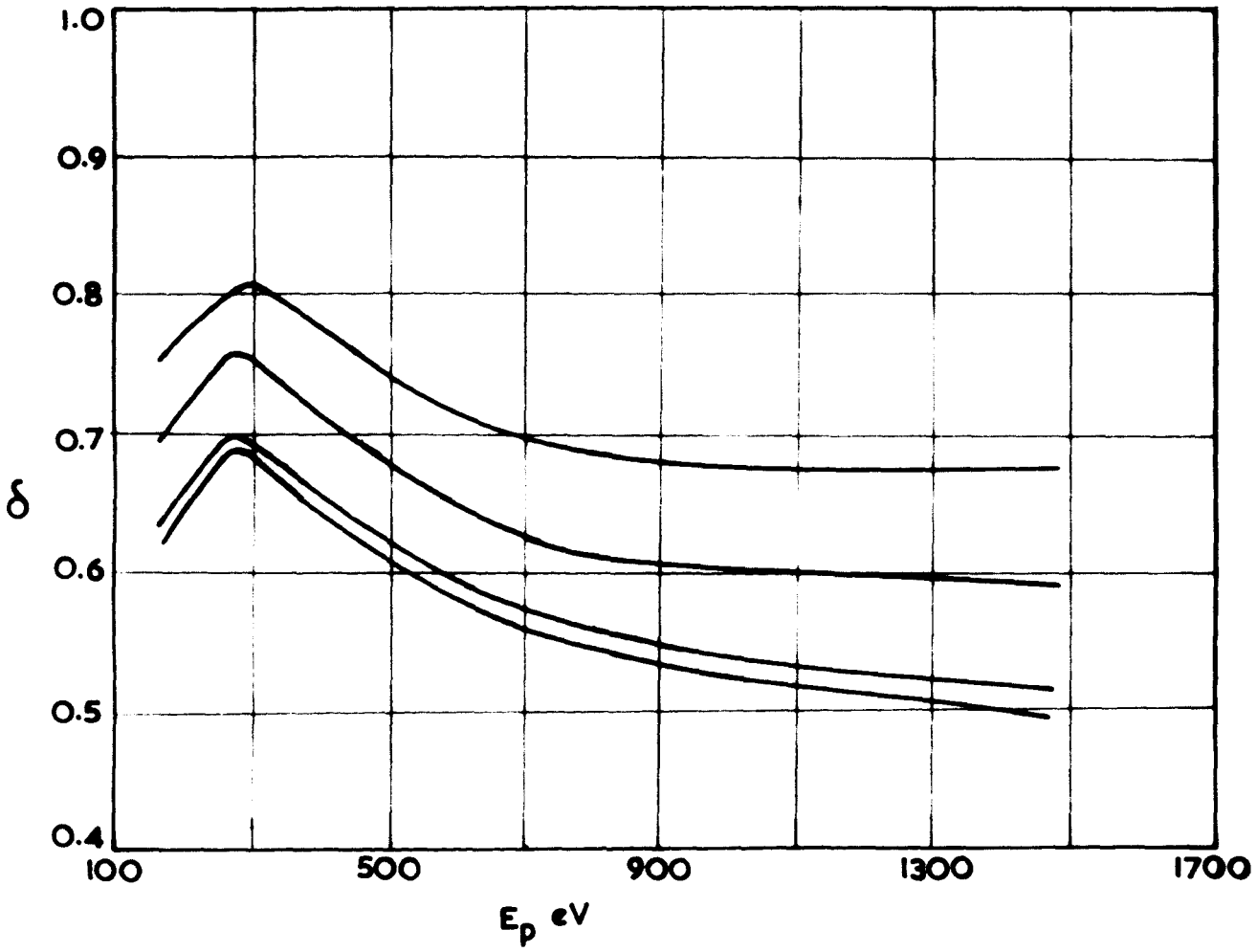

FIG·60. PROGRESSIVE LOWERING OF YIELD FROM A 'ROUGH' T_aC TARGET WITH HEAT TREATMENT.

6.3 Yield Measurements

6.3.a Tantalum carbide

It has been said in section 2.3 that Kreuchen and Diserens (79) suggested the use of TaC as a low yield surface to reduce the "multipactor effect" in klystrons. Owing to the lack of information on the SEE properties of TaC and the commercial importance of it as a low yield surface, the properties of TaC were studied. The secondary emission yield was measured from such a surface, with particular reference to the surface conditions. The present investigation provides the first published data on the secondary emission characteristics of tantalum carbide (192).

Initially, yield measurements were made on a "rough" TaC surface, the profile of which was measured on a "Talisurf" machine (Trace 1, fig. 59). At first the yield curve had an irregular shape presumably due to the rather unclean surface. The target was then heated to about 800°C for six hours, by the projection lamp filament located behind it. When the target was cold and the pressure conditions improved to about 10^{-9} torr, the experiment was repeated. Results obtained after successive heat treatment showed that the yield decreased with each progressive heat treatment (fig. 60). A stage was reached, however, when there was practically no change in the yield, even after further heating, presumably because the surface was thoroughly degassed and cleaned. The yield curve thus obtained is the one characteristic of the "rough" TaC surface. The maximum yield δ_{max}, for this surface was found to be 0.68 at a primary energy 270eV. The yield decreased to 0.5 at an E_p of about 1400eV.

Yield measurements were then made for a smoother TaC surface,

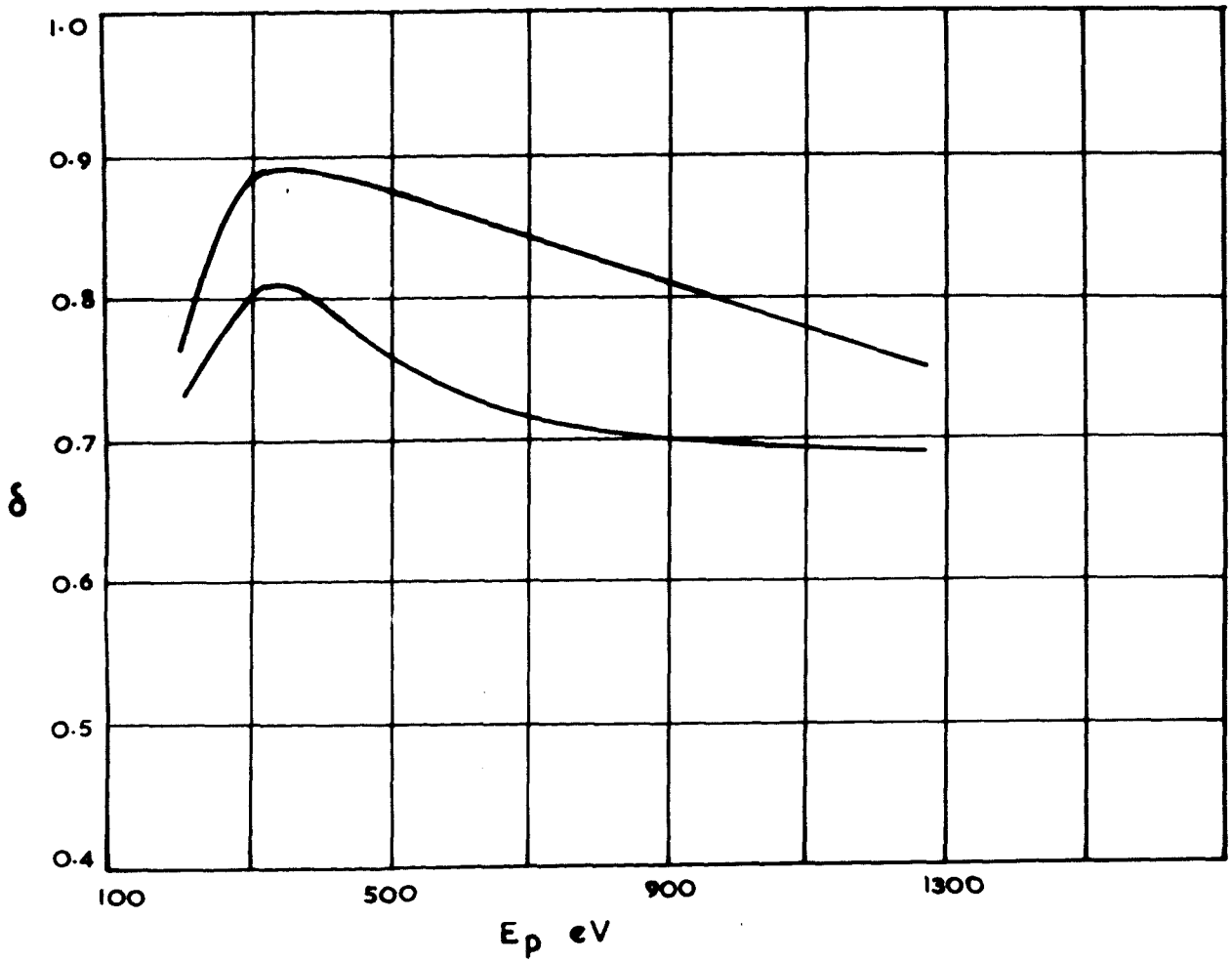

FIG. 61. PROGRESSIVE LOWERING OF YIELD FROM A 'SMOOTH' TaC TARGET WITH HEAT TREATMENT.

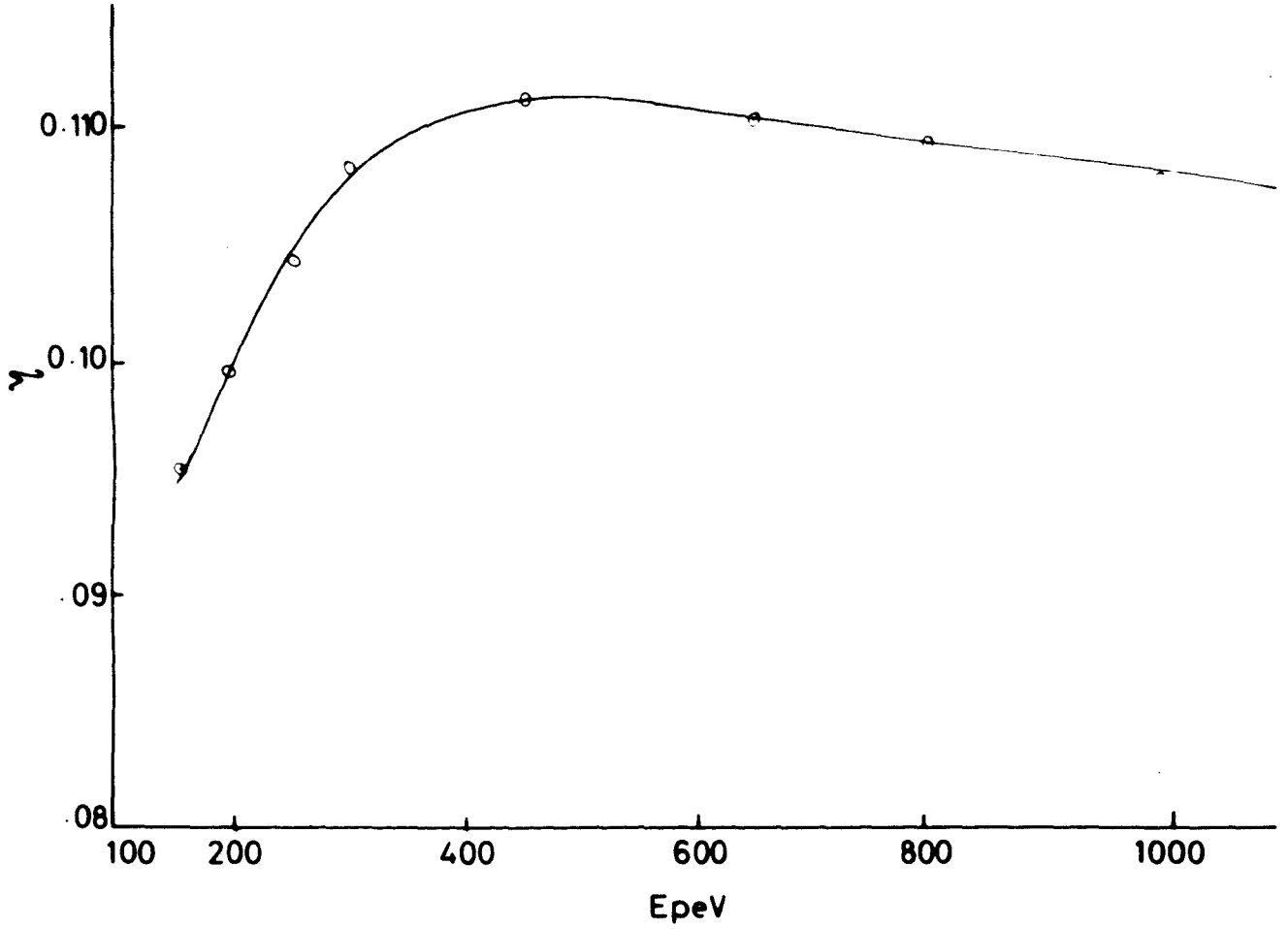

FIG. 62. η vs Ep FOR TANTALUM CARBIDE.

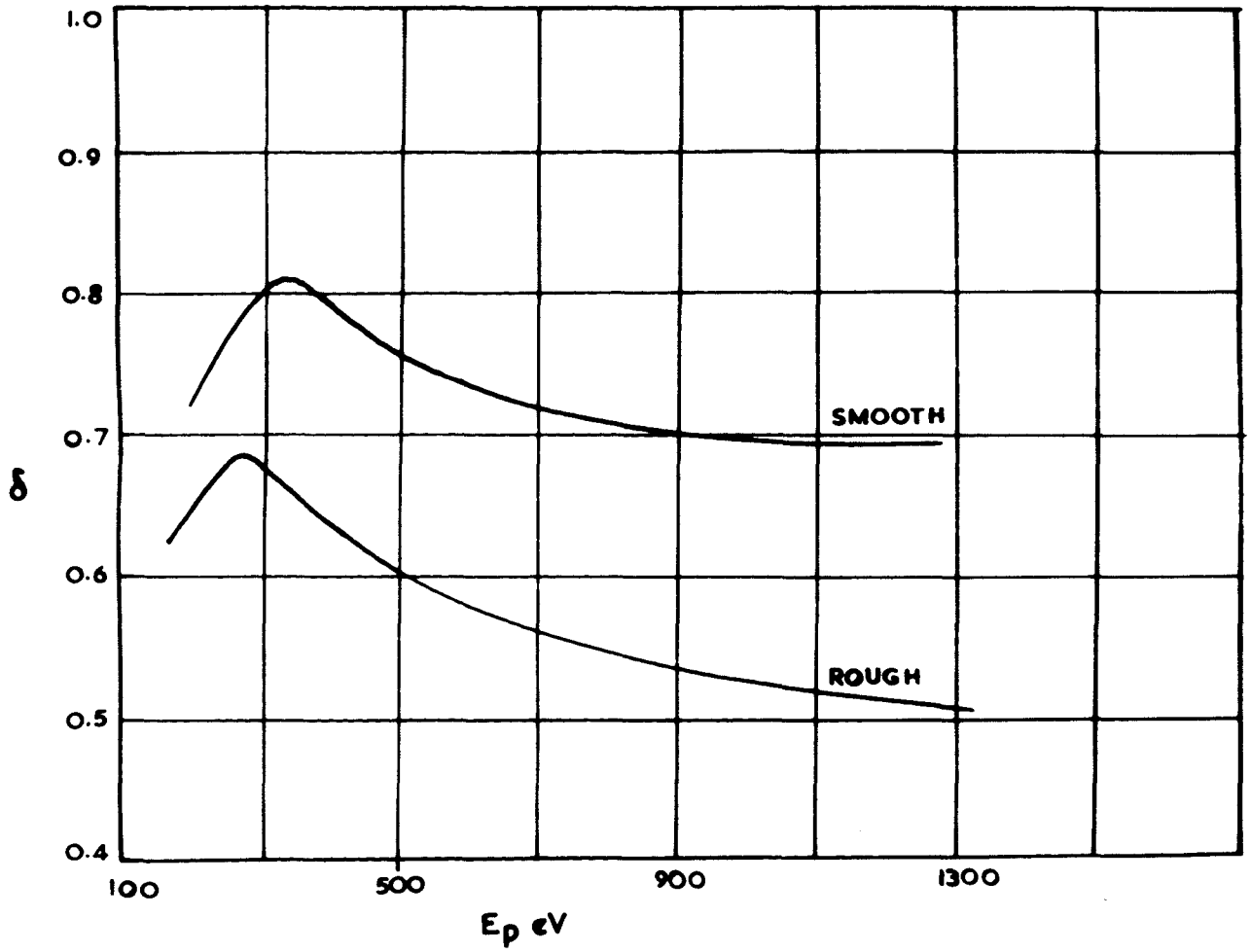

FIG. 63

the profile of which is shown in the lower trace of fig. 59. This target was also subjected to the same heat treatment procedure as before. In fig. 61 the lower curve represents the yield of this surface after the heat treatment cycle. For this "smoother" surface the yield was higher than that for the rough surface. δ_{max} had a value of 0.81 occurring at a primary energy of about 320eV. In the case of the smoother target it was also observed that the peak in the yield curve was flatter than for the rough surface. This makes it difficult to determine $E_{p_{max}}$ very accurately.

By deflecting the primary beam, using the 'X' and 'Y' plates the yield from neighbouring parts of the target was measured. A variation of 5 to 10% in the yield was noticed. This is quite understandable when one considers the non-uniformity of the surface.

The inelastic reflection coefficient, η , plotted against the primary energy is given in fig. 62. The maximum value of η is 0.11 occurring at a primary energy of about the same as $E_{p_{max}}$

The yield curves for the two "rough" and "smooth" surfaces are compared in fig. 63. The lower value of yield from a rough surface observed in the present investigation is in agreement with the evidence obtained by previous workers (3,11), who studied other surfaces. The comparison by Bruining (11) of a rough surface to a series of "holes" or "wells" (fig. 9) may be justified in the light of the profile of the surfaces shown in fig. 59. A secondary electron produced in the bottom of the well can get trapped on the sides and hence be prevented from being emitted at the surface. There is less chance of the secondary electron being trapped for a smoother surface and hence presumably the

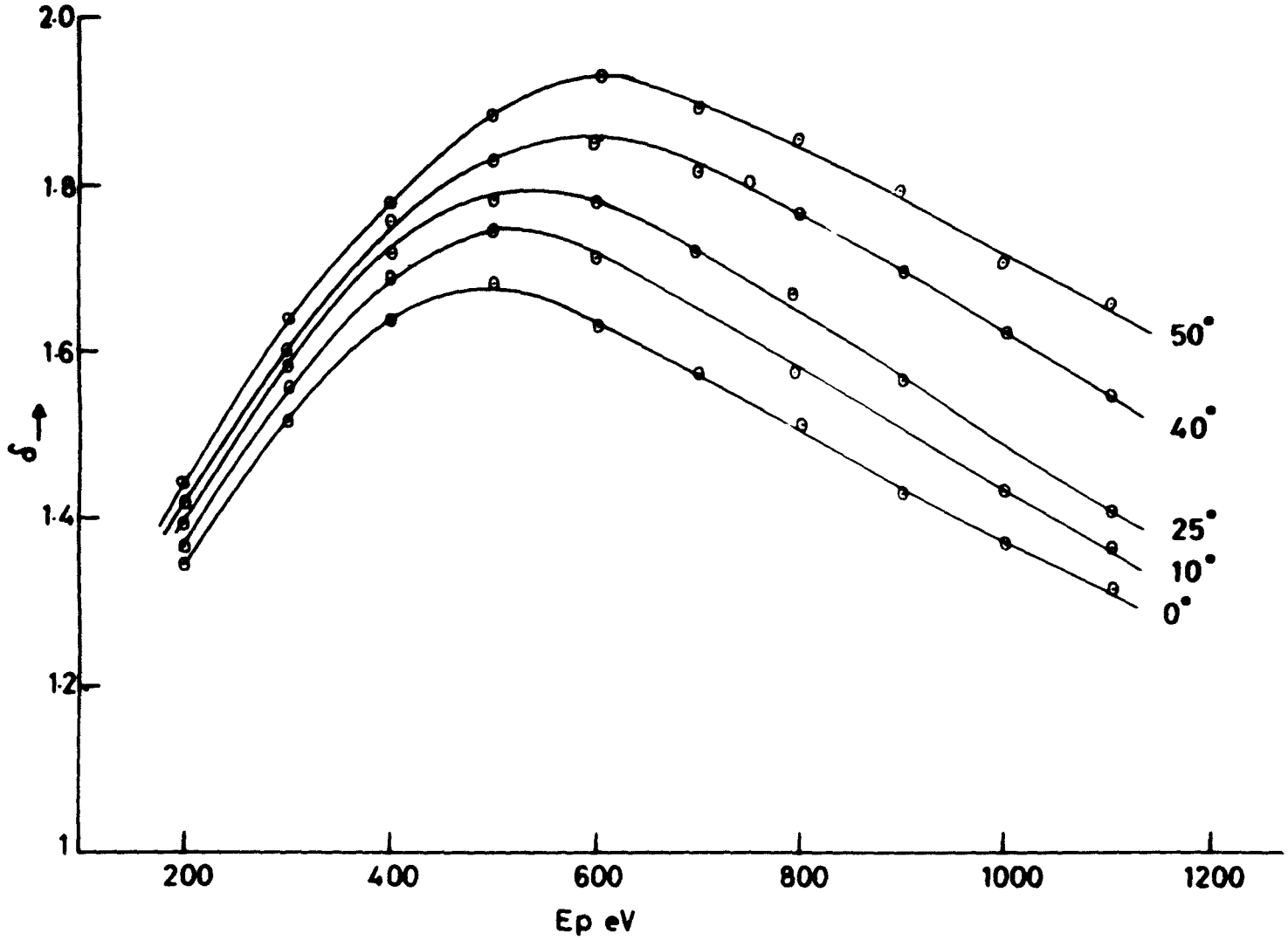

FIG.64. VARIATION OF YIELD WITH θ FOR NICKEL.

the yield is higher.

Though theoretically one should not expect any change in the value of $E_{p_{max}}$ with roughness, a definite change has been observed in this study. This could be ascribed to the geometrical nature of the surface, rather than to the characteristic of the material.

6.3.b Nickel

The total yield, δ, was measured from a highly polished nickel surface, first for normal incidence of the primary beam and then for different angles of incidence up to 60°. All measurements were made only after cleaning the surface by heat treatment. The $\delta - E_p$ curves for the different angles are given in fig. 64. δ_{max} at normal incidence was found to be 1.67 at about a primary energy, $E_{p_{max}}$ 460eV. As is seen from fig. 64, there is a general increase in the values of the yield with higher angles of incidence of the primary. $E_{p_{max}}$ also shifts towards higher energy with increase in angle of incidence. The variation of η, the inelastic reflection coefficient, with E_p is in excellent agreement with the results of Sternglass (165). The limiting value for η is 0.28 as compared to the value of 0.26 obtained by Sternglass.

The value of δ_{max} at normal incidence, is higher than the value 1.35 obtained by Bruining (11). The higher value of δ_{max} obtained in the present investigation could be due to the high smoothness and cleanliness of the surface. The poor vacuum conditions used by Bruining could account for the low yield value he got.

According to Bruining, the variation of the yield with angle of

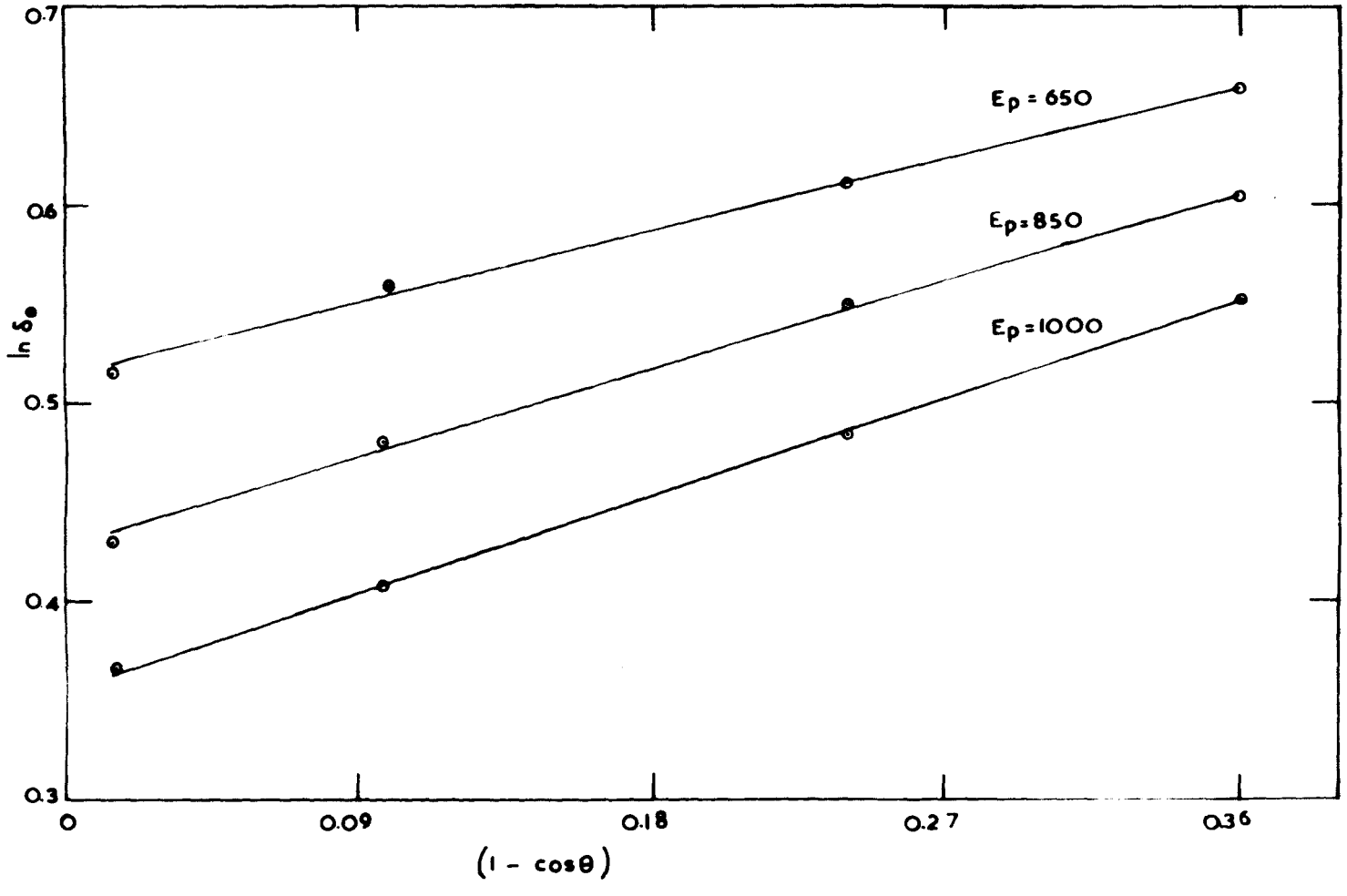

FIG. 65 $\ln \delta_0$ vs $(1-\cos\theta)$ FOR NICKEL.

incidence of the primary beam is given by equation (6), namely

$$\delta_\theta = \delta_o \exp \left[\alpha x_s (1 - \cos \theta) \right] \qquad (6)$$

where δ_θ and δ_o are the yields at angles of incidence θ° and 0°.

α - the absorption coefficient

x_s - the average depth of origin of the secondaries.

If one assumes this equation, a plot of $\ln \delta_\theta$ against $(1 - \cos \theta)$ should yield a straight line. From the above measurements, a plot was made, for the nickel target. For primary energies lower than $E_{p_{max}}$, the linearity of such a plot was not satisfactory. This is understandable when one considers the fact that the yield is governed mainly by the absorption coefficient only for primary energies greater than $E_{p_{max}}$ (section 1.8).

For E_p higher than $E_{p_{max}}$, graphs were plotted with $\ln \delta_\theta$ against $(1 - \cos \theta)$. Fig 65 gives a set of such graphs. These graphs are straight lines, the linearity being remarkably good for higher primary energies. The slope of these graphs gives the product αx_s. If the value of α is known, x_s can be calculated. Becker (37) from his study of high energy electrons, gives the value of α for nickel to be 1.5×10^6 cm.$^{-1}$. Assuming this value to be valid for the energy range concerned here, x_s was calculated. It was found that in the case of nickel, the mean depth of origin of the secondaries increased from 28Å for a primary energy of 600eV, to 38Å for 1200eV. Bruining from his experiments got a value of x_s = 30Å for nickel. The change in the value of x_s with primary energy, though not seen by Bruining, may be due to the oversimplified nature of equation (6) and because of the fact that the effect of n

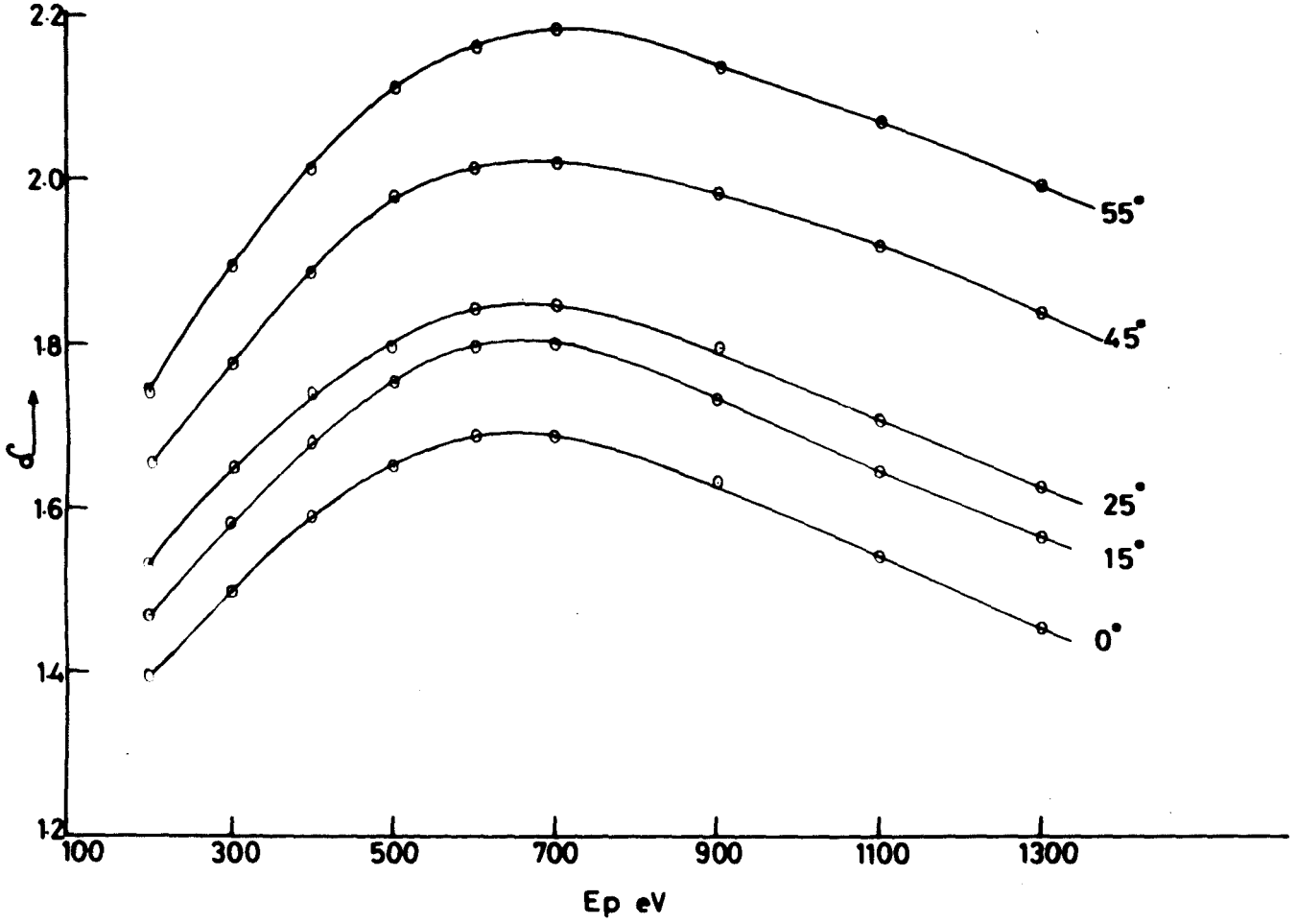

FIG. 66. VARIATION OF YIELD WITH ANGLE OF INCIDENCE θ FOR SILVER.

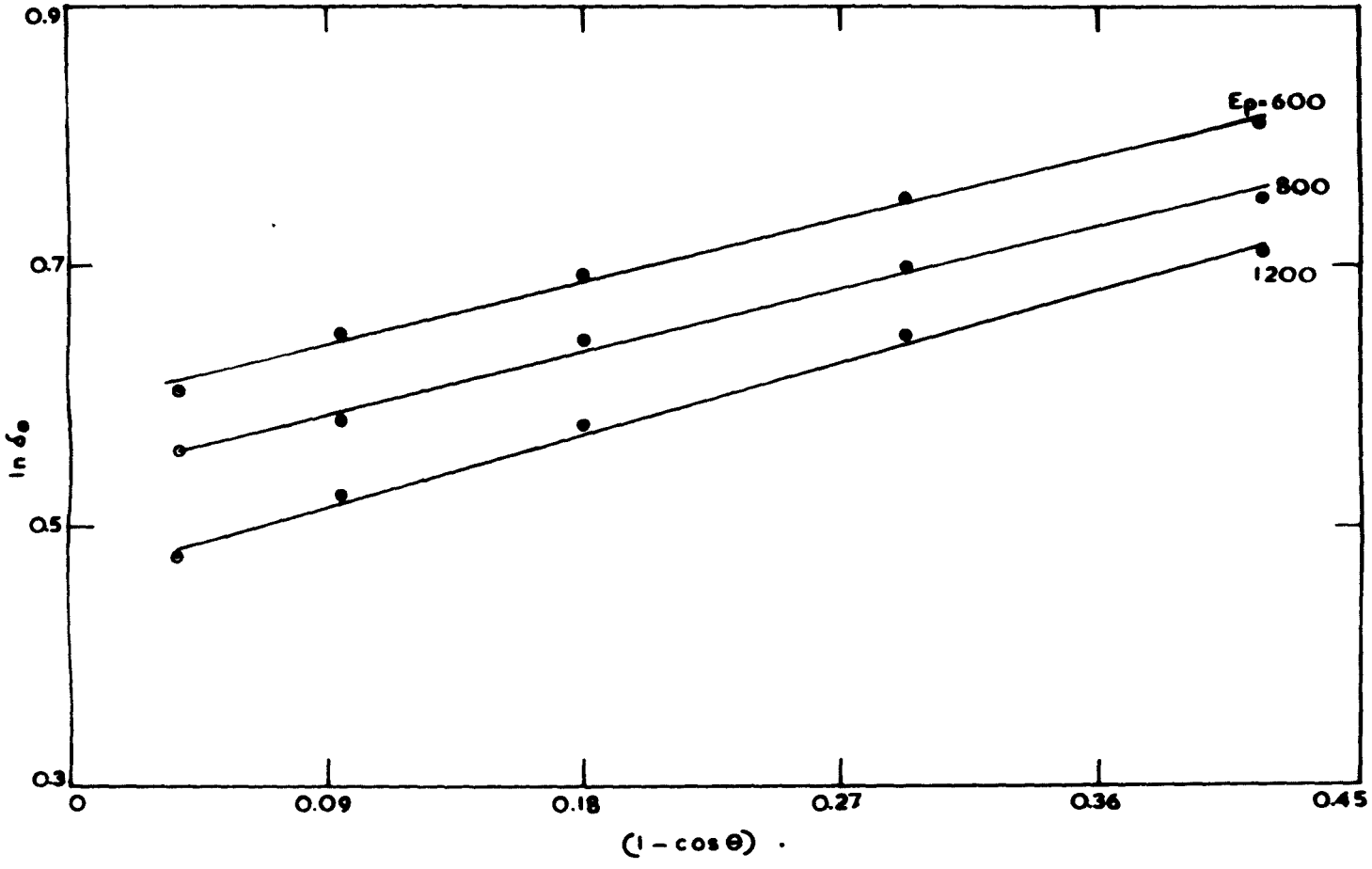

FIG. 67. $\ln \delta_0$ vs $(1-\cos\theta)$ FOR SILVER.

has been ignored. Despite the fact that Becker's value of α, for nickel is for high energy electrons, the above calculations do yield an approximate value of the mean depth of origin of the secondaries, which is in good agreement with the values obtainedby Bruining (11) and that obtained by Jonker (38) by an entirely different method.

6.3.c Silver

The silver target was prepared by evaporation. The total secondary emission yield for different angles of incidence of the primary beam, was measureed. The yield curves for angles 0°, 15°, 25°, 45° and 55° are given in fig. 66, At normal incidence δ_{max} has a value 1.63 occurring at $E_{p_{max}}$ = 680eV. The graphs drawn between ln δ_{θ} and (1 - Cos θ) are shown in fig. 67. The three graphs are for E_p = 800, 1000 and 1200eV.

Jonker (38) calculated a theoretical value for α of silver to be 3.3×10^{6} cm.$^{-1}$. However, considering the experimental value of Ni, he further suggests that this theoretical value of α is far too high and in practice the value may be only $\frac{1}{5}$ of the theoretical value. Following this suggestion a value of 6.6×10^{5} cm.$^{-1}$ was taken for α of silver, in calculating the mean depth of origin of secondaries. Assuming the above value for α, from the slope of the graphs x_s was calculated to be about 60 Å for silver. Bronshtein and Segal (4, 5) in their study on the inelastic reflection coefficient, experimentally determined the range of the secondaries (section 2.5.c). For silver they give a value for x_s of silver to be 12 - 20 atomic layers.

As in the case of nickel, even though there is a general increase

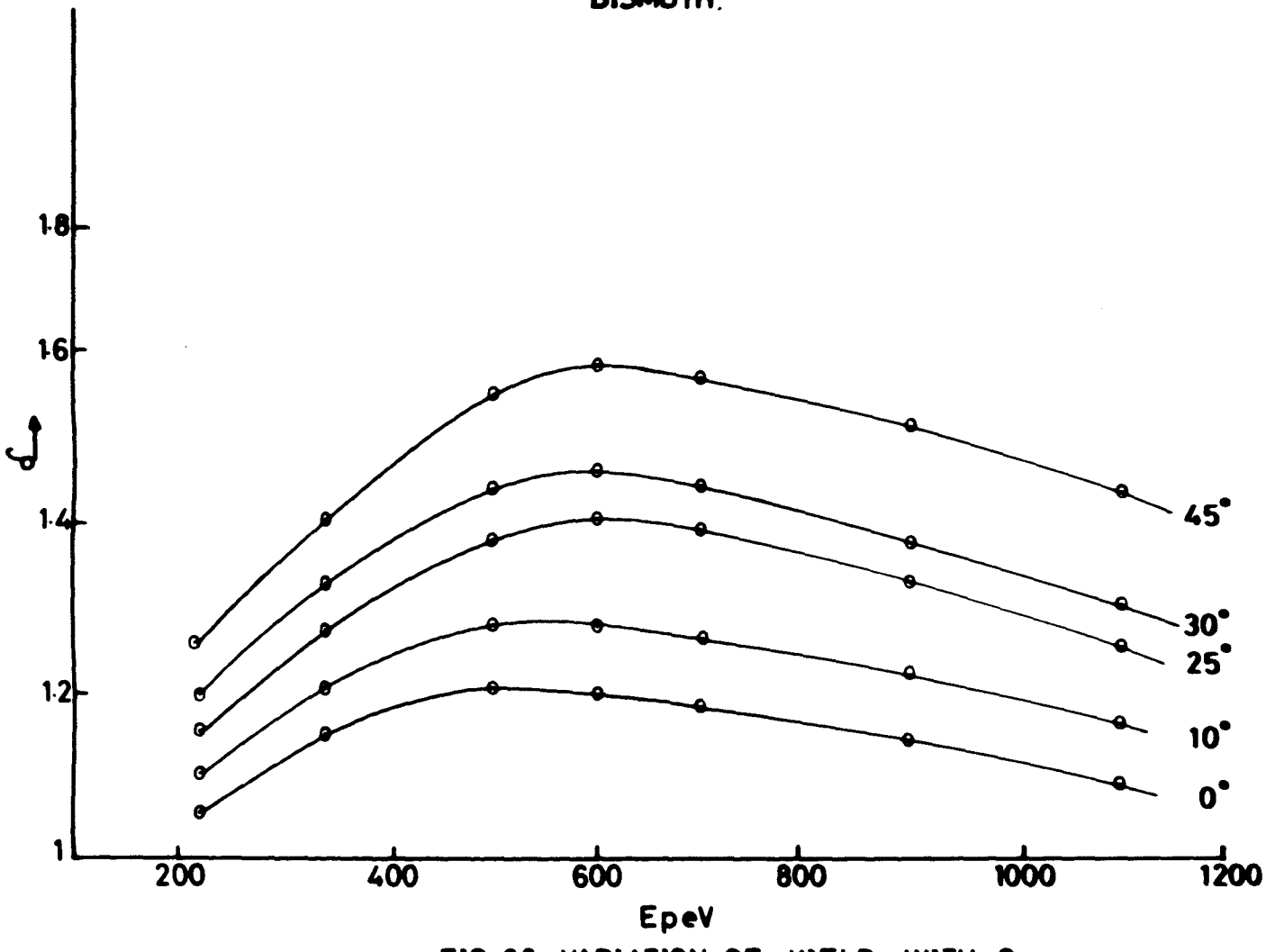

FIG.68. VARIATION OF YIELD WITH θ FOR BISMUTH.

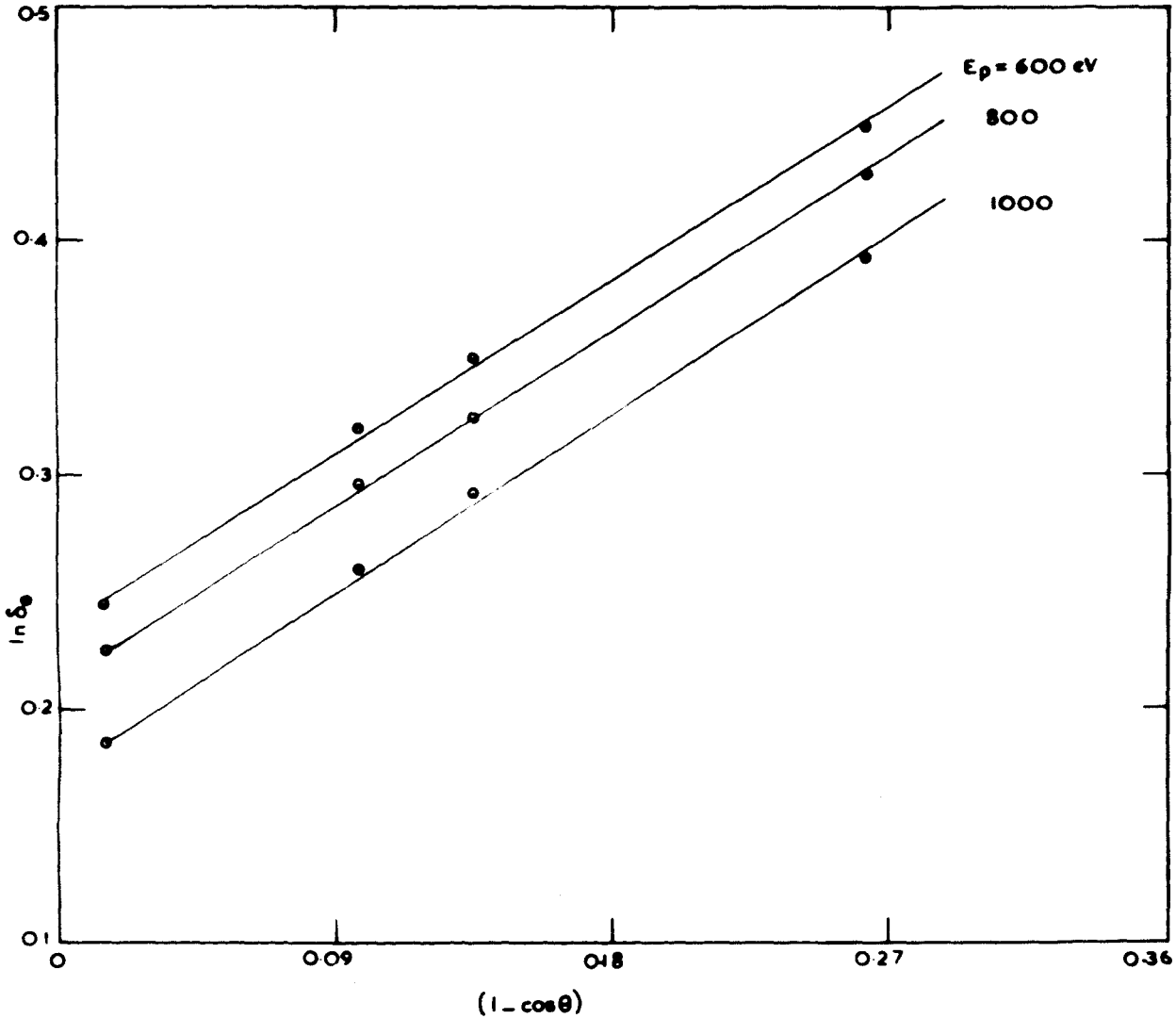

FIG. 69. $\ln \delta_e$ vs $(1-\cos\theta)$ FOR BISMUTH.

in the value of $E_{p_{max}}$ with increasing angle of incidence of the primaries, the variation is not strictly proportional to $\frac{1}{\sqrt{\text{Cos }\theta}}$. It must be said, however, that the rather flat peak of the yield curve made a very accurate determination of $E_{p_{max}}$ difficult.

6.3.d Bismuth

The angular dependence of the yield curve for an evaporated bismuth target is shown in fig. 68. The parameters δ_{max} and $E_{p_{max}}$ for Bi, obtained by Morozov (26) for normal incidence of the primary beam agree reasonably well with the values obtained in the present study. The value of δ_{max} is 1.22 as opposed to 1.15 obtained by Morozov. A set of graphs drawn betwen ln δ_θ and (1 - Cos θ) is given in fig. 69. A value for the absorption coefficient α of Bi, is not available from direct experimental evidence. Assuming α to be directly proportional to the density of the material, and inversely proportional to $E_{p_{max}}^{\ 2}$, a value for α of Bi, is extrapolated from Jonker's table of values for other materials (38). A value of 1.56 x 10^6 cm.$^{-1}$ is obtained by this extrapolation. Assuming this approximate value for α, x_s is calculated from the slope of the graphs in fig. 69. Thus x_s is found to be $\simeq$ 52Å. Bronshtein by depositing thin films on cold substrates finds a value of $\simeq$ 7 atomic layers ($\simeq$ 26Å) for x_s of Bi. However, on depositing onto warm substrates he gets a value much higher than 7 atomic layers. Even if one takes x_s = 7 atomic layers to be the correct one, the rather high value of 52Å may be due to the low value of α assumed in this case. A very accurate calculation of x_s, in this way is not possible until a more accurate value for α has been obtained from direct experiments.

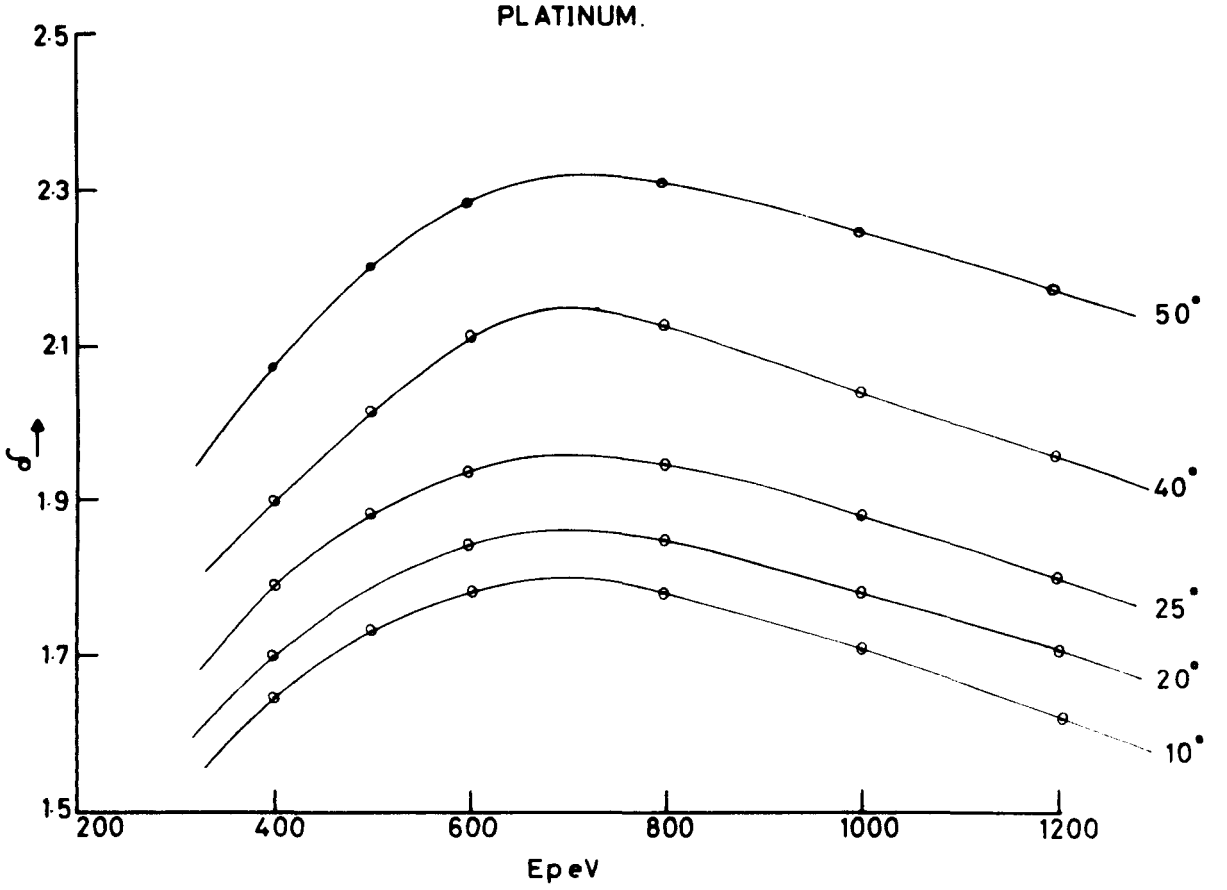

FIG. 70. VARIATION OF YIELD WITH θ FOR PLATINUM.

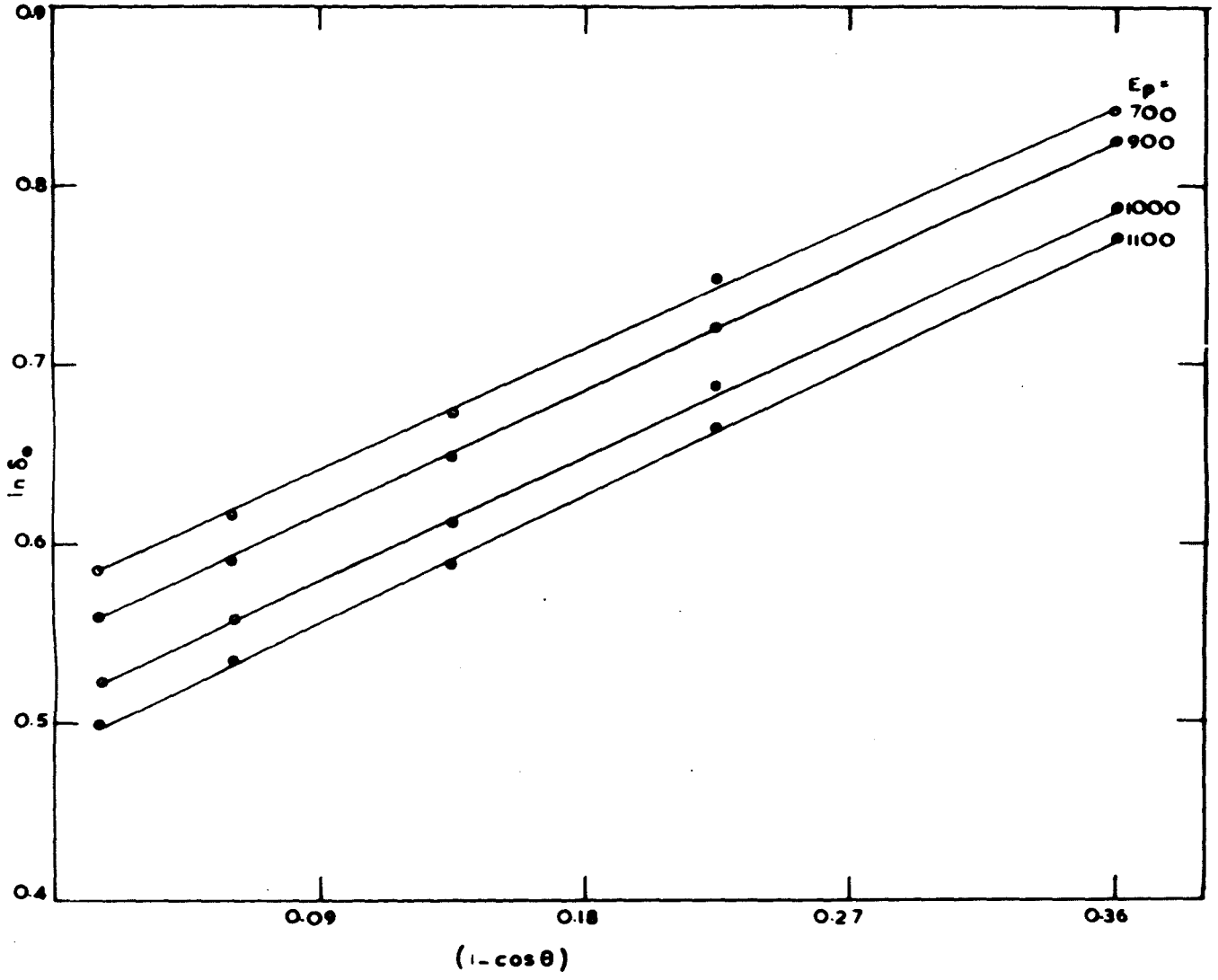

FIG. 71. $\ln\delta_0$ vs $(1-\cos\theta)$ FOR PLATINUM.

6.3.e Platinum

The secondary emission yield from a platinum ribbon, outgassed and cleaned by heat treatment was also measured, for various angles of incidence of the primaries. The yield curves for the different angles of incidence are given in fig. 70. For normal incidence, δ_{max} has a value 1.74 which is nearer to the value 1.8 obtained by Copeland (11) and Bronshtein and Segal (4) than the value 1.5 given by Kollath (23). $\ln \delta_\theta$ against $(1 - \cos \theta)$ was again plotted for primary energies above 700eV and a set of such graphs is given in fig. 71. In the case of platinum also, a value for α is not available from direct experimental evidence. However, as in the case of bismuth, a value for α may be extrapolated from the corresponding value for nickel. The value thus obtained for platinum is 3.42×10^6 cm.$^{-1}$. From the slope of the straight lines, x_s was calculated. For platinum, this value was found to be $\simeq 23$Å.

The different parameters of SEE for the metals studied are tabulated in Table 4. Since the values of α are not very accurately known in the energy range concerned, the calculated values of the mean depths of origin of secondaries may only be taken as approximate. However, such a determination of the mean depth of origin of secondaries from the variation of the yield with the angle of incidence of the primary beam does yield values of the right order which tend to confirm that the secondary emission is largely a surface phenomenon.

TABLE 4

SEE parameters of the materials investigated

Material	δ_{max}	$E_{p_{max}}$	α (cm^{-1})	x_s (Å)
Nickel	1.67	460	1.5×10^6	28 - 38
Silver	1.63	680	6.6×10^5	60
Platinum	1.74	650	3.42×10^6	23
Bismuth	1.22	480	1.56×10^6	52
Tantalum Carbide	0.68	270	- -	-

FIG. 72. ENERGY LOSSES FROM SILVER.

PRIMARY ENERGY 400eV.

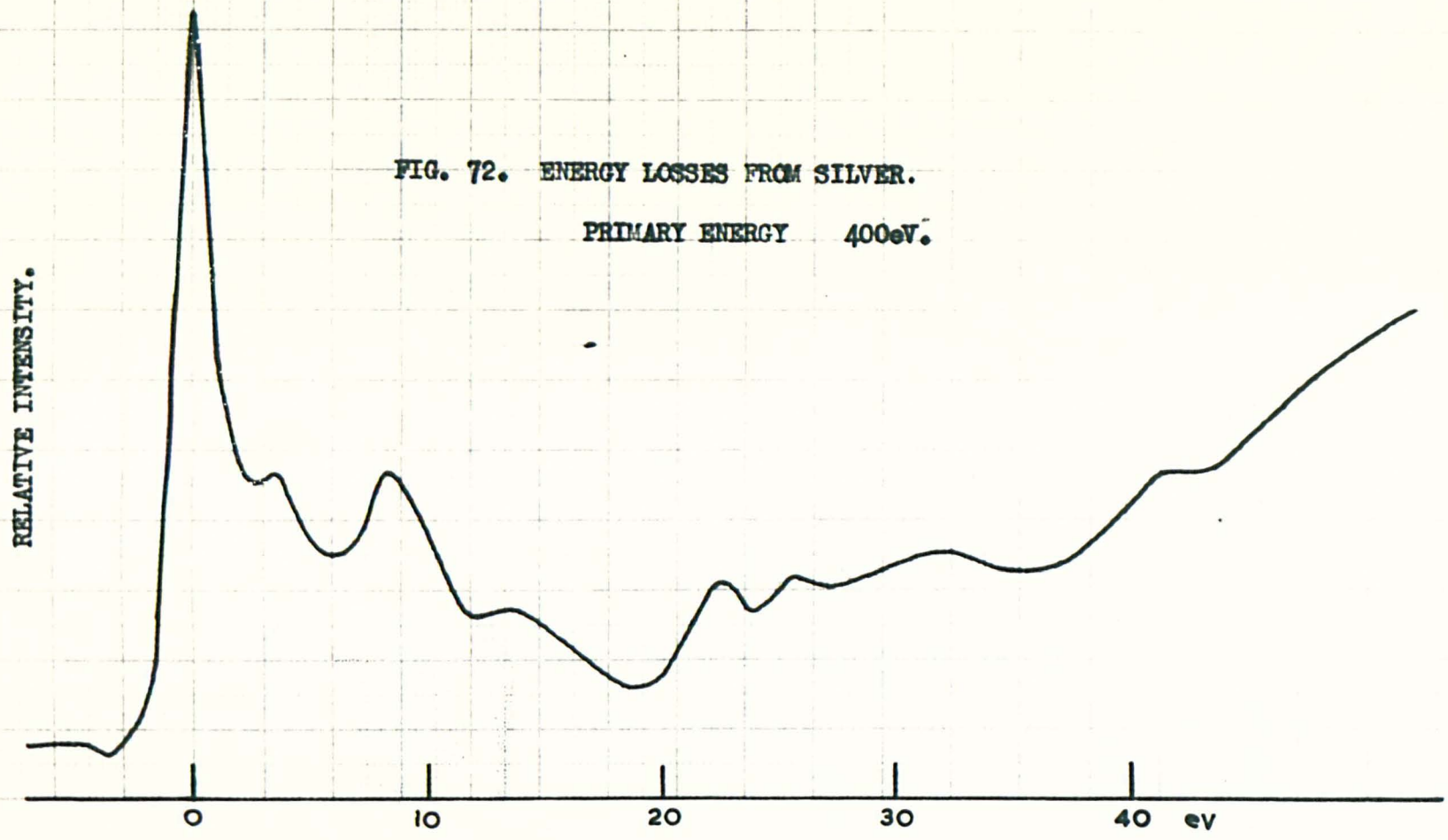

6.4 Characteristic Energy Loss Studies

6.4.a Silver

Characteristic energy losses from silver have been studied by many authors, both by the transmission and reflection methods. The loss spectrum from silver is very complicated and the explanations of the energy losses are varied. In the present investigation, energy losses from an evaporated silver target were measured, by using the retarding field energy analyser. A typical energy loss spectrum for a primary energy of 400eV is shown in fig. 72. Measurements using four different primary energies ranging from 200eV to 450eV did not show any change in the enrgy loss values. The spectrum could be scanned both ways - increasing and decreasing the retarding field - by reversing the motor driving the helipot. This reversal produced no change in the spectrum and always loss values were calculated as the mean of the two obtained this way. The modulating voltage was 350mV at a frequency 450 Hz. The elastically reflected primary peak had a half width of 2eV for a primary energy of 400eV.

The loss values obtained from the present investigation may be compared with the experimental results obtained previously by a few authors (Table 5).

TABLE 5

Characteristic Energy Losses (in eV) in Silver

as found in the present work and by other authors

Present Work	4.1	8.6	13.5	16.7	23.4	25.5	33.5	43.1
Robins (195)	4.1	7.3		17.2		25	33.5	
Rudberg (90)	4.6	7.4				24.8		
Marton et al. (107)	3.4	7		16.7		24.8		
Jull (201)	3.3	6.8	14.3		23.8			44.8
Watanabe (198)	3.4	8		17.5		25	34	
Gauthe (193)		7.5			22.1	26	36	43

There seems to be good general agreement for most loss values. Many of the previous workers could not however resolve the 23.4 and 25.5eV peaks. Most authors observe the loss peak at about 4.1eV, though the values vary from 3.4 to 4.6eV. The loss at 8.6 is the predominant one. The corresponding value obtained by other authors ranges from 6.8 to 8eV. A new loss at 13.5eV is observed in this study, though it appears only with small intensity. Very few workers find the two peaks 23.4 and 25.5eV, except Gauthe, probably because of the poor resolution of the analyser and surface conditions of the target. In addition to the above losses, two more losses at 33.5 and 43.1eV are distinguishable.

There are a wide variety of interpretations of these loss peaks by different authors. From the reflectance data of silver Ehrenreich and Philipp (157) found an energy loss peak occurring at 3.9eV which they explained as due to an interband transition of 4d electrons

to the Fermi level. The optical work of Taft and Philipp (194) leads to the prediction of two energy losses one at 3.75eV which may be explained as due to collective oscillations, and another one at about 8eV. Furthermore, Steinmann (148) and Brown et al. (149) have observed radiation arising from silver corresponding to an energy 3.75eV, which tends to suggest that the loss at 3.75eV is due to collective oscillations.

If one considers Ag to have one "free" electron per atom, the "plasmon" energy calculated from equation (55), $\hbar\omega_p = 28.8\ (\frac{Zd}{A})^{\frac{1}{2}}$eV, has a value 9.2eV. Ehrenreich and Philipp argue that owing to the strong influence of interband transitions, the value is displaced to 3.75eV. So this value would represent a volume plasmon. They however, indicate that this is not a free electron resonance as given by the plasma theory, but rather a "hybrid resonance" resulting from the cooperative behaviour of both the 4d and 5s electrons. However, since this hybrid resonance energy of 3.75eV is so close to the interband transition of 3.9eV, it is difficult to distinguish them experimentally. Hence the experimental value of 4.1eV may be due either to the hybrid resonance or to an interband transition or perhaps both. However, Pines (121) is of the opinion that at such low energies the interband transitions will dominate and hence the loss 4.1eV must be ascribed to interband transitions.

From their optical data, Ehrenreich and Philipp found a peak in the energy loss function $\mathrm{Im}\left|\frac{1}{\varepsilon}\right|$ at an energy 7.5eV, which is ascribed to the collective oscillation of the conduction electrons alone. The loss value of 8.6eV, obtained in the present study, may be due to such a collective oscillation. Robins (195) however, considers this loss to be a surface

plasma loss. It is difficult to agree with his argument, especially since he considers that 25eV is the volume loss. If 25eV were the volume loss, a surface loss should occur at 17.8eV. Though he finds a loss at 17.2eV, he leaves it as "unexplained".

A small peak is found to occur at about 13.5eV, which most other authors do not observe. However, referring to the Robins' loss spectrum, one can see a small hump at about this value, though he does not quote it as a loss. Jull (201) observed a loss at 14.3eV, which might be the same loss as observed in this study. This loss might be due to an interband transition or perhaps a combination of the 4.1eV and 8.6eV losses.

The loss at 16.7eV agrees with the values obtained by previous workers. Robins leaves this loss as "unexplained". From the X-ray fine structure studies of the K-absorption edge, a maximum in the absorption spectrum is observed at an energy 17eV (196). This value agrees with the observed loss 16.7eV. Hence it is likely that this loss is due to the excitation of conduction band electrons to the allowed unoccupied levels. If, however, 8.6eV is the volume plasma loss, the peak at 16.7eV could very well be due to the electrons having excited two plasmons.

The loss at 23.4eV agrees well with the absorption maximum in the X-ray spectrum which corresponds to 24eV, and hence may be due to the excitation of conduction electrons. The losses at 25.5 and 33.5eV are thought of as due to electrons having excited 3 or 4 plasmons. However, the loss 33.5eV agrees with the value of 33eV corresponding to an absorption maximum in the X-ray spectrum. The loss 43.1eV agrees with the 44eV obtained from X-ray fine structure, which hence may be due to the excitation of conduction electrons.

FIG. 73. ENERGY LOSSES FROM BERYLLIUM.

PRIMARY ENERGY 300eV.

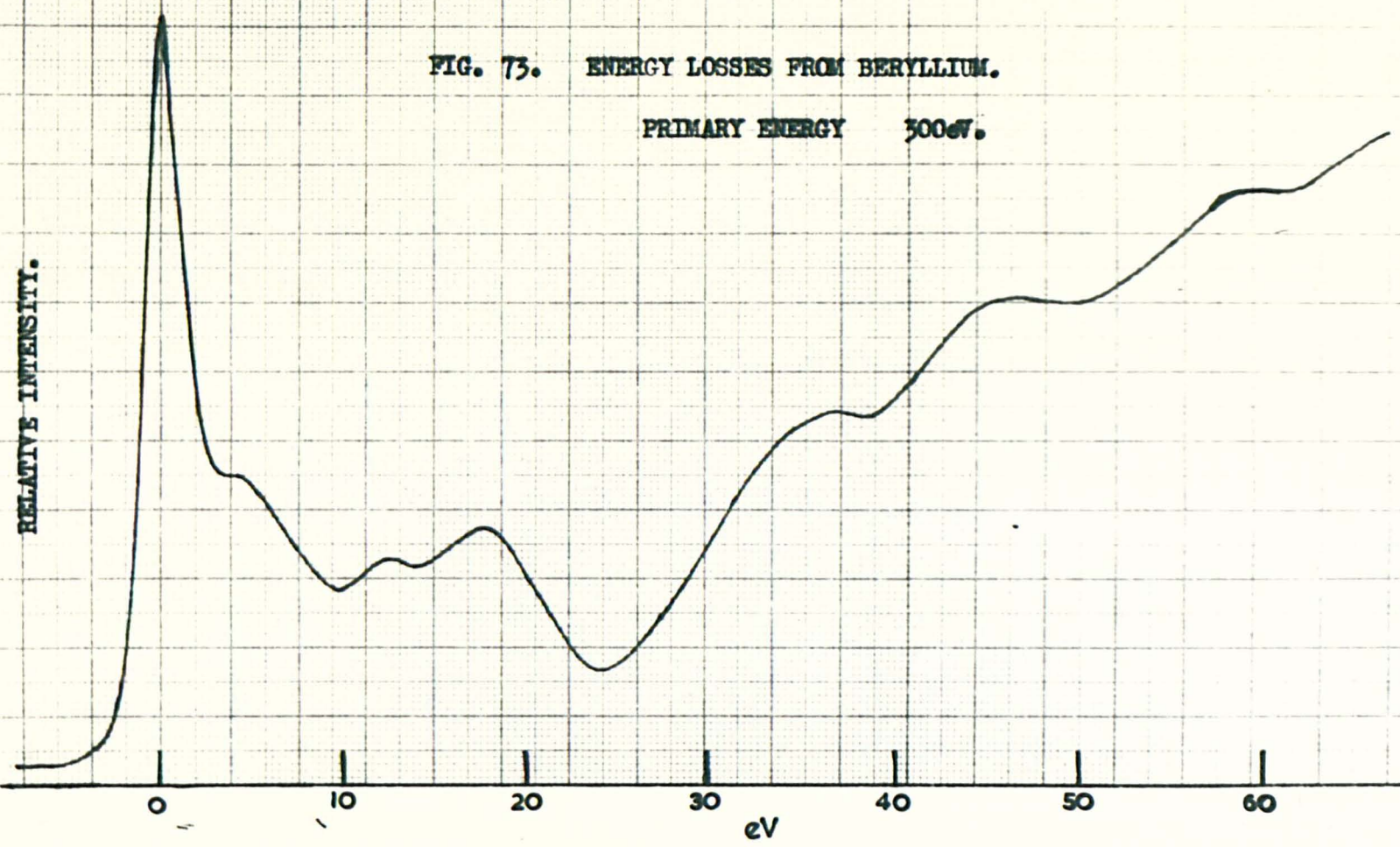

6.4b Beryllium

Characteristic energy losses from an evaporated beryllium target were measured using the same analyser. A typical loss spectrum for a primary energy 300eV is shown in fig. 73. The different energy loss values are compared with those observed by previous workers, in Table 6.

TABLE 6

Characteristic Energy Losses (in eV) in Be

as found in the present work and by other authors

Present Work	4.4	12.1	18.9	28	37.4	43.5	57.8
Powell (105)		11.9	19.9		39.4		58.4
Marton and Leder (103)	6.5		18.9				
Gauthe (193)			19	28	38.1		
Kleinn (102)			17.3		36.7		54

There is general agreement in most of the values except for a loss at 4.4eV which has not been observed by others. However, Marton and Leder (103) observe a loss at 6.5eV. The loss at 4.4eV cannot be explained on the basis of collective oscillations of the valence electrons. Perhaps this could be due to an interband transition. If it is assumed that in Be there are two electrons per atom free, capable of collective oscillations, the theoretical value of the volume plasmon energy will be 18.4eV, which agrees well with the loss 18.9eV observed in the present study.

The loss at 12.1eV is identified as the surface plasmon loss, since

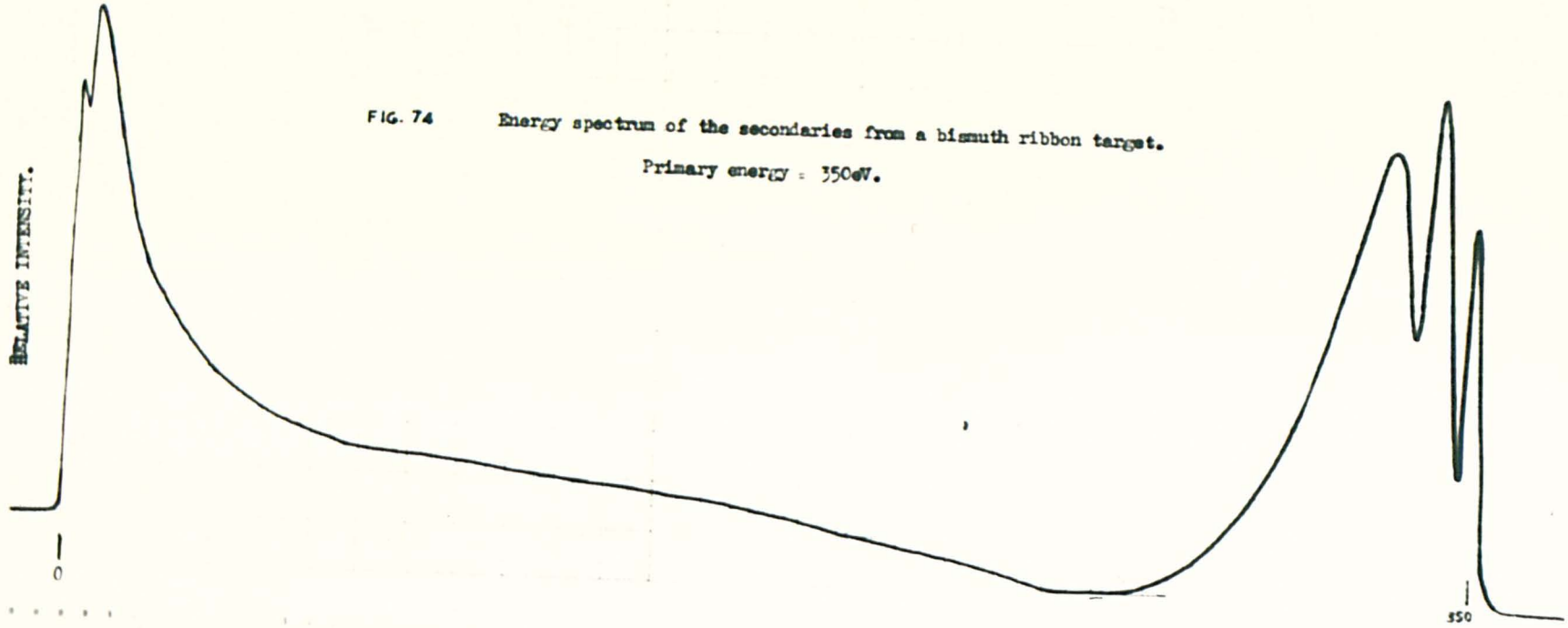

FIG. 74 Energy spectrum of the secondaries from a bismuth ribbon target.
Primary energy = 350eV.

it agrees approximately with the theoretical value of $\frac{\hbar \omega_p}{\sqrt{2}}$ = 13eV. The losses 37.4eV and 57.8eV could be due to the electrons having excited two and three volume plasmons respectively. However, in the X-ray absorption spectra there do occur fine structures corresponding to 35.8 and 56.9eV (196). Hence it may be argued that the above two losses are due to interband transitions. Nevertheless simply because of the fact that fine structures occur at these energies, it is not necessarily true that the losses are due to interband transitions as has been suggested by Pines (123). Some of the fine structures in the X-ray absorption spectrum might very well be due to the collective oscillations of electrons. The small "hump" occurring at 43.5eV, though not observed by many others, may be due to an interband transition, especially since an absorption maximum is observed near this energy, in the X-ray spectrum.

6.4.c Bismuth

Initially, a bismuth ribbon obtained commercially (Purity 4N) was used as the target. A complete energy distribution of the secondary electrons from this target was plotted. One such distribution curve for a primary energy of 350eV is shown in fig. 74. The true secondary peak occurs at about 2.5eV. One interesting feature of the spectrum is the large number of inelastically reflected primaries. There are two large loss peaks occurring at 7.4eV and 19.7eV. These two loss peaks are, in fact, found to be more intense than the primary peak. The 7.4eV peak has a half width smaller than that of 19.7eV. Since the target had been exposed to air, it is very likely that the surface was oxidised.

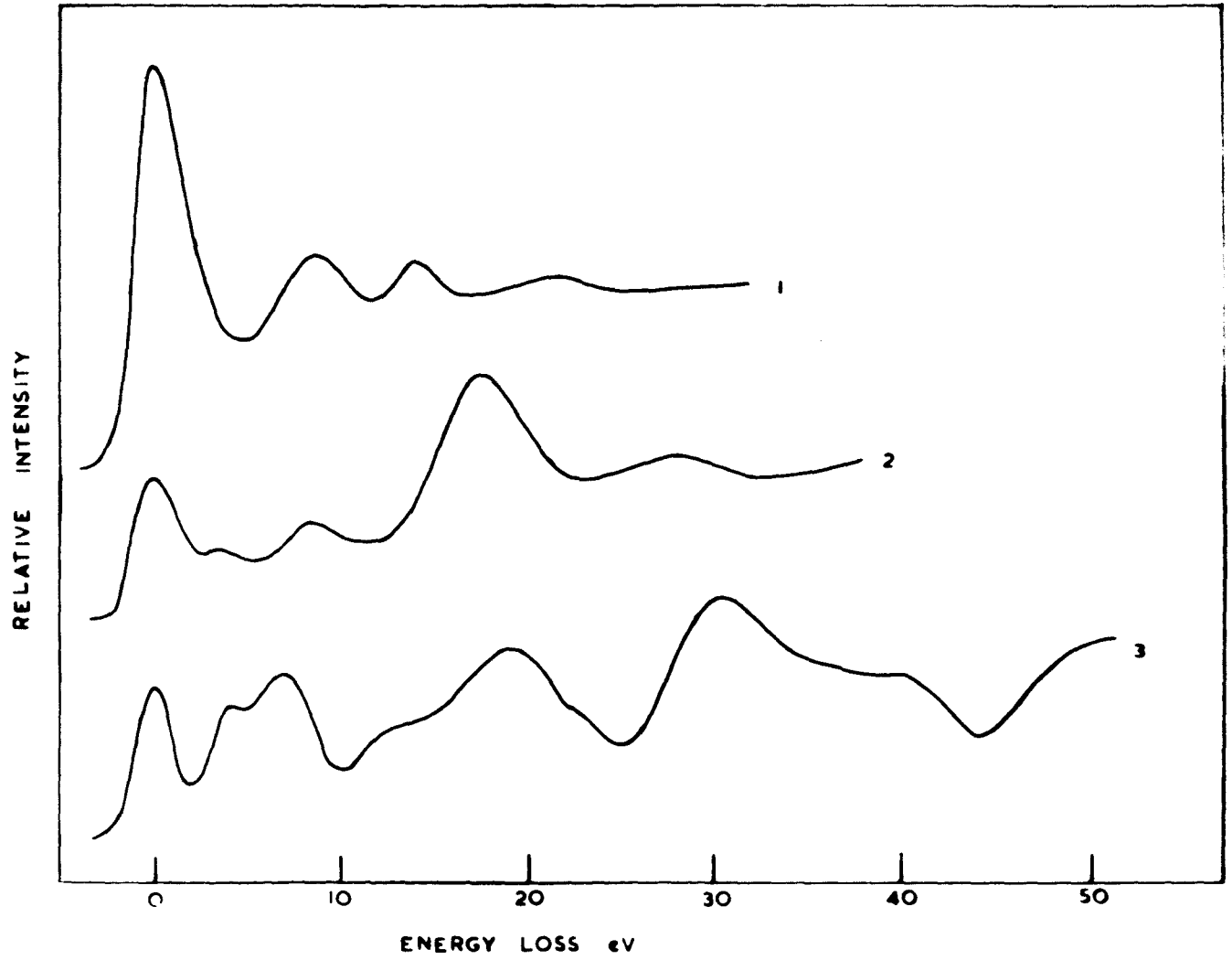

FIG. 75 EFFECT OF CONTAMINATION ON THE C.E.L SPECTRUM FROM BISMUTH

These loss peaks might be characteristic of bismuth oxide rather than Bi. Later experiments tend to confirm this.

Next a bismuth target was prepared by evaporation 'in vacuo'. An energy loss spectrum was scanned immediately after the evaporation of Bi and the spectrum is shown in fig. 75. There are three main loss peaks at 8.6, 14.1 and 22.4eV. The CEL values are compared with the results of previous workers in Table 7.

TABLE 7

Characteristic Energy Losses in Bi

Present Work	8.6	14.1	22.4	
Powell (105)	9.9	14.7	24.8	29
Marton and Leder (103)		13	25.2	

However, within an hour or so, the spectrum began to change in shape and within a few hours the whole spectrum was completely changed (fig. 75). This could either be due to Bi getting oxidised or due to the adsorption of contaminating layers. For the contaminated target there were a larger number of energy losses visible, at 4.2, 7, 14.7, 19.5, 22.7, 32.5 and 41eV. In addition, the primary peak was relatively very small. These losses are not considered to be characteristic of pure Bi at all.

The three energy losses from a freshly evaporated target can be explained as due to plasmon excitations. Assuming all the five valence electrons to be free to participate in collective oscillations, the volume plasmon energy is calculated to be 13.9eV and the surface plasmon energy

9.8eV. These values agree with the values of 14.1 and 8.6eV obtained in the present study. Hence it may be concluded that these two losses are due to volume and surface plasmon excitation. The loss at 22.4eV could be due to a combination of volume and surface plasmon excitation. However, from optical data Walker et al. (197) conclude that an interband transition can occur at 24eV. Hence it may be that the loss 22.4eV is due to such a process or perhaps a combination of both interband transition and plasmon excitation.

The fact that the energy loss spectrum of Bi changes in shape and size so quickly, emphasises the necessity for maintaining the surface free from contaminations. In the present investigation even after using such clean ultra-high vacuum, it takes only very little time to alter the spectrum completely. Since this is so, one must question the surface condition of the target and hence the results when a vacuum not better than 10^{-6} torr is used (as indeed Powell in his many investigations (104, 105) and others did). It is somewhat surprising that Powell et al. quote values thought to be genuinely characteristic of Bi! As can be seen from fig. 75, the loss values and the intensity of the loss peaks change with contamination of the surface. Apart from the surface plasmon loss being extremely sensitive to adsorbed layers, the fact that the volume loss also changes reveals the fact that even under such ultrahigh vacuum conditions ($< 10^{-9}$ torr) bismuth gets covered completely with contaminating layers within an hour or so. This emphasises the necessity for maintaining the surface clean, in any study of plasmon excitation.

FIG.76. ENERGY LOSSES FROM TANTALUM.

PRIMARY ENERGY 300eV.

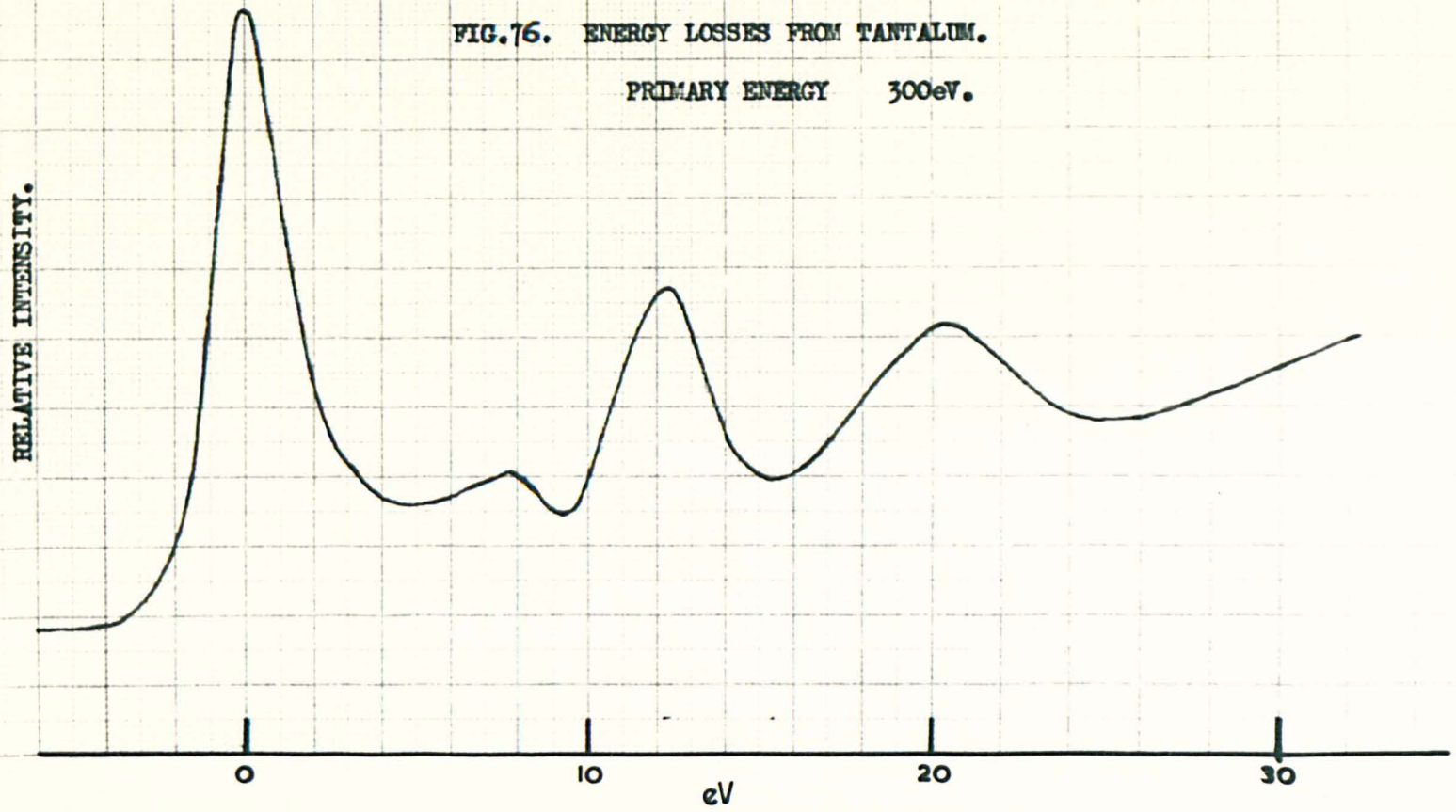

6.4.d Tantalum

Since tantalum carbide was one of the materials studied, it was felt necessary to also investigate the characteristic energy losses of tantalum, in order to make a comparison of the two. Only one author - Kleinn in 1954 (102) - has studied so far the properties of Ta and that too by the transmission method. In the present study, the target was in the form of a plate 1 sq. cm. cleaned by heat treatment. A typical CEL spectrum is shown in fig. 76. There are three main losses occurring at 7.9, 12.4 and 20.1eV, as opposed to the two losses at 19.7 and 47.7eV observed by Kleinn. Kleinn did not find the two lower losses. There might be a loss at 47.7eV, but it was found difficult to establish with certainty the existence of this loss in the present investigation.

On the basis of the plasma theory, taking the number of "free" electrons in Ta to be 5, the calculated value of the "plasmon" energy is 19.5eV. This agrees reasonably well with the experimental value of 20.1eV, observed in the present study. Hence it may be concluded that the loss at 20.1eV is due to the excitation of a volume plasmon. However, it must be said that the ionisation potentials of N_7 and N_6 shells are 18V and 20V respectively. Hence it may even be argued that the 20.1eV loss is due to the ionisation of one or the other of the above shells. The loss at 12.4eV is thought to be due to the excitation of surface plasmon, since it satisfies approximat-ely the relation $\hbar\omega_s = \frac{\hbar\omega_p}{\sqrt{2}}$. This surface plasmon loss could not be observed when the primary beam was incident normally on the target, and in the actual case the beam was incident at an angle 30° to the normal to the target. The loss at 7.9eV observed in the present study seems to be inexplicable on the basis of the plasma theory.

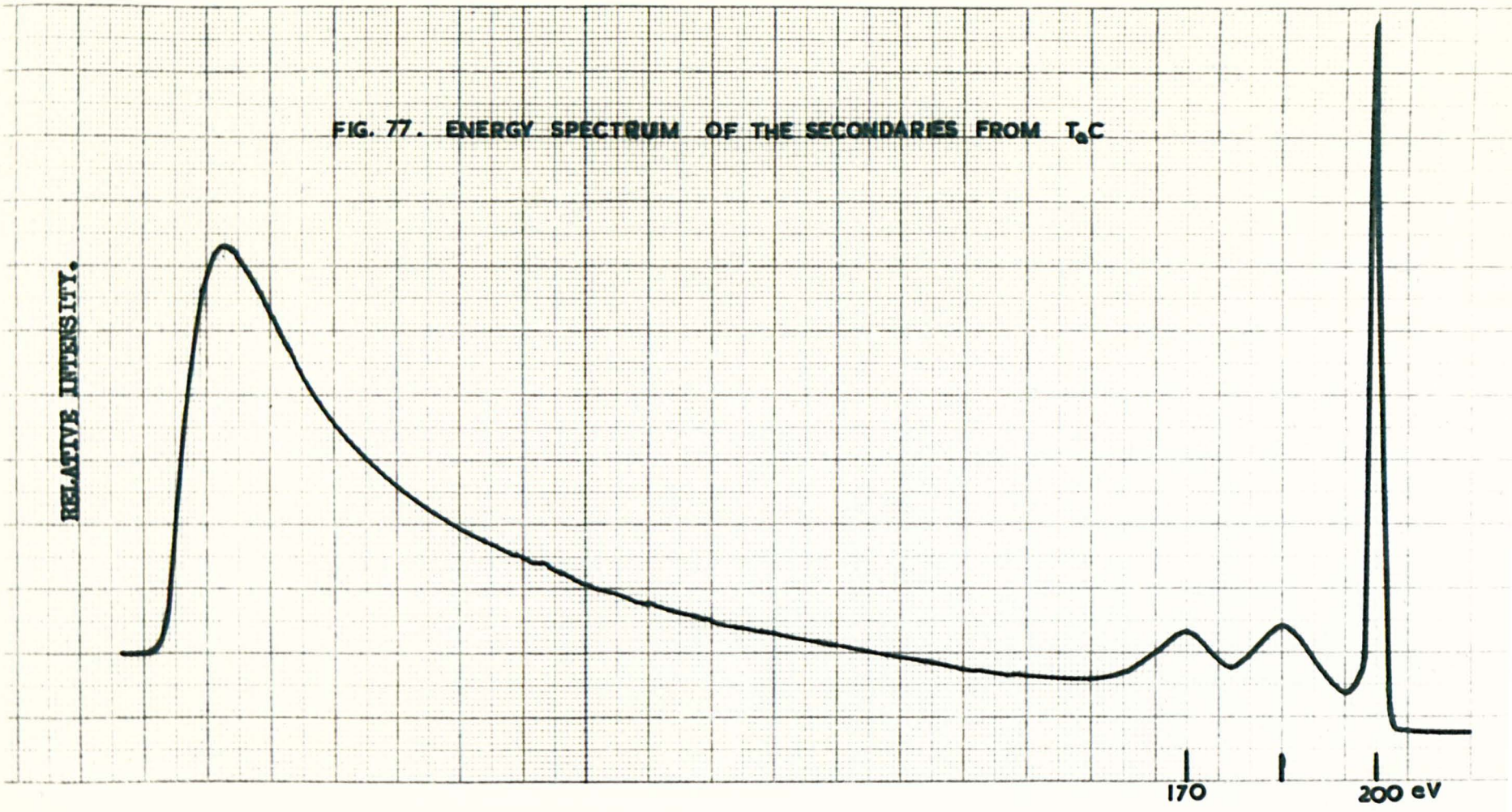

6.4.e Tantalum carbide

As a part of the study of the secondary emission characteristics of tantalum carbide, which has not been studied, the energy distribution of the secondary electrons was measured by the retarding field analyser. A typical energy distribution curve of the secondaries is shown in fig. 77, for a primary energy 200eV. The most interesting feature of this distribution curve is the presence of two energy loss peaks occurring at 15eV and 30eV. The 15eV loss is considered to be the single volume plasma loss and 30eV corresponding to electrons having excited two plasmons.

In explaining these two losses, it is interesting to compare the loss values of the component elements Ta and C. As has already been noted, the volume plasmon in Ta has a value 19.5eV. For graphite, Watanabe (198), Leder and Suddeth (199) and Scheibner and Tharp (202) observe two losses at 25eV and 7.5eV. The 25eV loss is explained as a volume plasma loss owing to the collective oscillation of all the four valence electrons in C. Ichikawa (200) explains the loss at 7.5eV as due not to surface plasmons but as due to the oscillation of the π electrons in carbon. This interpretation is, however, still subject to question (203) and some authors associate this loss with a simple interband transition between π electron levels (202). From the present investigation it is seen that the compound TaC has losses not the same as those of the component elements. This is not surprising since many other compounds do exhibit a similar property.

The depression in the loss value from the "plasmon" energy of Ta

may be due to the tight valence binding, when a compound is formed with carbon. Pines is of the opinion that such a tight valence binding will give rise to important high frequency band to band transitions which decrease the plasmon energy from the theoretical value. If one assumes that all the five electrons in Ta and the four electrons in C are free - which however may not be true in actual practice,- to participate in collective oscillations, a theoretical value for the plasmon energy may be obtained for TaC. The theoretical value thus obtained is 23eV, which is much higher than the observed value of 15eV. It is not surprising at all, owing to the tight valence binding and core-polarizability in the case of the compound. Even if one assumes that the core polarizability is negligible on the grounds that the core is tightly bound, the tight valence binding is by no means negligible. Because of this, there will be a depression in the theoretical value of the plasmon energy. This may explain the experimentally observed low value of the plasma loss. Hence it may be concluded that the two losses 15eV and 30eV in the case of TaC are in fact due to a single and double plasmon excitation respectively.

For tantalum carbide the whole energy range of the secondary electrons was scanned through and the energy spectrum thus obtained is shown in fig. 77. The shape is quite similar to that for other metals. Even though the present spectrometer was capable of good resolution, no fine structure in the lower energy range was observed.

CHAPTER VII

Conclusions and Suggestions for further Work

The experimental apparatus of the present investigation has proved to be a valuable tool in the study of some aspects of secondary electron emission under ultra-high vacuum conditions. It is possible to maintain clean surfaces only under such conditions and most previous experimental work has been open to the criticism of comparatively poor vacuum conditions and this factor has possibly accounted for the large discrepancies from author to author in the published data on SEE.

Using the spherical manifold system the total yield of secondaries from Ni, Ag, Pt, Bi and TaC has been measured. A quantitative assessment of the variation of the primaries has also been made. The total yield at normal incidence of the primary beam has been measured before, from Ni, Ag, Pt and Bi. On the other hand despite its commercial importance as a low yield material, TaC has not been studied hitherto. For the first four above-mentioned metals a more accurate value of the yield has been obtained in this study.

For normal incidence δ_{max} from nickel has a value 1.62 which is higher than the value 1.4 obtained by previous workers. This higher value for δ_{max} is thought to be due to the high smoothness and the cleanliness of the surface. In addition most previous workers have ignored the effect of tertiary electfons from the collector which might be one reason for the lower value that they observed. The higher value of δ_{max} found in the present study may hence partly be due to the action of this grid.

It is felt that such a grid is essential for accurate measurements.

In the case of platinum, different authors quote varied values for δ_{max} ranging from 1.4 to 1.8. The present study yields a value 1.74 for δ_{max} from Pt which agrees more with the value found by Bronshtein and Segal (4) who again used a suppressor or so-called anti-dynatron grid. This value tends to suggest that Pt is one of the high yield metals. For silver the value of δ_{max} has a value 1.64 as opposed to the value of 1.56 quoted by Kollath. This increase may again be due to the reasons given above. However, there does not seem to be any great difference in the value of δ_{max} for Bi between the present study and previous work. For all these materials, the yield is found to be generally higher, which may be ascribed to the ultra-high vacuum environment and the effect of the anti-dynatron grid. Owing to this noticeable effect of ultra-high vacuum on SEE it may be essential to repeat the experiments for other materials in such conditions.

The yield values from tantalum carbide are of particular interest because of its intrinsic importance as a low yield material used in the valve industry. The value of δ_{max} is found to be < 1, in fact only 0.68. This value is somewhat higher for a smoother TaC surface.

It may be concluded that TaC is a low yield material which may be used to minimise the secondary emission where it has adverse effects. Furthermore the value of inelastic reflection coefficient which is found to be only 0.11 suggests that the majority of the secondary electrons have energies less than 50eV.

A quantitative determination of the dependence of the total yield

on the angle of incidence of the primary beam and the mean depth of origin of secondaries has been made in the present study. For larger angles of incidence of the primary beam the total yield is higher. This is expected from elementary theory. The mean depth of origin of secondaries x_s, in the case of Ni has a value 28 - 38 Å in the primary range 600eV - 1200eV which is compatible with the value of 30 Å found by Bruining. The values of x_s for Ag, Bi and Pt found in the present study cannot be compared with other work owing to the lack of data.

For all the materials investigated the mean depths of origin of secondaries are only a few tens of Å units (Table 4) which suggest that the secondary electron emission may be considered to be more of a surface phenomenon. It must be admitted that the values of x_s are only approximate because of the lack of accurate data on the absorption coefficient of slow electrons in these materials in the energy range concerned. More transmission experiments need to be done in the lower energy range to determine the absorption coefficient before a very accurate measurement of the mean depth of origin of secondaries can be made by this method.

The roughly linear relationship observed between ln δ_θ and (1 - Cos θ) suggests that the variation of the yield with the angle of incidence of the primaries may very well be represented above the primary energy $E_{p_{max}}$, by the equation (6)

$$\delta_\theta = \delta_o \exp \left[\alpha x_s (1 - \cos \theta) \right]$$

An outstanding feature of the present experimental set-up has been its ability to measure both yield and energy distribution of the

secondaries and in particular the energy distribution of inelastically reflected electrons, which reveals the characteristic energy losses. The energy loss values obtained from this study clearly reveal the immense potential of this spherical retarding field energy analyser as a very accurate device in the measurement of the characteristic energy losses, by analysing the reflected electrons. The a.c modulation technique used in differentiating the retarding field curve has proved a great success. The resolution of the above analyser has been remarkably good. The half-width of the elastically reflected primary peak had a typical value less than 2eV for a primary energy 400eV. This could possibly be improved upon by reducing the size of the target or increasing the diameter of the spherical retarding grid and replacing the oxide-coated cathode in the electron gun by a tungsten filament. The electronic differentiation of the integral plot by the a.c modulation technique and the consequent detection by a phase sensitive detector eliminate some of the possible errors normally associated with other retarding field energy analysers. In addition, since the total number of electrons emerging through an angle 2π , is available for analysis, a very small primary beam current density only is required.

The characteristic energy losses from silver, beryllium, bismuth tantalum and tantalum carbide measured by using the present energy analyser can be explained as due to the excitation of volume plasmons, surface plasmons or a combination of the two, and due to interband transitions. The two losses 15eV and 30eV, observed in the energy spectrum from TaC

and measured for the first time may be considered to be due to the excitation of volume plasmons. These losses are different from the losses observed in either Ta or C, showing that TaC belongs to the group of compounds which have CEL spectra different from the respective elements. The variation of the intensity of the loss peaks and the change in the spectrum observed in the case of Bi, reveal a significant effect of contamination on the loss spectrum. It is to be concluded that for reproducible energy loss spectra, genuinely characteristic of the material investigated, one should prepare clean surfaces and maintain them in ultra-high vacuum. The energy losses found in the different materials tend to support strongly the concept of plasma oscillations in metals and plasmon excitation as a possible mechanism by which electrons can lose energy. However, it is to be emphasised that plasmon excitation is not, by any means, the only mechanism by which energy losses can occur. Electrons can obviously lose energy through interband transitions, intraband transitions, Auger transition, etc.

It is evident that a great deal of work lies ahead before we may feel that our understanding of the energy loss spectra is truly satisfactory. The existing discrepancies among the experimental results of different investigators on the same material surely ought to be resolved. Certainly there is scope for further improvement in the existing techniques. There may be special difficulties germane to the very accurate measurement of the energy losses which should in fact induce one to look for new techniques rather than being pessimistic about the older ones. New spectrometers with enhanced energy resolution should and can be designed, particularly in the low energy reflection type experiments as in the

present study.

A few suggestions may be made regarding further study of SE properties and characteristic energy losses using a similar "dual-purpose" system. So far, the plotting of the yield curve has been done manually, which is time-consuming. By incorporating an operational amplifier and an analogue module as an electronic divider and sweeping the primary voltage, a yield curve could be plotted in a few minutes, which would make it possible to investigate the likely variation of the yield with short times, and changing environmental conditions.

In the present study, only the variation of the total yield with the angle of incidence of the primaries has been studied. It is equally easy to make a quantitative determination of the variation of the inelastic reflection coefficient with the angle of incidence. Furthermore, by depositing thin films of one material onto another and measuring the total yield and inelastic reflection coefficient, one can verify the conclusions drawn by Bronshtein and Segal (4,5) regarding the "effectiveness" of inelastically reflected primaries in the production of true secondaries and also the depth of origin of secondaries. The thickness of the condensed films can be controlled to finer limits by using an automatic evaporation controller, coupled with a quartz crystal monitor.

Since the present investigation was directed towards a measurement of the energy losses of electrons, the spectrum of inelastically reflected primaries only was studied. However, the same set-up may be easily adapted to study the whole energy spectrum of the secondaries, by using an arrangement shown in fig. 55. Such a study will reveal the

existence - if any - of the fine structures in the energy spectrum which have been explained as due to Auger transitions. Recently the interest in this process of energy loss and excitation of electrons has been revived (202).

The present energy analyser is particularly suitable for the study of characteristic energy losses and their dependence on the angle of incidence of the primary beam. Very little work has been done in this direction particularly in the reflection type experiments. Recently Thirlwell (204) reported that the ratio of the intensity of surface plasmon loss to that of the volume plasmon loss increases with larger angles of incidence of the primary beam. This offers in fact, an easy means of identification of the surface plasmons.

There have been only a few scattered investigations on the characteristic energy losses in alloys. As stated in section 3.7, for an alloy, an intermediate loss between the individual losses of the components and varying in position with concentration would be expected, on the basis of the plasma theory. A study of this aspect and the variation with the chemical composition would yield a better knowledge of the interaction of electrons in alloys and provide a crucial test for the plasma oscillation theory.

With the recent progress in plasmon studies, surface plasmons have been favoured as a tool for the investigation of surface conditions (205). For a metal surface of perfect planar geometry the surface plasma frequency is given by $\omega_s = \frac{\omega_p}{\sqrt{2}}$ and the corresponding energy $\hbar\omega_s$ can be experimentally measured. However, if the surface is covered with a layer

of frequency - independent dielectric constant ε , the surface plasmon energy is shifted to $\frac{\hbar \omega_p}{\sqrt{1+\varepsilon}}$. This change in the surface plasmon energy can be employed as a test for the cleanliness of the metal surface. Also, an experimental determination of ε by this method and the comparison of the value of this dielectric constant from optical measurements should provide a test for the existance of surface plasmons.

Another interesting aspect of the plasmons which can be studied in this experimental set-up is the existence of interfacial plasmons i.e. plasma oscillations between the boundaries of two free electron plasmas. This may be studied by depositing a very thin layer of one metal onto another and examining the energy losses. For example Mg may be deposited onto Al and the interfacial surface plasmon energy will be $\hbar \omega_s = \hbar \left[\frac{1}{2}(\omega_{p_1}^2 + \omega_{p_2}^2)\right]^{\frac{1}{2}}$ where ω_{p_1} and ω_{p_2} are the volume plasmon frequencies in the two metals.

The experimental evidence of all these aspects of plasmons will confirm the validity of the concept of plasma oscillations in metals and the excitation of these oscillations as a means of energy loss of electrons in solids. Particularly, the existence of surface plasmons should open up new techniques in the study of surfaces. Properly developed, surface plasmons may turn out to be as good a tool in the study of surfaces as low energy electron diffraction. There are a large number of varied aspects of plasmons, like plasma radiation, excitation of plasmons by photons, which have not been investigated. The study of plasmons is still only in its infancy and certainly the near future should bring about remarkable progress in this field which would in turn yield extremely interesting and important results and help enlarge our present knowledge of this attractive field of solid state physics.

LIST OF SYMBOLS

A	Atomic weight
$(2A)$	Whiddington's constant
Å	Angstrom unit
α	Absorption coefficient of secondaries
c	Velocity of light
d	Density of the metal
δ	Yield of secondary electrons
δ_{max}	Maximum yield
δ_{true}	Fraction of the secondaries below 50eV
e	Electronic charge
E_p	Primary electron energy
$E_{p_{max}}$	Primary energy corresponding to maximum yield
ε	Dielectric constant
ζ_o	Fermi Energy
$\hbar$	$\frac{h}{2\pi}$
η	Inelastic reflection coefficient
θ	Angle of incidence of primaries
λ	Wavelength of the plasma wave
k	Wave number of the plasmon
k_c	Cut-off plasma wave vector
m	Mass of the electron
N	Avogadro's number

n_o	Free electron density
R	Range of primary electrons
r_e	Inter-electronic distance
S	'Effectiveness' of inelastically reflected primaries in secondary production
τ	Relaxation time
ϕ	Work function
v	Velocity of the electron
x_s	Mean depth of origin of secondaries
Z	Atomic number
ω_p	Volume plasmon frequency
ω_s	Surface plasmon frequency

REFERENCES

1.	Austin, L. Starke, H.	Ann. Physik	9	271	(1902)
2.	Hachenberg, O. Brauer, W.	Advan. Electron. Electron Phys.	11	413	(1959)
3.	McKay, K.G.	Advances in Electronics	1	65	(1948)
4.	Bronshtein, I.M. Segal, R.B.	Sov. Phys. Solid State	1	1365	(1960)
5.	Bronshtein, I.M. Segal, R.B.	Sov. Phys. Solid State	1	1375	(1960)
6.	Dekker, A.J.	Solid State Physics, MacMillan & Co., London			(1964)
7.	Mott, N.F., Jones, H.	Theory of the Properties of Metals and Alloys, Oxford.			(1936)
8.	Rudberg, E.	Phys. Rev.	50	138	(1936)
9.	Lenard, P.	Quantitatives über kathodenstrahlen, Heidelberg.			(1918)
10.	McKay, K.G.	Phys. Rev.	74	1606	(1948)
11.	Brüining, H.	Physics and Applications of Secondary Electron Emission, Pergamon Press			(1954)
12.	Kollath, R.	Phys. Z.	38	202	(1937)
13.	Van der Ziel, A.	Solid State Physical Electronics. Prentice Hall Co.			(1957)
14.	Brown, S.C.	Basic Data of Plasma Physics. John Wiley & Son.			(1959)
15.	Sproull, R.L.	Modern Physics. John Wiley & Son.			(1956)

16.	Becker, J.A.	Rev.Mod.Phys.	7	95	(1935)
17.	De Boer, J.H., Bruining, H.	Physica	6	941	(1939)
18.	Sixtus, K.	Ann. Phys. Lpz.	3	1017	(1929)
19.	Treloar, L.R.G.	Proc. Phys. Soc. Lond.	49	392	(1937)
20.	Coomes, E.A.	Phys. Rev.	55	1270	(1939)
21.	McKay, K.G.	Phys. Rev.	61	708	(1942)
22.	Barcody, E.M.	Phys. Rev.	78	780	(1950)
23.	Kollath, R.	Hanbuch d. Physik	21	232	(1956)
24.	Treloar, L.R.G., Landon, D.H.	Proc. Phys. Soc. Lond.	50	625	(1938)
25.	Kushniv, Yu. M., Milyutin, I.	J. Tec. Phys. U.S.S.R.	9	267	(1939)
26.	Morozov, P.M.	J. Exp. Theoret. Phys. U.S.S.R.	11	402	(1941)
27.	Wooldridge, D.E.	Phys. Rev.	57	1080	(1940)
28.	Wooldridge, D.E.	Phys. Rev.	58	316	(1940)
29.	Blankenfeld, G.	Ann. Physik	9	48	(1950)
30.	Sternglass, E.J.	Westinghouse Res. Lab. Research Rept. R. 94413-3-J			
31.	Johnson, J.B., McKay, K.G.	Phys. Rev.	93	668	(1953)
32.	Tate, J.T.	Phys. Rev.	17	394	(1921)
33.	Baltruschat, M. Starke, H.	Phys. Z.	23	403	(1922)
34.	Bruining, H.	Physica	5	901	(1938)
35.	Bruining, H.	Physica	3	1046	(1936)
36.	Müller, H.O.	Z. Phys.	104	475	(1937)

37.	Becker, A.	Ann. Phys. Lpz.	2	249	(1929)
38.	Jonker, J.L.H.	Philips Res. Rept.	7	1	(1952)
39.	Young, J.R.	Phys. Rev.	103	292	(1956)
40.	Nichols, M.H.	Phys. Rev.	57	297	(1940)
41.	Beckow, G.	Phys. Z.	42	144	(1941)
42.	Wooldridge, D.E.	Phys. Rev.	56	562	(1939)
43.	Rashkovskii, S.F.	Radio Eng. Electron.	3	87	(1958)
44.	Park, R.L. Farnsworth, H.C.	J. Chem. Phys.	43	2351	(1965)
45.	Palluel, P.	Compt. rend.	224	1492, 1551	(1947)
46.	Holliday, J.E., Sternglass, E.J.	J. Appl. Phys.	28	1189	(1957)
47.	Bronshtein, I.M., Fraiman, B.S.	Sov. Phys. Solid State	3	816	(1961)
48.	Gomoyunova, M.V., Ivanov, G.A.	Sov. Phys. Solid State	2	294	(1960)
49.	Bohm, D., Pines, D.	Phys. Rev.	82	625	(1951)
50.	Pines, D., Bohm, D.	ibid.	85	338	(1952)
51.	Bohm, D., Pines, D.	ibid	92	609	(1953)
52.	Sternglass, E.J.	Phys. Rev.	95	345	(1954)
53.	Everhart, T.E.	J. Appl. Phys.	31	1483	(1960)
54.	Nakhodkin, N.G. et al.	Sov. Phys. Solid State	4	1112	(1962)
55.	Archard, G.D.	J. Appl. Phys.	32	1905	(1961)
56.	Muller, R.H.	Phys. Rev.	93	891	(1954)
57.	Saldick, J., Allen, A.O.	J. Chem. Phys.	22	438	(1954)

58.	Gomoyunova, M.V., Letunov, N.A.	Sov. Phys. Solid State	7	311	(1965)
59.	Jonker, J.L.H.	Philips Res. Rept.	6	372	(1951)
60.	Jonker, J.L.H.	ibid.	12	249	(1957)
61.	Alekseev, V.A., Borisov, V.L.	Sov. Phys. Solid State	4	191	(1962)
62.	Burns, J.	Phys. Rev.	119	102	(1960)
63.	Haworth, L.J.	Phys. Rev.	48 50	88 216	(1935) (1936)
64.	Kollath, R.	Ann. Physik.	1	357	(1947)
65.	Harrower, G.A.	Phys. Rev.	102	340	(1956)
66.	Zinke, O.H.	Phys. Rev.	106	1163	(1957)
67.	Lander, J.J.	Phys. Rev.	91	1382	(1953)
68.	Burhop, E.H.S.	The Auger Effect and other Radiationless Transitions - University Press, Cambridge.			(1952)
69.	Melter, L.	Phys. Rev.	50	48	(1936)
70.	Koller, L.R., Johnson, R.P.	Phys. Rev.	52	519	(1937)
71.	Allen F.G., et al.	J. Appl. Phys.	30	1563	(1959)
72.	Ehrlich, G.	J. Phys. Chem.,	60	1388	(1956)
73.	Bloomer, R.N., Haine, M.E.	Vacuum	3	128	(1954)
74.	Becker, J.A., et al.	J. Appl. Phys.	32	411	(1961)
75.	Cooper, E.G., Muller, E.W.	Rev. Sci. Inst.	29	309	(1958)
76.	Gibbons, D.J.	Handbook of Vacuum Physics, Vol. 2. Pergamon Press.			(1966)
77.	Bruining, H. et al.	Physica	4	267	(1937)

78.	Boumeester, H.G.	Philips Tec. Rev.	2	115	(1937)
79.	Kreuchen, K.H., Diserens, N.J.	Proc. I.E.E. Pt. B. Supt.		860	(1958)
80.	Johnson, J.B.	Phys. Rev.	66 73	352 1058	(1944) (1948)
81.	Valentine, J.H., Curran, S.C.	Repts. Progr. Phys.	21	2	(1958)
82.	Kanter, H.	Phys. Rev.	121	677	(1961)
83.	Stehberger, K.H.	Ann. Physik	86	825	(1928)
84.	Dobretsov, L.N., Matskevich, T.L.	Sov. Phys-Tech. Phys.	2	663	(1957)
85.	Kanter, H.	Phys. Rev.	121	681	(1961)
86.	Hughes, A. Ll., Rojansky, V.	Phys. Rev.	34	284	(1929)
87.	Hughes, A. Ll., McMillen, J.H.	Phys. Rev.	34	291	(1929)
88.	Schulz	Phys. Rev.	125	229	(1962)
89.	Ramsauer, C.	Ann. Physik (4)	45	961	(1914)
90.	Rudberg, E.	Proc. Phys. Soc.	A127	111	(1930)
91.	Kollath, R.	Z. tech. Phys. Ann. Physik (5)	21 39	328 59	(1940) (1941)
92.	Brown, D., Whiddington, R.	Proc. Leeds Phil. Lit. Soc.	1	162	(1927)
93.	Rudberg, E., Slater, J.C.	Phys. Rev.	50	150	(1936)
94.	Haworth, L.J.	Phys. Rev.	48	88	(1935)
95.	Haworth, L.J.	ibid.	50	216	(1936)
96.	Turnbull, J.C., Farnsworth, H.E.	Phys. Rev.	54	509	(1938)
97.	Reichertz, P.P., Farnsworth, H.E.	Phys. Rev.	75	1902	(1949)

98.	Ruthemann, G.	Naturwissenschaften	29 30	648 145	(1941) (1942)
99.	Ruthemann, G.	Ann. Physik.	2(6)	113	(1948)
100.	Möllenstedt, G.	Optik	5	499	(1949)
101.	Watanabe, H.	J. Phys. Soc. Japan	9 10 11	920 321 112	(1954) (1955) (1956)
102.	Kleinn, W.	Optik	11	226	(1954)
103.	Marton, L., Leder, L.B.	Phys. Rev.	94	203	(1954)
104.	Powell, C.J., Swan, J.B.	Phys. Rev.	115	869	(1959)
105.	Powell, C.J.	Proc. Phys. Soc.	76	593	(1960)
106.	Marton, L.	Phys. Rev.	28	172	(1956)
107.	Marton, L., Leder, L.B., Mendlowitz, H.	Advanc. Electron. Electron Physics	7	183	(1955)
108.	Best, P. E.	Proc. Phys. Soc. Lond.	79	133	(1962)
109.	Gauthe, B.	Phys. Rev.	114	1265	(1959)
110.	Powell, C.J.	Austrl. J. Phys.	13	145	(1960)
111.	Klemperer, O., Shepherd, J.P.G.	Brit. J. Appl. Phys.	14	89	(1963)
112.	Minor, R.S.	Ann. Physik.	10	581	(1903)
113.	Richardson, O.W.	Proc. Roy. Soc.	A128	63	(1930)
114.	Cauchois, Y.	Acta Cryst.	5	351	(1952)
115.	Leder L.B. et al.	Phys. Rev.	101	1460	(1956)
116.	Sternglass, E.J.	Nature	178	1387	(1956)
117.	Tonks, L., Langmuir, I.	Phys. Rev.	33	195, 990	(1929)

118.	Hartree, D.R.	Proc. Camb. Phil. Soc.	24	89	(1928)
119.	Raimes, S.	The Wave Mechanics of Electrons in Metals. North Holland Publishing Co.			(1967)
120.	Raimes, S.	Repts. on Progr. in Phys.	10	1	(1957)
121.	Pines, D.	Elementary Excitations in Solids. W. A. Benjamin, New York.			(1963)
122.	Pines, D.	Solid State Phys.	1	367	(1955)
123.	Pines, D.	Revs. Mod. Phys.	28	184	(1956)
124.	Ritchie, R.H.	Phys. Rev.	106	874	(1957)
125.	Stern, E.A., Ferrell, R.A.	Phys. Rev.	20	130	(1960)
126.	Nozieres, P., Pines, D.	Phys. Rev.	109	1062	(1958)
			113	1254	(1959)
		Nuovo Cimento	9	470	(1958)
127.	Pines, D.	Physica	26	5103	(1960)
128.	Wolff, P.A.	Phys. Rev.	92	18	(1953)
129.	Hubbard, J.	Proc. Phys. Soc.	A67	1058	(1954)
130.	Kanazawa, H.	Progr. Theore. Phys. Japan	13	227	(1955)
131.	Adams, E.N.	Phys. Rev.	98	947	(1955)
132.	Frohlich, H., Pilzer, H.	Proc. Phys. Soc.	A68	525	(1955)
133.	Hubbard, J.	Proc. Phys. Soc.	A68	441	(1955)
134.	Raether, H.	Solid State Excitations by Solids. Springer Tracts in Modern Physics. Vol. 38		(1965)	
135.	Ditchburn, R.W.	Light. Blackie and Son. Ltd., London.			

136.	Klemperer, O., Shepherd, J.P.G.	Advanc. Phys.	12	355	(1963)
137.	Robins, J.L., Swan, J.B.	Proc. Phys. Soc.	76	857	(1960)
138.	Blackstock, A.W., Ritchie, R.H., Birkhoff, R.D.	Phys. Rev.	100	1078	(1955)
139.	Quinn, J.J.	Phys. Rev.	126	1435	(1962)
140.	Schmuser, P.	Z. Physik	180	105	(1964)
141.	Miller, W.R., Axelrod, N.N.	Solid State Comm.	3	133	(1965)
142.	Creuzburg, M.	Z. Physik	174	511	(1963)
143.	Kunz. C.	Z. Physik	180	127	(1964)
144.	Kunz, C., Raether, H.	Solid State Comm.	1	214	(1963)
145.	Powell, C.J., Swan, J.B.	Phys. Rev.	116, 118	81 640	(1960) (1960)
146.	Klemperer, O., Thirlwell, J.	Solid State Comm.	4	15	(1966)
147.	Ferrell, R.A.	Phys. Rev.	111	1214	(1958)
148.	Steinmann, W.	Phys. Rev. Letters Z. Physik	5 163	470 92	(1960) (1961)
149.	Brown, R.W., Wessel, P., Trounson, E.P.	Phys. Rev. Letters	5	472	(1960)
150.	Arakawa, E.T., Herickoff, R.J., Birkhoff, R.D.	Phys. Rev. Letters	12	319	(1964)
151.	Herickoff, R.J. et al.	Phys. Rev.	137	A1433	(1965)
152.	Ferrell, R.A., Stern, E.A.	Am. J. Phys.	30	810	(1962)
153.	McAlister, A.J., Stern, E.A.	Phys. Rev.	132	1599	(1963)
154.	Brambring, J., Raether, H.	Phys. Rev. Letters	15	882	(1965)

155.	Ritchie, R.H.	Surface Science	4	497	(1965)
156.	Williams, M.W., Arakawa, E.T., Emerson, L.C.	Surface Science	6	127	(1967)
157.	Ehrenreich, H., Phillip, H.R.	Phys. Rev.	128	1622	(1962)
158.	Mayer, H., Hietel	Optical Properties and Electronic Structure of Metals and Alloys. Ed. Abeles, F. North Holland Publishing Co.			(1966)
159.	Arakawa, E.T. et al.	ibid			
160.	Salow, H.	Z. tech. Physik	21	8	(1940)
161.	Dekker, A.J.	Solid State Phys.	6	251	(1958)
162.	Whiddington, R.	Proc. Roy. Soc.	A86	360	(1912)
163.	Terrill, H.M.	Phys. Rev.	22	161	(1922)
164.	Hoffmann, O.	Z. Physik	143	147	(1955)
165.	Sternglass, E.J.	Westinghouse Res. Lab. Sci. Paper No. 6-94410-2-709			(1957)
166.	Bethe, H.A.	Ann. Physik	5	325	(1930)
167.	Izmailov, S.V.	Sov. Phys. - Solid State	4	1873	(1963)
168.	Kadyschevitsch, A.E.	J. Phys. U.S.S.R.	2 4 9	115 341 431	(1940) (1941) (1945)
169.	Fröhlich, H.	Ann. Physik	13	229	(1932)
170.	Dekker, A.J., van der Ziel, A.	Phys. Rev.	92	34	(1953)
171.	Marshall, J.F.	Phys. Rev.	88	416	(1952)
172.	Baroody, E.M.	Phys. Rev.	89 101	910 1679	(1953) (1956)
173.	van der Ziel, A.	Phys. Rev.	92	35	(1953)

174.	Neufield, J., Ritchie, R.H.	Phys. Rev.	98	1632	(1955)
175.	Fröhlich, H.	Proc. Phys. Soc.	B68	657	(1955)
176.	Wolff, P.A.	Phys. Rev.	95	56	(1954)
177.	Marshak, R.E.	Rev. Mod. Phys.	19	185	(1947)
178.	Bills, D.G., Evett, A.A.	J. Appl. Phys.	30	564	(1959)
179.	Hall, L.D.	5th National Vacuum Symposium Transactions			(1958)
180.	Todd, C.J.	J. Sc. Inst.	42	755	(1965)
181.	Klemperer, O.	Electron Optics Cambridge Univ. Press			(1953)
182.	Klemperer, O.	Rept. on Progr. in Phys.	28	77	(1965)
183.	Caulton, M.	RCA Review	26	217	(1965)
184.	Simpson, J.A.	Rev. Sci. Inst.	32	1283	(1961)
185.	Boersch, H.	Z. Phys.	139	118	(1954)
186.	Boersch, H.	Z. Phys.	134	156	(1953)
187.	Soboleva, N.A.	Radiotech i Elektron	3	339	(1958)
188.	Leder, L.B., Simpson, J.A.	Rev. Sci. Inst.	29	571	(1958)
189.	Hunten, D.M.	Introduction to Electronics Holt, Rinehart and Winston, Inc. New York.			(1964)
190.	Faulkner, E.A., Stanneth, R.H.O.	Electronic Engineering	36	159	(1964)
191.	Englander-Golden, P., Rapp, D.	Lockhead Missiles and Space Co. Rept.			(1965)
192.	Thomas, S., Pattinson, E.B.	Proc. of 8th International Conference on ionised phenomena in gases - Vienna		(1967)	

193.	Gauthe, B.	Ann. Phys. Paris	3	915	(1958)
194.	Taft, E.A., Philipp, H.R.	Phys. Rev.	121	1100	(1961)
195.	Robins, J.L.	Proc. Phys. Soc.	78	1177	(1961)
196	Munier J.H. et al.,	Phys. Rev.	58	537	(1940)
197.	Walker, W.C. et al.,	J. Opt. Soc. Amer.	49	491	(1951)
198.	Watanabe, H.	J. Electronmicroscopy	4	24	(1956)
199.	Leder, L.B., Suddeth, J.A.	J. Appl. Phys.	31	1422	(1960)
200.	Ichikawa, Y.H.	Phys. Rev.	109	653	(1958)
201.	Jull, G.W.	Proc. Phys. Soc.	B69	1237	(1956)
202.	Scheibner, E.J., Tharp, L.N.	Surface Science	8	247	(1967)
203.	Carter, J.G. et al.	Phys. Rev.	137	639	(1965)
204.	Thirlwell, J.	Proc. Phys. Soc.	91	552	(1967)
205.	Raether, H.	Surface Science	8	233	(1967)